

Divambal APPAVOO-GUPTA

Chimiste diplômée de l'Université de Johannesburg, Johannesburg (Afrique du Sud)

**Exploring New Avenues for Arene-Ruthenium Complexes:
Coordination to [60]Fullerene, Hydrogen Bonding
Assemblies and Liquid-Crystalline Materials**

Thèse présentée à la Faculté des Sciences,

Pour l'obtention du grade de Docteur ès Sciences

Membres du jury:

| | |
|-------------------------|---|
| Prof. Robert Deschenaux | Université de Neuchâtel, Directeur de thèse |
| Prof. Bruno Therrien | Université de Neuchâtel, Rapporteur interne |
| Prof. Gilles Gasser | Université de Zurich, Rapporteur externe |



Institut de Chimie

Université de Neuchâtel

Soutenue le 20 July 2015

IMPRIMATUR POUR THESE DE DOCTORAT

La Faculté des sciences de l'Université de Neuchâtel
autorise l'impression de la présente thèse soutenue par

Madame Divambal APPAVOO-GUPTA

Titre:

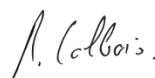
**“Exploring New Avenues for Arene-Ruthenium
Complexes: Coordination to Fullerene,
Hydrogen Bonding Assemblies
and Liquid-Crystalline Materials”**

sur le rapport des membres du jury composé comme suit:

- Prof. Robert Deschenaux, directeur de thèse, Université de Neuchâtel
- Prof. ass. Bruno Therrien, Université de Neuchâtel
- Prof. Gilles Gasser, Université de Zürich

Neuchâtel, le 7 octobre 2015

Le Doyen, Prof. B. Colbois



Acknowledgements

Professor Robert Deschenaux, thank you for having welcomed me in your group. You have been of constant support during my entire Ph.D. and I am grateful for that.

Professor Bruno Therrien, thank you for having given me the opportunity to do research in Switzerland.

Professor Gilles Gasser, thank you for accepting to be in my jury.

Dr Diego Carnevale, thank you for the NMR analysis. Your contribution has been crucial to my work.

Dr Armelle Vallat, thank you for MS spectrometry analysis and for your advice.

I am very grateful to my previous and current colleagues, without whom I would probably not be where I am today. Thank you Luyen, Anaïs, Nguyet, Sébastiano, Sylvain, Virginie, Tung, Ester, LeAnh and Steeve. Marion and Aurélie, thank you for your huge support and for keeping the “Hakuna Matata” and joyful ambiance in the lab.

I want to thank Damien and Christian for their useful advice as well as Thomas, David and Bing, who helped me whenever I needed an inorganic expert's advice.

A big thank you to all my friends here in Neuchâtel who made my stay a bit more fun and comfortable, Jon, Manu, Ana, Christian, Simla, Theju, Bindhu and Justin.

I want to give an enormous thank you to my parents, mom, dad and Sel and my entire family for always caring and supporting me. Finally, thank you Mayank, for standing by my side, for trusting and believing in me more than I believe in myself.

Summary

The thesis aims at using arene-ruthenium complexes as building blocks for the synthesis of diverse compounds to obtain potential mesomorphic and/or biological properties. The thesis consists of three main projects.

The first project deals with supramolecular assemblies. New supramolecular di- and tetranuclear ruthenium arrangements, the latter bearing a cavity, were designed. H-bonding was the key interaction involved in the synthesis of the spacer ligands, which exist as dimers. Different spacer ligands and different ruthenium clips were used in synthesizing a whole family of the corresponding ruthenium assemblies/cages. Several analytical methods were employed to characterise the compounds and to study their arrangements.

The second project involves more classical ruthenium cages, including hexanuclear prisms and octanuclear cubes. Anthracene- and pyrene-core dendrimers were developed as potential guests, using key reactions such as click, Suzuki and Sonogashira coupling. Owing to the poor stability of the anthracene derivatives, their proper characterization and encapsulation could not be carried out. Pyrene derivatives showed better stability and were therefore studied further. The pyrene dendrimers, bearing cyanobiphenyl dendrons, displayed liquid-crystalline properties. Two pyrene dendrimers could be successfully encapsulated into hexanuclear arene-ruthenium prisms by the carceplex method. However, no mesomorphic properties were observed for the encapsulated systems.

The third project had as objective to study the biological properties of a system comprising of an arene-ruthenium moiety and [60]fullerene. Two such compounds were successfully synthesised. However, these compounds could not be tested for their potential biological activities because of their poor solubility in aqueous media.

Table of Contents

| | |
|---|-----------|
| 1 Introduction | 1 |
| 1.1 Ruthenium Complexes..... | 3 |
| 1.1.1 Catalytic Applications..... | 3 |
| 1.1.2 Biological Applications | 4 |
| 1.1.3 Arene-Ruthenium Complexes..... | 7 |
| 1.1.4 Mononuclear Arene-Ruthenium Complexes as Anticancer Drugs..... | 8 |
| 1.1.5 Multinuclear Arene-Ruthenium Complexes for Anticancer Treatment | 9 |
| 1.2 Host-Guest Chemistry | 12 |
| 1.2.1 Carceplex Systems | 13 |
| 1.2.2 Trojan Horse Concept..... | 14 |
| 1.2.3 Encapsulation of Pyrene-Core Dendrimers and their Biological Properties | 15 |
| 1.3 Aim of the Present Thesis..... | 16 |
| | |
| 2 Hydrogen Bonded Metallo-Assemblies | 19 |
| 2.1 Hydrogen Bonding..... | 21 |
| 2.2 Aim | 29 |
| 2.3 Synthesis | 29 |
| 2.3.1 Synthesis of the Spacer Ligands | 29 |
| 2.3.2 Macromolecular Assemblies..... | 31 |
| 2.4 Characterization..... | 33 |
| 2.4.1 Proton NMR Spectroscopy | 33 |
| 2.4.2 DOSY..... | 36 |
| 2.4.3 NOE/ROE and DFT Calculations..... | 38 |
| 2.4.4 UV-Vis Spectroscopy | 42 |
| 2.4.5 Electrospray Ionization Mass Spectrometry | 45 |
| 2.5 Conclusion | 46 |
| 2.6 Experimental Part | 46 |
| | |
| 3 Encapsulation of Anthracene-Core Dendrimers into Arene-Ru Metallo-Cycles | 69 |
| 3.1 Introduction..... | 71 |
| 3.1.1 Anthracene | 71 |
| 3.1.2 Suzuki Coupling Reaction | 71 |
| 3.1.3 Click Chemistry | 73 |
| 3.1.4 Sonogashira Coupling Reaction..... | 75 |
| 3.2 Aim | 77 |
| 3.3 Synthesis | 77 |
| 3.3.1 Synthesis of Anthracene Compounds | 77 |
| 3.3.2 Carceplex Assemblies..... | 81 |
| 3.4 Characterization..... | 83 |
| 3.4.1 Proton NMR Spectroscopy | 83 |

| | |
|--|------------|
| 3.5 Conclusion | 84 |
| 3.6 Experimental Part | 85 |
| 4 Encapsulation of Pyrene-Core Dendrimers into Arene-Ru Metallo-Cycles..... | 93 |
| 4.1 Introduction..... | 95 |
| 4.2 Aim | 96 |
| 4.3 Synthesis | 96 |
| 4.3.1 Synthesis of Pyrene Dendrimers..... | 96 |
| 4.3.2 Carceplex Assemblies..... | 98 |
| 4.4 Characterization..... | 104 |
| 4.4.1 Proton NMR Spectroscopy | 104 |
| 4.4.2 DOSY..... | 105 |
| 4.4.3 X-Ray Crystallography | 107 |
| 4.4.4 Mesomorphic Properties | 108 |
| 4.5 Conclusion | 113 |
| 4.6 Experimental Part | 114 |
| 5 [60]Fullerene-Ruthenium Complexes..... | 131 |
| 5.1 The [60]Fullerene | 133 |
| 5.2 Aim | 137 |
| 5.3 Synthesis | 137 |
| 5.4 Characterization..... | 140 |
| 5.4.1 Proton NMR Spectroscopy | 140 |
| 5.4.2 UV-Vis Spectroscopy | 141 |
| 5.5 Conclusion | 142 |
| 5.6 Experimental Part | 142 |
| 6 Conclusion and Perspectives | 149 |
| 6.1 Conclusion | 151 |
| 6.2 Perspectives | 152 |
| 7 References | 155 |
| Abbreviations..... | 167 |
| Annex 1..... | 171 |
| Annex 2..... | 177 |
| Annex 3..... | 179 |

Chapter 1: Introduction

1.1 Ruthenium Complexes

1.1.1 Catalytic Applications

Ruthenium, the d-block element that belongs to the “platinum group metals”, is one of the rarest metals on Earth. It is obtained commercially from the wastes of nickel refining. Ru complexes are mostly used as catalysts for several, mechanically diverse, processes. Their ability to assume a vast range of oxidation states (-II to +VIII) and coordination geometries, and the major influence of ligands on the complexes have made Ru complexes very versatile catalysts.^[1] Before the 1980s, a limited number of reactions, such as oxidation with RuO₄ and hydrogenation with ruthenium hydroxide were known.^[2] Since then, the chemistry of Ru has progressed and is better understood, leading to higher scope for Ru catalysts. Thus, their ability of high electron transfer, high Lewis acidity, low redox potentials and their stability have given rise to the development of a large number of new reactions catalysed by Ru complexes, some of which are listed below:^[3]

- Hydrogenation: homogeneous or heterogeneous catalysis of the hydrogenation of substrates, like olefins, with either molecular hydrogen or by hydrogen transfer reactions.
- Oxidation: oxidative transformations of alcohols, amines, amides and hydrocarbons catalysed by low-valent Ru complexes.
- Isomerization: isomerization, like Claisen rearrangement of β,γ -unsaturated oxygen and nitrogen containing compounds catalysed by low-valent Ru complexes.
- Nucleophilic addition: nucleophilic attack on alkynes and nitriles activated by Ru catalysts.
- C-C bond formation: selective C-C bond formation reactions catalysed by low-valent Ru complexes.

Among all these Ru-catalysed reactions, the C-C bond formation, more specifically olefin metathesis, is a powerful method used extensively in organic synthesis. The work on olefin metathesis has been pioneered by Yves Chauvin, Robert H. Grubbs and Richard R. Schrock who were awarded the Nobel Prize in 2005. Ruthenium alkylidenes have been successful catalysts for metathesis transformations, including ring-closing metathesis, cross-metathesis, enyne metathesis and ring-opening metathesis polymerisation (Figure 1.1). Most of these reactions are catalysed by Grubbs 1st and 2nd generation Ru catalysts or Hoveyda-Grubbs Ru catalysts (Figure 1.2).^[4]

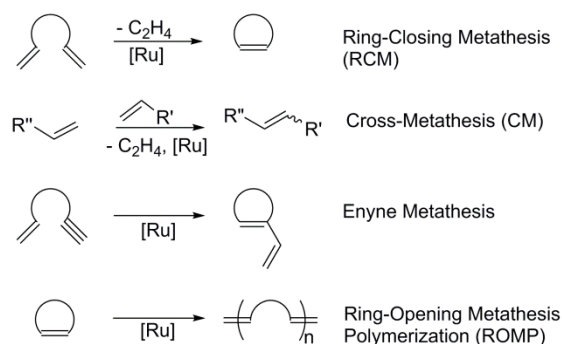
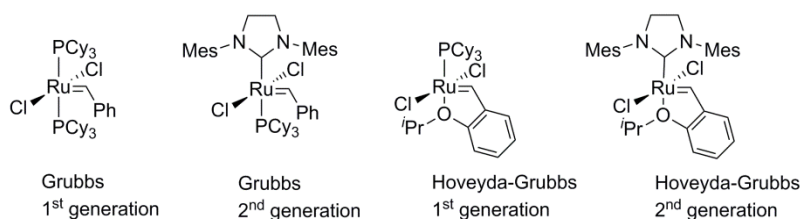


Figure 1.1 Schematic representation of common Ru catalysed metathesis reactions

Figure 1.2 The 1st and 2nd generation of Grubbs and Hoveyda-Grubbs catalysts

Besides the widespread applications of Ru as catalysts, the unique properties of this precious metal have made its complexes to find interesting applications in other fields. For instance, many Ru complexes are being explored for their potential biological activities.^[5]

1.1.2 Biological Applications

Belonging to the same group, ruthenium has mostly been inspired by the well-established chemistry and applications of platinum and its compounds. Just as in the case of catalysis, Ru has followed in the steps of Pt into biological applications. The area of metal-based anticancer drugs has been dominated by the Pt drug, cisplatin and closely related Pt antitumor agents, such as carboplatin and oxaliplatin (Figure 1.3). Since it got FDA (US Food and Drug Administration) approval in 1978, cisplatin has been used extensively in the treatment of several cancers including ovarian and testicular cancers.^[6] Despite its resounding success in treating some cancers, cisplatin has several limitations, among which kidney toxicity, nausea, and bone marrow suppression are a few.^[6c] Hence, the search for a better anticancer drug continues.

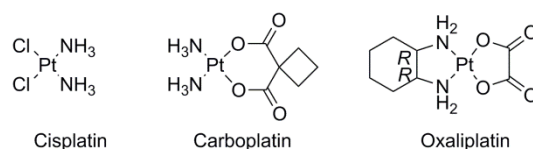
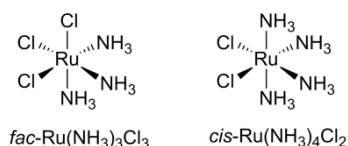


Figure 1.3 Structures of cisplatin, carboplatin and oxaliplatin

The application of platinum compounds in the treatment of cancer questions the ability of other metal complexes to do the same. In fact, metals such as Fe,^[7] Ti,^[8] Ga,^[9] and Ru^[10] have compounds that show interesting medicinal properties. Among these metals, Ru has attracted the attention of several research groups worldwide as complexes of this d^7 metal display ligand exchange kinetics similar to those of platinum complexes.^[11] Ruthenium is being considered as a promising alternative to platinum because it shows many advantages compared to platinum. Ru has more coordination sites, can undergo more changes in oxidation state, is less toxic than Pt and is able to mimic Fe in binding to biomolecules. All these properties have led many researchers to believe that the future of metal-based anticancer drug might be a Ru drug that will show anticancer activity similar to or even better than cisplatin and that can treat a broader range of tumours and with less side effects.^[12]

The idea of using Ru complexes as potential anticancer agent first came to Clarke in 1980 after Durig *et al.* reported, in 1976, the ability of *fac*-Ru(NH₃)₃Cl₃ to induce filamentous growth of *E. Coli* cells in a manner comparable to cisplatin.^[13] Following this discovery, Clarke *et al.* tested the anticancer properties of *fac*-Ru(NH₃)₃Cl₃ and related *cis*-Ru(NH₃)₄Cl₂ (Figure 1.4). Despite their good antitumor activity, the poor solubility of both compounds made them unsuitable for pharmaceutical use.^[14]

Figure 1.4 Structures of *fac*-Ru(NH₃)₃Cl₃ and *cis*-Ru(NH₃)₄Cl₂

This work of Clarke instigated the study of the cytotoxic properties of Ru complexes, eventually resulting in a large number of these compounds that can be categorised according to the ligand type; amine and imine: {*mer*-Ru(tpy)Cl₃, where tpy = 2,2':6',2''-terpyridine^[15] and (HIm)[*trans*-(Im)₂Cl₄Ru],^[16] where Im = imidazole}, polyaminopolycarboxylate: {Cl₂(cdta)Ru,^[17] where cdta = 1,2-cyclohexanediaminetetraacetate and *cis*-Cl₂(pdta)Ru,^[18]

where pdta = 1,2-propylenediaminetetraacetate}, DMSO: *cis*- and *trans*-Cl₂(MeSO)₄Ru^[19] (Figure 1.5).

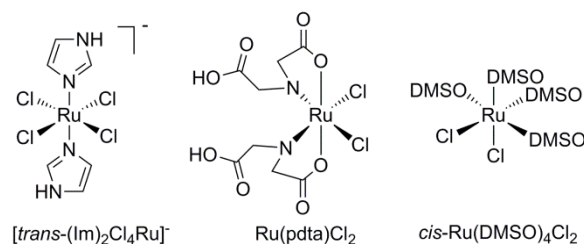


Figure 1.5 Structures of octahedral cytotoxic Ru complexes

From all the biologically active ruthenium complexes, only two entered clinical trials, imidazolium-*trans*-dimethylsulfoxide-imidazole-tetrachlororuthenate (NAMI-A) and imidazolium-*trans*-bis(1H-indazole)-tetrachlororuthenate (KP1019) (Figure 1.6).^[6c, 14, 20] Even though their structures resemble, these two Ru(III) complexes have different modes of action as anticancer drugs. While NAMI-A shows little cytotoxicity towards many cancer cell lines, KP1019 has high antitumoral activity and NAMI-A has pronounced antimetastatic effects (ability to prevent the release of cancer cells from the tumour into other parts of the body) on several cancer models whereas none is shown by KP1019.^[21]

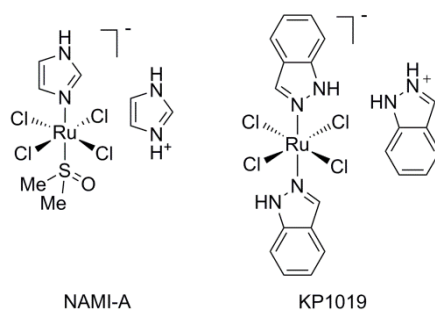


Figure 1.6 Structures of NAMI-A and KP1019

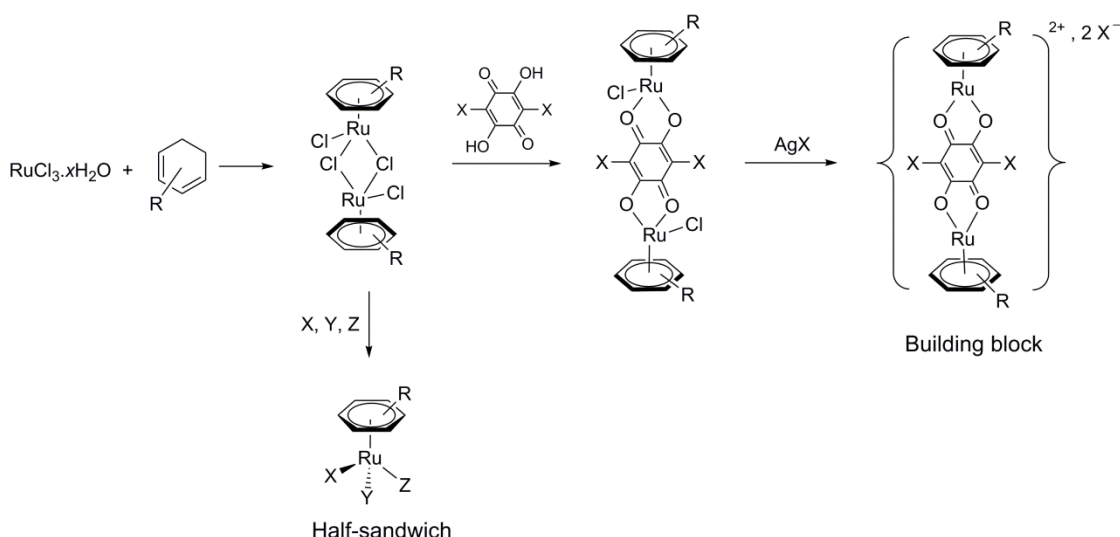
Both Ru(III) complexes have successfully completed Phase I of clinical trial and it has been observed that the reduction of the Ru(III) of NAMI-A to Ru(II), with ascorbic acid prior to administration, gives rise to increased antimetastatic activity. This is in agreement with the hypothesis made earlier by Clarke about “activation by reduction”, whereby the Ru(III) is believed to be reduced to Ru(II) species, the transformation being favoured by the chemically reducing environment created by the low molecular oxygen concentration and lower pH in tumour cells than in healthy ones.^[11b, 14, 22] Ru(II) species, in general, show better binding

ability and hence better reactivity than Ru(III). In view of this, the area of Ru(II) arene complexes is rapidly growing, with the synthesis and evaluation of a series of these compounds for their potential biological activities.^[5, 6c, 23]

1.1.3 Arene-Ruthenium Complexes

Arene is a ligand that commonly binds to a metal through more than two atoms. η^6 -Arene, whereby the ligand gives three electron pairs to the metal, tends to maintain its planar structure after coordination to the metal. For these ligands, a mixture of π -bonding (co-axial bonding from the p orbitals of the ligand to the vacant d orbitals of the metal) and back π -bonding (lateral bonding from filled d orbitals of the metal to the π^* antibonding p orbitals of the ligand) helps to generate stable complexes. This and its strong π -acceptor behaviour has made arene one of the mostly used ligands in Ru(II) chemistry.^[6c, 12, 23-24]

Hence, since the discovery of the first dinuclear chloride-bridged arene complexes $[(\eta^6\text{-arene})\text{Ru}(\mu_2\text{-Cl})\text{Cl}]_2$ by Winkhaus and Singer in 1967, this area of Ru chemistry has undergone exponential expansion. These dimers, which can be easily synthesised from $\text{RuCl}_3 \cdot x\text{H}_2\text{O}$ starting material, show very good stability under atmospheric conditions and hence do not require special storage. They also show good solubility in common organic solvents as well as in water. This very important amphiphilic property of the arene-Ru unit comes from the hydrophobic nature of the arene ligand combined with the hydrophilicity of the metal centre. Moreover, the chloride ligands on the dimers undergo facile replacement with other ligands, while the arene remains intact, due to the robust Ru-arene bond (Scheme 1.1). All these properties make them popular building blocks for metallo-assemblies.^[1] The arene also plays the crucial role of protecting the metal against oxidation to Ru(III). Among the many different assemblies, arene-ruthenium metallo-cages are under intensive investigation. Their adaptable cavity and their host-guest properties make these arene-Ru metallo-cages versatile drug-delivery systems.^[23c, 24c] In our group, a wide range of η^6 -arene ligands have been used to coordinate to Ru(II), such as benzene, hexamethylbenzene, p -cymene and other functionalised arenes.^[6c, 23]



Scheme 1.1 The synthesis of arene-Ru building blocks

1.1.4 Mononuclear Arene-Ruthenium Complexes as Anticancer Drugs

A large number of mononuclear Ru complexes have been synthesised and evaluated for their antitumor activity after the entrance of NAMI-A and KP1019 into clinical trial. Furthermore, with the discovery of the higher activity of Ru(II) compared to Ru(III), research has been growing in the Ru(II) chemistry. As seen from the previous section, arene is found to be a crucial ligand for many reasons, one of which being the stability of the Ru(II) species. Also, the facile cleavage of the chloride bridges allows for the synthesis of a series of half-sandwich arene-Ru complexes, which in turn allows multiple anchoring possibilities to introduce biologically active groups to the three coordination sites.

Recently, two classes of ruthenium anticancer agents have been developed, centred on arene-Ru compounds (Figure 1.7). The first class, developed by Sadler, consists of an arene-Ru with a chelating ethylenediamine ligand (en) and a chloride occupying the three remaining coordination sites, $[(\eta^6\text{-arene})\text{Ru}(\text{en})\text{Cl}]^+$ (Figure 1.7(a)).^[24g] It is water soluble and shows activity against A2780 human ovarian cancer cells *in vitro* and *in vivo*. Its cytotoxicity against primary tumours was found to be similar to anticancer agent carboplatin and it shows better activity than cisplatin.^[12]

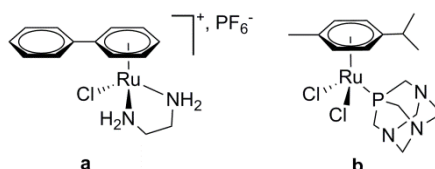


Figure 1.7 The two half-sandwich mononuclear arene-Ru complexes, (a) $[(\eta^6\text{-biphenyl})\text{Ru}(\text{en})\text{Cl}]^+ \text{PF}_6^-$ and (b) RAPTA-C

The second class comprises of the ruthenium arene pta (pta = 1,3,5-triaza-7-phosphaadamantane), RAPTA agents developed by Dyson. The RAPTA complexes are a family of Ru(II) compounds with monodentate pta ligand and a η^6 -arene ligand. The synthesis is very simple, leading to mononuclear arene-Ru complexes that are stable under physiological environment.^[25] RAPTA-C, the most popular member of the RAPTA family, displays antimetastatic activity *in vivo* and is able to selectively target cancer cell lines (Figure 1.7(b)). It has a relatively lower activity than cisplatin, but it exhibits selective cytotoxicity towards TS/A (a metastasizing mouse cell line) cancer cell lines *in vivo*, with the pta ligand playing a crucial role in determining the selectivity.^[26]

1.1.5 Multinuclear Arene-Ruthenium Complexes for Anticancer Treatment

Inspired by the higher cytotoxicity shown by the trinuclear platinum complex, [*trans, trans, trans*-(NH_3)₂ $\text{NH}_2\text{Pt}(\text{Cl})(\text{CH}_2)_6\text{NH}_2\text{Pt}(\text{NH}_3)_2\text{NH}_2(\text{CH}_2)_6\text{NH}_2\text{Pt}(\text{NH}_3)_2(\text{Cl})$][NO_3]₄,^[27] researchers started exploring the possibility of having better anticancer activities from multinuclear complexes.^[28] Mendoza-Ferri *et al.* reported the structure-activity relationships of dinuclear pyridinone-derived arene-Ru complexes (Figure 1.8(a)). *In vitro* studies show the antiproliferative activity, determined against the human cancer cell lines SW480 (colon) and A2780 (ovary), to be similar to oxaliplatin in SW480 and better cytotoxicity than cisplatin in A2780.^[29] Inspired by these results, other groups started research in this area, one of which is the diruthenium complex, $[(\text{Ru}(\text{tpy})\text{Cl})_2(\mu\text{-bb}_n)]^{2+}$ (tpy = 2,2':6',2''-terpyridine and bb_n = bis[4(4'-methyl-2,2'-bipyridyl)]⁻¹ (Figure 1.8(b)). For the complex $n = 12$, higher activity compared to cisplatin was observed against two breast cancer cell lines.^[30]

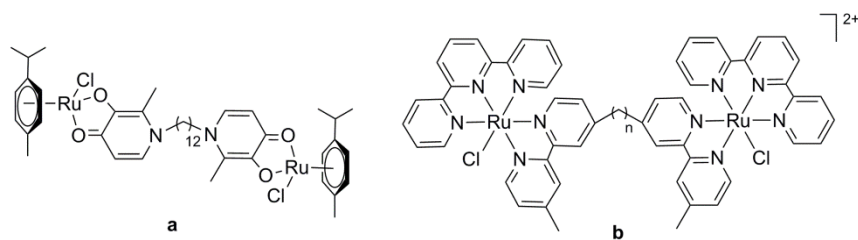


Figure 1.8 Dinuclear Ru complexes, (a) pyridinone-derived arene-Ru complex and (b) $[(\text{Ru}(\text{tpy})\text{Cl})_2(\mu\text{-bb}_n)]^{2+}$

The chemistry of multinuclear complexes does not stop at dinuclear compounds. Numerous molecular assemblies, tetra-, hexa-, octanuclear Ru complexes have been produced by combining two different strategies developed by Stang and Fujita who work on “molecular clip”^[31] and “molecular panelling”^[32] respectively. These two strategies constitute a very important part in modern supramolecular chemistry. With controlled architecture of the shape and size of the complex, a variety of coordination-driven self-assembled 2D and 3D supramolecular ensembles have been built. The desired frameworks can be obtained by the choice of appropriate building blocks. Hence, if the precursor units of rigid structures with predefined bite angles are combined in the appropriate stoichiometric ratio, the desired arrangement is formed. A panorama of spatially and electronically tunable supramolecular arrangements now exists and some have found applications in the biomedical field. For instance, a cationic hexanuclear metallo-prism is formed from arene-Ru building blocks with $OO \cap OO$ bridges and triazine trigonal panels (or spacer ligands); these complexes show anticancer properties (Figure 1.9).^[33]

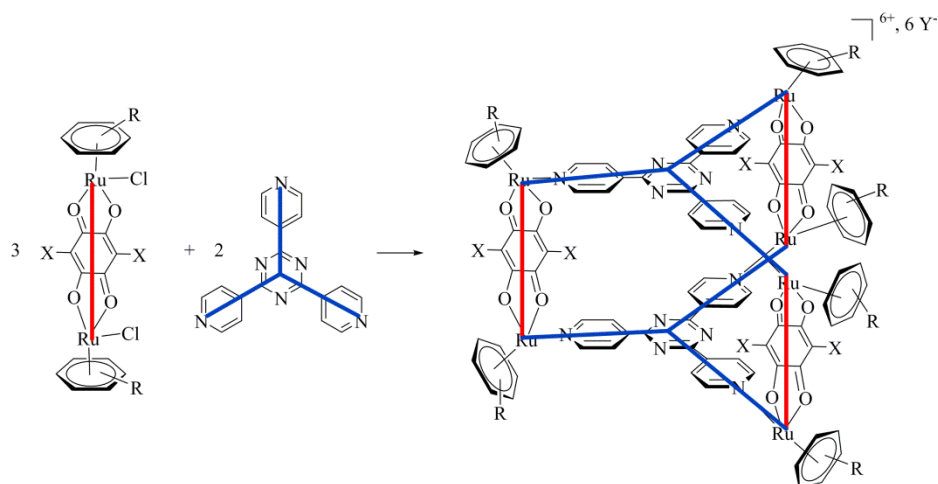
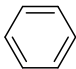
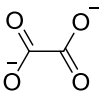
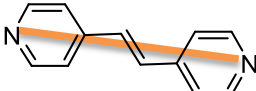

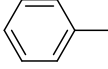
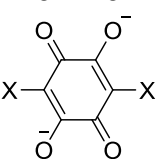
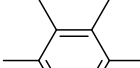
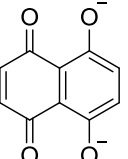
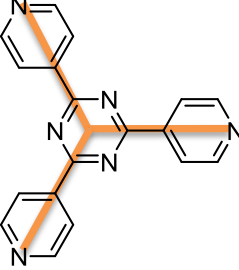
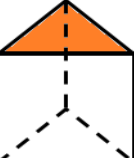
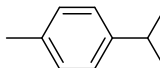
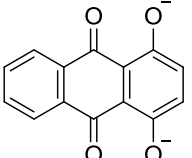
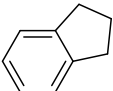
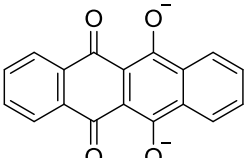
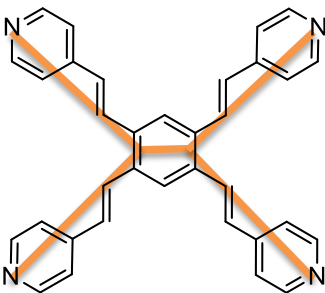
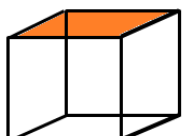
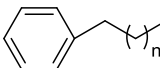
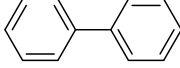
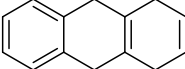


Figure 1.9 Supramolecular assembly of a metallo-prism

Among the many research groups whose work was inspired by this supramolecular chemistry, our group has reported the synthesis of a wide range of multinuclear arene-ruthenium complexes in the form of metallo-cages.^[23b] These cages are supramolecular arrangements bearing a cavity formed during the assembly of the different subunits. Changing the Ru clips and the spacer ligands changes the shape and size of the cavity. Generally, the spacer ligand is the one that determines the geometry of the metallo-assembly, giving rise to the formation of cages in the shape of rectangles, prisms and cubes (Table 1.1). There are some cases where the clip has an as important role to play in the architecture of the assembly as the spacer ligand. For instance, two complexes of platinum and palladium have been reported recently, consisting of π -extended tetrathiafulvalene ligand with four pyridyl units that bind to the metal centres, each metal coordinated to a (diphenylphosphino)ferrocene unit.^[34] These octacationic self-assembled complexes possess an ovoid internal cavity, which is different from the common cubic or cuboid formed by tetradentate spacer ligands (Figure 1.10).

Table 1.1 The different clips and spacer ligands and examples of the geometries they give

| Ru Clips | | Spacer ligand N \cap N | Geometry of assembly |
|---|---|--|---|
| Arene | OO \cap OO | | |
|  |  |  |  |
|  |  | | |
|  |  |  |  |
|  |  | | |
|  |  |  |  |
|  | | | |
|  | | | |
|  | | | |

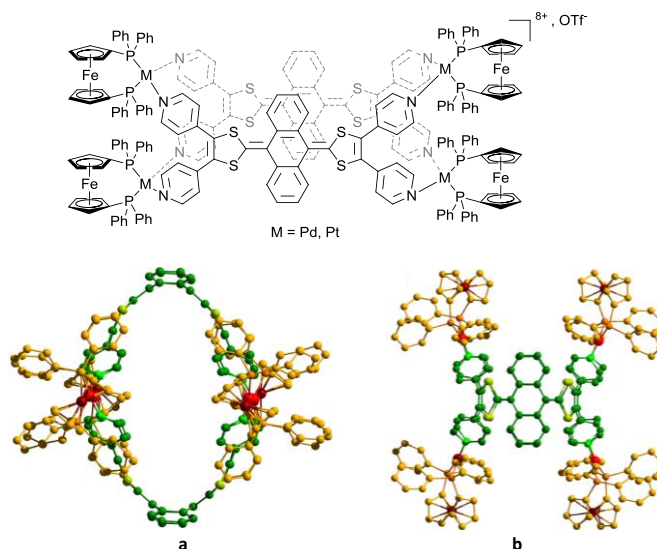


Figure 1.10 The X-ray crystal structures of the Pd complex (a) lateral view and (b) top view^[34]

1.2 Host-Guest Chemistry

The term “Host-Guest Chemistry” was coined by Cram in 1974, to describe the “complexation and decomplexation” happening during an enzymatic reaction during which molecular recognition is of utmost importance for the substrate-enzyme systems.^[35] In 1967, Pedersen reported the binding of metal ions with crown ethers to give highly structured complexes.^[36] Two years later, Lehn, Sauvage and Dietrich published their work on cryptands that involved the study of the binding properties of these molecules.^[37] The basic principle behind this chemistry is the size compatibility between the host and the guest. Also, the complementary binding forces, which are weak non-covalent interactions like van der Waals, eventually leading to the assembly of the host and the guest are crucial.^[35a] In 1987, Donald J. Cram, Jean-Marie Lehn and Charles J. Pedersen were awarded the Noble Prize for their work on this concept, which has found widespread applications. The term host-guest chemistry is well defined in the following citation by Cram:^[35a]

“... a host-guest relationship involves a complementary stereoelectronic arrangement of binding sites in host and guest... the host component is defined as an organic molecule or ion whose binding sites converge in the complex... the guest component is defined as any molecule or ion whose binding sites diverge in the complex...”

Thus, the host possesses convergent binding sites while the guest has divergent ones. The interactions existing in the host-guest system are important in determining the stability of the

assembly. These interactions can be hydrophobic, H-bonding, π - π aromatic interactions and ion-ion and dipole interactions. Apart from the selective binding affinity between the host and the guest, the two components need to have complementary geometric size/shape according to the lock and key principle.

In order to get a better understanding of how the host-guest strategy works, thermodynamic experiments, like isothermal titration calorimetry, were performed. Results from the experiments between guest molecules and the cavity confirmed that depending on the type of interaction happening inside the cavity, the encapsulation will be either entropy- or enthalpy-driven. Since entropy changes occur mostly when there is desolvation or a change in conformation, the host-guest systems, in general, are most likely to be enthalpy-driven. Thus, the π - π and C-H- π interactions between the guest molecule and the inner surface of the cavity give rise to enthalpic combination. Therefore, encapsulation is mainly enthalpy-driven, with probably some favourable entropic changes in terms of loss of solvent molecules surrounding the guest during encapsulation.^[38]

Chemists have designed a large array of host-guest systems ranging from crown ethers to cyclodextrins to calixarenes, capable of hosting guest molecules or ions based on complementary/attractive forces between the two species. Host-guest chemistry is now applied in many areas including catalysis, sensors and pharmaceuticals. Host-guest systems have become a very popular method of drug-delivery in recent years and are believed to give rise to improvement in efficiency and biocompatibility.^[23b] Researchers have even encapsulated cisplatin in order to reduce the severe side effects of the drug.^[39] Thus, the arene-ruthenium arrangements allow the encapsulation of organic molecules of sizes that can fit in the cavity. The guest, usually a planar aromatic compound, is held by π -stacking to the spacer ligand of the host. A series of these complexes have been tested for their medicinal properties and interesting results have been obtained, comparable to cisplatin.^[40]

1.2.1 Carceplex Systems

For small aromatic molecules that need to be encapsulated, the concept of host-guest has worked very well, allowing the guest molecule to enter and exit the cavity without disruption of the host molecule (Figure 1.11(a)). But in the case of highly branched aromatic molecules that can fit in the cavity, the movement in and out of the cage is restricted as the passage is not large enough.^[41] In such instances, carceplex systems are used, whereby the guest molecule

gets trapped permanently as the host is assembled around it (Figure 1.11**(b)**). The driving force for the incarceration is the interaction between the guest molecule and the interior of the forming shell.^[42] With the portal size being too small, the guest molecule can only be liberated *via* rupture of the cage. It is also possible for several molecules to be imprisoned inside the cavity that is big enough to accommodate the guests.^[43] Besides its growing use in drug-delivery, carceplex systems are being applied in other areas, for instance, it is being employed as stabilizers for highly reactive species.^[43b]

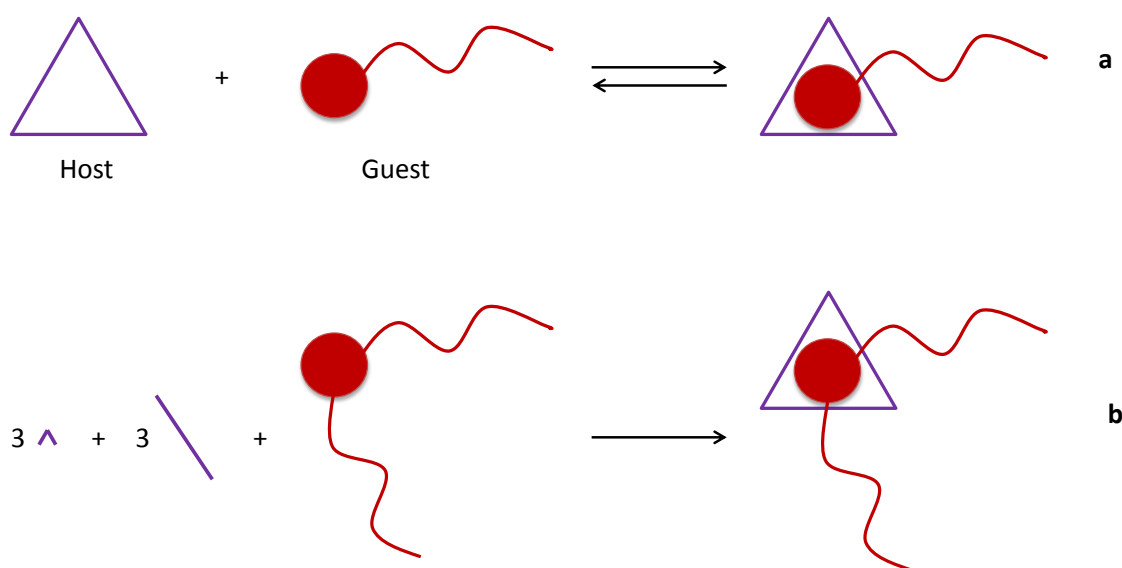


Figure 1.11 Schematic representation of encapsulation of a guest molecule by the (a) host-guest and (b) carceplex methods

1.2.2 Trojan Horse Concept

Drug-delivery strategies are engineered technologies that allow controlled release of drugs into targeted cells. This system has helped in avoiding many side effects associated with unwanted interactions of the drug with parts of the body that are not targeted. Trojan-Horse is a common way of referring to drug-delivery based on the strategy of transporting potential drugs, which are not water-soluble, inside the hydrophobic cavity of a cage with hydrophilic exterior and releasing the drug in the target cells. Drug-delivery employing Trojan-Horse concept can be advantageous compared to other modes used. Some of the advantages can be the higher local drug concentration and improved therapeutic efficacy.^[44] From the various types of Trojan-Horse published, the horse was found to adopt different forms such as liposomes, engineered viruses,^[45] nanotubes^[46] and supramolecular assemblies.^[23d, 47]

Introduced by our group, the supramolecular assemblies have been used to encapsulate drugs into the hydrophobic cavity of the metallo-assembly, with two main objectives: (1) transportation of mostly hydrophobic drug and (2) release of the treatment inside the targeted cancer cells.^[47a] The first supramolecular Trojan Horse system involved the encapsulation of non-water soluble $M(\text{acac})_2$ complexes into water-soluble hexanuclear arene-ruthenium prism *via* carceplex assembly until its release in the cancer cells (Figure 1.12). This “complex-in-a-complex” assembly was confirmed by X-ray crystallography, which demonstrates the bending of the plane of the triazine ligands due to strong interactions with the guest complex.

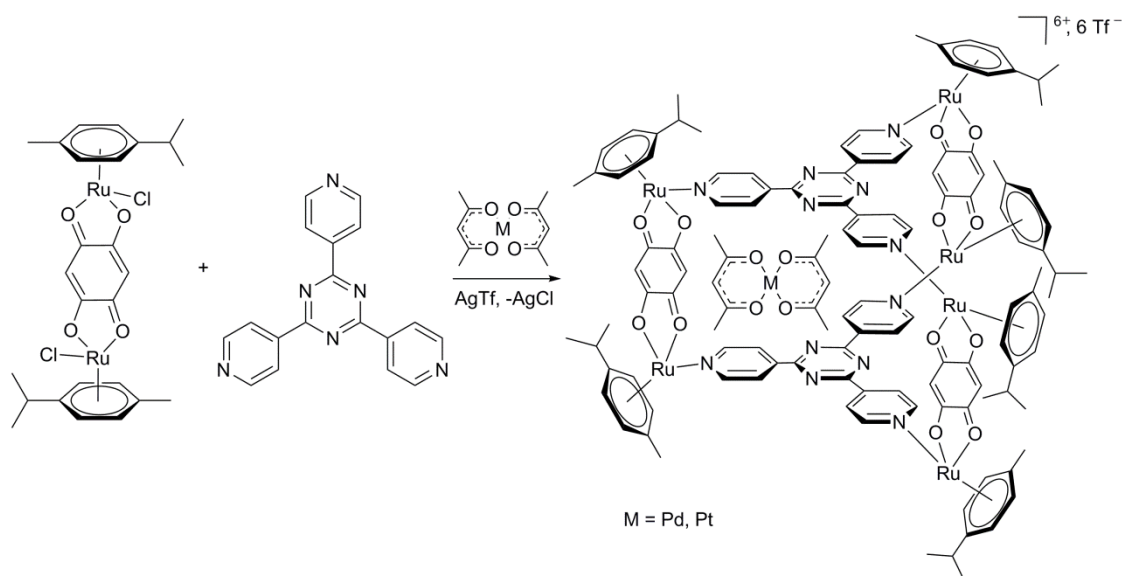


Figure 1.12 Encapsulation of $M(\text{acac})_2$ into supramolecular Trojan Horse

1.2.3 Encapsulation of Pyrene-Core Dendrimers and their Biological Properties

In our group, a series of successful arene-Ru assemblies showing interesting anticancer properties have been developed. One such example is a family of pyrene-core dendrimers encapsulated in tetra- and hexanuclear arene-Ru complexes with the pyrene-core inside the hydrophobic cavity of the cage and the dendritic arm left dangling out (Figures 1.13, 1.14). This system was found to exhibit enhanced cytotoxicity compared to either the host or the guest alone. The IC_{50} values (the half maximal inhibitory concentration that indicates how much of a particular drug is needed to inhibit a given biological process by half) of these systems were comparable to those of cisplatin when evaluated against human ovarian A2780 (cisplatin sensitive) and A2780cisR (acquired resistance to cisplatin) cancer cell lines.^[48]

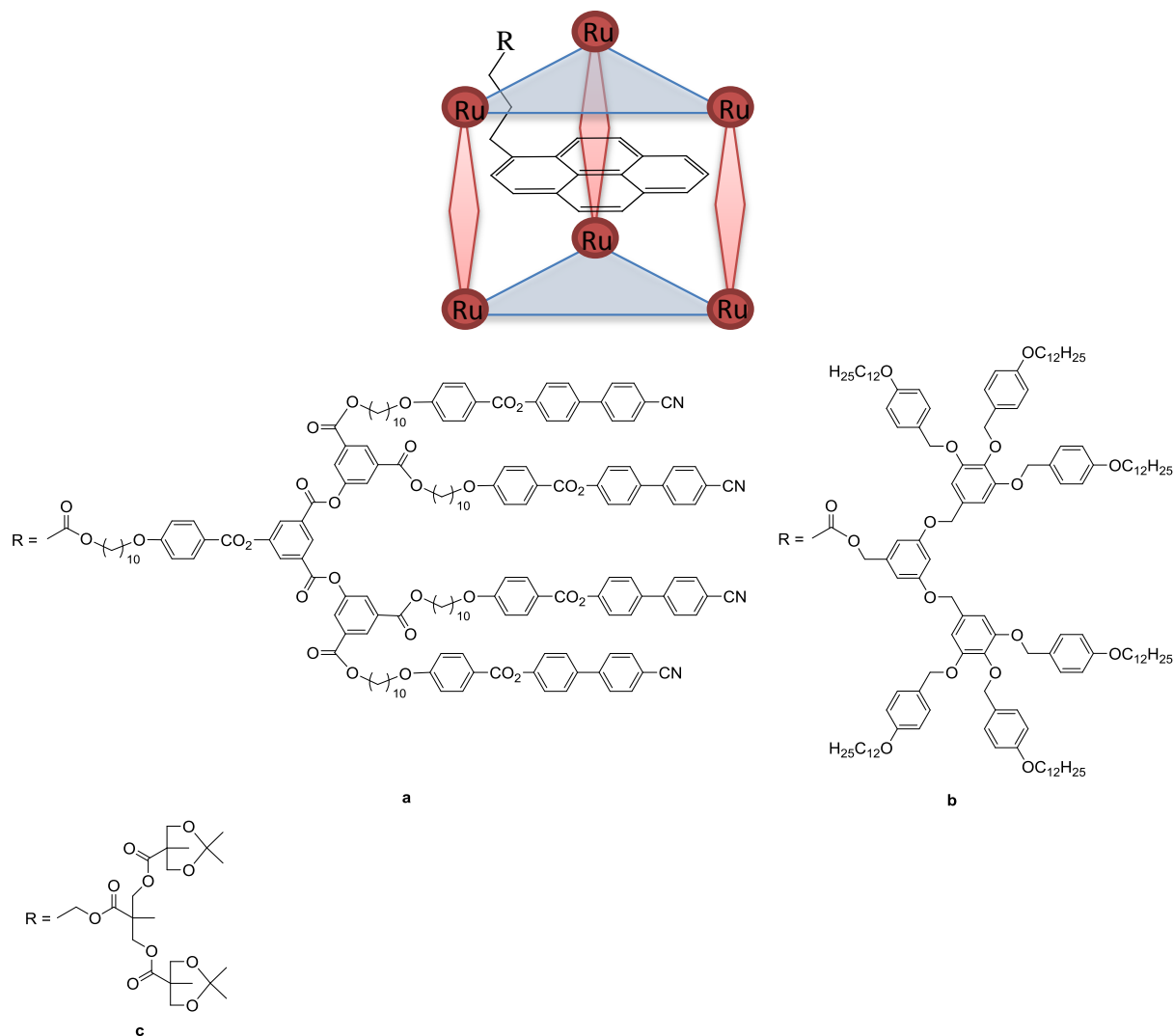


Figure 1.13 Encapsulation in a hexanuclear metallo-cage of dendrimers of second generation: (a) poly(arylester), (b) poly(benzylether) and (c) polyester

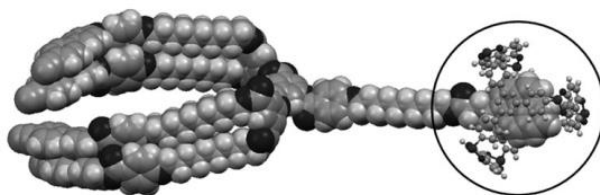


Figure 1.14 HyperChem simulation of the structure of the encapsulation of the poly(arylester) dendrimer of second generation into a hexanuclear Ru prism

1.3 Aim of the Present Thesis

The work done by Anaís Pitto-Barry during her thesis has shown that dendrimers displaying liquid-crystalline properties could be successfully encapsulated into arene-Ru metallo-cages

by host-guest chemistry.^[48] Moreover, these macromolecular assemblies show biological activities against human ovarian cancer cells. This thesis work is a continuation of the project initiated by Anaïs Pitto-Barry, consisting of the synthesis and the study of liquid-crystalline dendrimers in combination with arene-Ru metallo-cages as potential anticancer drugs and as hybrid liquid-crystalline materials.

So far, only monosubstituted pyrene-core dendrimers have been tested for their biological activities, alone and encapsulated. Therefore, the goal of this work was to synthesise new aromatic-core dendrimers possessing two dendritic chains that have liquid-crystalline properties and to encapsulate them into arene-Ru metallo-cages in order to determine any possible biological activities they might display inside cancer cells. Moreover, studying the liquid-crystalline property of the host-guest systems was also envisaged.

Furthermore, there were two other objectives for this work. One was to use a different approach in assembling the supramolecular cages other than the coordination-driven method; hence, self-assembly of arene-Ru cages by H-bonding was tested. The description of new and larger spacer ligands and the syntheses of the corresponding half-sandwich complexes and metallo-rectangles have been studied. The properties of these new metallo-assemblies as host-guest as well as carceplex systems have been evaluated. The other aim involved the association of arene-Ru units with [60]fullerene. Half-sandwich mononuclear [60]fullerene-based arene-Ru complexes were thus synthesised for their potential biological activities. The introduction for these two topics, hydrogen bonding self-assembly and [60]fullerene, will be done in the corresponding chapters.

Chapter 2: Hydrogen Bonded Metallo-Assemblies

2.1 Hydrogen Bonding

When hydrogen is bonded to electronegative atoms, such as N, O and F, the covalently bonded electron pair is pulled strongly to the nucleus of the electronegative atom, leaving a partial positive charge on the hydrogen atom and a partial negative charge on the electronegative atom. The partial positive charge allows the hydrogen to attract negatively charged species, an anion or a lone pair of electrons. This dipole-dipole attraction between the H atom, covalently bonded to an electronegative atom, and another electronegative atom is called hydrogen bonding. Hence, the IUPAC definition of hydrogen bonding is the “association between an electronegative atom and a hydrogen atom attached to a second, relatively electronegative atom”. The terms “donor” and “acceptor” are commonly used when dealing with hydrogen bonding: the donor (D) is the electronegative atom (X) to which the H atom is covalently bonded and the acceptor (A) is the neighbouring electronegative atom (Y) that possesses the negative charge or lone pair of electrons (Figure 2.1).^[49]

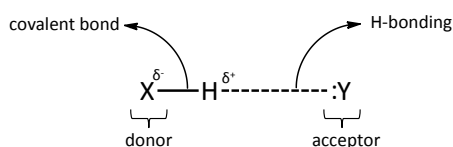


Figure 2.1 Schematic representation of a H-bonded system

The strength of H-bond is intermediate between that of dipole forces between molecules and covalent bonds within a molecule. The H-bond is about 1/10 as strong as covalent bonds. Nevertheless, multiple H-bonds between two molecules result in a union that displays sufficient strength and good stability.

There have not been any Nobel Prize winners for the discovery of H-bonding because since the realization of its significance in the early 1900s, many important researchers have been working on and contributed to the understanding of this complex concept, among whom were Werner, Huggins, Rodebush and Pauling.^[50] Hydrogen bond is still today a growing area of research due to its enormous importance. One example of the role of H-bonding is water (Figure 2.2). Each water molecule can potentially form four intermolecular hydrogen bonds with neighbouring water molecules. Compared to other binary compounds formed between hydrogen and elements of group 6, like H₂S, where H-bonding is absent, H₂O has the highest boiling point, despite its smaller molar mass. Also, compared to other larger molar mass

molecules where H-bonding is present, like HF, the boiling point of H₂O is still higher as it partakes in more hydrogen bonds per molecule. Hence, H-bonding can account for the unique properties of water (Figure 2.2).^[51]

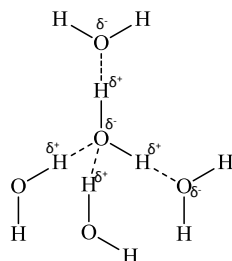


Figure 2.2 Hydrogen bonding in water

H-bonding has a very important role to play in the structure and function of several biological systems, like DNA. The double strands in DNA are held together by hydrogen bonds between the H atoms attached to N on one strand and lone pairs on another N or an O on the other strand. The H-bonding between the complementary nucleotide Watson-Crick base pairs and π -stacking interactions give rise to the stable double helical structure of DNA. Two H-bonds occur between the adenosine and the thymine base pairs and triple hydrogen bonds exist between the cytosine and the guanine (Figure 2.3(a)). Furthermore, the construction of polypeptides uses extensively H-bonds between N-H and C=O groups. Intra- and inter-chain H-bonding interactions in α -helices and β -sheets, respectively, establish the secondary structure of proteins (Figure 2.3(b)).^[49]

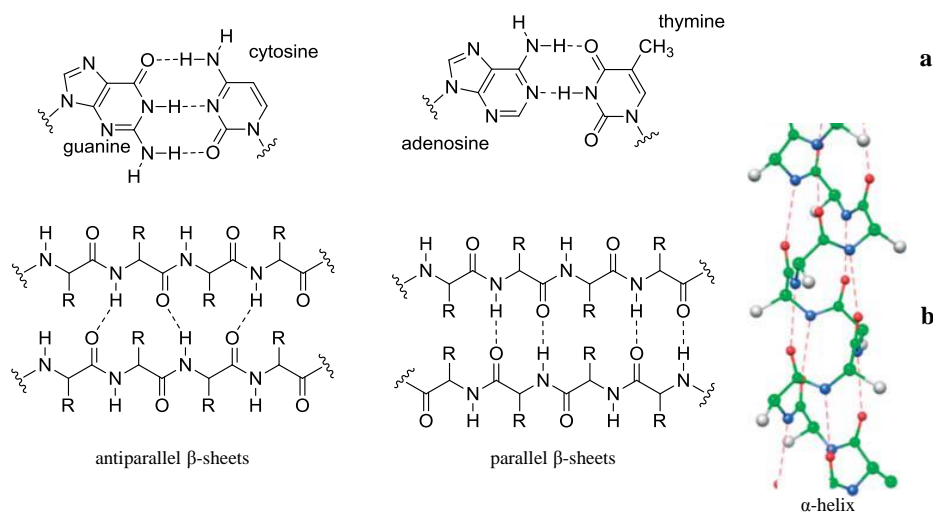


Figure 2.3 Hydrogen bonding between base pairs (a) and peptides (b)

Supramolecular chemistry, as defined by Nobel Prize winners Lehn, Cram and Pedersen, is the “chemistry beyond the molecule”, and two fundamental features of this discipline are molecular recognition and self-assembly. Non-covalent interactions are used for the synthesis of supramolecules, enabling preparation of these complex assemblies from simple fragments, which may sometimes be difficult by covalent interactions. Hydrogen bonding is one of the preferred types of non-covalent interactions in supramolecular chemistry because H-bonded mediated self-assembly has been shown to be a good strategy for creating well-defined supramolecular architectures. Its directionality, stability, reversibility and specificity constitute some of the features that make H-bonding so versatile compared to other non-covalent interactions.^[52] Appropriate choice of donor/acceptor pairs makes it possible for H-bonding to be directional and to have tunable strengths. Hence, H-bonds can be classified as follows:

- Strong H-bonds: formed between charged species and have bond strengths in the range 15-40 kcal·mol⁻¹ and have the shortest bond lengths.
- Moderate H-bonds: are mostly electrostatic interactions found in biomolecules with bond strengths in the order 4-15 kcal·mol⁻¹ with moderate bond lengths.
- Weak H-bonds: formed between an electronegative species and a significantly less electronegative complement of bond strengths less than 4 kcal·mol⁻¹ and have the longest bond lengths.

Based on the several biological examples where H-bonding exists, researchers have been inspired to build synthetic systems with H-bonding to benefit from its unique properties. The careful selection of acceptor/donor pairs is able to give the desired strength and stability of each hydrogen bond as well as the number and arrangement of the hydrogen bonds in the system. Similar to the base pairing in DNA, the well-defined through-space directionality and hence high selectivity of H-bonds have been used by many researchers. Thus, many examples of supramolecular assemblies involving H-bonding interactions have been reported in different fields of chemistry, especially in organic and polymer chemistry.^[52a, 53]

Studies have shown that H-bonds could be made stronger and/or more selective by introducing arrays of donors (D) and acceptors (A) sites. These H-bonded systems are built by the use of parallel arrays of H-bonds and they feature two or more contiguous H-bonds on a heterocyclic scaffold. Units consisting of up to six consecutive H-bonds have been reported, but those of the triple and quadruple units are the most studied derivatives in molecular

recognition and self-assembly processes. It was found that the arrangement of the D and A sites, as well as the solvent in which the complexes are formed are determining factors for the strength of the H-bonds, called the association constant (K_a) or dimerization constant (K_{dim}) in case of homodimers.^[52c]

For triple H-bonded complexes, the general trend in their stability is as follows:



The DDD-AAA arrangement was found to have the highest association constant ($K_a = 10^5$ - 10^6 M^{-1}) and ADA-DAD pair the lowest ($K_a = 10^2$ - 10^3 M^{-1}).^[54] With the same primary H-bonding interactions between the D/A pairs, the difference in K_a can only be the result of another type of interaction. Hence, Jorgensen rationalised these differences as the impact of the secondary electrostatic interactions on the stability of H-bonding arrays.^[55] Since the D/A partners are in close proximity, due to the H-bonding between them, this gives rise to substantial electrostatic interactions. The partial positive charges on the protons and the partial negative charges on the electronegative atoms result in attractive forces between opposite charges and repulsive forces between like charges. The net of the secondary interactions can therefore account for the stronger/weaker binding, depending on the arrangement of the D/A sites in the molecules. Hence, parallel H-bond arrays, having all the H-bond donor groups in one partner and the acceptor sites in the other in an AAA-DDD arrangement seems to result in the strongest association with all secondary electrostatic interactions between neighbouring H-bond pairs being attractive.^[52c]

Among the many triple H-bonding modes, the H-bonded melamine-cyanuric acid motif with a ADA-DAD array has been one of the most widely used in the formation of the so-called “rosette” supramolecular structures. In this system, a single rosette constitutes of a cyclic aggregate of three melamine and three cyanuric acid units. The lattice formed in organic solution shows very good stability arising from nine hydrogen bonds surrounding each melamine or cyanuric acid molecule (Figure 2.4).^[56] Based on this arrangement, a series of macromolecules have been developed using melamine and cyanuric acid derivatives. Two strategies were adopted in designing these rosette structures: preorganization and peripheral crowding, favouring the formation of 1:1 cyclic aggregates.^[56-57]

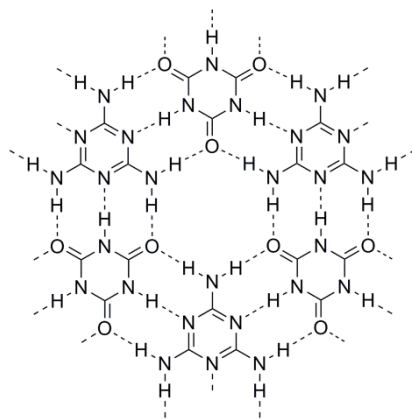
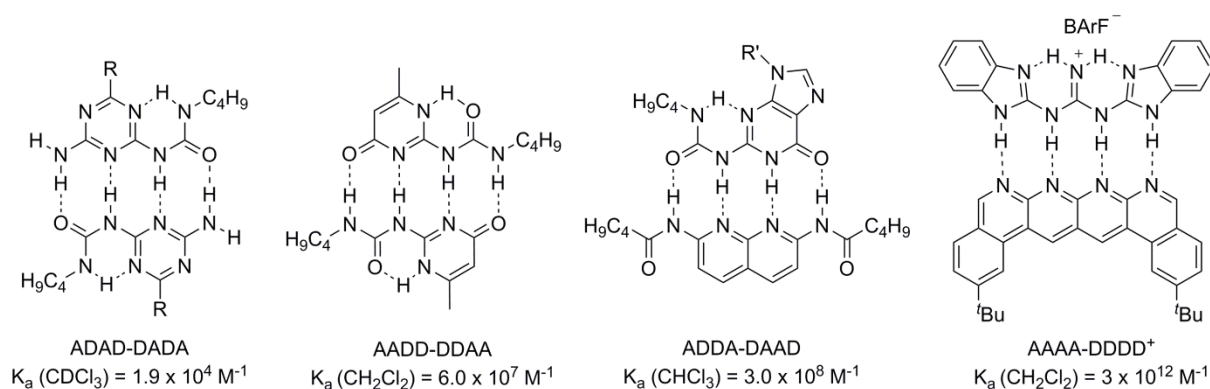


Figure 2.4 Melamine and cyanuric acid rosette structure

Four H-bonding systems have also attracted the attention of many research groups, as a result of which a vast series of quadruple H-bond complexes have been synthesised. Out of the six possible H-bond permutations, only three have been extensively studied: ADAD-DADA, AADD-DDAA, ADDA-DAAD (Figure 2.5).^[52c, 58] The AAAA-DDDD array is not much explored and even though these complexes with four consecutive H-bond donors and acceptors show the highest stability ($K_a > 10^{12} \text{ M}^{-1}$), similar to triple systems, their application is not so popular. One example of an AAAA-DDDD quadruple H-bond array is the highly stable cationic complex formed by the equimolar assembly between guanidinium dibenzimidazole and diisoquinoline-[1,8]-naphthyridine (Figure 2.5).^[58c]

Figure 2.5 Examples of quadruple H-bond arrays and their K_a values

Many different scaffolds have been used in designing and building up quadruple H-bonding self-assembled systems, and the most popular one is probably the 2-ureido-4-[1H]-pyrimidinone (UPy). Upy dimers, with a DDAA H-bond array, have high dimerization constants ($K_{\text{dim}} > 10^7 \text{ M}^{-1}$) and they can be readily synthesised.^[61f] The high dimerization constant of UPy arises from the limited repulsive secondary interactions and two attractive

secondary interactions within the motif, as well as the intramolecular H-bond that creates order within the molecule by prearrangement of the motif.^[59] UPy unit can also associate with other units to form heterocomplexes that are stable with high association constants. Thus, Meijer and co-workers have developed a series of UPy derivatives.^[60] UPy consisting of a linear four H-bond DDAA-AADD array has been used as building block for the construction of various assemblies. Inspired by this unit, numerous derivatives of UPy have been used as DDAA modules, with varying dimerization constants (Figure 2.6).^[52b, 52d, 53c, 61]

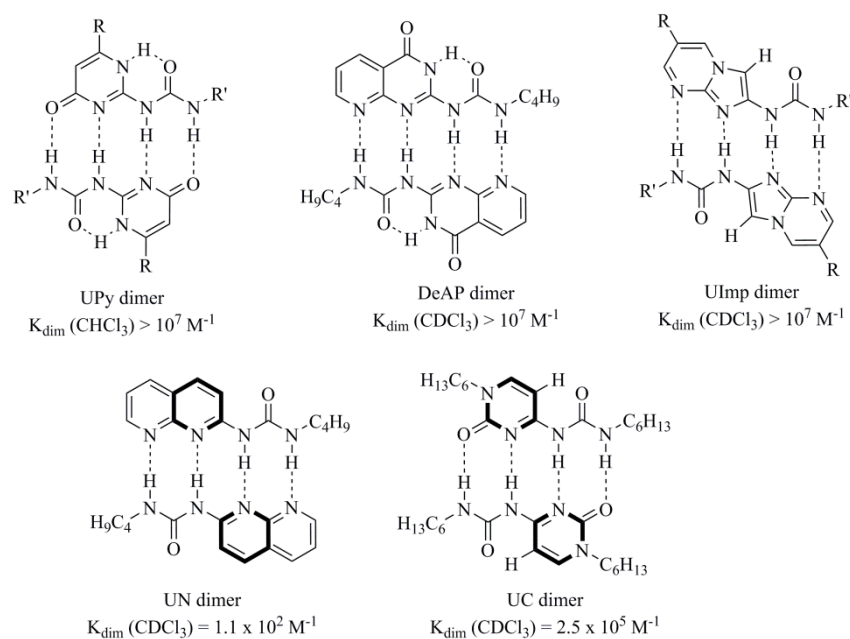


Figure 2.6 Homodimer structures of DDAA-AADD array modules, UPy, DeAP, UN and UC

Developed by Zimmerman and co-workers in the late 1990s, ureidodeazapterin (DeAP) shows very high stability (Figure 2.6). Three major DDAA-AADD dimers are present in the DeAP systems: two homodimers, X.X and Y.Y (arising from the two possible tautomers) and one heterodimer X.Y. Some undesired DADA-ADAD homodimers, Z.Z, are also detected in small amount (Figure 2.7).^[53c]

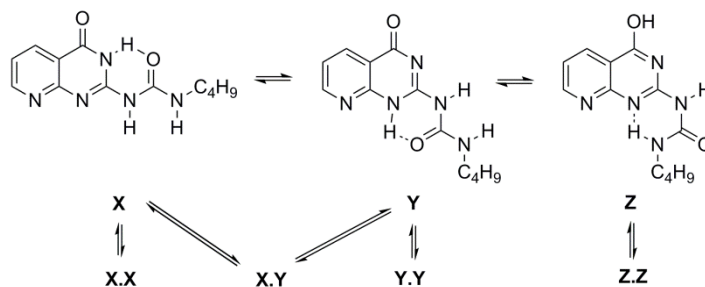


Figure 2.7 The different protomeric forms of the AADD H-bonding array of DeAP

A few years later, the same group developed a ureidodeazapterin-based module, linking two DeAP units with a semi-rigid spacer bearing a Fréchet-type dendron (of first, second and third generation) attached to it. This molecule exists as two tautomers, with a DDAADDAA H-bond array in both forms. The two different conformations, symmetrical and non-symmetrical, give rise to different aggregates, polymeric and cyclic, respectively (Figure 2.8).^[52a]

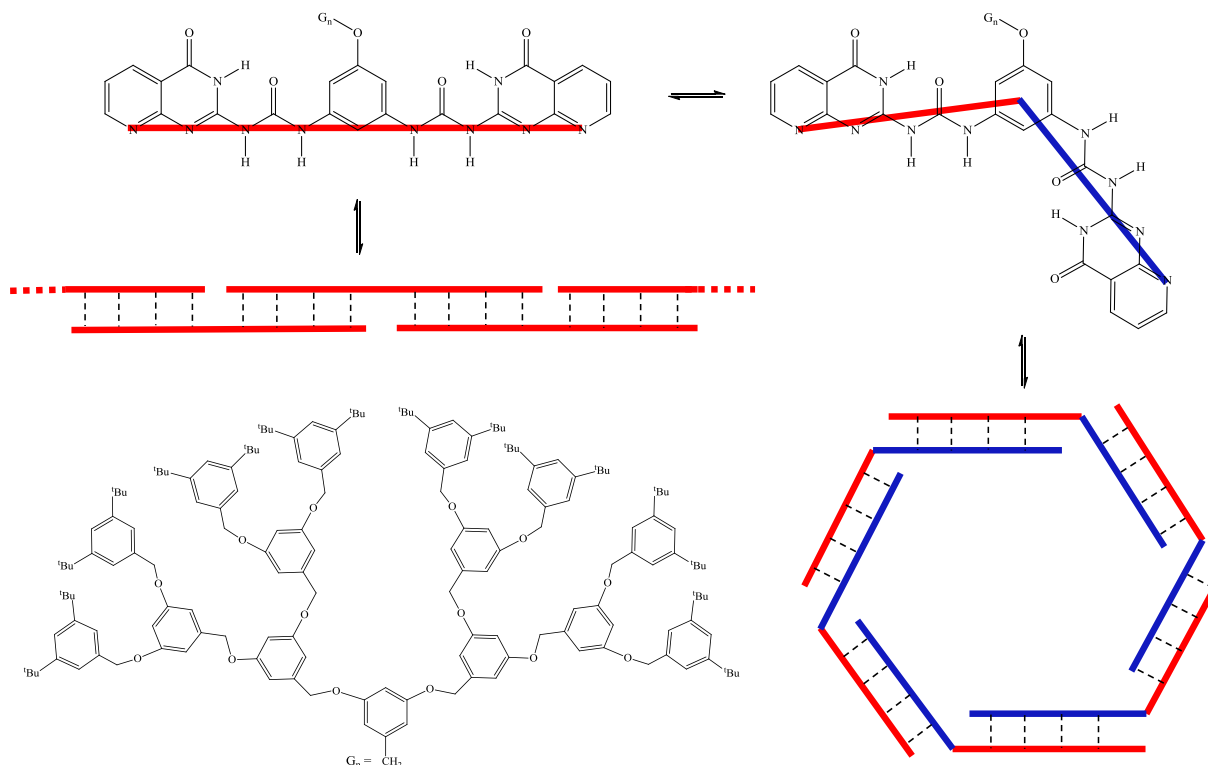


Figure 2.8 Different conformations of spacer unit DeAP and the corresponding assemblies with third generation dendron

The dimerization constant of ureidonaphthyridine (UN) is the lowest in this series because intramolecular H-bonding occurs to stabilise the folded conformer rather than the unfolded

one (Figure 2.9).^[62] This problem is less in the ureidocytosine (UC) units, developed by Hailes and co-workers, where the unfolded dimer is the most stable conformer.^[63] Similar to UC, ureidoimidazo[1,2-a]pyrimidine (UImp) has highly stable unfolded dimer.^[52b]

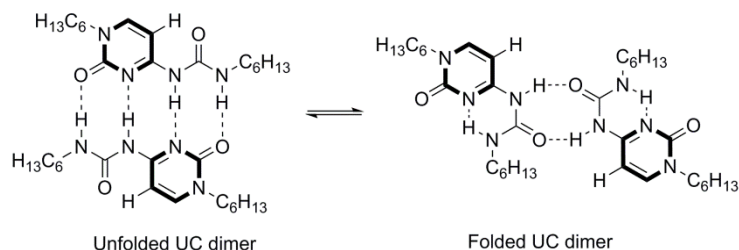


Figure 2.9 The folded and unfolded conformers of UC dimer

Among the different macrostructures that have been successfully designed and constructed by H-bonds, there are several networks bearing cavities that have been formed as a result of non-covalent, complementary interactions. The formation of these cyclic aggregates, or cages, by H-bonding requires a high binding/association constant and a highly preorganised monomeric subunit.^[61a] Another type of interaction that has been found to produce macrocycles and cages is metal coordination. Fujita and Stang have worked, independently, on the design of cyclic frameworks by coordinating different ligands, like 4,4'-dipyridine, to the metal centres, like Pt(II).^[32c, 64] Mendoza *et al.* generated molecular squares and triangles by combining H-bonding and metal-templated self-assembly. Upon mixing the difunctional UPy dimers, which can easily be preorganised by functionalisation of the phenylene ring or the amine, and a Pd(II) species in a 1:1 molar ratio, different cyclic aggregates were formed (Figure 2.10). These results led to the start of the application of H-bonding and metal complexation in designing molecular architectures of higher complexity.^[61f]

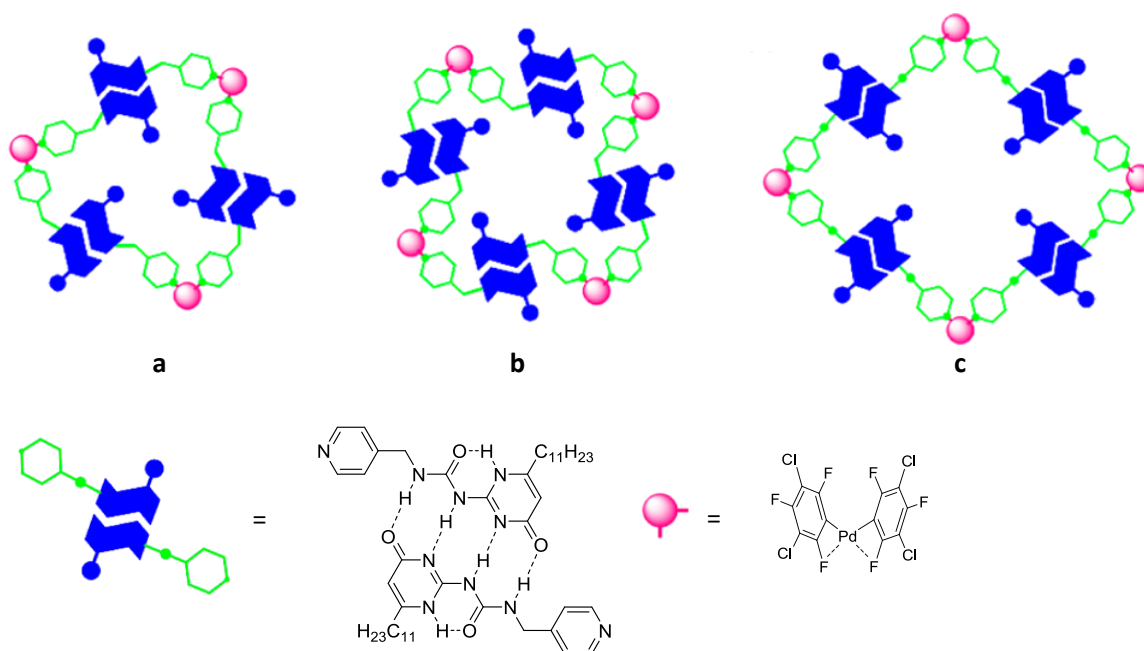


Figure 2.10 Schematic representation of cyclic aggregates (a) propeller-shaped triangle, (b) propeller-shaped square and (c) tubular-shaped tetramer.

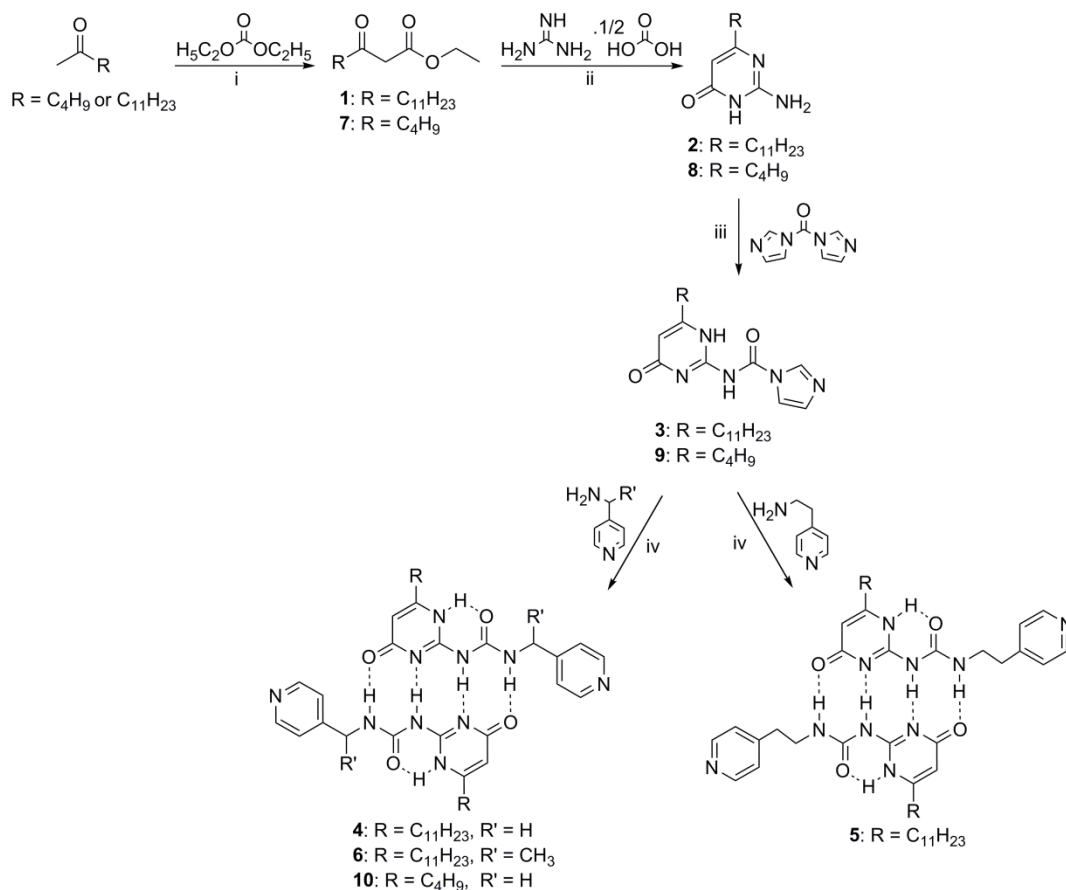
2.2 Aim

Supramolecular chemistry combining H-bonding and metal complexation has flourished since Mendoza and co-workers published their findings on this method. Thus, the objective of this project was to move from directional-bonding coordination-driven self-assembly of Ru cages to H-bonding and metal coordination self-assembly, in order to take advantage of the pool of information associated with each technique. Hence, a series of new assemblies was developed consisting of arene-Ru clips and ureidopyrimidone derivatives with a DDAA H-bond array as the spacer ligand. Five new dinuclear Ru panels and a family of new arene-Ru rectangles were generated from this work.

2.3 Synthesis

2.3.1 Synthesis of Spacer Ligands

Four different ligands (**4-6**, **10**) were synthesised by a four step synthetic route (Scheme 2.1). The first step involves an alkylation reaction between diethyl carbonate and a ketone in the presence of NaH in refluxing THF. The product obtained after purification was found to be a mixture of tautomers: the enol form and the desired ketone form as the major product (**1** and **7**). Isolation of the ketone was not carried out, and the product was used for further reactions without separation.



Scheme 2.1 Synthesis of H-bonded systems (**4-6**, **10**). Reagents and conditions: i. NaH, THF, 66°C, 16h, **1**: 76%, **7**: 88%, ii. EtOH, 90°C, 16h, **2**: 75%, **8**: 43%, iii. THF, rt, 8h, **3**: quantitative yield, **9**: 64%, iv. DMF/ NEt_3 , 70°C, 16h, **4**: 37%, **5**: 72%, **6**: 50%, **10**: 73%

The second step is the ring-closure of the β -ketoester (**1** and **7**) with guanidinium carbonate in refluxing ethanol. The isocytosine derivative (**2** and **8**) reacts with 1,1'-carbonyldiimidazole (CDI) in THF, due to limited solubility of the isocytosines, to give the blocked isocytosine isocyanate derivative (**3** and **9**). An excess (two equivalents) of CDI was used to ensure complete conversion of the isocytosine. The imidazolide was then reacted with different amines in DMF/ NEt_3 solvent mixture in a sealed tube to produce head-to-tail ureidopyrimidinone dimer with a DDAA H-bond array (**4**, **6** and **10**). The different ligands were synthesised to test the effect of: (1) adding a methyl group to the methylene spacer, (2) elongating the spacer chain, hence increasing flexibility and (3) reducing the length of the aliphatic chain from C_{11} to C_4 .

2.3.2 Macromolecular Assemblies

$[(\eta^6\text{-}p\text{-cym})\text{Ru}(\mu_2\text{-Cl})\text{Cl}]_2$, its hexamethylbenzene derivative, $[(\eta^6\text{-hmb})\text{Ru}(\mu_2\text{-Cl})\text{Cl}]_2$, and four other dinuclear arene-Ru clips synthesised from $[(\eta^6\text{-}p\text{-cym})\text{Ru}(\mu_2\text{-Cl})\text{Cl}]_2$ were used for molecular assembly. As in the case of the ligands, different clips were used for complexation to test the effect of the bridge and the arene on the ability of the resulting product to self-assemble and to form monocrystals.

Clips **11-14** (Figure 2.11) were synthesised, following literature procedures.^[43a, 47a] In these complexes, each ruthenium is coordinated to a chloride ligand that allows substitution by other ligands.

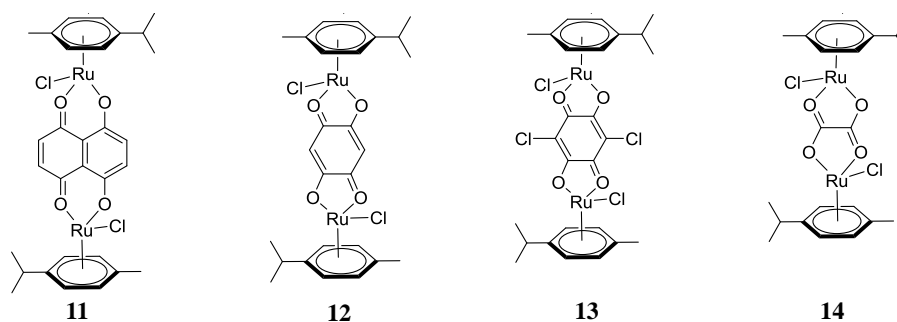
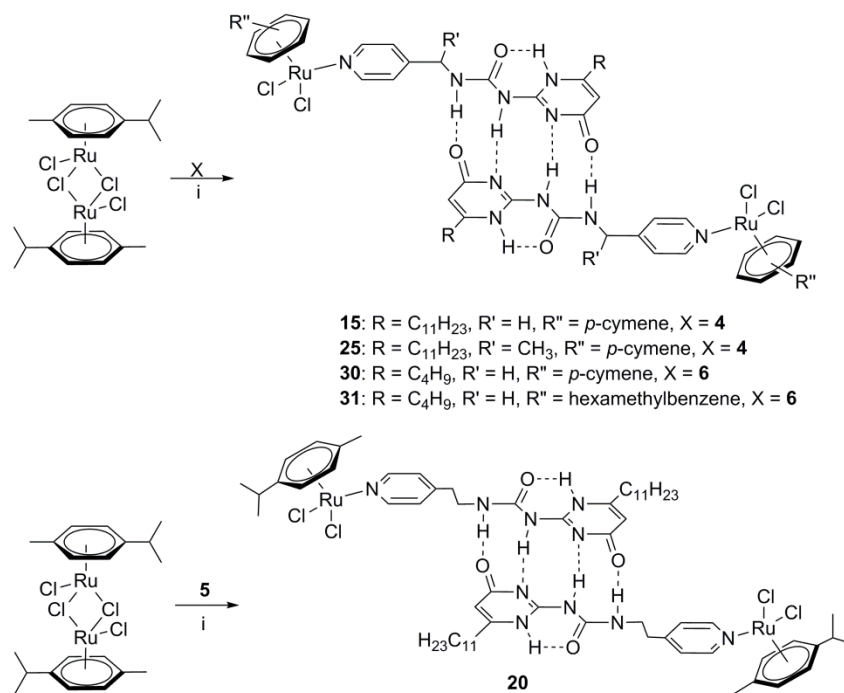


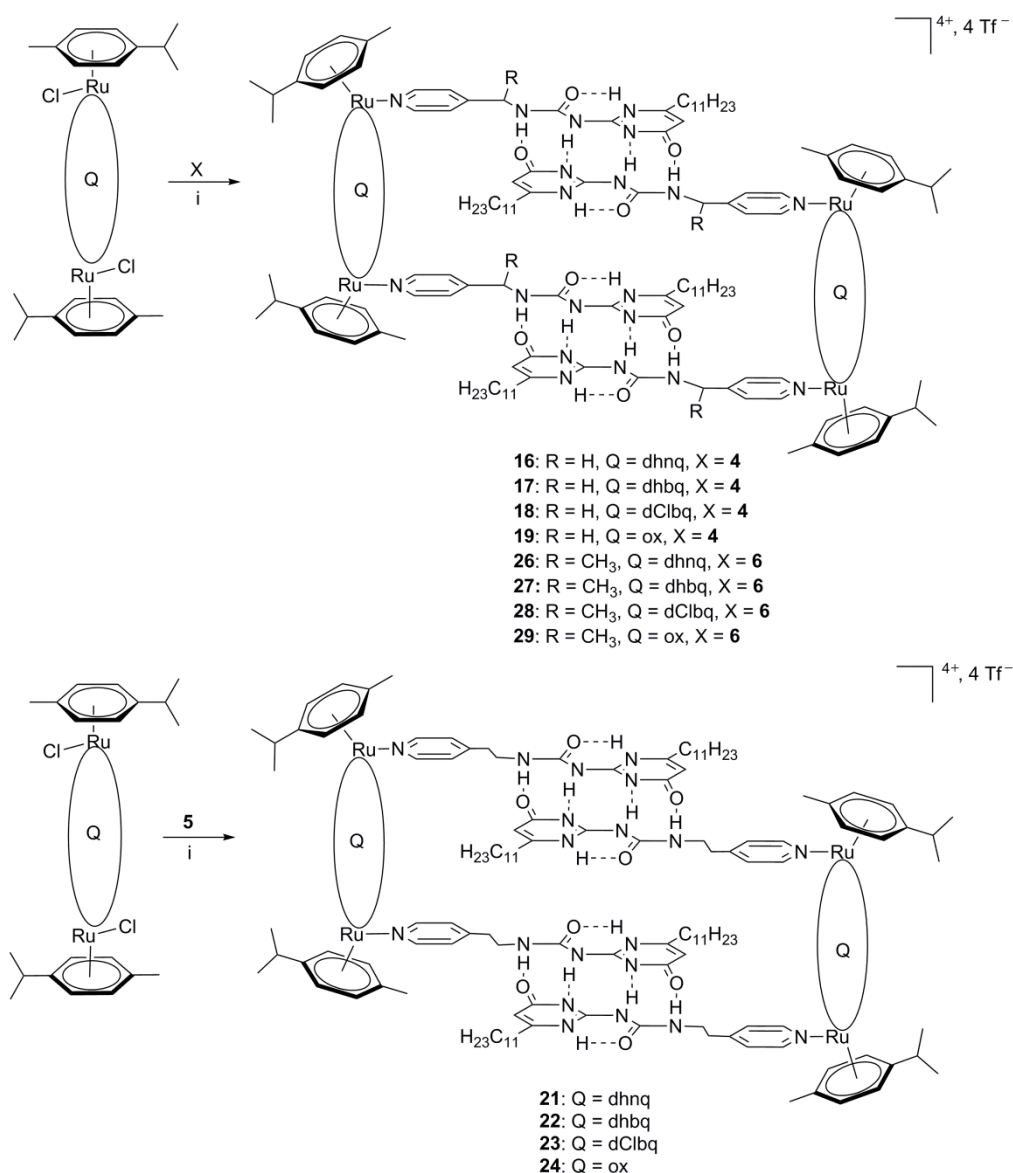
Figure 2.11 Structures of Ru clips **11-14**

These Ru clips were then reacted with the ureido dimers under different conditions to give either the dinuclear panels (**15, 20, 25, 30, 31**) or the tetranuclear rectangular assemblies (**16-19, 21-24, 26-29**) (Schemes 2.2 and 2.3). The dinuclear panels are obtained by simply stirring the ruthenium dimer with the ligand in CHCl_3 at room temperature for 24h. In these panels, the dichloro-bridge is broken, leaving each Ru with two chloride ligands and one vacant site that is taken up by the ureido ligand with the coordination of the pyridyl nitrogen to the Ru(II). With the ligand behaving as one single component with two available coordinating sites, two ruthenium dichloride species get attached to the two pyridyl nitrogen atoms of every bidentate ligand (Scheme 2.2).



Scheme 2.2 Synthesis of dinuclear Ru assemblies (**15**, **20**, **25**, **30**, **31**). Reagents and conditions: i. CHCl₃, rt, 24h, **15**: 98%, **20**: 96%, **25**: 93%, **30**: 95%, **31**: 90%

In the case of the cages, a vacant site is created on each Ru centre by loss of the chloride ligand in the form of AgCl, resulting in the *in-situ* preparation of the activated intermediate species in the *syn* symmetry exclusively. When the ligand is added to the mixture, two bidentate dimers link together two Ru clips to form a cationic tetrameric cyclic arrangement adopting a rectangular shape, with four triflate counter anion (Scheme 2.3).



Scheme 2.3 Synthesis of tetranuclear Ru assemblies (**16-19**, **21-24**, **26-29**). Reagents and conditions: i. AgCF₃SO₃, CH₂Cl₂, rt, 24h or MeOH, rt, 16h, **16**: 23%, **17**: 72%, **18**: 72%, **19**: 38%, **21**: 46%, **22**: 65%, **23**: 53%, **24**: 23%, **26**: 21%, **27**: 61%, **28**: 57%, **29**: 21%

2.4 Characterization

2.4.1 Proton NMR Spectroscopy

For all the ligands (**4-6**, **10**), sharp ¹H NMR spectra in CDCl₃ were observed (Figure 2.12). Well-defined typical signature for UPy's NH was observed downfield, in the region expected for H-bonded dimers. It was also observed that changes brought to the molecule gave rise to shifting of some proton signals (Figure 2.12). For instance, adding a methyl group to the spacer results in an upfield shift for H₅ and H₆ protons from 12.16 and 11.03 ppm to 12.10 and 10.81 ppm, respectively. In the case of elongating the spacer by one carbon atom, an

upfield shift of H₅ and H₆ protons is observed from 12.16 and 11.03 ppm to 11.91 and 10.42 ppm. On the other hand, shortening the aliphatic side chain from C₁₁ to C₄ causes no change in the chemical shifts of H₅ and H₆ protons (Figure 2.12). The H₄ protons are the most downfield in **5**, when the spacer is more flexible and shortening the aliphatic side chain results in an upfield shift of the H₄ proton from 13.02 ppm in **5** to 12.95 ppm in **4** (Figure 2.12). Hence, alterations brought to the dimer have an effect on the H-bonds holding the dimer together and inter- and intramolecular H-bondings are affected in different ways.

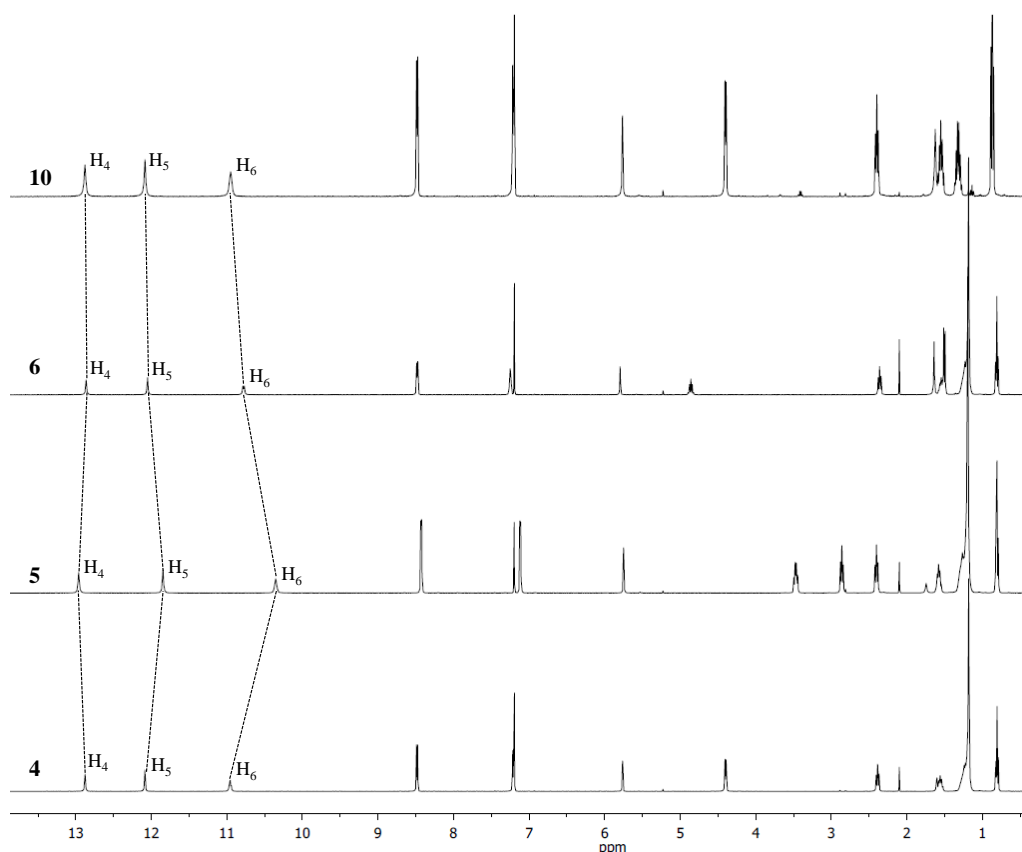


Figure 2.12 ¹H NMR spectra (400 MHz, CDCl₃) of ligands **4-6** and **10**

The effect of concentration on the chemical shifts of the NH protons (H₄, H₅ and H₆) in dimer **4** was tested. There was no apparent change in the chemical shift across a broad range of concentration (1 mM to 50 μM). From this observation, only a lower limit to the dimerization constant, $K_{\text{dim}} > 10^7 \text{ M}^{-1}$ could be estimated, which is among the largest stability constants reported to date for neutral, H-bonded species.

For the two sets of Ru complexes, the dinuclear and the tetranuclear, the resolution of the proton signals was found to differ. The spectra of the dinuclear species show peaks that are

sharp and well-defined, like in the case of the uncoordinated dimers (Figure 2.13). Besides a slight upfield shift of the H₄ proton of the ureido derivatives after coordination of the dimer to the Ru, the other two NH signals (H₅ and H₆) did not undergo any major shifting. The H₉ peaks, however, underwent a downfield shift due to their close proximity to the Ru centre. Only a slight upfield shift was observed for the H₈ peaks, being further away and therefore less affected by the Ru(II) centre. An example of the comparison between uncoordinated ligand and the corresponding dinuclear Ru complex is shown in Figure 2.13, whereby the ¹H NMR spectra of compound **4** and its dinuclear Ru complex **15** are compared. The shifts observed between the two spectra are indicated by dotted lines, namely the shifting of the H₄, H₆, H₈ and H₉ protons.

In the case of the rectangles, for most of the complexes, broad and ill-defined peaks were obtained, with some signals not visible on the spectra. For instance, the NH signals (H₄, H₅, H₆) are broadened completely into the baseline for most of the rectangular systems (see Figure 2.20 for ¹H NMR spectrum of **17**).

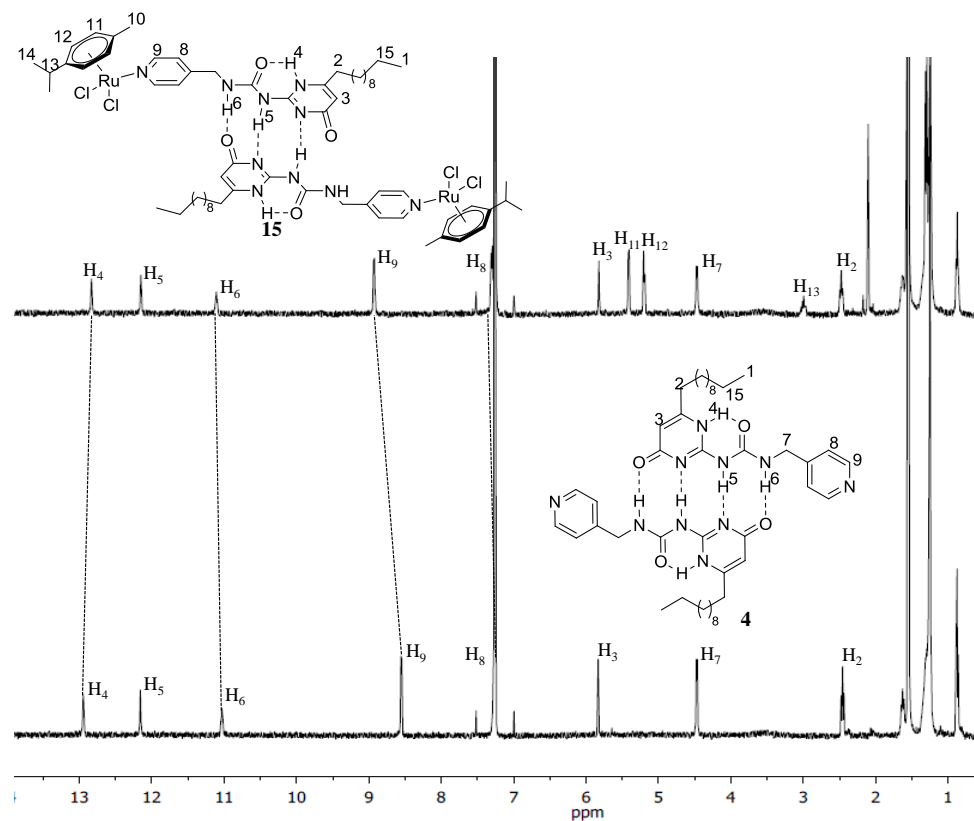


Figure 2.13 ¹H NMR spectra (400 MHz, CDCl₃) of **4** and **15**

2.4.2 DOSY

Diffusion-ordered NMR spectroscopy (DOSY) is a 2D NMR experiment developed in 1992 to measure diffusion coefficients and in case of spherical molecules, the hydrodynamic radii of such molecules in solution using the Stokes-Einstein equation can be determined.^[65] The 2D spectrum consists of one axis representing typical chemical shift information and diffusion coefficient (D) on another. This technique allows the different species contained in a mixture to be distinguished, as D is related to the size of the particle. The diffusion coefficient is dependent on the size and shape of the molecule in a particular solvent at a particular temperature.^[66] This NMR tool has found widespread applications in biology and chemistry where DOSY is being used to determine the dimensions of polydispersed supramolecular aggregates.^[67]

In order to confirm the composition of the metal coordination/H-bonding self-assembly of the Ru/ureido systems, DOSY experiments were run on the complexes. For all the dinuclear complexes (**15**, **20**, **25**, **30** and **31**) DOSY experiments were run in CDCl₃ using similar concentrations and at room temperature. Figure 2.14 shows the 2D spectra of compounds **15**, **20** and **25**, which display single diffusion coefficient for each compound, indicating the formation of single species. It was also observed that the diffusion coefficients differ only very slightly for the five complexes ($-9.30 > \log D > -9.41$) and hence, the standard errors associated with the differences between these values are too significant to be ignored. Comparing the DOSY spectrum of the free ligand to its corresponding dinuclear Ru complex, a decrease in $\log D$ value was observed. For example, compound **4** has $\log D$ value of -9.25 while compound **15** has a $\log D$ value around -9.32. It can be concluded that for the dinuclear system, the complexes have very similar diffusion coefficients and that the minor differences among the UPy ligands do not have any apparent significance on the diffusion of the corresponding complexes, which have similar hydrodynamic volumes in solution.

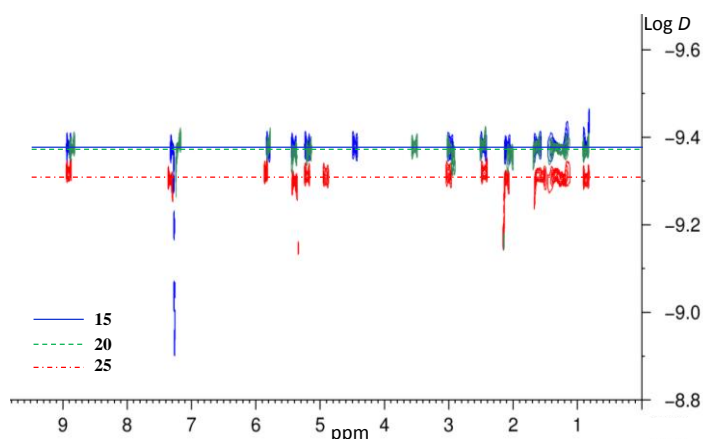


Figure 2.14 DOSY spectra (400 MHz, CDCl_3) of compounds **15**, **20** and **25**

For the tetranuclear complexes, the DOSY experiments were run mostly in CD_3CN , and it was observed that the complexes have diffusion coefficients in the range of -9.12 to -9.30×10^{10} . Similar to the dinuclear system, the differences are too small to account for any structure/diffusion relationship among these complexes. Thus, even with clips of different lengths, for example **11** and **14**, their corresponding complexes show very close D values and hence have almost the same hydrodynamic volumes in solution. The difference in D values is however slightly more important when comparing a tetranuclear assembly to its corresponding dinuclear complex bearing the same UPy ligand. Thus, complexes **15** and **17** have diffusion coefficients of -9.38×10^{10} and -9.54×10^{10} respectively in CDCl_3 . This difference can be associated to the larger hydrodynamic volume of the rectangle than the dinuclear panel. An example of the comparison of free ligand **4** and its corresponding tetranuclear Ru complex **17** is shown in Figure 2.15.

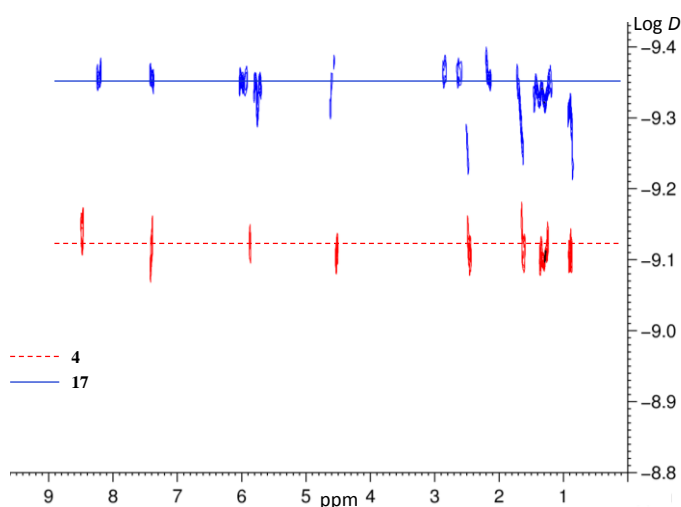


Figure 2.15 DOSY spectra (400 MHz, CDCl_3) of **4** and **17**

2.4.3 NOE/ROE and DFT Calculations

A very powerful tool in NMR spectroscopy for structural studies of chemical systems is the Nuclear Overhauser Effect (NOE). This technique relies on relaxation phenomena between dipolar coupled spins and manifests itself in changes in signal intensities of nuclear sites when other specific nuclear sites are perturbed by means of a radio-frequency (*rf*) pulse.^[68] Therefore, the experimental observation of NOE supplies information about, and implies, spatial proximities between given nuclear sites and can prove extremely useful in structural studies of the supramolecular systems considered in this thesis (See Annex 2).^[69] A widespread variation of the NOE experiment is the Rotating-frame Overhauser Effect (ROE), where an *rf* pulse is applied so as to spin-lock the magnetization in the transverse plane. This technique is utilised in cases where NOE enhancements are close to zero. Also this latter technique may therefore be utilised for structural studies aiming to determine internuclear distances between sites experiencing non-negligible dipolar couplings.

In order to corroborate the experimental findings, a computational study has also been undertaken (See Annex 2).^[70] The structures thus obtained were used to calculate the magnetic shielding tensors of both ^1H and ^{13}C nuclei with the GIAO method at the same level of theory of the DFT optimizations.^[71] The geometry optimizations supplied internuclear distances to be compared to those determined experimentally by means of NMR/NOE measurements whereas the calculations of the magnetic shieldings allowed comparison with the experimental ^1H and ^{13}C chemical shifts observed for structure **4** in simple 1D solution-phase NMR spectra.

Structure **4** is expected to form in solution a dimer *via* formation of four H-bonds, resulting in the head-to-tail configuration as shown in Figure 2.16.

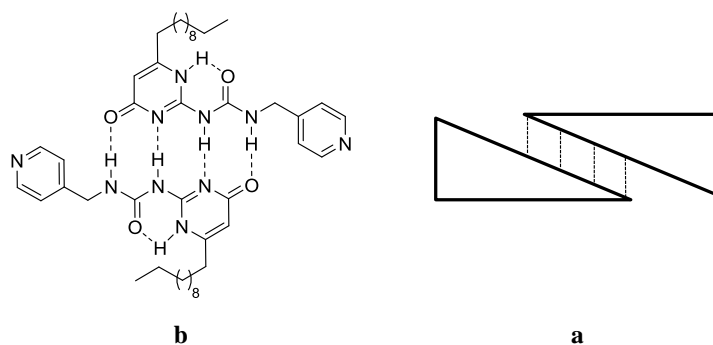


Figure 2.16 Dimeric structure of **4** in a head-to-tail configuration

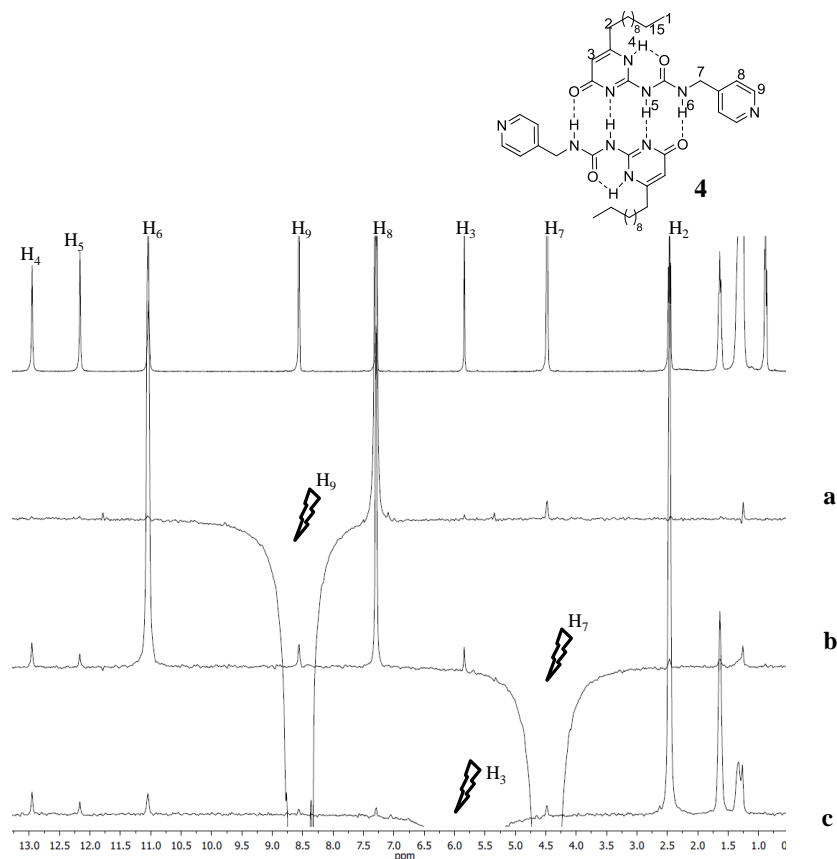


Figure 2.17 1D ROE spectra (400 MHz, CDCl_3) of **4** with protons H_9 (a), H_7 (b) and H_3 (c) irradiated

Figure 2.17(a), (b) and (c) shows 1D ROE spectra obtained when irradiating protons H_3 , H_7 and H_9 , respectively. Figure 2.18 shows, as histogram, the differences between internuclear distances measured from the NOE enhancements of the spectra in (a), (b) and (c), and those obtained from the structures optimised with DFT methods. The smaller those differences, the better the agreement between experiments and calculations are. In this histogram, the differences calculated, assuming a monomeric non-H-bonded structure **4**, are shown in blue whereas those calculated, assuming the head-to-tail dimer, are shown in red. This histogram clearly shows a much better agreement of the experimental data sets when the dimeric structure is considered, with differences generally smaller than 1 \AA in both cases (Figure 2.18). In particular, proton sites that are on opposite sides of structure **4**, such as, H_3 and H_9 , necessarily require intermolecular pathways that may only exist in the dimeric form in order to interpret the experimentally-observed NOE enhancements.

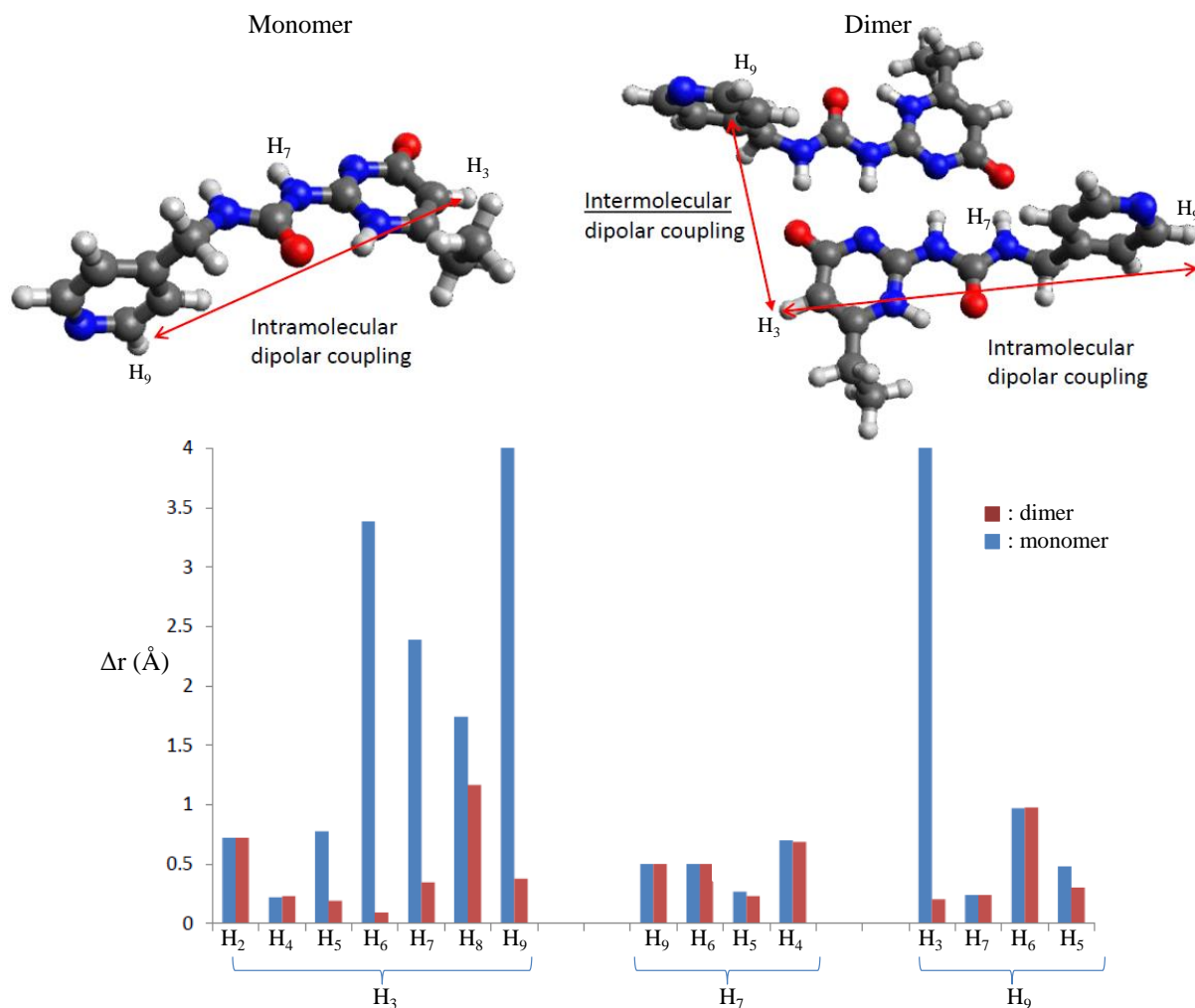


Figure 2.18 Difference in Δr between DFT-calculated and ROE measured distances

The experimental data based on ROE measurements strongly suggests the existence of **4** as a H-bonded dimer in solution. An independent further assessment may be also carried out by considering the chemical shifts of the ^{13}C and ^1H resonances as measured in conventional 1D spectra and as calculated with DFT methods, as described above. Figure 2.19(a) shows the correlation between experimental ^{13}C chemical shifts and those calculated for the monomeric structure. The quality of the correlation may be indicated by a coefficient $R^2 = 0.996$. Figure 2.19(b) shows the good correlation when the dimeric structure was used to calculate the chemical shifts. In this latter case $R^2 = 0.999$, with all carbon sites being very accurately described by DFT calculations. Figure 2.19(c) shows the correlation between experimental ^1H chemical shifts and those calculated for the monomeric structure. In this case, the NH protons lay completely out of the correlation line where all other proton sites may be found. These protons are involved in the H-bonding network that assembles the dimeric structure. If solvent effects are included in the calculations, no substantial improvement is obtained. Figure

2.19(d) shows the analogous correlation when the dimeric structure was considered in the calculations. In this case the chemical shifts of the NH protons correlate very well with the calculated ones, with a coefficient $R^2 = 0.998$. These results indicate that, in order to interpret the chemical shifts observed experimentally for ^{13}C and ^1H in structure **4**, a dimeric arrangement needs to be considered. This is particularly true for the protons of the NH groups involved in the H-bonding system.

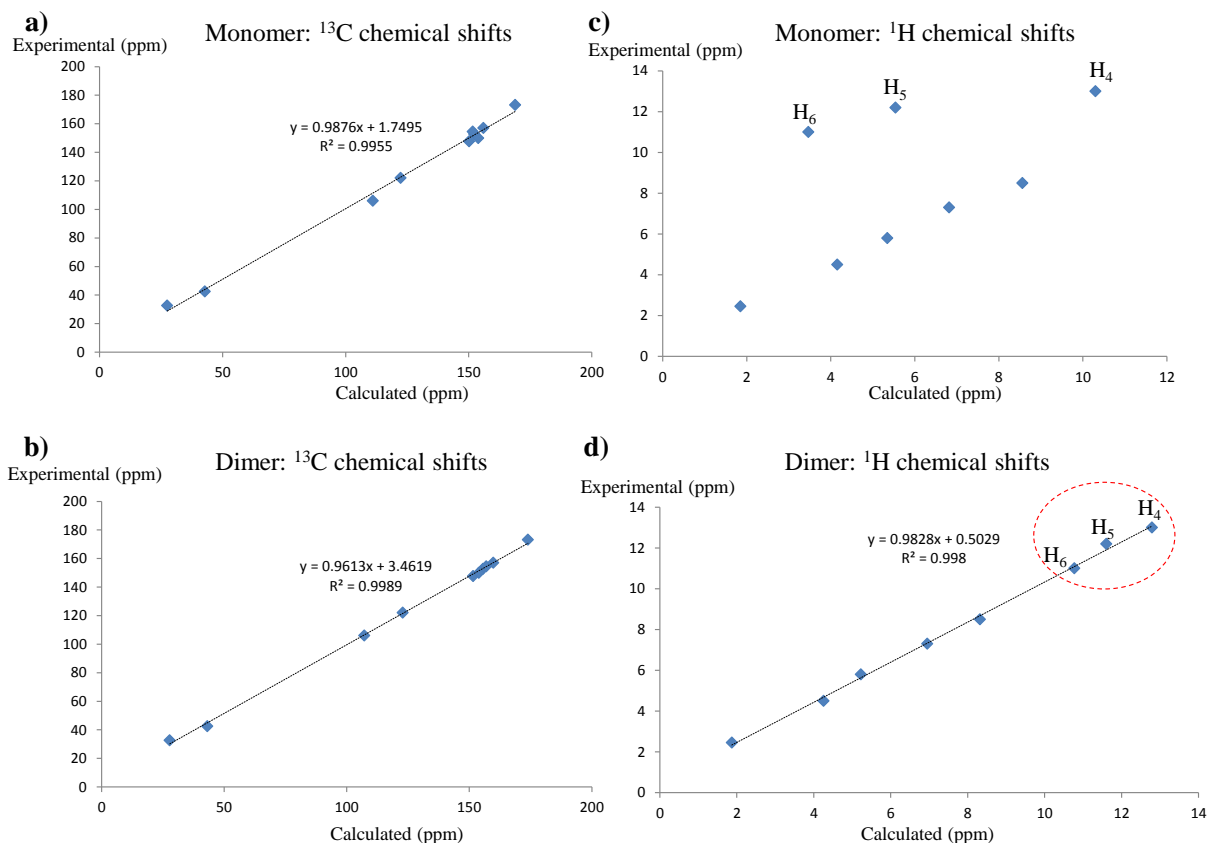


Figure 2.19 Experimental v/s DFT-calculated ^{13}C and ^1H chemical shifts for the (a and c) monomeric and (b and d) dimeric forms

All the NMR data experimentally observed as ROE ^1H enhancements and ^1H and ^{13}C chemical shifts strongly support the hypothesis of a structure **4** existing as a head-to-tail dimer in solution. In the case of the tetranuclear species, qualitative ROE/NMR analysis of compound **17** confirms the predicted rectangular self-assembled arrangement. Figure 2.20 shows the NOE spectrum of **17**: with H_9 being irradiated, the peak corresponding to the benzoquinone Ru bridge of the clip, H_{19} was observed on the spectrum (See Annex 2).

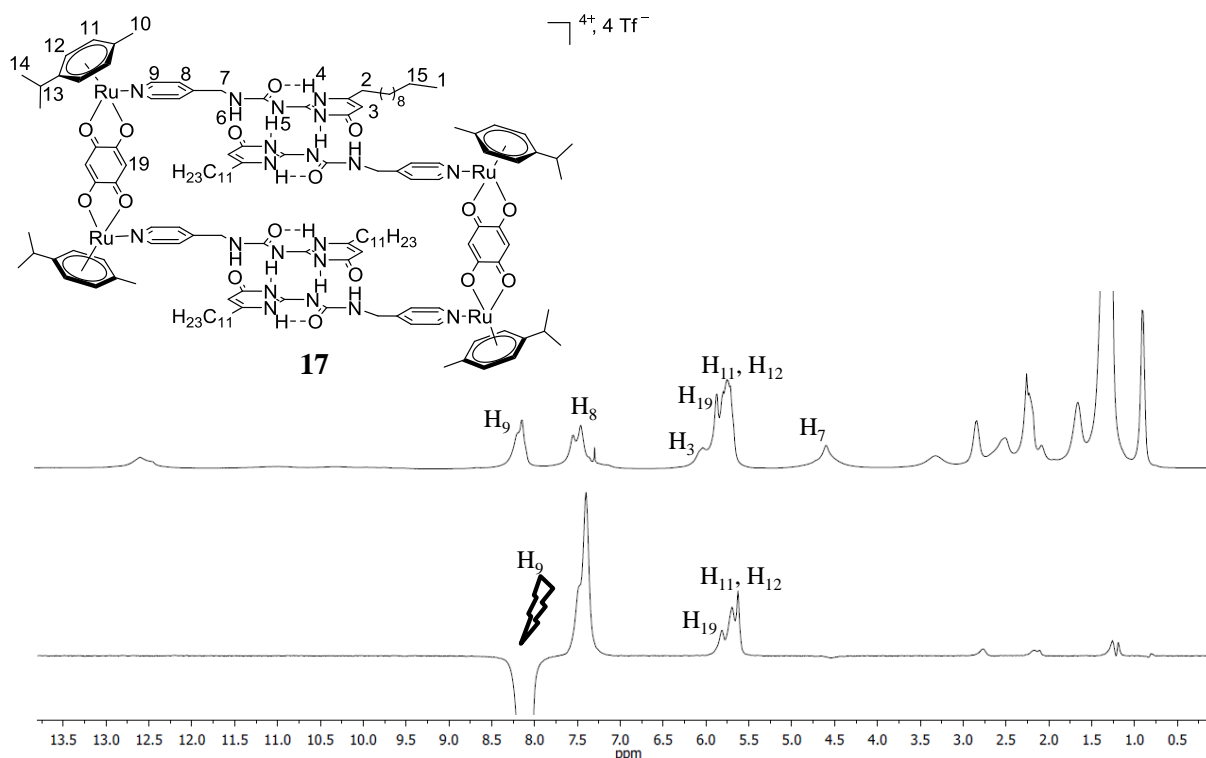


Figure 2.20 1D ROE spectra (400 MHz, CDCl_3) of **17** with protons H_9 (a) and H_{19} (b) irradiated

2.4.4 UV-Vis Spectroscopy

The binding of the various metallo-assemblies were studied by UV-visible spectroscopy; the electronic absorption spectra were acquired in CH_2Cl_2 at concentrations around 10^{-5} M in the range 250-700 nm (Table 2.1). The di- and tetranuclear complexes were found to have different spectra. The dinuclear complexes have similar spectra, with a high energy shoulder around 288 nm, which may be attributed to ligand $\pi \rightarrow \pi^*$ transitions and a broad and low energy band at around 410 nm.^[72] The latter may be assigned to mixed metal-ligand charge transfer (MLCT), intra-ligand charge transfer (ILCT) from spacer ligand to $OO \cap OO$ bridging ligand and ligand $\pi \rightarrow \pi^*$ transitions.^[73] Figure 2.21 shows the stacking of the UV-Vis spectra of compounds **16**, **21** and **26** measured in CH_2Cl_2 and the similarity between these three naphthoquinone ruthenium derivatives. The spectra show that the differences between the three compounds bearing three different spacer ligands are negligible.

Table 2.1 λ_{\max} values of the different series of metallo-cycles

| Clips | Metallo-cycles | λ_{\max} (nm) | ε ($M^{-1}\cdot cm^{-1}$) x 10^5 |
|-------|----------------|-----------------------|--|
| 11 | 16 | 306 | 2.38 |
| | | 433 | 1.66 |
| | | 639 | 0.55 |
| | | 693 | 0.62 |
| | 21 | 310 | 2.56 |
| | | 434 | 4.32 |
| | | 644 | 0.55 |
| | | 696 | 0.58 |
| | 26 | 310 | 2.57 |
| | | 434 | 1.57 |
| | | 641 | 0.51 |
| | | 693 | 0.51 |
| 12 | 17 | 299 | 3.64 |
| | | 498 | 3.39 |
| | 22 | 300 | 3.72 |
| | | 497 | 2.23 |
| | 27 | 298 | 3.42 |
| | | 496 | 3.07 |
| 13 | 18 | 324 | 2.27 |
| | | 504 | 2.27 |
| | 23 | 326 | 2.20 |
| | | 509 | 2.28 |
| | 28 | 325 | 2.31 |
| | | 503 | 2.40 |
| 14 | 19 | 383 | 0.28 |
| | 24 | 384 | 0.26 |
| | 29 | 387 | 0.28 |

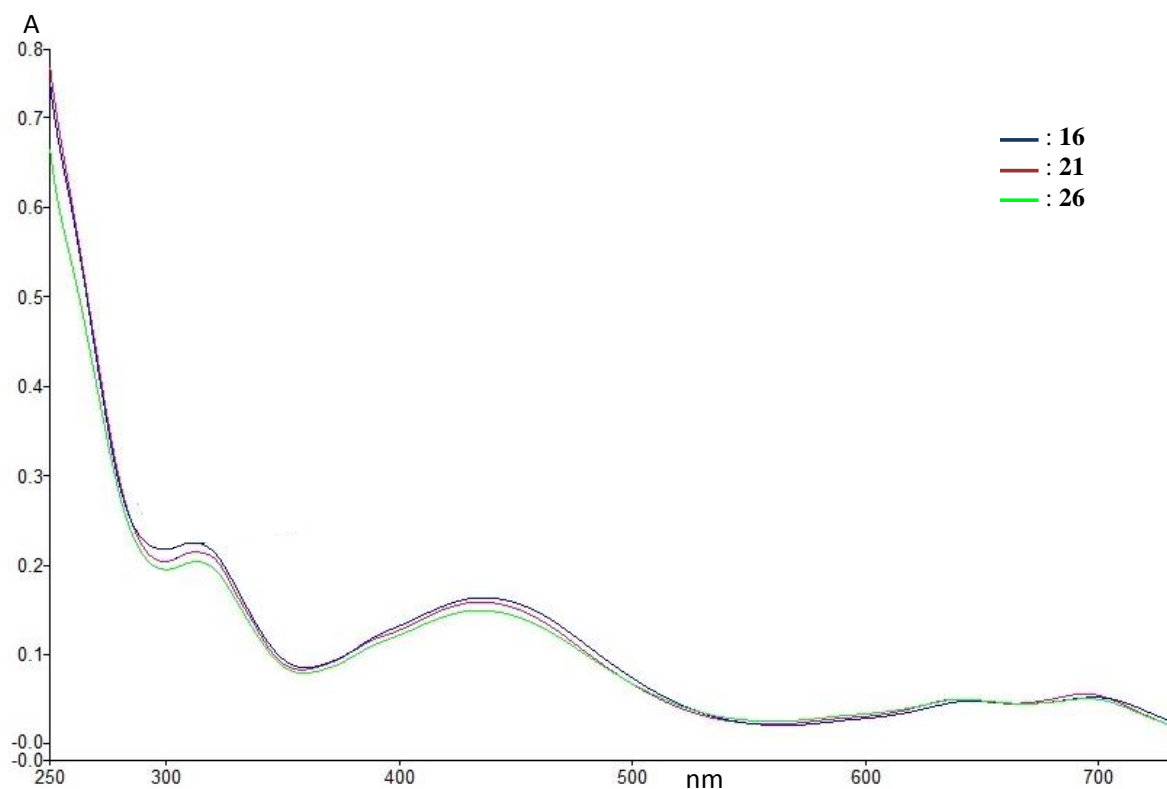


Figure 2.21 UV spectra of compounds **26**, **21** and **16** in CH_2Cl_2

Changing the spacer ligand coordinated to the Ru(II) does not change the spectra of the di- and tetranuclear complexes. However, the spectra change a lot when modifying the bridging ligand of the Ru clip. Thus, complexes bearing the same Ru clip have similar spectra. Comparing those similar spectra allows the effect of the different ligands to be determined. But like in the case of dinuclear complexes, the differences in the spacer ligands cannot be seen by this technique. When the different series bearing the different clips were compared with each other, the effect of the Ru clip can be studied. For instance, relative to the dinuclear systems, the series of complexes bearing clip **14** undergo a hypsochromic shift of about 20 nm (Table 2.1).

Moreover, comparing the metallo-cycles obtained from Ru clips **11** and **12**, more bands are observed for the series from clip **11** and a slight bathochromic shift with Ru clip **12** (about 10 nm) is observed (Table 2.1). A presumably lower contribution to ILCT between the spacer ligand and the benzoquinone compared to the same charge transfer between the same ligand and the naphthoquinone bridging ligand of clip **11**.^[72b, 74] Similarly, addition of a chloride on the benzoquinone bridge results in a bathochromic shift of the bands of the metallo-cycle from Ru clip **13** compared to those of clip **12** (Table 2.1).

2.4.5 Electrospray Ionization Mass Spectrometry

The electrospray ionization (ESI) mass spectra of ligands **4-6** and **10**, run in CH_2Cl_2 and MeOH, show the peak of highest intensity corresponding to either $[\text{M}_{\text{monomer}}+\text{H}]^+$ or $[\text{M}_{\text{monomer}}-\text{H}]^-$ for the positive and negative modes, respectively. A possible reason for the observation of the monomer and not the dimer of the ligands may be the presence of methanol molecules that undergo an exchange with monomer, hence obstructing the dimer formation.

In the case of the Ru(II) complexes, the ESI MS was run in acetonitrile to avoid any exchange to take place between the solvent molecule and the complex. The spectra of the dinuclear complexes **15**, **20**, **25**, **30** and **31** all show the peak corresponding to the m/z of $[\text{M}_{\text{dimer}}-\text{Cl}]^+$ with a separation of 1 Da between the components of the mentioned peak, which is expected of a singly charged ion. For example, the ESI mass spectrum of complex **20** shows several species, among which the $[\text{M}-\text{Cl}]^+$ peak observed at $m/z = 1403.2$. An expansion of this peak reveals the characteristic Ru_8 isotope pattern with a 1 Da separation between the peaks (Figure 2.22).

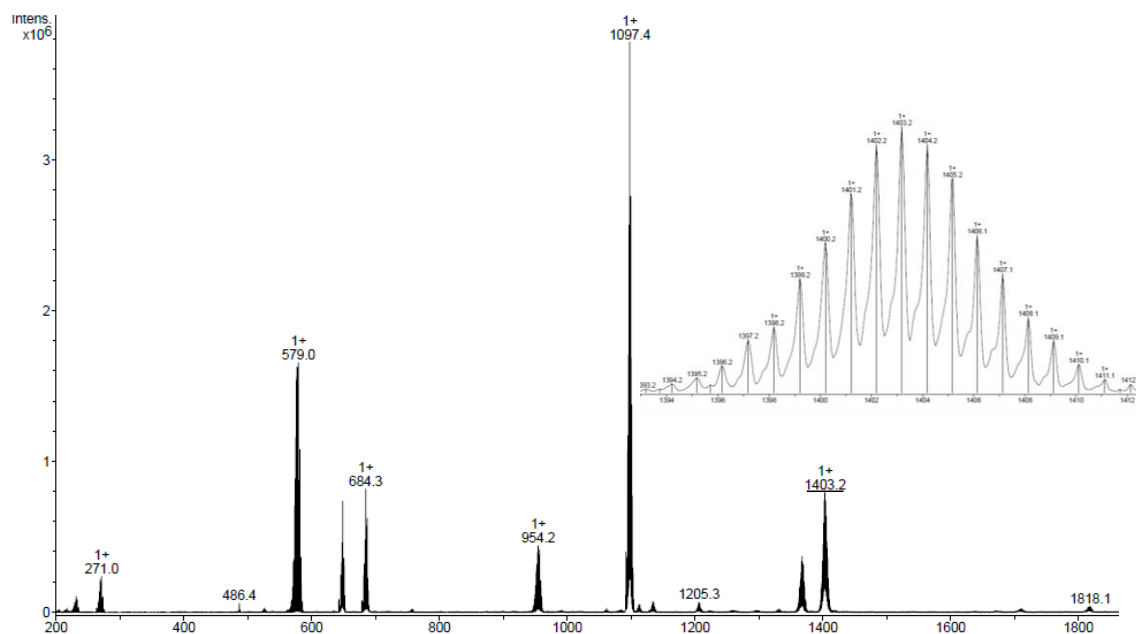


Figure 2.22 The ESI mass spectra of complex **20** in acetonitrile

For the tetranuclear complexes, the ESI mass spectra show the peak of the ion $[\text{M}_{\text{dinuclear}}+\text{Tf}]^{2+}$, with the isotope peaks that differ by 0.5 Da, characteristic of doubly charged ions. Hence, the tetranuclear assembly is confirmed as the mass detected corresponds to that of the tetranuclear complex. For instance, the spectrum of complex **17** shows the peak at m/z

= 1556 that corresponds to the mass of the tetranuclear system after the loss of two triflate ions (Figure 2.23).

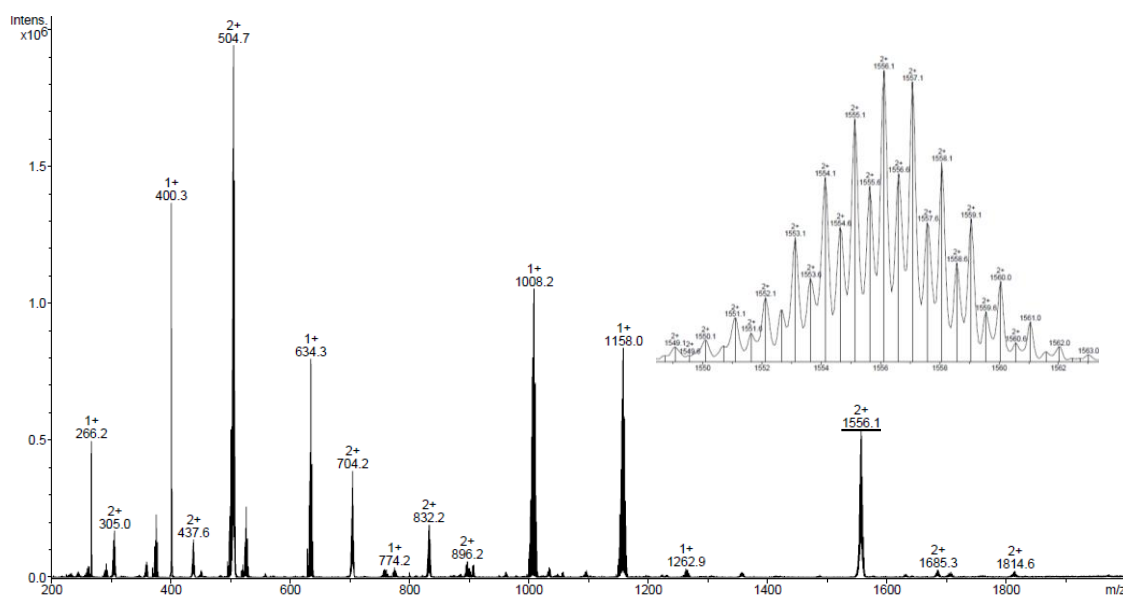
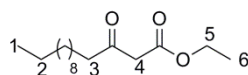


Figure 2.23 The ESI mass spectra of complex **17** in acetonitrile

2.5 Conclusion

A series of novel multinuclear arene-Ru(II) assemblies were synthesised and characterised. The use of H-bonding self-assembly together with metal coordination to make metallo-cages has proven to be successful. The arrangements originating from this straightforward synthetic route show good stability under atmospheric conditions. A major part of the characterization of these complexes was made using the different tools associated with the NMR: ^1H NMR, DOSY and NOE/ROE, complemented by DFT calculations. IR, UV-visible and ESI mass spectrometry supported the observations and conclusions made from NMR analysis.

2.6 Experimental Part



1

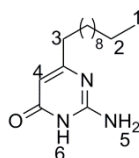
A suspension of NaH on dispersion oil (3.55 g, 88.7 mmol) and diethyl carbonate (8 mL, 65.9 mmol) in dry THF (55 mL) was heated under reflux under argon. A solution of 2-tridecanone (5.68 g, 28.6 mmol) in dry THF (10 mL) was added dropwise over 2h to the mixture and was heated under reflux overnight. The dense suspension was carefully poured into a mixture of

saturated aqueous NH_4Cl , 5% HCl and ice and extracted with diethyl ether. The organic layer was washed with saturated aqueous NH_4Cl and dried over MgSO_4 and the solvent evaporated. The crude product was purified by CC (eluent hexane/diethyl ether, 10/1). **1** was formed with the enol isomer (15%) as a transparent liquid with a yield of 76% (5.89 g).

^1H NMR (400 MHz, CDCl_3 , ppm): $\delta = 4.22$ (q, $^3J_{\text{H-H}} = 7.1$ Hz, 2H, H_5), 3.42 (s, 2H, H_4), 2.52 (t, $^3J_{\text{H-H}} = 7.4$ Hz, 2H, H_3), 1.60 (t, $^3J_{\text{H-H}} = 7.4$ Hz, 3H, H_6), 1.25-1.33 (m, 18H, aliphatic chain), 0.88 (t, $^3J_{\text{H-H}} = 6.8$ Hz, 3H, H_1).

$^{13}\text{C}\{^1\text{H}\}$ NMR (100 MHz, CDCl_3 , ppm): $\delta = 203.00$; 167.28; 61.25; 49.32; 43.05; 31.91; 29.60; 29.44; 29.36; 29.33; 29.03; 23.48; 22.68; 14.10.

MS (ESI(+)) = 271.5 $[\text{M}+\text{H}]^+$



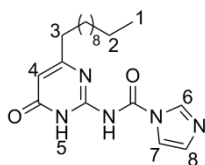
2

A suspension of guanidinium carbonate (0.48 g, 2.70 mmol) and **1** (1.47 g, 5.40 mmol) in ethanol (20 mL) was heated under reflux. After overnight stirring, mixture was cooled to rt, the white precipitate formed was filtered off and washed with ethanol. The residue was dried under vacuum. **2** was obtained as a white solid with a yield of 75% (0.53 g).

^1H NMR (400 MHz, DMSO, ppm): $\delta = 10.57$ (s, 1H, H_6), 6.42 (s, 2H, H_5), 5.35 (s, 1H, H_4), 2.20 (t, $^3J_{\text{H-H}} = 7.6$ Hz, 2H, H_3), 1.48-1.56 (m, 2H, H_2), 1.24-1.30 (m, 16H, aliphatic chain), 0.85 (t, $^3J_{\text{H-H}} = 6.6$ Hz, 3H, H_1).

$^{13}\text{C}\{^1\text{H}\}$ NMR (100 MHz, DMSO, ppm): $\delta = 170.22$; 163.23; 155.93; 100.03; 37.46; 31.71; 29.44; 29.41; 29.39; 29.27; 29.12; 29.05; 27.93; 22.51; 14.38.

MS (ESI(-)) = 529.2 $[2\text{M}-\text{H}]^-$

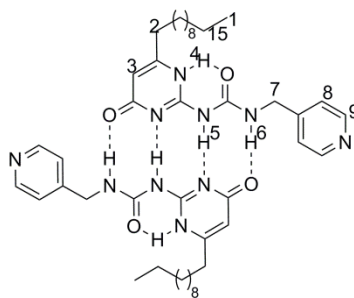
**3**

A suspension of **2** (0.40 g, 0.94 mmol) and CDI (0.30 g, 1.89 mmol) in dry THF (35 mL) was stirred under argon at rt for 8h. The solvent was removed and the residue was triturated with acetone (60 mL). The precipitate was filtered and the residue dried under vacuum. **3** was obtained as a white solid with a quantitative yield (0.42 g).

^1H NMR (400 MHz, CDCl_3 , ppm): δ = 12.16 (s, 1H, H_5), 8.85 (m, 1H, H_6), 7.64 (m, 1H, H_7), 7.01 (m, 1H, H_8), 5.81 (s, 1H, H_4), 2.65 (t, $^3J_{\text{H-H}} = 7.7$ Hz, 2H, H_3), 1.75 (quint, $^3J_{\text{H-H}} = 7.6$ Hz, 2H, aliphatic chain), 1.26-1.43 (m, 16H, aliphatic chain), 0.87 (t, $^3J_{\text{H-H}} = 6.6$ Hz, 3H, H_1).

$^{13}\text{C}\{^1\text{H}\}$ NMR (100 MHz, CDCl_3 , ppm): δ = 160.80; 157.17; 156.67; 138.01; 127.85; 117.69; 104.04; 76.72; 32.90; 31.91; 29.58; 29.44; 29.33; 29.27; 29.10; 27.58; 22.69; 14.13.

MS (ESI(+)) = 360.4 $[\text{M}+\text{H}]^+$

**4**

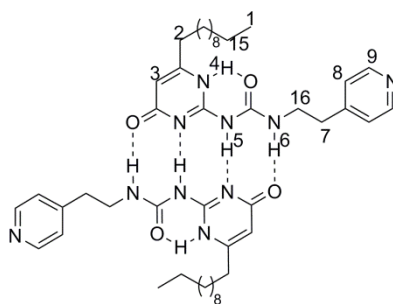
4-(Aminomethyl)pyridine (0.44 mL, 5.06 mmol) and **3** (2.00 g, 5.56 mmol) were placed in a sealed tube containing dry DMF (20 mL). To this solution, triethylamine (7.5 mL) was added and the mixture was stirred at 70°C. After overnight reaction, the mixture was cooled to rt, the solvent was removed under vacuum and the residue was triturated in methanol. The mixture was filtered and the residue washed with methanol, chloroform and EtOAc. **4** was obtained as a white solid with a yield of 37% (0.74 g).

^1H NMR (400 MHz, CDCl_3 , ppm): $\delta = 12.95$ (s, 2H, H_4), 12.16 (s, 2H, H_5), 11.03 (t, $^3J_{\text{H-H}} = 6.0$ Hz, 2H, H_6), 8.55 (d, $^3J_{\text{H-H}} = 5.9$ Hz, 4H, H_9), 7.27 (d, $^3J_{\text{H-H}} = 5.4$ Hz, 4H, H_8), 5.83 (s, 2H, H_3), 4.46 (d, $^3J_{\text{H-H}} = 5.7$ Hz, 4H, H_7), 2.46 (t, $^3J_{\text{H-H}} = 7.7$ Hz, 4H, H_2), 1.59-1.64 (m, 4H, aliphatic chain), 1.25-1.35 (m, 32H, aliphatic chain), 0.87 (t, $^3J_{\text{H-H}} = 6.8$ Hz, 6H, H_1).

$^{13}\text{C}\{^1\text{H}\}$ NMR (100 MHz, CDCl_3 , ppm): $\delta = 173.20$; 157.01; 152.54; 152.79; 150.01; 147.76; 122.09; 106.09; 42.49; 31.91; 29.58; 29.56; 29.43; 29.32; 29.15; 28.86; 26.97; 22.70; 14.13.

MS (ESI(-)) = 398.5 [$\text{M}_{\text{monomer}}\text{-H}$] $^-$

IR (KBr) (cm^{-1}) = 1699 (s, NH), 1658 (s, NH), 1590 (s, NH); 1260 (s, CN).



5

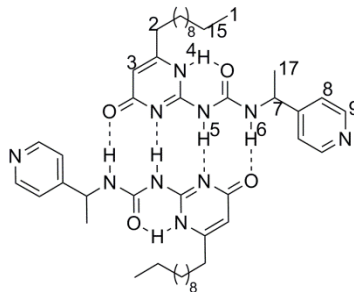
4-(2-Aminoethyl)pyridine (0.11 g, 0.91 mmol) and **3** (0.35 g, 1.00 mmol) were reacted following the procedure for **4** in DMF (5 mL) and triethylamine (1.5 mL) at 70°C overnight. The product was purified by the same method used for compound **4**. **5** was obtained as a white solid with a yield of 72% (0.27 g).

^1H NMR (400 MHz, CDCl_3 , ppm): $\delta = 13.02$ (s, 2H, H_4), 11.91 (s, 2H, H_5), 10.42 (t, $^3J_{\text{H-H}} = 5.4$ Hz, 2H, H_6), 8.49 (d, $^3J_{\text{H-H}} = 6.1$ Hz, 4H, H_9), 7.18 (d, $^3J_{\text{H-H}} = 6.1$ Hz, 4H, H_8), 5.81 (s, 2H, H_3), 3.54 (dt, $^3J_{\text{H-H}} = 8.1$ Hz, $^4J_{\text{H-H}} = 6.1$ Hz, 4H, H_{16}), 2.94 (t, $^3J_{\text{H-H}} = 7.5$ Hz, 4H, H_7), 2.47 (t, $^3J_{\text{H-H}} = 7.7$ Hz, 4H, H_2), 1.64 (quint, $^3J_{\text{H-H}} = 7.6$ Hz, 4H, aliphatic chain), 1.26-1.38 (m, 32H, aliphatic chain), 0.87 (t, $^3J_{\text{H-H}} = 6.5$ Hz, 6H, H_1).

$^{13}\text{C}\{^1\text{H}\}$ NMR (100 MHz, CDCl_3 , ppm): $\delta = 173.12$; 156.66; 154.59; 152.66; 149.82; 148.09; 124.23; 105.91; 40.21; 34.97; 32.73; 31.91; 29.59; 29.58; 29.45; 29.33; 29.18; 28.87; 26.99; 22.770; 14.13.

MS (ESI(+)) = 414.9 $[M_{\text{monomer}}+H]^+$

IR (KBr) (cm^{-1}) = 1702 (s, NH), 1654 (s, NH), 1579 (s, NH); 1256 (s, CN).



6

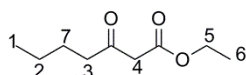
4-(1-Aminoethyl)pyridine (0.11 g, 0.91 mmol) and **3** (0.35 g, 1.00 mmol) were reacted following the procedure for **4** in DMF (5 mL) and triethylamine (1.5 mL) at 70°C overnight. The product was purified by the same method used for compound **4**. **6** was obtained as a white solid with a yield of 50% (0.19 g).

^1H NMR (400 MHz, CDCl_3 , ppm): δ = 12.91 (s, 2H, H_4), 12.10 (s, 2H, H_5), 10.81 (d, $^3J_{\text{H-H}} = 7.2$ Hz, 2H, H_6), 8.52 (d, $^3J_{\text{H-H}} = 6.0$ Hz, 4H, H_9), 7.30-7.33 (m, 4H, H_8), 5.87 (s, 2H, H_3), 4.92 (quint, $^3J_{\text{H-H}} = 7.0$ Hz, 2H, H_7), 2.43 (t, $^3J_{\text{H-H}} = 7.7$ Hz, 4H, H_2), 1.56-1.63 (m, 10H, H_{17} , aliphatic chain), 1.25-1.28 (m, 32H, aliphatic chain), 0.86 (t, $^3J_{\text{H-H}} = 6.4$ Hz, 6H, H_1).

$^{13}\text{C}\{^1\text{H}\}$ NMR (100 MHz, CDCl_3 , ppm): δ = 173.08; 156.10; 154.60; 153.40; 152.60; 150.09; 121.16; 106.12; 49.42; 32.71; 31.91; 29.58; 29.56; 29.42; 29.33; 29.15; 28.86; 26.96; 22.70; 21.98; 14.14.

MS (ESI(+)) = 412.4 $[M_{\text{monomer}}-H]^-$

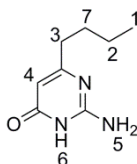
IR (KBr) (cm^{-1}) = 1695 (s, NH), 1662 (s, NH), 1593 (s, NH); 1265 (s, CN)

**7**

A suspension of NaH on dispersion oil (3.55 g, 88.7 mmol), diethyl carbonate (8 mL, 65.9 mmol) and 2-hexanone (3.5 mL, 28.6 mmol) were stirred in dry THF (55+10 mL) following same procedure as for **1**. **7** was obtained as a transparent liquid with the yield of 88% (4.33 g).

^1H NMR (400 MHz, CDCl_3 , ppm): $\delta = 4.19$ (q, $^3J_{\text{H-H}} = 7.2$ Hz, 2H, H_5), 3.43 (s, 2H, H_4), 2.53 (t, $^3J_{\text{H-H}} = 7.4$ Hz, 2H, H_3), 1.52-1.63 (m, 2H, H_7), 1.26-1.31 (m, 5H, H_2 , H_6), 0.91 (t, $^3J_{\text{H-H}} = 7.2$ Hz, 3H, H_1).

$^{13}\text{C}\{^1\text{H}\}$ NMR (100 MHz, CDCl_3 , ppm): $\delta = 203.01$; 168.12; 61.05; 48.89; 41.73; 25.46; 22.20; 14.1; 13.89.

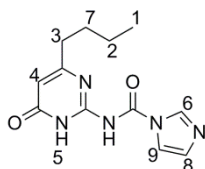
**8**

Guanidinium carbonate (2.26 g, 12.0 mmol) and **7** (4.33 g, 25.0 mmol) were stirred in ethanol (50 mL) following the procedure of **2**. **8** was obtained as a white solid with a yield of 43% (1.82 g).

^1H NMR (400 MHz, DMSO, ppm): $\delta = 10.60$ (s, 1H, H_6), 6.44 (s, 2H, H_5), 5.37 (s, 1H, H_4), 2.20 (t, $^3J_{\text{H-H}} = 7.7$ Hz, 2H, H_3), 1.50 (quint, $^3J_{\text{H-H}} = 8.3$ Hz, 2H, H_2), 1.28 (sept, $^3J_{\text{H-H}} = 7.2$ Hz, 2H, H_7), 0.87 (t, $^3J_{\text{H-H}} = 7.6$ Hz, 3H, H_1).

$^{13}\text{C}\{^1\text{H}\}$ NMR (100 MHz, DMSO, ppm): $\delta = 155.56$; 99.66; 64.88; 29.63; 21.71; 15.13; 13.62.

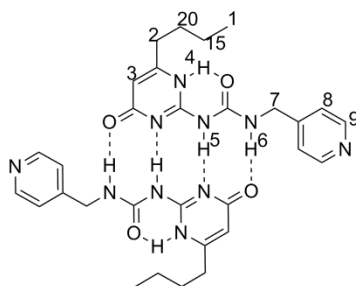
MS (ESI(+)) = 168.4 $[\text{M}+\text{H}]^+$

**9**

8 (1.67 g, 10.0 mmol) and CDI (3.24 g, 20.0 mmol) were stirred in dry THF (160 mL) following similar procedure as **3**. **9** was obtained as a white solid with a yield of 64% (1.67 g). ^1H NMR (400 MHz, CDCl_3 , ppm): δ = 8.82 (m, 1H, H_6), 7.64 (m, 1H, H_9), 7.03 (m, 1H, H_8), 5.82 (s, 1H, H_4), 2.65 (t, $^3J_{\text{H-H}} = 7.7$ Hz, 2H, H_3), 1.68-1.79 (m, 2H, H_7), 1.43-1.53 (m, 2H, H_2), 0.99 (t, $^3J_{\text{H-H}} = 7.3$ Hz, 3H, H_1).

$^{13}\text{C}\{^1\text{H}\}$ NMR (100 MHz, CDCl_3 , ppm): δ = 160.75; 156.60; 137.99; 128.03; 117.66; 104.08; 32.64; 29.54; 22.24; 13.72.

MS (ESI(+)) = 261.2 $[\text{M}+\text{H}]^+$

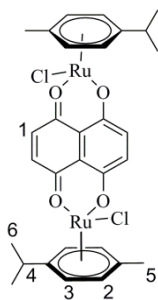
**10**

4-(Aminomethyl)pyridine (0.10 mL, 1.0 mmol), **9** (0.28 g, 1.1 mmol) and triethylamine (1.5 mL) were stirred in dry DMF (5 mL) following similar procedure as **4**. **10** was obtained as a white solid with a yield of 73% (0.21 g).

^1H NMR (400 MHz, CDCl_3 , ppm): δ = 12.90 (s, 1H, H_4), 12.16 (s, 1H, H_5), 11.03 (s, 1H, H_6), 8.55 (d, $^3J_{\text{H-H}} = 6.1$ Hz, 2H, H_9), 7.27 (d, $^3J_{\text{H-H}} = 6.0$ Hz, 2H, H_8), 5.84 (s, 1H, H_3), 4.48 (d, $^3J_{\text{H-H}} = 5.8$ Hz, 2H, H_7), 2.45 (t, $^3J_{\text{H-H}} = 7.7$ Hz, 2H, H_2), 1.62 (quint, $^3J_{\text{H-H}} = 7.4$ Hz, 2H, H_{20}), 1.39 (sext, $^3J_{\text{H-H}} = 7.4$ Hz, 2H, H_{15}), 0.93 (t, $^3J_{\text{H-H}} = 7.3$ Hz, 3H, H_1).

$^{13}\text{C}\{^1\text{H}\}$ NMR (100 MHz, CDCl_3 , ppm): δ = 173.18; 157.01; 154.53; 152.75; 49.99; 147.76; 122.10; 106.10; 42.49; 32.44; 28.99; 21.99; 13.61.

MS (ESI(+)) = 302.4 $[M_{\text{monomer}}+H]^+$

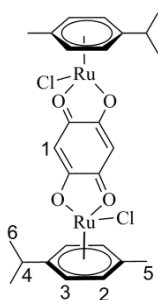


11

A mixture of $[(\eta^6\text{-}p\text{-cym})\text{Ru}(\mu_2\text{-Cl})\text{Cl}]_2$ (0.63 g, 1.00 mmol), anhydrous sodium acetate (0.16 g, 2.00 mmol) and 5,8-dihydroxy-1,4-naphthaquinone (0.19 g, 1.00 mmol) in ethanol (75 mL) was stirred at 90°C for 16h. The precipitate formed was then filtered and washed with ethanol, water, acetone, diethyl ether and pentane to give **11** as a green solid in a yield of 80% (0.58 g).

^1H NMR (400 MHz, CDCl_3 , ppm): δ = 6.95 (s, 4H, H_1), 5.48 (d, $^3J_{\text{H-H}} = 5.7$ Hz, 4H, H_2), 5.22 (d, $^3J_{\text{H-H}} = 5.7$ Hz, 4H, H_3), 2.87 (sept, $^3J_{\text{H-H}} = 6.7$ Hz, 2H, H_4), 2.22 (s, 6H, H_5), 1.30 (d, $^3J_{\text{H-H}} = 6.9$ Hz, 12H, H_6).

$^{13}\text{C}\{^1\text{H}\}$ NMR (100 MHz, CDCl_3 , ppm): δ = 170.91; 137.05; 111.92; 100.30; 98.04; 82.80; 79.59; 30.72; 22.40; 17.93.

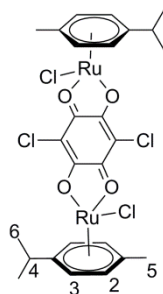


12

$[(\eta^6\text{-}p\text{-cym})\text{Ru}(\mu_2\text{-Cl})\text{Cl}]_2$ (0.31 g, 0.50 mmol), anhydrous sodium acetate (0.08 g, 1.00 mmol) and 2,5-dihydroxy-1,4-benzoquinone (0.07 g, 0.50 mmol) in ethanol (30 mL) were reacted and purified following the procedure for **11**. **12** was obtained as a red solid with a yield of 89% (0.30 g).

^1H NMR (400 MHz, CDCl_3 , ppm): $\delta = 5.79$ (s, 2H, H_1), 5.62 (d, $^3J_{\text{H-H}} = 5.7$ Hz, 4H, H_2), 5.38 (d, $^3J_{\text{H-H}} = 5.7$ Hz, 4H, H_3), 2.91 (sept, $^3J_{\text{H-H}} = 7.0$ Hz, 2H, H_4), 2.29 (s, 6H, H_5), 1.31 (d, $^3J_{\text{H-H}} = 6.9$ Hz, 12H, H_6).

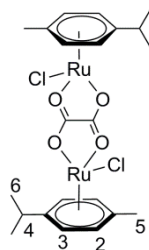
$^{13}\text{C}\{^1\text{H}\}$ NMR (100 MHz, CDCl_3 , ppm): $\delta = 184.45$; 139.12; 119.46; 102.29; 97.03; 81.55; 79.60; 31.70; 22.87; 19.09.

**13**

$[(\eta^6\text{-}p\text{-cym})\text{Ru}(\mu_2\text{-Cl})\text{Cl}]_2$ (0.31 g, 0.50 mmol), anhydrous sodium acetate (0.08 g, 1.00 mmol) and chloranilic acid (0.10 g, 0.50 mmol) were stirred in methanol (30 mL) at rt for 2h. The mixture was filtered and the residue washed with diethyl ether to afford **13** as a red solid with a yield of 87% (0.32 g).

^1H NMR (400 MHz, CDCl_3 , ppm): $\delta = 5.72$ (d, $^3J_{\text{H-H}} = 5.7$ Hz, 4H, H_2), 5.47 (d, $^3J_{\text{H-H}} = 5.7$ Hz, 4H, H_3), 2.94 (sept, $^3J_{\text{H-H}} = 7.0$ Hz, 2H, H_4), 2.34 (s, 6H, H_5), 1.36 (d, $^3J_{\text{H-H}} = 6.9$ Hz, 12H, H_6).

$^{13}\text{C}\{^1\text{H}\}$ NMR (100 MHz, CDCl_3 , ppm): $\delta = 184.72$; 137.45; 118.41; 102.36; 98.62; 82.07; 76.44; 31.72; 21.53; 18.59.

**14**

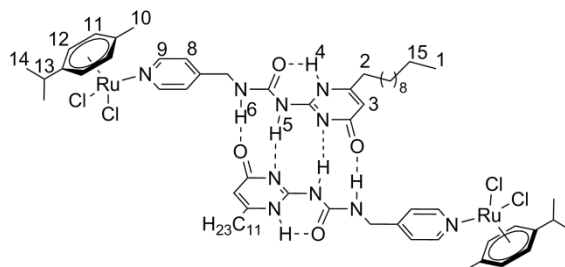
$[(\eta^6\text{-}p\text{-cym})\text{Ru}(\mu_2\text{-Cl})\text{Cl}]_2$ (0.63 g, 1.00 mmol) and ammonium oxalate monohydrate (0.14 g, 1.00 mmol) were added to a $\text{CHCl}_3/\text{MeOH}$ (20/20 mL) solvent mixture and heated at 62°C for

6h. The mixture was filtered and washed with cold methanol to afford **14** as an orange solid with a yield of 90% (0.57 g).

^1H NMR (400 MHz, CDCl_3 , ppm): $\delta = 5.55$ (d, $^3J_{\text{H-H}} = 5.7$ Hz, 4H, H_2), 5.32 (d, $^3J_{\text{H-H}} = 5.8$ Hz, 4H, H_3), 2.87 (sept, $^3J_{\text{H-H}} = 2.8$ Hz, 2H, H_4), 2.21 (s, 6H, H_5), 1.29 (d, $^3J_{\text{H-H}} = 6.9$ Hz, 12H, H_6).

$^{13}\text{C}\{^1\text{H}\}$ NMR (100 MHz, CDCl_3 , ppm): $\delta = 171.78$; 99.88; 95.57; 80.49; 78.48; 31.19; 22.51; 18.60.

General procedure for dinuclear panels (**15**, **20**, **25**, **30** and **31**): a mixture of Ru dichloride dimer (**15**, **20**, **25**, **30**: $[(\eta^6\text{-arene})\text{Ru}(\mu_2\text{-Cl})\text{Cl}]_2$ (0.03 g, 0.06 mmol) and **31**: $[(\eta^6\text{-hmb})\text{Ru}(\mu_2\text{-Cl})\text{Cl}]_2$ (0.06 g, 0.09 mmol)) and UPy derivative (**15** and **30**: **4** (0.04 g, 0.06 mmol), **20**: **5** (0.05 g, 0.06 mmol), **25**: **6** (0.05 g, 0.06 mmol) and **31**: **10** (0.04 g, 0.09 mmol)) was stirred in CHCl_3 (2 mL) at rt for 16h. Diethyl ether was added to precipitate the product that was obtained by filtration.



15

Yield = 98% (0.17 g)

^1H NMR (400 MHz, CDCl_3 , ppm): $\delta = 12.83$ (s, 2H, H_4), 12.15 (s, 2H, H_5), 11.10 (s, 2H, H_6), 8.92 (d, $^3J_{\text{H-H}} = 6.0$ Hz, 4H, H_9), 7.30 (d, $^3J_{\text{H-H}} = 5.8$ Hz, 4H, H_8), 5.82 (s, 2H, H_3), 5.40 (d, $^3J_{\text{H-H}} = 5.8$ Hz, 4H, H_{11}), 5.19 (d, $^3J_{\text{H-H}} = 5.8$ Hz, 4H, H_{12}), 4.46 (d, $^3J_{\text{H-H}} = 5.7$ Hz, 4H, H_7), 2.99 (sept, $^3J_{\text{H-H}} = 6.9$ Hz, 2H, H_{13}), 2.47 (t, $^3J_{\text{H-H}} = 7.8$ Hz, 4H, H_2), 2.10 (s, 6H, H_{10}), 1.63 (quint, $^3J_{\text{H-H}} = 7.5$ Hz, 4H, aliphatic chain), 1.23-1.36 (m, 44H, H_{14} , aliphatic chain), 0.87 (t, $^3J_{\text{H-H}} = 6.8$ Hz, 6H, H_1).

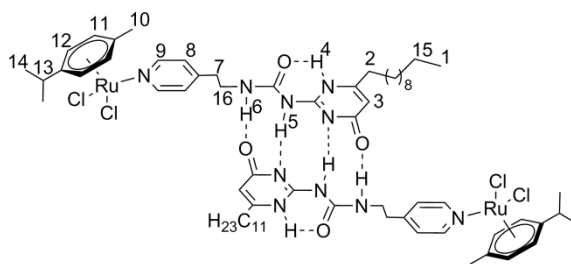
$^{13}\text{C}\{^1\text{H}\}$ NMR (100 MHz, CDCl_3 , ppm): $\delta = 194.92; 156.76; 154.60; 152.99; 123.17; 106.01; 103.60; 82.63; 82.35; 31.84; 30.61; 29.53; 29.41; 29.27; 29.10; 28.83; 26.88; 22.64; 22.27; 18.29; 14.09; 0.97$.

MS (ESI(+)) = 1375.1 $[\text{M}-\text{Cl}]^+$

Anal. Calcd. (found) for $\text{C}_{64}\text{H}_{94}\text{N}_{10}\text{O}_4\text{Cl}_4\text{Ru}_2$ (1411.46) = C, 54.06 (54.46); H, 6.75 (6.71); N, 9.80 (9.92)%

UV-Vis (CH_2Cl_2 , 1.0×10^{-5} M): $\lambda_{\text{max}} = 408$ nm ($\epsilon = 0.15 \times 10^5 \text{ M}^{-1} \cdot \text{cm}^{-1}$)

IR (KBr) (cm^{-1}) = 3421 (s, NH); 1697 (s, NH); 1660 (s, NH); 1587 (s, NH); 1257 (s, CN).



20

Yield = 96% (0.17 g)

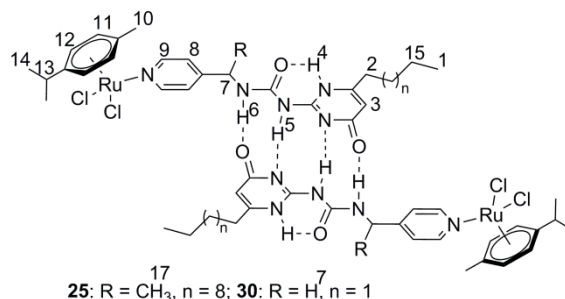
^1H NMR (400 MHz, CDCl_3 , ppm): $\delta = 12.91$ (s, 2H, H_4), 11.86 (s, 2H, H_5), 10.41 (s, 2H, H_6), 8.85 (d, $^3J_{\text{H-H}} = 5.7$ Hz, 4H, H_9), 7.20 (d, $^3J_{\text{H-H}} = 5.7$ Hz, 4H, H_8), 5.79 (s, 2H, H_3), 5.40 (d, $^3J_{\text{H-H}} = 5.7$ Hz, 4H, H_{11}), 5.18 (d, $^3J_{\text{H-H}} = 5.7$ Hz, 4H, H_{12}), 3.53 (q, $^3J_{\text{H-H}} = 6.5$ Hz, 4H, H_{16}), 2.92-2.99 (m, 6H, H_7 , H_{13}), 2.47 (t, $^3J_{\text{H-H}} = 7.7$ Hz, 4H, H_2), 2.04 (s, 6H, H_{10}), 1.66 (quint, $^3J_{\text{H-H}} = 7.6$ Hz, 4H, aliphatic chain), 1.24-1.37 (m, 44H, H_{14} , aliphatic chain), 0.86 (t, $^3J_{\text{H-H}} = 6.6$ Hz, 6H, H_1).

$^{13}\text{C}\{^1\text{H}\}$ NMR (100 MHz, CDCl_3 , ppm): $\delta = 173.12; 156.51; 154.36; 152.79; 150.66; 125.13; 105.80; 103.39; 96.96; 82.79; 82.14; 39.57; 34.27; 32.68; 32.85; 30.58; 29.53; 29.41; 29.27; 29.13; 28.86; 26.88; 22.64; 22.26; 18.17; 14.10$.

MS (ESI(+)) = 1403.2 $[\text{M}-\text{Cl}]^+$

UV-Vis (CH_2Cl_2 , $1.0 \times 10^{-5} \text{ M}$): $\lambda_{\text{max}} = 402 \text{ nm}$ ($\epsilon = 0.18 \times 10^5 \text{ M}^{-1} \cdot \text{cm}^{-1}$)

IR (KBr) (cm^{-1}) = 3425 (s, NH); 1698 (s, NH); 1659 (s, NH); 1586 (s, NH); 1255 (s, CN).



25

Yield = 93% (0.16 g)

^1H NMR (400 MHz, CDCl_3 , ppm): $\delta = 12.81$ (s, 2H, H₄), 12.09 (s, 2H, H₅), 10.90 (d, $^3J_{\text{H-H}} = 6.9 \text{ Hz}$, 2H, H₆), 8.90 (d, $^3J_{\text{H-H}} = 5.7 \text{ Hz}$, 4H, H₉), 7.32 (d, $^3J_{\text{H-H}} = 4.6 \text{ Hz}$, 4H, H₈), 5.84 (s, 2H, H₃), 5.39 (q, $^3J_{\text{H-H}} = 5.4 \text{ Hz}$, 4H, H₁₁), 5.20 (q, $^3J_{\text{H-H}} = 4.7 \text{ Hz}$, 4H, H₁₂), 4.91 (quint, $^3J_{\text{H-H}} = 7.1 \text{ Hz}$, 2H, H₇), 3.00 (sept, $^3J_{\text{H-H}} = 7.1 \text{ Hz}$, 2H, H₁₃), 2.44 (t, $^3J_{\text{H-H}} = 7.8 \text{ Hz}$, 4H, H₂), 2.10 (s, 6H, H₁₀), 1.63 (quint, $^3J_{\text{H-H}} = 7.5 \text{ Hz}$, 4H, aliphatic chain), 1.23-1.30 (m, 44H, H₁₄, aliphatic chain), 0.86 (t, $^3J_{\text{H-H}} = 6.6 \text{ Hz}$, 6H, H₁).

$^{13}\text{C}\{^1\text{H}\}$ NMR (100 MHz, CDCl_3 , ppm): $\delta = 173.01$; 165.76; 155.92; 154.72; 154.34; 152.76; 122.18; 115.94; 106.04; 103.77; 96.75; 82.44; 82.33; 49.08; 32.63; 31.85; 30.58; 29.53; 29.39; 29.27; 29.10; 28.82; 26.83; 22.64; 22.23; 21.51; 18.21; 14.09.

MS (ESI(+)) = 1402.2 [M-Cl]⁺

UV-Vis (CH_2Cl_2 , $1.0 \times 10^{-5} \text{ M}$): $\lambda_{\text{max}} = 409 \text{ nm}$ ($\epsilon = 0.18 \times 10^5 \text{ M}^{-1} \cdot \text{cm}^{-1}$)

IR (KBr) (cm^{-1}) = 3421 (s, NH); 1698 (s, NH); 1658 (s, NH); 1585 (s, NH); 1255 (s, CN).

30

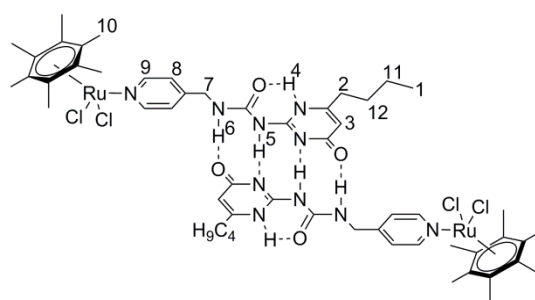
Yield = 95% (0.07 g)

^1H NMR (400 MHz, CDCl_3 , ppm): $\delta = 8.93$ (d, $^3J_{\text{H-H}} = 6.3$ Hz, 2H, H_9), 7.30 (d, $^3J_{\text{H-H}} = 5.7$ Hz, 2H, H_8), 5.83 (s, 2H, H_3), 5.43-5.47 (m, 4H, H_{11}), 5.22-5.33 (m, 4H, H_{12}), 4.46-4.50 (m, 2H, H_7), 2.95-3.02 (m, 2H, H_{13}), 2.45-2.49 (m, 4H, H_2), 2.09 (s, 6H, H_{10}), 1.27-1.41 (m, 20H, H_{14} , aliphatic chain), 0.92-0.95 (m, 6H, H_1).

$^{13}\text{C}\{^1\text{H}\}$ NMR (100 MHz, CDCl_3 , ppm): $\delta = 155.86$; 154.74; 154.33; 128.91; 126.22; 123.24; 103.69; 103.69; 102.00; 82.58; 82.22; 65.81; 32.31; 30.63; 22.79; 22.38; 22.21; 21.92; 18.23; 15.22; 13.97; 13.90; 13.64; 13.56.

MS (ESI(+)) = 1178.8 $[\text{M-Cl}]^+$

UV-Vis (CH_2Cl_2 , 5.0×10^{-5} M): $\lambda_{\text{max}} = 414$ nm ($\epsilon = 0.01 \times 10^5 \text{ M}^{-1} \cdot \text{cm}^{-1}$)



31

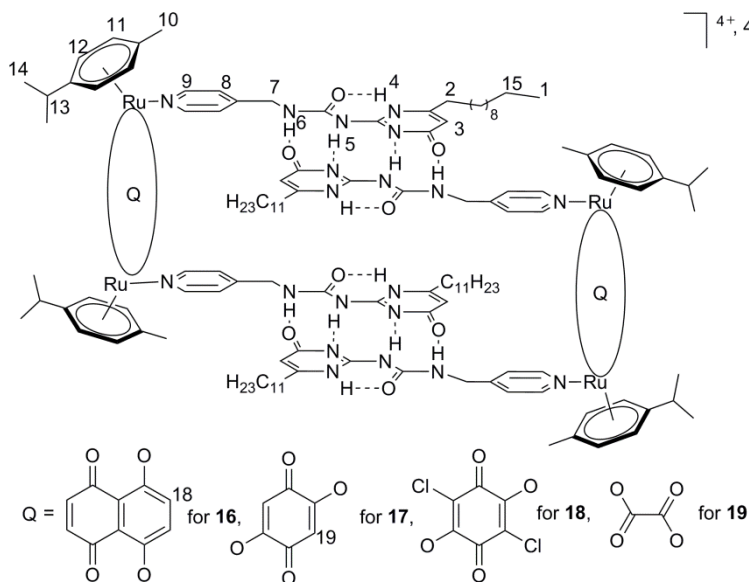
Yield = 90% (0.10 g)

^1H NMR (400 MHz, CDCl_3 , ppm): $\delta = 12.83$ (s, 2H, H_4), 12.11 (s, 2H, H_5), 11.06 (s, 2H, H_6), 8.65-8.70 (m, 4H, H_9), 7.14-7.30 (m, 4H, H_8), 5.80 (s, 2H, H_3), 5.54 (s, 4H, H_7), 2.45-2.55 (m, 4H, H_2), 1.97-2.13 (m, 36H, H_{10}), 1.60-1.65 (m, 4H, H_{11}), 1.30-1.37 (m, 4H, H_{12}), 0.86-0.97 (m, 6H, H_1).

$^{13}\text{C}\{^1\text{H}\}$ NMR (100 MHz, CDCl_3 , ppm): $\delta = 154.37$; 154.22; 123.27; 123.11; 101.75; 93.24; 92.43; 91.26; 91.22; 90.64; 89.54; 42.11; 32.39; 31.52; 29.09; 29.00; 28.86; 22.12; 22.08; 21.95; 21.88; 16.78; 16.29; 16.16; 15.86; 15.74; 15.61; 15.56; 15.40; 13.75; 13.66; 13.58.

MS (ESI(+)) = 1233.9 $[\text{M-Cl}]^+$

General procedure for cyclic tetramers (**16-19**, **21-24** and **26-29**): a mixture of one equivalent of Ru clip (**16**, **21**, **26**: **11** (0.04g, 0.06 mmol), **17**, **22**, **27**: **12** (0.04g, 0.06 mmol), **18**, **23**, **28**: **13** (0.04g, 0.06 mmol), **19**, **24**, **29**: **14** (0.04g, 0.06 mmol)) and three equivalents of AgCF₃SO₃ (0.04 g, 0.18 mmol) was stirred in methanol (4 mL) for **16** or CH₂Cl₂ (4 mL) for **17** at rt for 2h, after which the mixture was filtered. UPy derivative (**16-19**: **4** (0.04 g, 0.06 mmol), **21-24**: **5** (0.04 g, 0.06 mmol), **26-29**: **6** (0.05 g, 0.06 mmol)) was added to the filtrate and the mixture stirred overnight at rt. In case of MeOH, the solvent was evaporated and the residue was redissolved in CH₂Cl₂ (2 mL) and in the case of CH₂Cl₂ as solvent of reaction, the volume of the solvent was halved. Diethyl ether was added to precipitate the product, which was collected by filtration.

**16**

Yield = 23% (0.10 g)

¹H NMR (400 MHz, CD₃OD, ppm): δ = 8.34 (d, ³J_{H-H} = 5.8 Hz, 8H, H₉), 7.32 (d, ³J_{H-H} = 6.1 Hz, 8H, H₈), 7.17 (s, 8H, H₁₈), 5.90 (s, 4H, H₃), 5.80 (d, ³J_{H-H} = 6.1 Hz, 8H, H₁₂), 5.57 (d, ³J_{H-H} = 6.1 Hz, 8H, H₁₁), 4.54 (s, 8H, H₇), 2.79 (sept, ³J_{H-H} = 4.8 Hz, 4H, H₁₃), 2.57 (quint, ³J_{H-H} = 6.9 Hz, 8H, H₂), 2.07 (s, 12H, H₁₀), 1.64-1.71 (m, 8H, aliphatic chain), 1.26-1.31 (m, 88H, H₁₄, aliphatic chain), 0.87 (t, ³J_{H-H} = 6.0 Hz, 12H, H₁).

$^{13}\text{C}\{^1\text{H}\}$ NMR (100 MHz, CD_3CN , ppm): $\delta = 172.67; 170.71; 156.85; 154.31; 153.34; 151.64; 137.30; 125.87; 123.68; 122.68; 119.49; 111.38; 105.27; 103.32; 98.97; 83.88; 82.91; 41.42; 31.81; 31.65; 30.37; 29.29; 29.12; 28.83; 28.47; 26.36; 22.39; 21.27; 16.28; 13.40$.

MS (ESI(+)) = 1607.0 [M-2Tf] $^{2+}$

UV-Vis (CH_2Cl_2 , 3.6×10^{-6} M): $\lambda_{\text{max}} = 306$ nm ($\epsilon = 2.38 \times 10^5 \text{ M}^{-1} \cdot \text{cm}^{-1}$), 434 nm ($\epsilon = 1.66 \times 10^5 \text{ M}^{-1} \cdot \text{cm}^{-1}$), 639 nm ($\epsilon = 0.55 \times 10^5 \text{ M}^{-1} \cdot \text{cm}^{-1}$), 693 nm ($\epsilon = 0.62 \times 10^5 \text{ M}^{-1} \cdot \text{cm}^{-1}$)

IR (KBr) (cm^{-1}) = 3334 (s, NH); 1704 (s, NH); 1659 (s, NH); 1535 (s, NH); 1274 (s, CN).

17

Yield = 72% (0.12 g)

^1H NMR (400 MHz, CD_3CN , ppm): $\delta = 12.73$ (s, 4H, H_4), 11.98 (s, 4H, H_5), 11.06 (t, $^3J_{\text{H-H}} = 6.0$ Hz, 4H, H_6), 8.04-8.10 (m, 8H, H_9), 7.30-7.37 (m, 8H, H_8), 5.85-5.89 (m, 8H, H_{12}), 5.74 (s, 44H, H_{19}), 5.63-5.69 (m, 8H, H_{11}), 5.62 (s, 4H, H_3), 4.38 (d, $^3J_{\text{H-H}} = 5.1$ Hz, 8H, H_7), 2.82 (sept, $^3J_{\text{H-H}} = 5.6$ Hz, 4H, H_{13}), 2.44 (t, $^3J_{\text{H-H}} = 8.0$ Hz, 8H, H_2), 2.10 (s, 12H, H_{10}), 1.55-1.62 (m, 8H, aliphatic chain), 1.28-1.31 (m, 88H, H_{14} , aliphatic chain), 0.88 (t, $^3J_{\text{H-H}} = 6.0$ Hz, 12H, H_1).

$^{13}\text{C}\{^1\text{H}\}$ NMR (100 MHz, CD_3CN , ppm): $\delta = 183.53; 152.04; 128.57; 123.48; 122.43; 117.00; 83.08; 81.53; 31.66; 31.34; 30.79; 29.07; 28.96; 28.82; 28.69; 28.34; 26.23; 23.05; 22.11; 21.11; 16.99; 13.11$.

MS (ESI(+)) = 1557.1 [M-2Tf] $^{2+}$

UV-Vis (CH_2Cl_2 , 2.0×10^{-6} M): $\lambda_{\text{max}} = 299$ nm ($\epsilon = 3.64 \times 10^5 \text{ M}^{-1} \cdot \text{cm}^{-1}$), 496 nm ($\epsilon = 3.39 \times 10^5 \text{ M}^{-1} \cdot \text{cm}^{-1}$)

IR (KBr) (cm^{-1}) = 3330 (s, NH); 1700 (s, NH); 1659 (s, NH); 1521 (s, NH); 1257 (s, CN)

18

Yield = 72% (0.12 g)

^1H NMR (400 MHz, CD_3OD , ppm): $\delta = 8.24$ (d, $^3J_{\text{H-H}} = 5.8$ Hz, 8H, H_9), 7.44 (d, $^3J_{\text{H-H}} = 6.0$ Hz, 8H, H_8), 6.10 (d, $^3J_{\text{H-H}} = 6.1$ Hz, 8H, H_{12}), 5.91 (d, $^3J_{\text{H-H}} = 6.4$ Hz, 12H, H_{11} , H_3), 4.55 (s, 8H, H_7), 2.90 (sept, $^3J_{\text{H-H}} = 5.6$ Hz, 4H, H_{13}), 2.48-2.53 (m, 8H, H_2), 2.24 (s, 12H, H_{10}), 1.62-1.71 (m, 8H, aliphatic chain), 1.28-1.38 (m, 88H, H_{14} , aliphatic chain), 0.87-0.90 (m, 12H, H_1).

$^{13}\text{C}\{^1\text{H}\}$ NMR (100 MHz, CD_3OD , ppm): $\delta = 152.22$; 145.84; 135.10; 128.84; 126.16; 122.66; 119.47; 117.30; 84.94; 83.21; 82.76; 79.88; 33.39; 31.65; 31.20; 29.34; 29.11; 23.33; 22.41; 21.52; 19.92; 13.43; 13.38.

MS (ESI(+)) = 1625.0 $[\text{M}-2\text{Tf}]^{2+}$

UV-Vis (CH_2Cl_2 , 2.0×10^{-6} M): $\lambda_{\text{max}} = 324$ nm ($\epsilon = 2.27 \times 10^5 \text{ M}^{-1} \cdot \text{cm}^{-1}$), 508 nm ($\epsilon = 2.27 \times 10^5 \text{ M}^{-1} \cdot \text{cm}^{-1}$)

19

Yield = 38% (0.08 g)

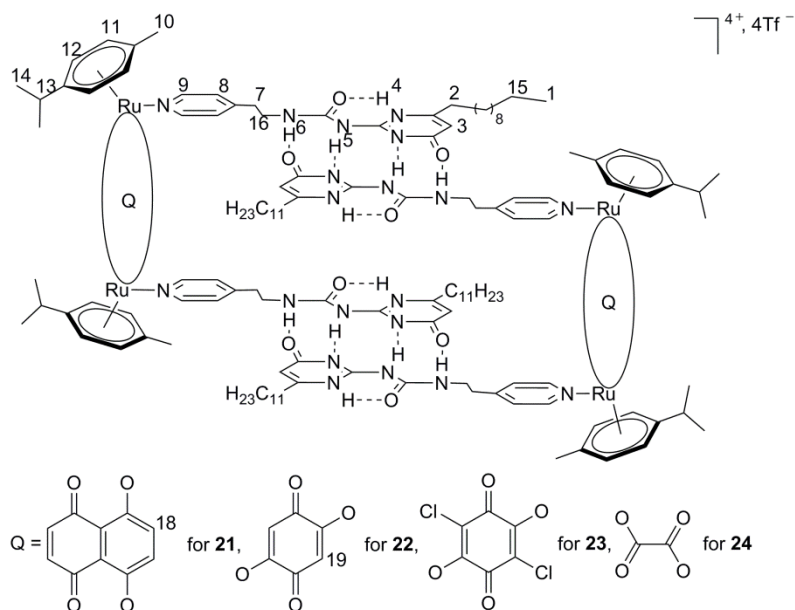
^1H NMR (400 MHz, CD_3CN , ppm): $\delta = 12.81$ (s, 4H, H_4), 12.06 (s, 4H, H_5), 10.98 (s, 4H, H_6), 8.29-8.38 (m, 8H, H_9), 7.85-7.88 (m, 8H, H_8), 5.66-5.81 (m, 12H, H_3 , H_{12}), 5.48-5.55 (m, 8H, H_{11}), 4.43-4.55 (m, 8H, H_7), 2.75-2.82 (m, 4H, H_{13}), 2.37-2.42 (m, 8H, H_2), 2.10 (s, 12H, H_{10}), 1.50-1.62 (m, 8H, aliphatic chain), 1.23-1.36 (m, 88H, H_{14} , aliphatic chain), 0.86 (t, $^3J_{\text{H-H}} = 8.0$ Hz, 12H, H_1).

$^{13}\text{C}\{^1\text{H}\}$ NMR (100 MHz, CD_3CN , ppm): $\delta = 172.81$; 170.59; 156.73; 154.38; 153.35; 151.61; 151.56; 123.56; 122.67; 119.48; 105.33; 101.72; 97.36; 82.18; 81.58; 31.90; 31.63; 30.88; 29.34; 29.24; 29.20; 29.08; 28.95; 28.64; 26.56; 22.38; 21.55; 21.43; 21.37; 21.24; 17.23; 13.39.

MS (ESI(+)) = 1507.1 $[\text{M}-2\text{Tf}]^{2+}$

UV-Vis (CH_2Cl_2 , 1.0×10^{-5} M): $\lambda_{\text{max}} = 383$ nm ($\epsilon = 0.28 \times 10^5 \text{ M}^{-1} \cdot \text{cm}^{-1}$)

IR (KBr) (cm^{-1}) = 3067 (s, NH); 1698 (s, NH); 1661 (s, NH); 1589 (s, NH); 1260 (s, CN).



Yield = 46% (0.10 g)

^1H NMR (400 MHz, CD_2Cl_2 , ppm): δ = 8.18 (d, $^3J_{\text{H-H}} = 5.6$ Hz, 8H, H_9), 7.23-7.25 (m, 8H, H_8), 7.15 (s, 8H, H_{19}), 5.60 (d, $^3J_{\text{H-H}} = 6.1$ Hz, 12H, H_{12} , H_3), 5.42 (d, $^3J_{\text{H-H}} = 6.0$ Hz, 12H, H_{11}), 3.30 (q, $^3J_{\text{H-H}} = 6.6$ Hz, 4H, H_{16}), 2.80-2.87 (m, 4H, H_{13}), 2.77 (q, $^3J_{\text{H-H}} = 6.7$ Hz, 4H, H_7), 2.47-2.54 (m, 4H, H_2), 2.07 (s, 12H, H_{10}), 1.27-1.34 (m, 88H, H_{14} , aliphatic chain), 0.89 (t, $^3J_{\text{H-H}} = 6.5$ Hz, 12H, H_1).

$^{13}\text{C}\{^1\text{H}\}$ NMR (100 MHz, CD_2Cl_2 , ppm): δ = 172.56; 171.51; 170.62; 156.24; 155.86; 154.50; 153.76; 153.00; 152.79; 152.21; 151.83; 151.65; 137.22; 136.83; 126.24; 126.05; 125.89; 122.70; 119.51; 112.23; 111.62; 105.18; 103.20; 103.03; 99.11; 98.31; 84.06; 83.70; 83.05; 82.76; 39.95; 34.45; 31.94; 31.71; 31.63; 30.40; 30.36; 29.42; 29.33; 29.23; 29.18; 29.15; 29.07; 29.01; 28.72; 28.46; 26.39; 22.45; 22.39; 21.29; 21.11; 16.30.

MS (ESI(+)) = 1635.1 $[\text{M}-2\text{Tf}]^{2+}$

UV-Vis (CH_2Cl_2 , 2.8×10^{-6} M): $\lambda_{\text{max}} = 310$ nm ($\epsilon = 2.56 \times 10^5 \text{ M}^{-1} \cdot \text{cm}^{-1}$), 435 nm ($\epsilon = 1.83 \times 10^5 \text{ M}^{-1} \cdot \text{cm}^{-1}$), 644 nm ($\epsilon = 0.55 \times 10^5 \text{ M}^{-1} \cdot \text{cm}^{-1}$), 696 nm ($\epsilon = 0.58 \times 10^5 \text{ M}^{-1} \cdot \text{cm}^{-1}$)

IR (KBr) (cm^{-1}) = 3336 (s, NH); 1710 (s, NH); 1659 (s, NH); 1535 (s, NH); 1274 (s, CN).

22

Yield = 65% (0.13 g)

^1H NMR (400 MHz, CD_3OD , ppm): δ = 8.17 (d, $^3J_{\text{H-H}} = 5.8$ Hz, 8H, H_9), 7.38 (d, $^3J_{\text{H-H}} = 5.7$ Hz, 8H, H_8), 6.01 (d, $^3J_{\text{H-H}} = 6.0$ Hz, 4H, H_{12}), 5.79 (d, $^3J_{\text{H-H}} = 6.1$ Hz, 12H, H_{11} , H_3), 3.13-3.23 (m, 8H, H_{16}), 2.83-2.90 (m, 4H, H_{13}), 2.57 (t, $^3J_{\text{H-H}} = 7.6$ Hz, 8H, H_7), 2.17 (s, 6H, H_{10}), 1.66-1.72 (m, 8H, aliphatic chain), 1.28-1.36 (m, 96H, H_{14} , aliphatic chain), 0.90 (t, $^3J_{\text{H-H}} = 6.5$ Hz, 12H, H_1).

$^{13}\text{C}\{^1\text{H}\}$ NMR (100 MHz, CD_3OD , ppm): δ = 153.78; 127.89; 123.44; 120.27; 84.79; 83.13; 33.11; 32.60; 30.79; 30.54; 23.78; 22.54; 14.49.

MS (ESI(+)) = 1585.1 $[\text{M}-2\text{Tf}]^{2+}$

UV-Vis (CH_2Cl_2 , 2.2×10^{-6} M): $\lambda_{\text{max}} = 497$ nm ($\epsilon = 2.23 \times 10^5 \text{ M}^{-1} \cdot \text{cm}^{-1}$)

IR (KBr) (cm^{-1}) = 3421 (s, NH); 1524 (s, NH); 1257 (s, CN)

23

Yield = 53% (0.11 g)

^1H NMR (400 MHz, CD_3CN , ppm): δ = 11.74 (s, 4H, H_5), 10.75 (s, 4H, H_6), 8.12 (d, $^3J_{\text{H-H}} = 5.9$ Hz, 8H, H_9), 7.30 (d, $^3J_{\text{H-H}} = 5.8$ Hz, 8H, H_8), 5.96 (d, $^3J_{\text{H-H}} = 6.3$ Hz, 8H, H_{12}), 5.76 (d, $^3J_{\text{H-H}} = 6.1$ Hz, 8H, H_{11}), 5.58 (s, 4H, H_3), 3.06-3.15 (m, 8H, H_{16}), 2.87 (sept, $^3J_{\text{H-H}} = 6.9$ Hz, 12H, H_{13} , H_7), 2.50 (t, $^3J_{\text{H-H}} = 7.6$ Hz, 8H, H_2), 2.10 (s, 12H, H_{10}); 1.64-1.66 (m, 8H, aliphatic chain); 1.29-1.38 (m, 88H, H_{14} , aliphatic chain), 0.90 (t, $^3J_{\text{H-H}} = 6.5$ Hz, 12H, H_1).

$^{13}\text{C}\{^1\text{H}\}$ NMR (100 MHz, CD_3CN , ppm): δ = 152.23; 128.57; 126.27; 122.43; 119.24; 83.09; 82.04; 31.36; 30.94; 29.07; 28.81; 28.76; 28.20; 26.13; 22.11; 21.05; 13.12.

MS (ESI(+)) = 1653.0 $[\text{M}-2\text{Tf}]^{2+}$

UV-Vis (CH_2Cl_2 , 2.1×10^{-5} M): $\lambda_{\text{max}} = 326$ nm ($\epsilon = 2.20 \times 10^5 \text{ M}^{-1} \cdot \text{cm}^{-1}$), 509 nm ($\epsilon = 2.25 \times 10^5 \text{ M}^{-1} \cdot \text{cm}^{-1}$)

IR (KBr) (cm^{-1}) = 3367 (s, NH); 1703 (s, NH); 1658 (s, NH); 1498 (s, NH); 1225 (s, CN).

24

Yield = 23% (0.09 g)

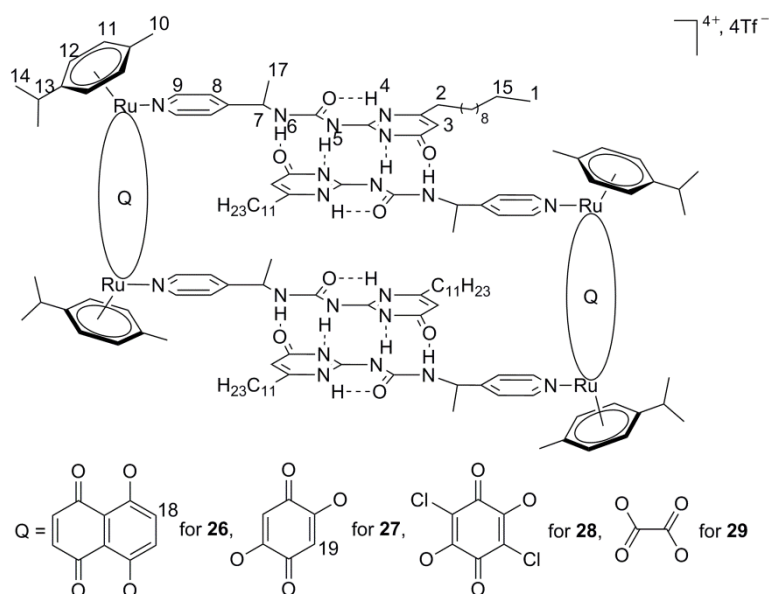
^1H NMR (400 MHz, CD_3OD , ppm): δ = 8.41 (d, $^3J_{\text{H-H}} = 5.8$ Hz, 8H, H_9), 7.50 (d, $^3J_{\text{H-H}} = 5.8$ Hz, 8H, H_8), 6.10 (s, 4H, H_3), 5.80 (d, $^3J_{\text{H-H}} = 5.9$ Hz, 8H, H_{12}), 5.58 (d, $^3J_{\text{H-H}} = 5.9$ Hz, 8H, H_{11}), 3.58 (t, $^3J_{\text{H-H}} = 6.6$ Hz, 8H, H_{16}), 3.00 (t, $^3J_{\text{H-H}} = 6.7$ Hz, 8H, H_7), 2.84 (sept, $^3J_{\text{H-H}} = 6.9$ Hz, 4H, H_{13}), 2.60 (t, $^3J_{\text{H-H}} = 7.7$ Hz, 8H, H_2), 2.13 (s, 12H, H_{10}), 1.64-1.68 (m, 8H, aliphatic chain), 1.28-1.40 (m, 88H, H_{14} , aliphatic chain), 0.90 (t, $^3J_{\text{H-H}} = 6.9$ Hz, 12H, H_1).

$^{13}\text{C}\{^1\text{H}\}$ NMR (100 MHz, CDCl_3 , ppm): δ = 166.16; 152.41; 127.65; 126.40; 118.76; 102.01; 97.31; 82.36; 80.46; 79.94; 77.48; 47.12; 46.90; 31.62; 29.28; 29.22; 29.14; 29.02; 28.93; 22.29; 21.19; 21.15; 16.50; 12.99.

MS (ESI(+)) = 1535.1 $[\text{M}-2\text{Tf}]^{2+}$

UV-Vis (CH_2Cl_2 , 1.0×10^{-5} M): $\lambda_{\text{max}} = 383$ nm ($\epsilon = 0.26 \times 10^5 \text{ M}^{-1} \cdot \text{cm}^{-1}$)

IR (KBr) (cm^{-1}) = 3338 (s, NH); 1706 (s, NH); 1657 (s, NH); 1632 (s, NH); 1258 (s, CN).



26

Yield = 21% (0.09 g)

^1H NMR (400 MHz, CD_3OD , ppm): δ = 8.38 (s, 8H, H_9), 7.40-7.44 (m, 8H, H_8), 7.15-7.18 (m, 8H, H_{18}), 5.81-5.89 (m, 12H, H_{12} , H_3), 5.56-5.59 (m, 12H, H_{11} , H_7), 2.79 (sept, $^3J_{\text{H-H}} = 7.2$ Hz, 4H, H_{13}), 2.46-2.52 (m, 8H, H_2), 2.07 (s, 12H, H_{10}), 1.46-1.63 (m, 20H, aliphatic chain, H_{17}), 1.26-1.36 (m, 88H, H_{14} , aliphatic chain), 0.86-0.91 (m, 12H, H_1).

$^{13}\text{C}\{^1\text{H}\}$ NMR (100 MHz, CD_3OD , ppm): δ = 153.00; 138.56; 123.42; 123.03; 120.26; 104.86; 100.85; 85.73; 83.95; 33.12; 33.08; 31.98; 30.73; 30.59; 30.49; 30.06; 23.80; 22.45; 17.35; 14.52.

MS (ESI(+)) = 1635.1 $[\text{M}-2\text{Tf}]^{2+}$

UV-Vis (CH_2Cl_2 , 3.1×10^{-6} M): $\lambda_{\text{max}} = 434$ nm ($\epsilon = 1.57 \times 10^5 \text{ M}^{-1} \cdot \text{cm}^{-1}$), 641 nm ($\epsilon = 0.51 \times 10^5 \text{ M}^{-1} \cdot \text{cm}^{-1}$), 693 nm ($\epsilon = 0.51 \times 10^5 \text{ M}^{-1} \cdot \text{cm}^{-1}$)

IR (KBr) (cm^{-1}) = 3286 (s, NH); 1703 (s, NH); 1659 (s, NH); 1532 (s, NH); 1275 (s, CN)

27

Yield = 61% (0.12 g)

^1H NMR (400 MHz, CD_3OD , ppm): δ = 8.21-8.26 (m, 8H, H_9), 7.44-7.49 (m, 8H, H_8), 5.93-6.00 (m, 12H, H_{12} , H_3), 5.74-5.79 (m, 12H, H_{11} , H_7), 2.86 (sept, $^3J_{\text{H-H}} = 7.7$ Hz, 4H, H_{13}), 2.47-2.53 (m, 4H, H_2), 2.17 (s, 12H, H_{10}), 1.52-1.66 (m, 20H, aliphatic chain, H_{17}), 1.29-1.35 (m, 88H, H_{14} , aliphatic chain), 0.87-0.91 (m, 12H, H_1).

$^{13}\text{C}\{^1\text{H}\}$ NMR (100 MHz, CD_3OD , ppm): δ = 185.48; 185.37; 154.15; 153.91; 153.85; 126.52; 125.02; 123.35; 120.18; 117.01; 105.06; 105.01; 104.78; 102.66; 99.87; 99.67; 84.76; 84.69; 83.58; 83.31; 83.18; 33.10; 33.07; 32.55; 30.79; 30.75; 30.66; 30.52; 30.49; 30.42; 30.11; 28.49; 23.77; 22.56; 22.51; 21.72; 18.20; 18.15; 14.49.

MS (ESI(+)) = 1585.1 $[\text{M}-2\text{Tf}]^{2+}$

UV-Vis (CH₂Cl₂, 2.2 x 10⁻⁶ M): λ_{max} = 298 nm (ϵ = 3.42 x 10⁵ M⁻¹·cm⁻¹), 496 nm (ϵ = 3.07 x 10⁵ M⁻¹·cm⁻¹)

IR (KBr) (cm⁻¹) = 3293 (s, NH); 1700 (s, NH); 1658 (s, NH); 1523 (s, NH); 1257 (s, CN).

28

Yield = 57% (0.12 g)

¹H NMR (400 MHz, CD₃OD, ppm): δ = 8.10-8.16 (m, 8H, H₉), 7.38-7.40 (m, 8H, H₈), 5.89-5.92 (m, 12H, H₁₂, H₃), 5.73-5.77 (m, 8H, H₁₁), 3.47-3.50 (m, 4H, H₇), 2.86 (sept, ³J_{H-H} = 6.0 Hz, 4H, H₁₃), 2.47-2.53 (m, 16H, H₂, H₁₆), 2.24 (s, 12H, H₁₀), 1.24-1.56 (m, 96H, H₁₄, aliphatic chain), 0.87-0.91 (m, 12H, H₁).

¹³C{¹H} NMR (100 MHz, CD₃OD, ppm): δ = 179.07; 153.80; 125.84; 125.34; 123.34; 120.17; 105.42; 84.74; 83.97; 33.11; 32.71; 30.74; 30.55; 30.02; 28.50; 23.76; 22.52; 21.64; 21.39; 18.20; 14.49.

MS (ESI(+)) = 1652.9 [M-2Tf]²⁺

UV-Vis (CH₂Cl₂, 2.3 x 10⁻⁶ M): λ_{max} = 325 nm (ϵ = 2.31 x 10⁵ M⁻¹·cm⁻¹), 506 nm (ϵ = 2.40 x 10⁵ M⁻¹·cm⁻¹)

IR (KBr) (cm⁻¹) = 3336 (s, NH); 1704 (s, NH); 1658 (s, NH); 1497 (s, NH); 1256 (s, CN).

29

Yield = 21% (0.09 g)

¹H NMR (400 MHz, CD₃OD, ppm): δ = 8.47 (d, ³J_{H-H} = 6.1 Hz, 8H, H₉), 7.55 (d, ³J_{H-H} = 6.0 Hz, 8H, H₈), 5.80-5.82 (m, 12H, H₁₂, H₃), 5.57 (d, ³J_{H-H} = 6.0 Hz, 8H, H₁₁), 2.86 (sept, ³J_{H-H} = 6.4 Hz, 12H, H₁₃, H₇), 2.52-2.61 (m, 8H, H₂), 2.29 (s, 12H, H₁₀), 1.52-1.63 (m, 20H, H₁₇, aliphatic chain), 1.28-1.40 (m, 88H, H₁₄, aliphatic chain), 0.88-0.91 (m, 12H, H₁).

$^{13}\text{C}\{^1\text{H}\}$ NMR (100 MHz, CD_3OD , ppm): $\delta = 154.25; 143.13; 125.92; 124.68; 123.38; 120.21; 103.59; 98.79; 83.79; 82.16; 81.18; 78.95; 33.07; 32.34; 30.73; 30.58; 30.48; 30.35; 30.04; 28.55; 23.74; 22.67; 22.65; 17.94; 14.46.$

MS (ESI(+)) = 1535.1 $[\text{M}-2\text{Tf}]^{2+}$

UV-Vis (CH_2Cl_2 , 1.0×10^{-5} M): $\lambda_{\text{max}} = 387$ nm ($\epsilon = 0.28 \times 10^5 \text{ M}^{-1} \cdot \text{cm}^{-1}$)

IR (KBr) (cm^{-1}) = 3276 (s, NH); 1660 (s, NH); 1633 (s, NH); 1242 (s, CN)

Chapter 3: Encapsulation of Anthracene-Core Dendrimers into Arene-Ru Metallo-Cycles

3.1 Introduction

3.1.1 Anthracene

Tricyclic aromatic hydrocarbon, anthracene, consists of a π electron cloud overlap that gives the molecule semiconductor properties. Anthracene is hence used as organic semiconductors for applications in organic solar cells and display devices like OLED (organic light-emitting diode).^[75] In the anthracene molecule, the 14 carbon atoms are not equivalent, with the “9” and “10” positions being the most reactive ones and therefore undergoing facile electrophilic substitutions. For instance, oxidation of anthracene gives anthraquinone, which is the starting material for the production of a large spectrum of dyes and pigments. Furthermore, 9,10-dibromoanthracene is one of the most common reactants employed to introduce the anthracene moiety in a molecule. With the availability of two reactive sites, 9,10-dibromoanthracene can undergo a number of organic transformations by reactions such as Suzuki coupling,^[76] click^[77] and Sonogashira coupling.^[78]

3.1.2 Suzuki Coupling Reaction

In 1979, Suzuki and co-workers published the successful cross coupling reaction of 1-alkenylboranes with 1-alkenyl halides, which had never been achieved before.^[79] This process, later termed the Suzuki coupling, is the reaction of organohalides or related electrophiles with organoboron reagents (Scheme 3.1). The coupling reaction was made possible by two important factors: (1) the use of palladium catalyst and (2) the introduction of a base in the reaction medium. Many Pd(0) catalysts have been used for Suzuki coupling reaction; Pd(PPh₃)₄, PdCl₂(PPh₃)₂ and Pd(OAc)₂ with PPh₃ being among the most common. The role played by the base is crucial because it speeds up the reaction and without a base, the reaction cannot occur. Hence, the choice of the appropriate base is fundamental for the success of the coupling reaction.^[79a] Moreover, it has been found that different halides give different reactivities since the relative reactivity of the halides decreases in the order: I > Br > Cl.^[80]

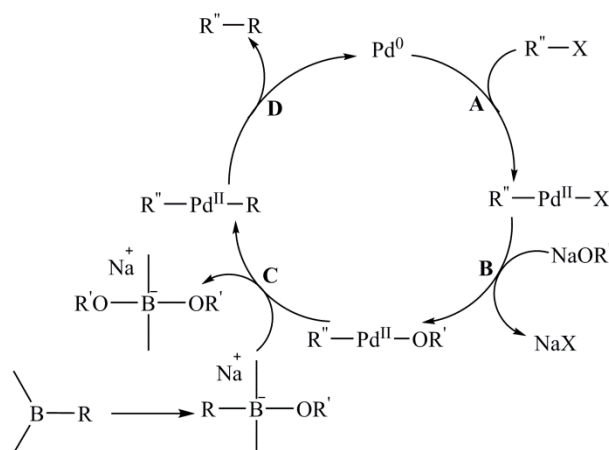
Suzuki coupling reaction provides many advantages that make it a crucial step in organic chemistry laboratories, including industries. The reaction is relatively simple, with readily available reagents, and is run under mild conditions. Furthermore, it is insensitive to the presence of water, highly tolerant of many functional groups on either coupling partners and is high yielding.^[79, 80b, 81] This straightforward methodology for various C-C bond formation is

also regio- and stereoselective, and all kinds of C-B bonds have been proven to undergo coupling reactions, including (sp³)C-B, (sp²)C-B and (sp)C-B bonds.^[81]

Experiments were carried out on the coupling reaction of alkenyl boranes and organohalides to study the mechanism of the reaction and a possible one was proposed as follows (Scheme 3.1):^[82]

- Step A: oxidative addition of the organic halide to the Pd(0) catalyst to generate Pd(II)R''X
- Step B: addition of a sodium alkoxide or hydroxide, resulting in the metathetical displacement of the halide ion from Pd(II)R''X to form an alkoxo- or hydroxopalladium(II) complex, Pd(II)R''OR'
- Step C: transmetalation of Pd(II)R''OR' with the alkenyl borane occurs, giving Pd(II)R''R
- Step D: reductive elimination of Pd(II)R''R giving the cross coupling product R''R and the catalyst is regenerated.

During the different steps, there is retention of configuration for alkenyl halide but in the case of allylic and benzylic halides, inversion of configuration occurs.^[80a, 82]



Scheme 3.1 Mechanism between alkenyl boranes (R-B(CH₃)₂) and organic halides (R''-X) catalysed by Pd(0) complexes and bases (NaOR')

Suzuki coupling reaction was used to functionalise anthracene derivatives. One example is the synthesis of 9,10-bis(1,2-diphenylstyryl)anthracene (BDSA) and 9,10-bis(4'-triphenylsilylphenyl)anthracene (BTSA), which contain anthracene as the main backbone and

1,2-diphenylstyryl or tetraphenylsilane as side units (Figure 3.1). BDSA and BTSA were used as blue-light emitting materials for deep blue OLEDs and one of the deepest blue for pure-blue emission was reported for OLEDs by these materials.^[76b]

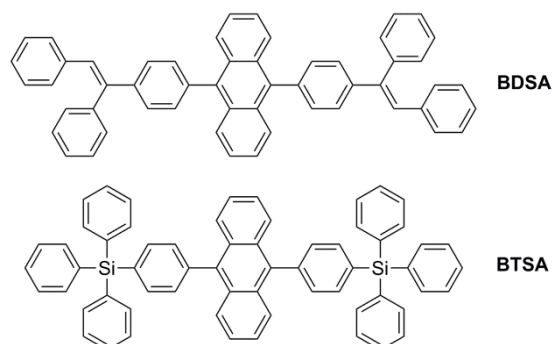


Figure 3.1 Structures of blue-light materials BDSA and DTSA

3.1.3 Click Chemistry

Click chemistry, termed by Sharpless *et al.* in 2001, is the assembly of two small units with heteroatom links; the reaction is versatile, efficient, high yielding with simple purification methods, stereospecific and conducted in easily removable solvents.^[83] Among the diverse examples of such reactions, Cu(I)-catalysed Huisgen 1,3-dipolar cycloaddition of azides and alkynes is one of the prime ones of click reaction.^[84] This reaction has drawn considerable attention because of the many advantages associated with it as compared to the thermal Huisgen reaction that requires elevated temperatures and is non-regioselective. Thus, on one hand, when the Cu-catalysed reaction is run under mild conditions it produces exclusively 1,4-disubstituted triazoles.^[85] On the other hand, click reactions catalysed by Ru complexes give the 1,5-disubstituted regioisomer.^[86]

Cu(I) catalysis has shown to boost the azide-alkyne cycloaddition reaction by being a fast, robust and regioselective method of synthesizing triazoles.^[87] Three sources of Cu(I) can be employed: (1) Cu(I) salts, (2) Cu(II) salts with a reducing agent and (3) oxidation of Cu(0) to Cu(I). Cu(II) salts are preferred because when used with a slight excess of the reducing agent, high level of Cu(I) is maintained at all times. One of the most common catalytic systems used is CuSO₄/sodium ascorbate because of the easy workup and the higher purity of the starting material.^[87-88]

The important features of click chemistry have made it useful in many fields and the reaction has found applications in supramolecular chemistry, medicinal chemistry and in making polymers, dendrimers and other complex structures.^[89] Moreover, obtaining highly functionalised 1,2,3-triazoles has given this heterocyclic scaffold various biological applications as well as in supramolecular and coordination chemistries.^[84a]

Many research groups have been working on understanding the mechanistic pathway of the Cu-catalysed azide-alkyne cycloaddition reaction. Combining computational and experimental studies, the mechanism can be suggested to proceed as described below (Scheme 3.2):^[84a]

Step A: Cu(I) undergoes π coordination with alkyne, increasing the CH acidity

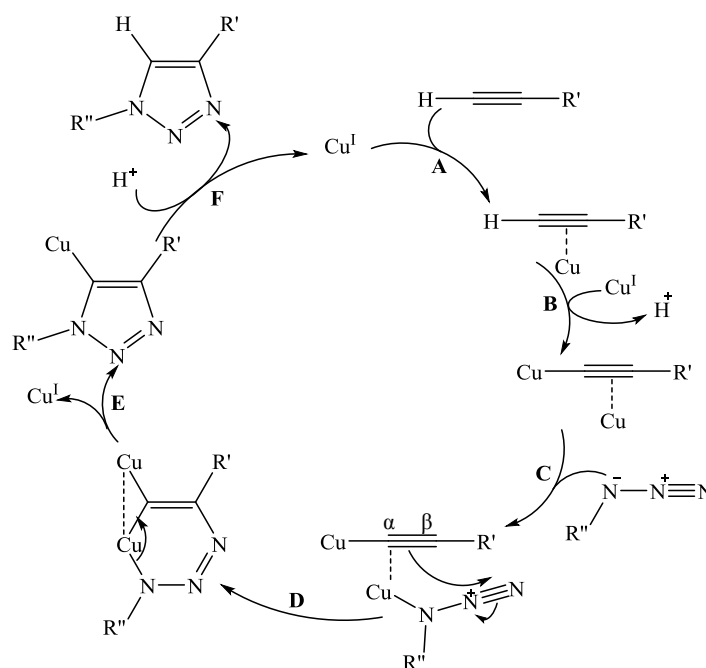
Step B: the rise in acidity allows the formation of a σ -coordinated Cu(I) acetylide alkyne and DFT calculations show that a second Cu(I) remains coordinated to the triple bond

Step C: coordination of an azide at the π -coordinated Cu(I) centre occurs

Step D: oxidative coupling

Step E: ring contraction and Cu(I)-bound exhaustion *via* reductive elimination

Step F: protonolysis of Cu(I) triazolide releasing free triazole and regenerating the Cu(I) catalyst



Scheme 3.2 Proposed mechanism of the copper catalysed azide-alkyne cycloaddition reaction.

Even if only few examples of click reaction in the chemistry of anthracene exist in literature, there are some interesting ones. For instance, a novel anthracene-based anion receptor was synthesised by click reaction done on 9-anthracenylmethyl azide with 5-*tert*-butyl-1,3-diethynylbenzene with $(\text{EtO}_3)\text{P}_3\cdot\text{CuI}$ as catalyst, followed by alkylation with trimethyloxonium tetrafluoroborate (Figure 3.2). The receptor, bearing two triazolium groups, is the first reported example of fluorescent triazolium receptor for anions.^[77b]

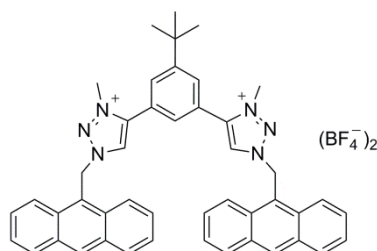


Figure 3.2 Anthracene-based anion receptor

3.1.4 Sonogashira Coupling Reaction

Sonogashira coupling reaction, discovered in 1975 by Sonogashira, Tohda and Hagihara, is a palladium catalysed sp^2 - sp coupling reaction between aryl or alkenyl halides or triflates and terminal alkynes, with or without Cu(I) co-catalyst in an amine solvent.^[90] Being one of the most popular ways of alkynylating aryl or alkenyl halides, Sonogashira coupling has been a crucial method in organic chemistry. In typical Sonogashira reactions, Cu(I) salts are used as co-catalyst as they accelerate the reaction by taking part in transmetalation of the alkynes, hence increasing the reactivity of the system, which allows room temperature alkynylation to take place. Yet, some shortcomings are associated with Cu(I) salts, one of which is the homocoupling of the terminal alkynes. In order to avoid the undesirable formation of the homocoupled products, the reaction has to be carried out in an oxygen-free atmosphere.^[91]

Some of the traditionally employed catalysts for the Sonogashira coupling reaction are the triphenylphosphane-based complexes $\text{Pd}(\text{PPh}_3)_4$ and $\text{Pd}(\text{PPh}_3)_2\text{Cl}_2$ and the bidentate ligand-based complexes like $\text{Pd}(\text{dppe})\text{Cl}_2$.^[91c] Hence, a broad spectrum of catalytical systems have been developed for this coupling reaction: (1) copper-free,^[92] (2) ligand-free Pd species,^[93] (3) non-Pd-based catalysts^[94] and (4) non-Cu-based co-catalysts.^[95] In spite of the wide range of catalytical systems and reaction conditions evaluated, the typical Sonogashira coupling conditions with Cu(I) co-catalyst are almost exclusively applied for all types of synthetic processes.^[91c]

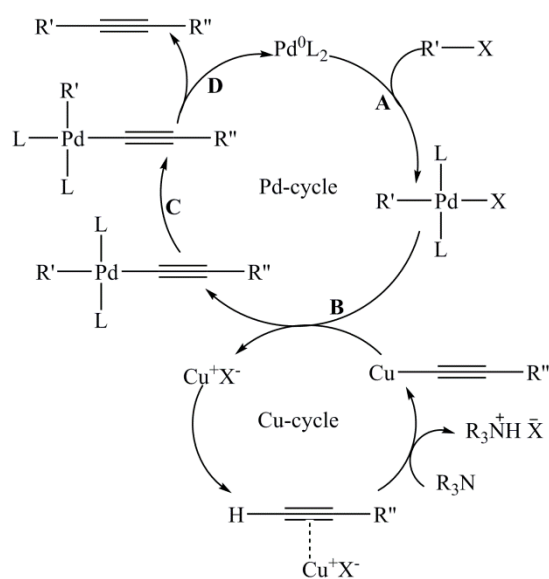
Even though the exact mechanism of the Sonogashira coupling with Pd/Cu catalytic system has not yet been fully understood, a possible one was established, proceeding *via* the “Pd-cycle” and the “Cu-cycle” (Scheme 3.3). The catalytically active Pd(0)L₂ species is first formed from either Pd(0) or Pd(II) complexes through the intermediate formation of a Pd(II)L₂(C≡CR'')₂ species that undergoes reductive elimination, generating Pd(0)L₂ and diyne.^[96] Also, the reduction of Pd(II) to Pd(0) can be made possible by amines *via* the formation of iminium cations.^[97] Once the activated catalyst is obtained, the mechanistic cycle is ready to start:

Step A: oxidative addition of the aryl or alkenyl halide to form Pd(II)R'L₂X

Step B: transmetalation of Pd(II)R'L₂X with a copper acetylide formed in the “Cu-cycle” into Pd(II)L₂R' (C≡CR'')

Step C: *cis/trans* isomerization

Step D: reductive elimination to form the desired alkyne with regeneration of the catalyst.



Scheme 3.3 Proposed mechanism for typical Pd/Cu catalysed Sonogashira coupling reaction

The oxidative addition is the rate determining step and the reactivity of different sp² species were found to vary: alkenyl substrates are more reactive than aryls and the halides affect the reactivity in the general order of reactivity of: RI > RBr > RCl. Furthermore, the base is believed to take part in the “Cu-cycle” in the formation of the copper acetylide. The base helps in the π-alkyne copper complex by making the alkyne terminal proton more acidic.^[91b]

Sonogashira coupling has been used in the functionalisation of anthracene molecules for different applications.^[78] One example is the synthesis of oligomers consisting of anthracene core unit and 4-alkylethynylbenzene end-capper (Figure 3.3). These oligomers show good thermal stability and high oxidation potentials, making them good candidates for organic field-effect transistors (OFETs) that are used in low-cost electronic devices and for their integrated circuits.^[98]

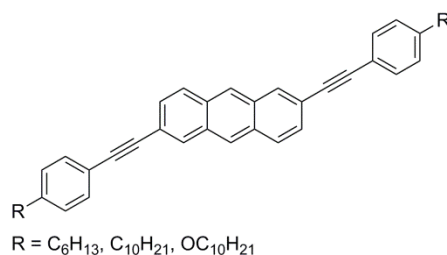


Figure 3.3 4-Alkylethynylbenzene end-capped oligomers of anthracene

3.2 Aim

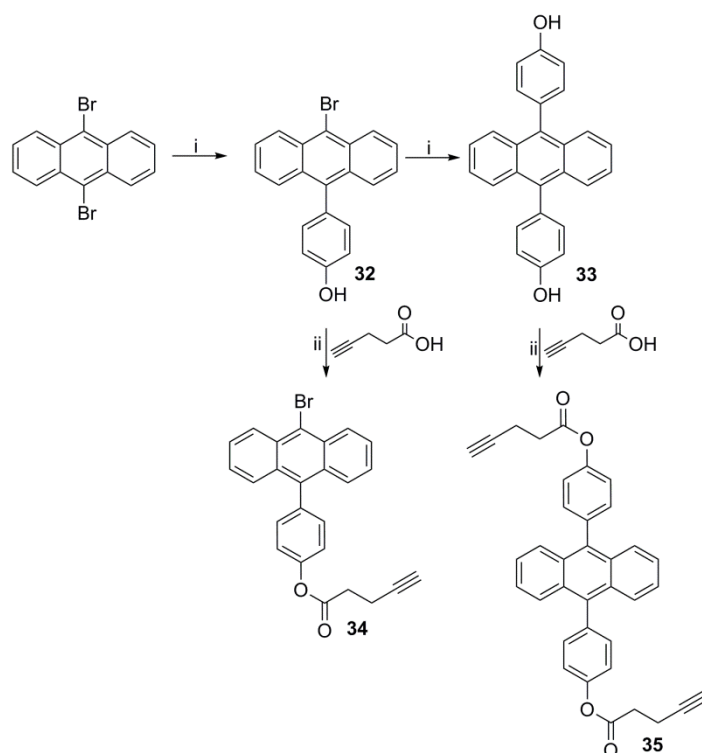
Anthracene can be used as the backbone for macromolecules because of the ease of functionalising the molecule. Hence, the introduction of dendrimers was envisaged onto anthracene in order to produce bis-functional anthracene-core dendrimers. Since the anthracene core is aromatic and planar, it can take part in π - π interactions making encapsulation into cages possible. Thus, the goal of the project is to synthesise anthracene-core dendrimers, to encapsulate them into arene-Ru cages, to study their interactions with the cages and to evaluate any potential anticancer activities of the organic molecules and the encapsulated systems.

3.3 Synthesis

3.3.1 Synthesis of Anthracene Compounds

The first step is a Suzuki coupling reaction on a 9,10-dibromoanthracene that was first reacted with 4-hydroxyphenylboronic acid in the presence of Pd(PPh₃)₄ and sodium carbonate in dry THF under reflux overnight (Scheme 3.4). After purification by extraction and column chromatography, the mono-functionalised product **32** was isolated as a yellow solid. Since double functionalisation could not be done in one step, compound **32** was reacted under the same conditions as the previous reaction to afford the disubstituted product **33** that was obtained as a yellow fluorescent solid.

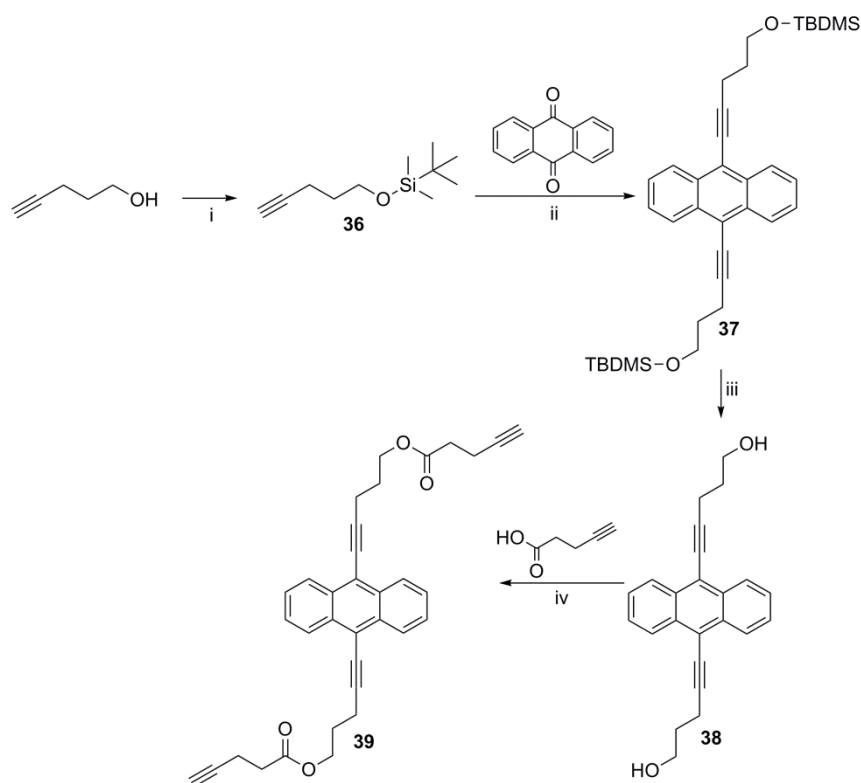
The mono- and disubstituted compounds, **32** and **33**, were esterified with 4-pentynoic acid in the presence of *N,N'*-dicyclohexylcarbodiimide (DCC) and 4-(dimethylamino)pyridinium *p*-toluenesulfonate (DPTS) in dry CH_2Cl_2 to give the mono- and diester **34** and **35**, respectively.^[99] Compound **35** was obtained in a low yield since the monoester was also formed during the reaction (Scheme 3.4). Compounds **32-35** were all found to readily undergo degradation and were therefore kept in the dark and at reduced temperatures. Because of the problem occurring during the following step of the reaction, as will be discussed in section 4.3.2 below, modifications had to be brought to the structure of the molecule.



Scheme 3.4 Synthesis of mono- and disubstituted anthracene compounds **34** and **35**. Reagents and conditions: i. 4-hydroxyphenylboronic acid, $\text{Pd}(\text{PPh}_3)_4$, Na_2CO_3 , THF, reflux, 16h, **32**: 66%, **33**: 62%, ii. DCC, DPTS, CH_2Cl_2 , 0°C to rt, 16h, **34**: 80%, **35**: 21%

The second series of ligand was synthesised by functionalising anthraquinone instead of 9,10-dibromoanthracene as described in Scheme 3.5. The first step involves the protection of the alcohol group of 4-pentyn-1-ol with *tert*-butyldimethylsilyl chloride (TBDMSCl) in the presence of triethylamine to give **36** as a colourless liquid.^[100] Upon addition of *n*-butyllithium (*n*-BuLi) to a solution of **36** in dry THF at 0°C , the solution turned from colourless to slightly yellow, forming a pentynyllithium intermediate. Anthraquinone was then added to the mixture and the solution turned rust-colour. After overnight stirring, wet

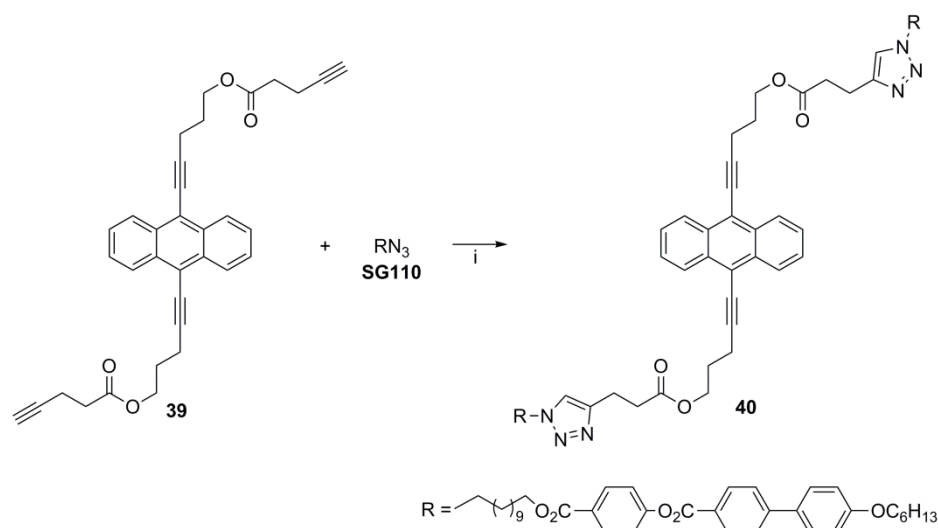
THF and stannous chloride ($\text{SnCl}_2 \cdot 2\text{H}_2\text{O}$) were added and deoxygenation took place.^[101] The dipentynyl substituted anthracene product **37** was isolated clean after extraction and two column chromatographies. Deprotection of the alcohol groups on **37** using tetrabutylammonium fluoride (TBAF) in THF from 0°C to room temperature results in diol **38**, purified by extraction and column chromatography (Scheme 3.5).^[102]



Scheme 3.5 Synthesis of compound **39**. Reagents and conditions: i. TBDMSCl, NEt_3 , CH_2Cl_2 , rt, 16h, 80%, ii. $n\text{-BuLi}$, $\text{SnCl}_2 \cdot 2\text{H}_2\text{O}$, THF, rt, 16h, 80%, iii. TBAF, THF, 0°C to rt, 2h, 70%, iv. EDC, DPTS, CH_2Cl_2 , 0°C to rt, 16h, 76%

Esterification of **38** with pentynoic acid in the presence of *N*-(3-dimethylaminopropyl)-*N'*-ethylcarbodiimide (EDC) and DPTS in dry CH_2Cl_2 gave diester **39**, which was isolated by extraction, column chromatography and recrystallization from heptane. A Huisgen 1,3-dipolar cycloaddition click reaction was then run on **39**, bearing two terminal alkyne groups, with a dendron having a terminal azide group, **SG110** (**SG110**, compound synthesised by Sebastiano Guerra) using CuSO_4 /sodium ascorbate catalytic system in THF/ H_2O mixture (Scheme 3.6).^[83, 84b, 84c, 84e, 85, 87-88] Reaction was run overnight, at room temperature, with the reaction mixture changing from yellow to pale yellow with blue deposit. After extraction, column

chromatography and recrystallization from acetone, the yellow product **40** was isolated in high yield.



Scheme 3.6 Synthesis of compound **40**. Reagents and conditions: i. CuSO_4 , NaAsc, THF/ H_2O , rt, 16h, 90%

As will be shown by the ^1H NMR data in section 3.4.1 below, compound **40** is very unstable and degradation takes place during the purification process. Two possible reasons for the degradation of the compound are: (1) the endoperoxide formation^[103] or (2) the photodimerization of the anthracene,^[104] both occurring at the 9 and 10 positions (Figure 3.4). The reason behind the degradation is the labile double bonds at these two positions of the anthracene. Even though the alkyne groups are supposed to stabilise these positions,^[105] degradation of the compound appears to be inevitable for this particular system.

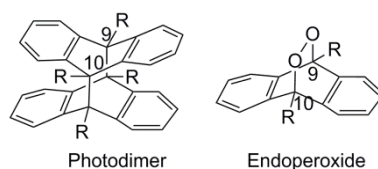
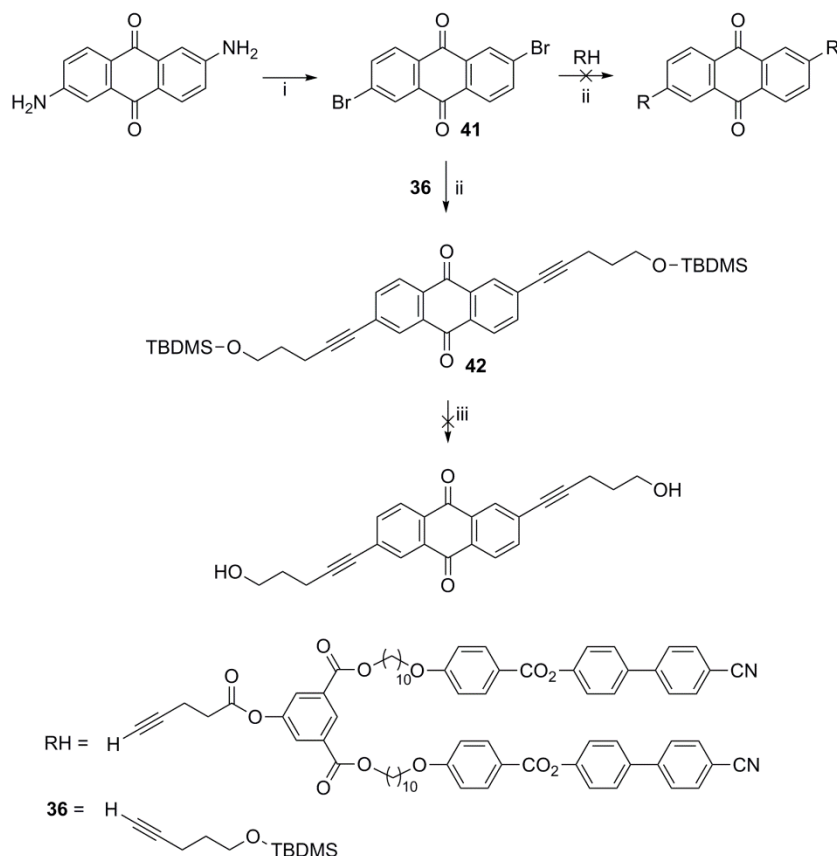


Figure 3.4 Structure of photodimer and endoperoxide from anthracene

To avoid the above problem, another anthracene core was chosen that does not possess any labile double bonds at the 9 and 10 positions. Therefore, anthraquinone, being a good substitute for anthracene, was used as starting material. Substitution of both amine groups by bromides on the anthraquinone derivatives was first carried out successfully using CuBr_2 and

tert-butyl nitrite (*t*BuONO) in refluxing acetonitrile for 2h (Scheme 3.7).^[106] Compound **41** was obtained as a yellow powder and was used for the next step, which is a Sonogashira coupling with **36** using a Pd(PPh₃)₄/CuI catalytic system in NEt₃/CH₂Cl₂ (3:1 ratio) at 60°C overnight. After column chromatography and washing the solid with warm methanol, clean product **42** was obtained in a good yield. The deprotection of the TBDMS group by TBAF with and without the use of acetic acid did not give the diol. Another attempt was made by direct Sonogashira coupling of **41** with a bismesogenic compound (RH) bearing a terminal alkyne, but isolation of the pure product failed after several column chromatographies (Scheme 3.7). Efforts made to recrystallise the pure products also failed due to rapid degradation of the compounds.

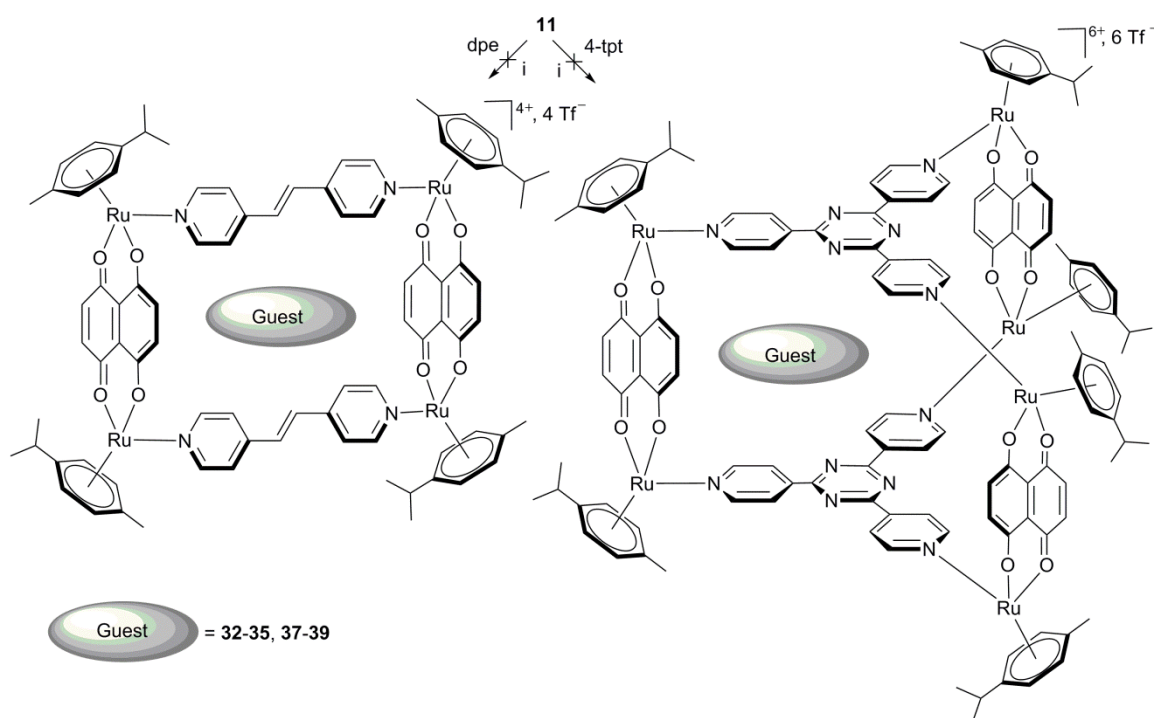


Scheme 3.7 Synthesis of 2,6-disubstituted anthracene compound **42**. Reagents and conditions: i. *t*BuONO, CuBr₂, CH₃CN, reflux, 2h, 70%, ii. Pd(PPh₃)₄, CuI, NEt₃/CH₂Cl₂ (3:1), 60°C, 16h, 83%, iii. TBAF, acetic acid, THF, 0°C to rt

3.3.2 Carceplex Assemblies

Since the anthracene-core is the part that should get encapsulated in the cage, reactions to encapsulate the mono- and disubstituted anthracene derivatives **32-35** were carried out

(Scheme 3.8). The reactions involved the carceplex assemblies, whereby the naphthoquinone Ru clip derivative, **11** (see Chapter 2 section 2.2.2) was first mixed with silver triflate in methanol for 2h. Mixture was then filtered and the spacer ligands, 2,4,6-tri(pyridine-4-yl)-1,3,5-triazine (tpt) or 1,2-bis(4-pyridyl)ethylene (dpe), and the guest molecule were added to the mixture and heated under reflux overnight for two days. After workup, it was found that encapsulation by carceplex of the first series of ligands failed, most probably due to the geometry of the molecule. The phenyl rings on either side of the anthracene core are believed to be perpendicular to the anthracene plane, therefore causing obstruction when attempting to build a cage around the molecule. In the second series of ligands, encapsulation of **37-39** was not possible into both hexanuclear (metallo-prism) and tetranuclear (metallo-rectangle) Ru cages because of the rapid degradation of the molecules. Since the degradation into either the endoperoxide or the photodimer disrupts the planarity of the molecules, entrapment into the cages becomes difficult.



Scheme 3.8 Encapsulation of guest molecules **32-35**, **37-39** into tetra- and hexanuclear Ru cages. Reagents and conditions: i. AgCF₃SO₃, guest (**32-35**, **37-39**), MeOH, reflux, 2 days

3.4 Characterization

3.4.1 Proton NMR Spectroscopy

Comparing **34** to **35**, a major upfield shift of H₁ proton from 8.60 to 7.69 ppm can be observed as a result of substitution of the bromide with a phenol group (Figure 3.5). Moreover, in **34**, H₁ protons appear as a doublet while in **35**, the same peak is doublet of doublets, due to the change in symmetry, as seen in Figure 3.5. On the other hand, when an alkyne group is attached to the anthracene instead of the phenol, the peak of the H₁ protons undergoes a downfield shift. Hence, H₁ protons in compound **35** appear at 7.70 ppm and are visible at 8.55 ppm in **38**. Also a slight upfield shift from 8.60 to 8.55 ppm is observed when comparing H₁ protons of compounds **34** and **38** caused by the replacement of the bromide by an alkyne group (Figure 3.5).

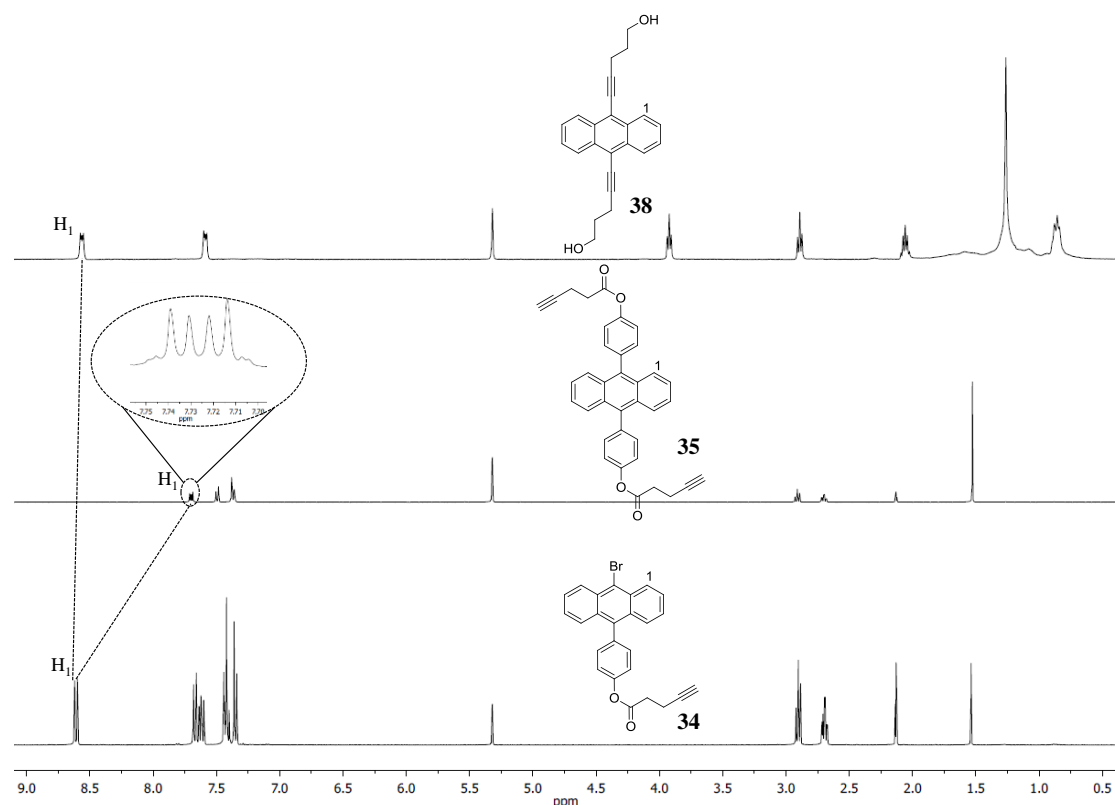


Figure 3.5 ¹H NMR spectra (400 MHz, CD₂Cl₂) of **34**, **35** and **38**

In the case of compound **40**, an unexpected phenomenon is observed from the different ¹H NMR spectra measured at different time intervals (Figure 3.6). The relative integrations of the peaks of the anthracene moiety to those of the dendron moiety were found to change with time. For instance, comparing H₁ to H₁₅ protons, the relative integrations for the peaks are changing, with the intensity of the H₁ proton decreasing with time (Figure 3.6). The change is

clearly seen for the aromatic protons. However, the aliphatic protons are more difficult to compare because of the poor resolution of the peaks.

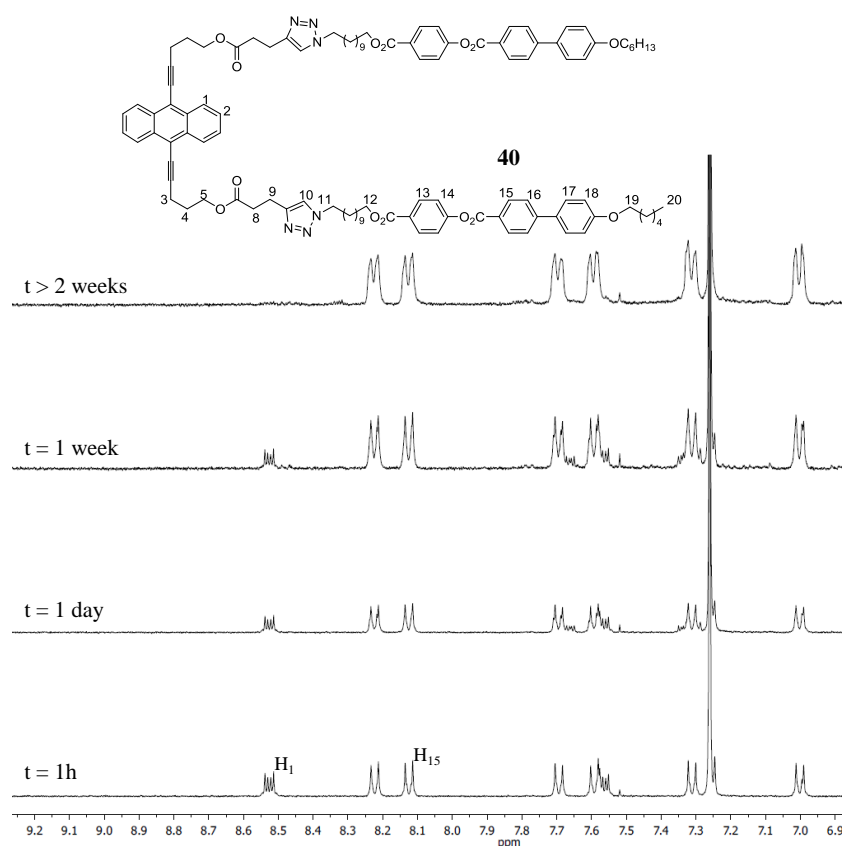
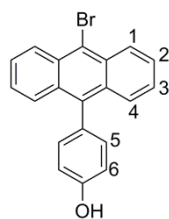


Figure 3.6 ^1H NMR spectra (400 MHz, CDCl_3) of **40** at different time intervals

3.5 Conclusion

Suzuki coupling, click and Sonogashira coupling reactions have been employed successfully in functionalising anthracene derivatives under typical reaction conditions. The Suzuki coupled products, which were the most stable anthracene derivatives synthesised, did not possess the correct geometry for encapsulation in the arene-Ru cages used. The click product showed very low stability, as was observed by the ^1H NMR spectroscopy and hence could not be used for encapsulation. Sonogashira coupling reaction on **41** gave the desired product **42**, but failure to deprotect the alcohol groups prevented further steps of the synthesis to be carried out. Therefore it can be concluded that anthracene-core dendrimers could not be synthesised due to stability problems and the reactions might be successful provided the environment under which the reactions are carried out is completely inert and oxygen-free.

3.6 Experimental Part

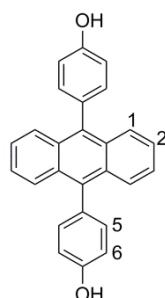
**32**

An aqueous solution of Na_2CO_3 (2M, 20 mL) was added to a THF solution of 9,10-dibromoanthracene (0.10 g, 0.30 mmol) under argon. 4-Hydroxyphenylboronic acid (0.08 g, 0.60 mmol) and $\text{Pd}(\text{PPh}_3)_4$ (0.06 g, 0.06 mmol) were added to the mixture and stirred under reflux. After overnight reaction, the mixture was allowed to cool to rt, then diethyl ether (40 mL) was added and brine was used to wash the mixture. The organic layer was washed with water and dried over MgSO_4 . The crude product obtained after evaporation of solvent was purified by CC (eluent CH_2Cl_2). **32** was obtained as a yellow powder with a yield of 66% (0.07 g).

^1H NMR (400 MHz, CDCl_3 , ppm): $\delta = 8.59$ (dt, $^3J_{\text{H-H}} = 8.9$ Hz, $^4J_{\text{H-H}} = 1.0$ Hz, 2H, H_1), 7.71 (dt, $^3J_{\text{H-H}} = 8.8$ Hz, $^4J_{\text{H-H}} = 1.0$ Hz, 2H, H_4), 7.59 (ddd, $^3J_{\text{H-H}} = 8.8$, 6.5 Hz, $^4J_{\text{H-H}} = 1.2$ Hz, 2H, H_2), 7.38 (ddd, $^3J_{\text{H-H}} = 8.8$, 6.5 Hz, $^4J_{\text{H-H}} = 1.2$ Hz, 2H, H_3), 7.28 (d, $^3J_{\text{H-H}} = 8.6$ Hz, 2H, H_5), 7.06 (d, $^3J_{\text{H-H}} = 8.6$ Hz, 2H, H_6).

$^{13}\text{C}\{^1\text{H}\}$ NMR (100 MHz, CDCl_3 , ppm): $\delta = 155.19$; 137.49; 132.45; 131.39; 130.68; 130.29; 127.87; 127.44; 126.94; 125.50; 122.63; 115.41.

MS (ESI(-)): 349.0 $[\text{M-H}]^-$

**33**

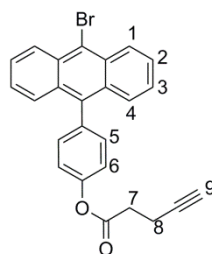
32 (0.17 g, 0.50 mmol), Na_2CO_3 (2M, 20 mL), 4-hydroxyphenylboronic acid (0.23 g, 1.00 mmol) and $\text{Pd}(\text{PPh}_3)_4$ (0.11 g, 0.10 mmol) were reacted in dry THF (80 mL) following similar

procedure as for **32**. After purification on two CC (eluent CH₂Cl₂/EtOAc 10/0.5), **33** was obtained as a yellow powder with a yield of 62% (0.11 g).

¹H NMR (400 MHz, CD₃OD, ppm): δ = 7.68 (dd, ³J_{H-H} = 6.8 Hz, ⁴J_{H-H} = 3.3 Hz, 4H, H₁), 7.29 (dd, ³J_{H-H} = 6.9 Hz, ⁴J_{H-H} = 3.3 Hz, 4H, H₂), 7.21-7.24 (m, 4H, H₅), 7.03-7.06 (m, 4H, H₆).

¹³C{¹H} NMR (100 MHz, CD₃OD, ppm): δ = 158.17; 138.21; 133.40; 131.65; 131.19; 128.01; 125.81; 116.35.

MS (ESI(+)): 362.3 [M+H]⁺



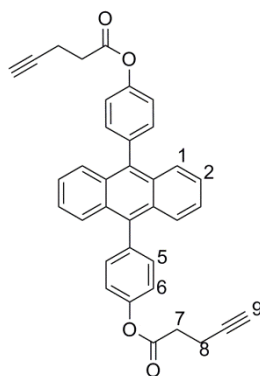
34

To a solution of **32** (0.10 g, 0.30 mmol) and 4-pentynoic acid (0.03 g, 0.30 mmol), in dry CH₂Cl₂ (50 mL) at 0°C, were added DCC (0.29 g, 1.40 mmol) and DPTS (0.08 g, 0.30 mmol). The mixture was stirred under argon, with the temperature rising gradually to rt. After overnight stirring, the solvent was evaporated and the crude product was purified on CC (eluent CH₂Cl₂/heptane 10/3.8). **34** was obtained as a shiny pale yellow solid with a yield of 80% (0.99 g).

¹H NMR (400 MHz, CD₂Cl₂, ppm): δ = 8.60 (dt, ³J_{H-H} = 8.9 Hz, ⁴J_{H-H} = 1.0 Hz, 2H, H₁), 7.67 (dt, ³J_{H-H} = 8.8 Hz, ⁴J_{H-H} = 1.0 Hz, 4H, H₄, H₅), 7.34-7.45 (m, 6H, H₂, H₃, H₆), 2.90 (t, ³J_{H-H} = 7.3 Hz, 2H, H₇), 2.67 (td, ³J_{H-H} = 7.4 Hz, ⁴J_{H-H} = 2.7 Hz, 2H, H₈), 2.12 (t, ³J_{H-H} = 2.6 Hz, 1H, H₉).

¹³C{¹H} NMR (100 MHz, CD₂Cl₂, ppm): δ = 170.72; 150.80; 137.21; 136.28; 132.54; 131.46; 130.57; 128.07; 127.59; 127.46; 126.14; 123.09; 122.08; 82.60; 69.53; 33.94; 14.80.

MS (ESI(+)): 453.1 [M+Na]⁺

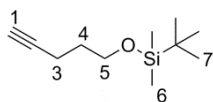
**35**

To a stirring solution of **33** (0.10 g, 0.20 mmol) and 4-pentynoic acid (0.05 g, 0.50 mmol) in dry CH_2Cl_2 (50 mL) at 0°C , were added EDC (0.23 mL, 1.30 mmol) and DPTS (0.08 g, 0.20 mmol). After overnight stirring with the temperature rising gradually to rt, the reaction mixture was washed three times with water. The organic phase was dried over MgSO_4 and the solvent removed. Purification was done by CC (eluent CH_2Cl_2 /heptane 10/3.8) and **35** was obtained as a shiny pale yellow solid with a yield of 21% (0.02 g).

^1H NMR (400 MHz, CD_2Cl_2 , ppm): $\delta = 7.69$ (dd, $^3J_{\text{H-H}} = 6.8$ Hz, $^4J_{\text{H-H}} = 3.3$ Hz, 4H, H_1), 7.54-7.50 (m, 4H, H_5), 7.37-7.42 (m, 8H, H_2 , H_6), 2.91 (t, $^3J_{\text{H-H}} = 7.1$ Hz, 4H, H_7), 2.73 (td, $^3J_{\text{H-H}} = 7.3$ Hz, $^4J_{\text{H-H}} = 2.7$ Hz, 4H, H_8), 2.12 (t, $^3J_{\text{H-H}} = 2.7$ Hz, 2H, H_9).

$^{13}\text{C}\{^1\text{H}\}$ NMR (100 MHz, CD_2Cl_2 , ppm): $\delta = 170.76$; 150.64; 136.94; 136.66; 132.68; 130.32; 127.13; 125.63; 122.05; 82.62; 69.50; 33.95; 14.81.

MS (ESI(+)): 545.3 $[\text{M}+\text{Na}]^+$

**36**

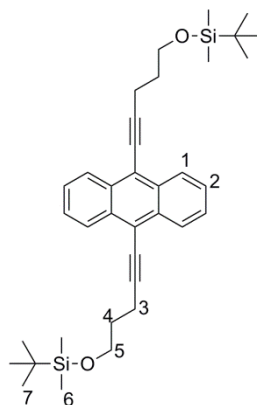
To a solution of 4-pentyn-1-ol (1.3 mL, 14.00 mmol), DMAP (0.08 g, 0.70 mmol) and triethylamine (2.38 mL, 16.80 mmol) in dry CH_2Cl_2 (100 mL), was added dropwise a solution of TBDMSCl (2.52 g, 16.80 mmol) in dry CH_2Cl_2 (50 mL). The mixture was stirred under argon at rt. After overnight reaction, extraction was done three times with brine. The aqueous layer was then washed three times with heptane. The combined organic phase was dried over

MgSO₄ and the solvent removed. The crude product was purified by CC (eluent heptane/CH₂Cl₂ 10/5) and **36** was obtained as a colourless liquid with a yield of 80% (2.21 g).

¹H NMR (400 MHz, CDCl₃, ppm): δ = 3.70 (t, ³J_{H-H} = 6.1 Hz, 2H, H₅), 2.27 (td, ³J_{H-H} = 7.1 Hz, ⁴J_{H-H} = 2.7 Hz, 2H, H₃), 1.92 (t, ³J_{H-H} = 2.7 Hz, 1H, H₁), 1.74 (quint, ³J_{H-H} = 7.1 Hz, 2H, H₄), 0.89 (s, 9H, H₇), 0.05 (s, 6H, H₆).

¹³C{¹H} NMR (100 MHz, CDCl₃, ppm): δ = 68.24; 61.47; 50.89; 31.53; 25.94; 14.85; -5.34.

MS (ESI(+)): 419.8 [2M+Na]⁺



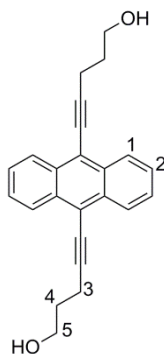
37

To a solution of **36** (2.38 g, 12.00 mmol) in dry THF (75 mL) at 0°C under argon was added an excess of ⁿBuLi (5.5 mL, 13.75 mmol) through a septum. The mixture was stirred at 0°C for 20 min during which the reaction mixture changed colour from colourless to slightly yellow. Anthraquinone (0.41 g, 2.00 mmol) was then added to the mixture and stirring was continued at rt overnight. The solution turned rust-red in colour upon the addition of anthraquinone. Wet THF (25 mL) was added after overnight stirring, followed by SnCl₂·2H₂O (0.90 g, 4.00 mmol). The mixture was further stirred for 30 min. After the reaction was over, the mixture was poured into hexane and extraction was done two times with 10% HCl and four times with water. The organic layer was dried over MgSO₄ and the solvent evaporated. Purification by two CC (eluent heptane/CH₂Cl₂ 10/5) gave **37** as a colourless liquid with a yield of 80% (0.91 g).

^1H NMR (400 MHz, CDCl_3 , ppm): $\delta = 8.55$ (dd, $^3J_{\text{H-H}} = 6.7$ Hz, $^4J_{\text{H-H}} = 3.3$ Hz, 4H, H_1), 7.54 (dd, $^3J_{\text{H-H}} = 6.7$ Hz, $^4J_{\text{H-H}} = 3.3$ Hz, 4H, H_2), 3.91 (t, $^3J_{\text{H-H}} = 6.1$ Hz, 4H, H_5), 2.85 (t, $^3J_{\text{H-H}} = 7.0$ Hz, 4H, H_3), 2.02 (quint, $^3J_{\text{H-H}} = 6.7$ Hz, 4H, H_4), 0.94 (s, 18H, H_7), 0.11 (s, 12H, H_6).

$^{13}\text{C}\{^1\text{H}\}$ NMR (100 MHz, CDCl_3 , ppm): $\delta = 132.25$; 127.50; 126.46; 102.30; 97.43; 77.95; 62.50; 31.90; 31.52; 25.94; 16.81.

MS (ESI(+)): 593.9 $[\text{M}+\text{Na}]^+$



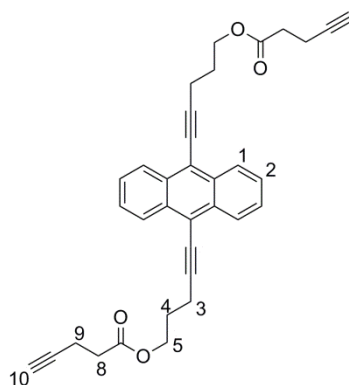
38

To a solution of **37** (1.35 g, 2.30 mmol) in THF (80 mL) at 0°C , was added an excess of TBAF (15 mL, 48.00 mmol). The mixture was stirred at rt for 2h and the solvent was evaporated. The residue was dissolved in CH_2Cl_2 and extraction was done with brine and saturated NH_4Cl solution. The organic phase was dried over MgSO_4 and the solvent evaporated. Purification of the crude product by CC (eluent $\text{CH}_2\text{Cl}_2/\text{EtOAc}$ 10/2) resulted in **38**, a yellow solid obtained with a yield of 70% (0.57 g).

^1H NMR (400 MHz, CDCl_3 , ppm): $\delta = 8.54$ (dd, $^3J_{\text{H-H}} = 6.7$ Hz, $^4J_{\text{H-H}} = 3.3$ Hz, 4H, H_1), 7.55 (dd, $^3J_{\text{H-H}} = 6.7$ Hz, $^4J_{\text{H-H}} = 3.3$ Hz, 4H, H_2), 3.98 (t, $^3J_{\text{H-H}} = 6.2$ Hz, 4H, H_5), 2.90 (t, $^3J_{\text{H-H}} = 7.0$ Hz, 4H, H_3), 2.09 (quint, $^3J_{\text{H-H}} = 6.7$ Hz, 4H, H_4).

$^{13}\text{C}\{^1\text{H}\}$ NMR (100 MHz, CDCl_3 , ppm): $\delta = 132.16$; 127.20; 126.46; 102.28; 97.42; 77.90; 61.97; 31.82; 16.84.

MS (ESI(+)): 365.5 $[\text{M}+\text{Na}]^+$

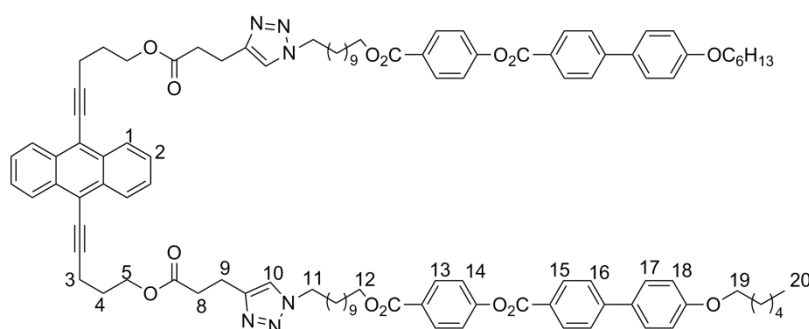
**39**

38 (0.47 g, 1.36 mmol), 4-pentynoic acid (0.39 g, 4.00 mmol), EDC (1.18 mL, 6.80 mmol) and DPTS (0.43 g, 1.36 mmol) were reacted in dry CH_2Cl_2 (100 mL) following the same procedure as **39**. Purification was done by CC (eluent $\text{CH}_2\text{Cl}_2/\text{EtOAc}$ 10/2) giving **39** as a yellow powder with a yield of 76% (0.52 g).

^1H NMR (400 MHz, CDCl_3 , ppm): δ = 8.52 (dd, $^3J_{\text{H-H}} = 6.6$ Hz, $^4J_{\text{H-H}} = 3.2$ Hz, 4H, H_1), 7.56 (dd, $^3J_{\text{H-H}} = 6.6$ Hz, $^4J_{\text{H-H}} = 3.2$ Hz, 4H, H_2), 4.42 (t, $^3J_{\text{H-H}} = 6.3$ Hz, 4H, H_5), 2.88 (t, $^3J_{\text{H-H}} = 7.0$ Hz, 4H, H_3), 2.53-2.61 (m, 8H, H_8 , H_9), 2.17 (quint, $^3J_{\text{H-H}} = 6.7$ Hz, 4H, H_4), 1.99 (t, $^3J_{\text{H-H}} = 2.4$ Hz, 2H, H_{10}).

$^{13}\text{C}\{^1\text{H}\}$ NMR (100 MHz, CDCl_3 , ppm): δ = 171.79; 132.15; 127.18; 126.53; 118.39; 101.49; 82.47; 78.13; 69.14; 63.63; 33.42; 28.23; 17.11; 14.46.

MS (ESI(+)): 525.7 $[\text{M}+\text{Na}]^+$

**40**

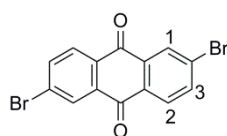
39 (0.50 g, 0.10 mmol) and the azide derivative **SG110** (0.13 g, 0.22 mmol) were dissolved in dry THF (9 mL) under argon. A suspension of CuSO_4 (0.02 g, 0.11 mmol) and NaAsc (0.04 g, 0.22 mmol) in water (1 mL) was added to the THF solution. The resulting yellow solution

was stirred overnight, after which a blue deposit was formed. The solvent was evaporated and CH_2Cl_2 was added to the residue. Extraction was done three times with water and the organic phase was dried over MgSO_4 . After evaporation of the solvent, the crude product was purified by CC (eluent $\text{CH}_2\text{Cl}_2/\text{EtOAc}$ 10/2). **40** was obtained as a yellow solid with a yield of 90% (0.15 g).

^1H NMR (400 MHz, CDCl_3 , ppm): δ = 8.52 (dd, $^3J_{\text{H-H}} = 6.8$ Hz, $^4J_{\text{H-H}} = 3.1$ Hz, 4H, H₁), 8.21 (d, $^3J_{\text{H-H}} = 8.5$ Hz, 4H, H₁₈), 8.11 (d, $^3J_{\text{H-H}} = 8.7$ Hz, 4H, H₁₄), 7.68 (d, $^3J_{\text{H-H}} = 8.2$ Hz, 4H, H₁₇), 7.55-7.60 (m, 4H, H₂, H₁₆), 7.32 (d, $^3J_{\text{H-H}} = 8.7$ Hz, 4H, H₁₃), 7.24 (s, 2H, H₁₀), 6.99 (d, $^3J_{\text{H-H}} = 8.3$ Hz, 4H, H₁₅), 4.37 (t, $^3J_{\text{H-H}} = 6.2$ Hz, 4H, H₅), 4.32 (t, $^3J_{\text{H-H}} = 6.7$ Hz, 4H, H₁₂), 4.19 (t, $^3J_{\text{H-H}} = 7.3$ Hz, 4H, H₁₉), 4.02 (t, $^3J_{\text{H-H}} = 6.6$ Hz, 4H, H₁₁), 3.03 (t, $^3J_{\text{H-H}} = 7.4$ Hz, 4H, H₉), 2.83 (t, $^3J_{\text{H-H}} = 7.0$ Hz, 4H, H₃), 2.78 (t, $^3J_{\text{H-H}} = 7.3$ Hz, 4H, H₈), 2.13 (quint, $^3J_{\text{H-H}} = 6.6$ Hz, 4H, H₄), 1.72-1.83 (m, 12H, aliphatic H), 1.21-1.50 (m, 42H, aliphatic H), 0.92 (t, $^3J_{\text{H-H}} = 6.3$ Hz, 6H, H₂₀).

$^{13}\text{C}\{^1\text{H}\}$ NMR (100 MHz, CDCl_3 , ppm): δ = 172.83; 165.96; 165.65; 159.70; 154.66; 146.31; 146.22; 132.13; 131.85; 131.19; 130.81; 128.42; 128.13; 127.17; 127.03; 126.68; 126.58; 121.79; 120.97; 118.38; 115.04; 101.57; 68.21; 65.26; 63.37; 50.20; 33.79; 31.62; 30.29; 29.47; 29.42; 29.36; 29.25; 28.98; 28.74; 28.17; 26.49; 26.03; 25.75; 22.64; 21.09; 17.08; 14.07.

MS (ESI(+)): 1753.4 $[\text{M}+\text{Na}]^+$



41

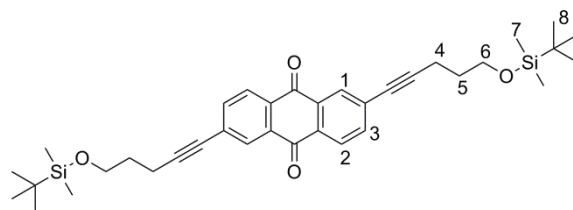
2,6-Diaminoanthraquinone (0.23 g, 1.00 mmol) and CuBr_2 (0.50 g, 2.25 mmol) were added to acetonitrile (50 mL), followed by $t\text{BuONO}$ (0.3 mL, 2.25 mmol). The mixture was stirred under reflux for 2 $\frac{1}{2}$ h during which evolution of gas was observed. 20% HCl (30 mL) was added to the mixture and stirred for 5 min. Water was then added and a light brown precipitate was formed, which was filtered off and washed with water. The residue was dissolved in boiling dioxane and charcoal was added to the mixture. Filtration of the hot

solution through celite gave a yellow filtrate. Upon cooling to rt, **41** precipitated from the solution and was collected as a pale yellow powder by filtration with a yield of 70% (0.25 g).

^1H NMR (400 MHz, CDCl_3 , ppm): $\delta = 8.43$ (s, 2H, H_1), 8.18 (d, $^3J_{\text{H-H}} = 8.3$ Hz, 2H, H_2), 7.95 (d, $^3J_{\text{H-H}} = 8.3$ Hz, 2H, H_3).

$^{13}\text{C}\{^1\text{H}\}$ NMR (100 MHz, CDCl_3 , ppm): $\delta = 182.13$; 137.41; 133.24; 130.38; 129.14; 128.16; 126.50.

MS (ESI(-)): 366.1 $[\text{M-H}]^-$



42

To a solution of **41** (0.36 g, 1.00 mmol) in dry and degassed CH_2Cl_2 (10 mL), were added CuI (0.01 g, 0.05 mmol) and degassed NEt_3 (30 mL) under argon. The mixture was stirred for 5 min, then $\text{Pd}(\text{PPh}_3)_4$ and **36** (0.59 g, 3.00 mmol) were added and stirred at 60°C overnight. After the reaction was complete, CH_2Cl_2 was added and extraction was done with water. After running CC (eluent CH_2Cl_2 /heptane 5/3), the product was stirred in methanol at 40°C . The suspension was filtered and the residue was dried. **42** was obtained as a pale yellow solid with a yield of 83% (0.56 g).

^1H NMR (400 MHz, CDCl_3 , ppm): $\delta = 8.27$ (s, 2H, H_1), 8.21 (d, $^3J_{\text{H-H}} = 8.3$ Hz, 2H, H_2), 7.75 (d, $^3J_{\text{H-H}} = 8.3$ Hz, 2H, H_3), 3.77 (t, $^3J_{\text{H-H}} = 6.1$ Hz, 4H, H_6), 2.57 (t, $^3J_{\text{H-H}} = 6.2$ Hz, 4H, H_4), 1.84 (quint, $^3J_{\text{H-H}} = 6.7$ Hz, 4H, H_5), 0.92 (s, 9H, H_8), 0.09 (s, 6H, H_7).

$^{13}\text{C}\{^1\text{H}\}$ NMR (100 MHz, CDCl_3 , ppm): $\delta = 182.18$; 136.63; 133.44; 131.86; 130.64; 130.20; 127.32; 96.00; 79.82; 61.51; 31.50; 25.97; 18.39; 16.07; -5.28.

MS (ESI(-)): 600.8 $[\text{M-H}]^-$

Chapter 4: Encapsulation of Pyrene-Core Dendrimers into Arene-Ru Metallo-Cycles

4.1 Introduction

Macromolecules, also referred to as polymer molecules, was termed by Nobel Prize winner Hermann Staudinger in the early 1920's.^[107] Biological macromolecules are critical components of the cells structure and are hence very important for life. Apart from biological macromolecules, there are other large molecules with great importance. Dendrimers, for instance, have a spectrum of applications including liquid crystal chemistry^[108] and biochemistry.^[109] Polyamidoamine derivatives (PAMAM)^[110] and poly-(2,2-bis(hydroxymethyl) propionic acids (bis-MPA))^[111] are two of the dendrimers used in drug-delivery systems.

In order to expand the spectrum of dendrimers with biological properties, our group has initiated the application of the well-known poly(benzyl ether) dendrimer, developed by Percec *et al.*,^[108a] as potential biological agents. As was briefly mentioned in Chapter 1 section 1.2.3, a series of different dendrimers of different generations were tested as anticancer agents.^[48b] Since the dendrimers are hydrophobic, they were transported in a hydrophilic vehicle that has a hydrophobic cavity. The dendrimers were attached to a planar π -conjugated pyrene moiety that gets encapsulated inside the hydrophobic cavity of the cage with the dendritic chain dangling out. The stability of these systems in biological media allowed their evaluation as potential drugs. Results show that the host-guest systems and the host alone show similar activities.^[48b] Another set of dendrimers tested was bis-MPA, which are water-soluble and biodegradable.^[48c] Unlike the poly(benzyl ether) systems, the biological activity of the pyrenyl bis-MPA dendrimers was determined, as well as that of the host-guest systems. Results show that the latter has higher activities than the host and guest alone.^[48c]

Apart from the biological activities of these macromolecules, their liquid-crystalline properties have a significant importance. It is well-known that dendrimers bearing mesogenic units tend to show liquid-crystalline properties. This property can however be affected or even be suppressed in some cases after coordination of the dendrimer to a metallic unit. In our group, the encapsulation of liquid-crystalline pyrenyl compounds, containing poly(arylester) dendrimers bearing cyanobiphenyl mesogens, into Ru cages has been studied. The encapsulated systems were evaluated on human ovarian cancer cell lines A2780 and A2780cis R.^[48a] For these systems to maintain the liquid-crystalline properties of the dendrimers, some conditions have to be met such as lowest possible global charge on the complex and soft counter anions, like dodecyl sulfate, that lower the melting points of the complex.^[99d] Hence,

the versatility, the ease of modification of the units and their potential to preferentially accumulate in tumour cells have made these systems a field of research with great perspectives.^[48a, 48c]

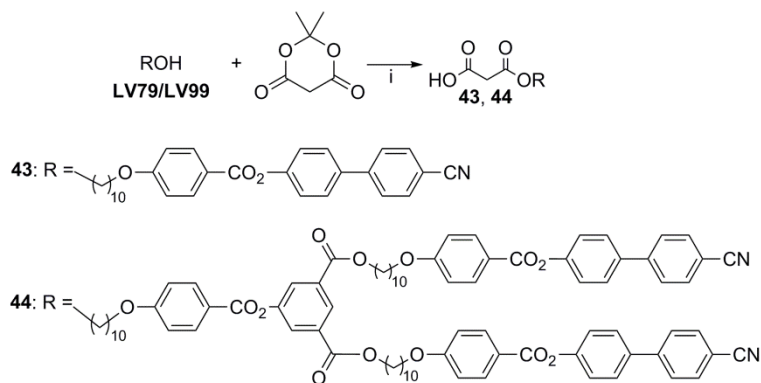
4.2 Aim

Following the work done on anthracene, a different approach was used to enable the success of the encapsulation of aromatic-core dendrimers into Ru cages. Hence, due to the low stability of anthracene moiety, the latter was replaced by pyrene, which shows greater stability than anthracene. Moreover, with disubstituted pyrenes, two isomers (1,6- and 1,8-) are possible, making the study of the encapsulation more interesting. Cyanobiphenyl units were used in the dendritic chain to introduce mesomorphic properties to the pyrene-core dendrimers. Hence, the effect of attaching the liquid-crystalline dendrimers to the pyrene was also studied as well as the influence encapsulation has on the mesomorphic properties of the systems. Two generations of dendrimers were used to study the behaviour of the different generations on the potential of the molecules to be trapped in arene-Ru cages.

4.3 Synthesis

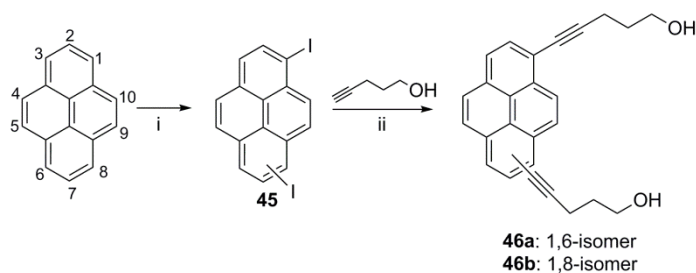
4.3.1 Synthesis of Pyrene Dendrimers

The two dendrimer chains were synthesised following literature procedures.^[99b] The final step of the synthesis is the reaction of the dendrimers bearing an alcohol end group (**LV79** and **LV99**, compounds synthesised by Thi Luyen Vuong. See Annex 3 for structures) with 2,2-dimethyl-1,3-dioxane-4,6-dione (Meldrum's acid) in toluene at 65°C (Scheme 4.1). At high temperatures, Meldrum's acid undergoes a pericyclic reaction with loss of acetone and carbon dioxide and produces ketene, a highly reactive compound that in turn reacts with the alcohol to form **43** and **44** (Scheme 4.1).^[112]



Scheme 4.1 Synthesis of compounds **43** and **44**. Reagents and conditions: i. toluene, 65°C, 24h, **43**: 16%, **44**: 76%

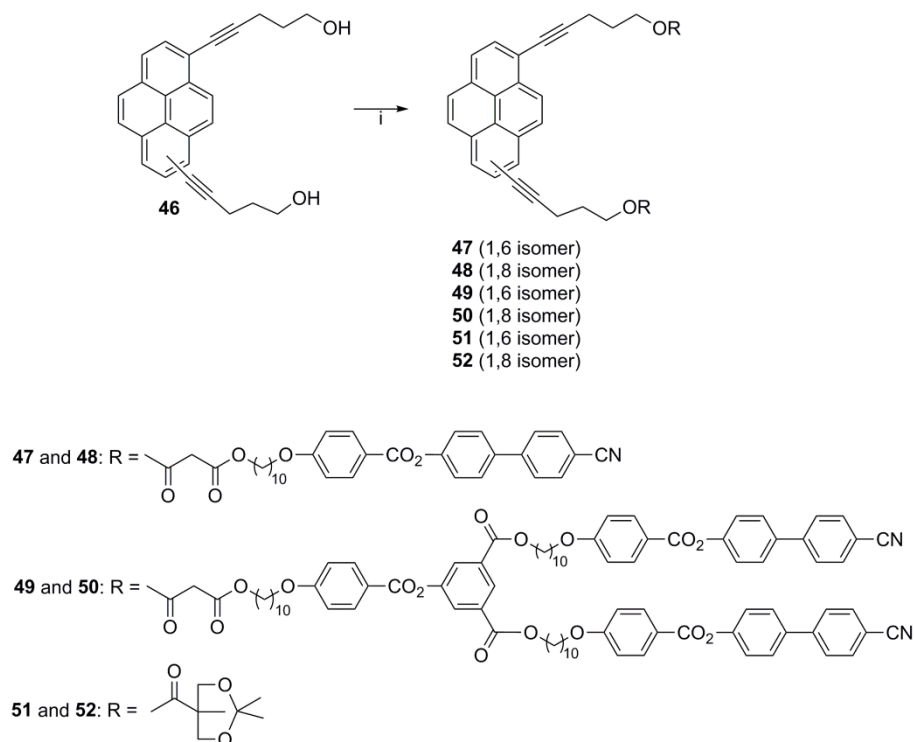
Pyrene was functionalised by iodination using I_2 and KIO_3 in an acetic acid, water and concentrated sulphuric acid (100:10:1 ratio) from 90°C to 40°C (Scheme 4.2).^[113] Two isomers of the diiodopyrene were obtained after recrystallization from hot toluene: the 1,6-isomer (**45a**) and the 1,8-isomer (**45b**). Separation of the isomers was not possible at this stage and the mixture of isomers was used for the following step, which involved a Sonogashira coupling with 4-pentyn-1-ol under the typical conditions: $\text{Pd(PPh}_3\text{)}_4/\text{CuI}$ catalytic system and $\text{CH}_2\text{Cl}_2/\text{NEt}_3$ (1:3 ratio).^[114] After several column chromatographies and recrystallizations, the 1,6- and 1,8-isomers were isolated separately as compounds **46a** and **46b**, respectively (Scheme 4.2).



Scheme 4.2 Synthesis of disubstituted pyrene compounds, **46a** and **46b**. Reagents and conditions: i. I_2 , KIO_3 , $\text{CH}_3\text{COOH}/\text{H}_2\text{O}/\text{H}_2\text{SO}_4$ (100:10:1 ratio), 90°C to 40°C, 4h, 25% ii. $\text{Pd(PPh}_3\text{)}_4$, CuI , $\text{CH}_2\text{Cl}_2/\text{NEt}_3$ (1:3 ratio), 60°C, 16h, **46a**: 7%, **46b**: 31%

Esterification using DCC and DPTS in CH_2Cl_2 was then carried out on the two isomers **46a** and **46b** with dendritic chains **43**, **44** and **zba01**, as shown in Scheme 4.3 (**zba01** was synthesised by Anaïs Pitto-Barry by the reaction between 2,2'-bis-(hydroxymethyl)propionic acid and 2,2'-dimethoxypropane in the presence of *p*-toluenesulfonic monohydrate in acetone

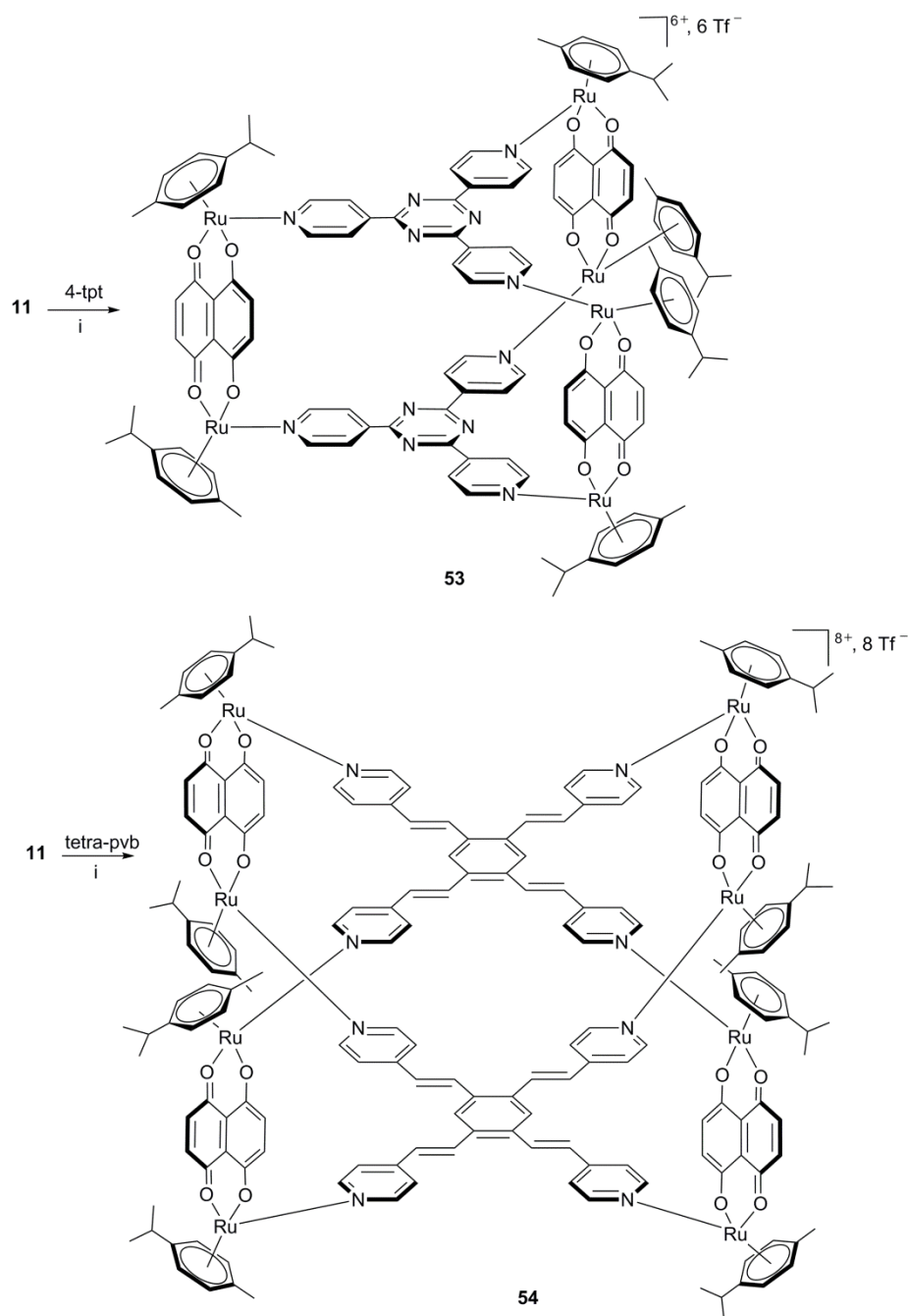
at room temperature for 2h. See Annex 3 for structure). After purification by several column chromatographies and preparative thick layer chromatographies, products **47-52** were isolated pure.



Scheme 4.3 Synthesis of compounds **47-52**. Reagents and conditions: i. ROH, DCC, DPTS, CH₂Cl₂, 0°C to rt, 16h, **47**: 52%, **48**: 25%, **49**: 63%, **50**: 55%, **51**: 51%, **52**: 80%

4.3.2 Carceplex Assemblies

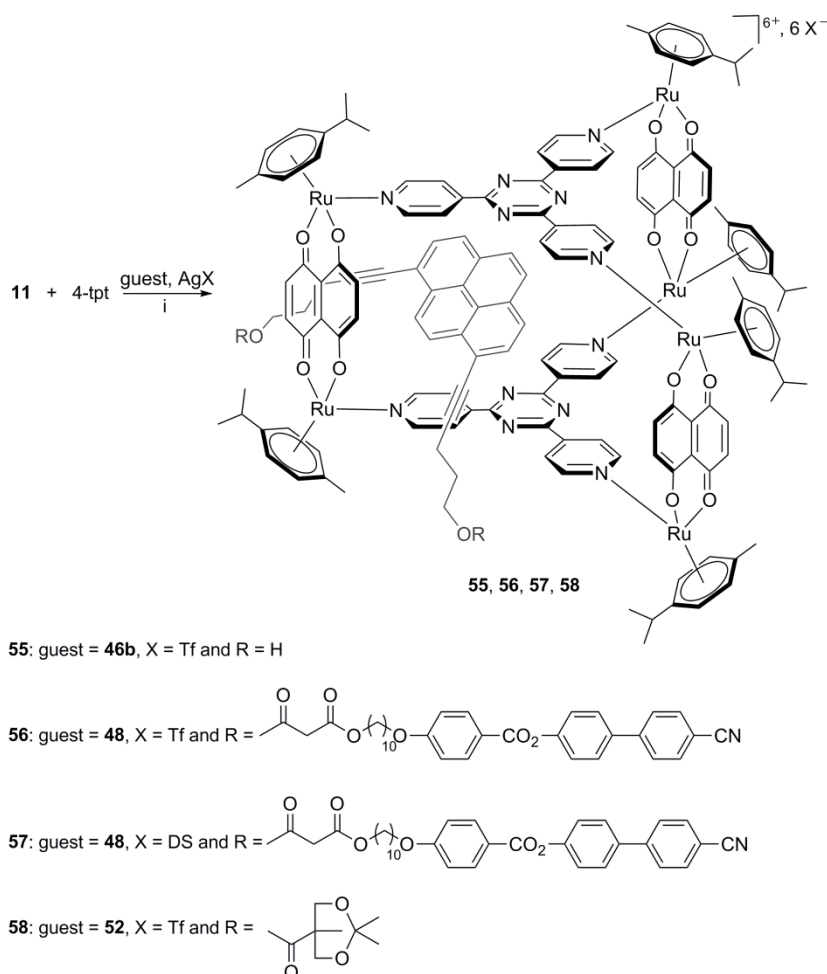
In the aim of encapsulating the dendrimers, carceplex method was used. Nevertheless, the empty cages were first synthesised to help in proper characterization of the encapsulation systems (Scheme 4.4). The Ru clip **11** was used in the synthesis of both the hexanuclear prism and the octanuclear cube. Silver triflate was used to remove the chlorides, followed by addition of the spacer ligand, which coordinated to the Ru. 2,4,6-Tris(pyridin-4-yl)-1,3,5-triazine (4-tpt) and 1,2,4,5-tetrakis(2-(pyridine-4-yl)vinyl)benzene (tetra-pvb) were used to afford the prism **53** and cube **54**, respectively (Scheme 4.4).



Scheme 4.4 Synthesis of hexa- and octanuclear Ru assemblies. Reagents and conditions: *i*. AgCF_3SO_3 , MeOH, reflux, 16h, **53**: 70%, **54**: 64%

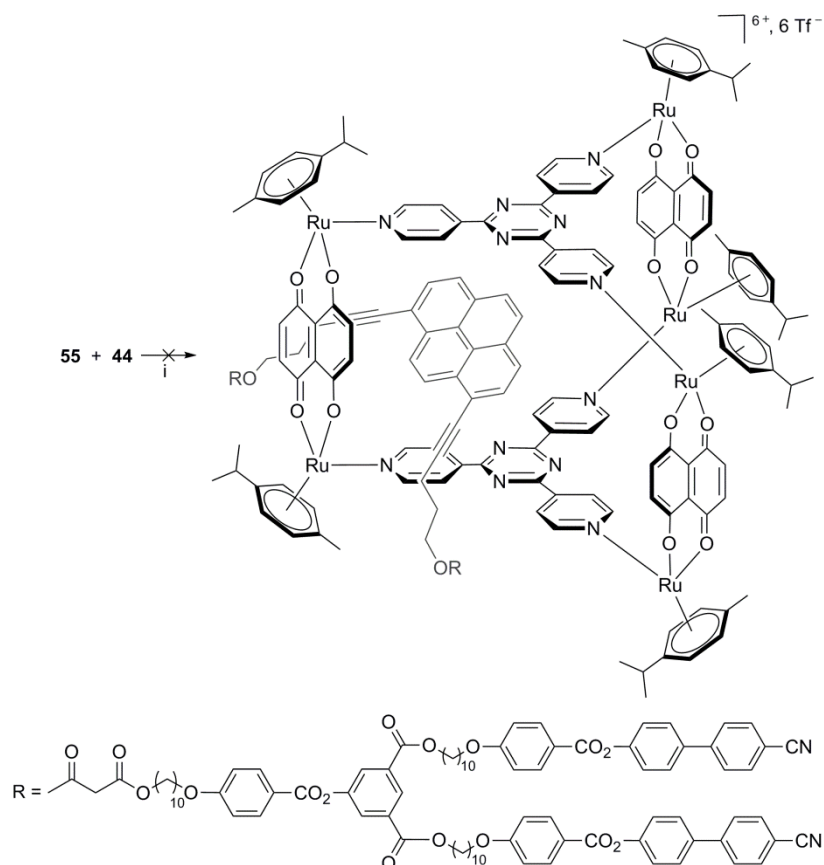
In order to test the ability of the pyrene-core dendrimers to be encapsulated in Ru cages, the intermediates **46a** and **46b** were first encapsulated by reacting clip **11**, spacer ligand 4-tpt and the potential guest in one step. On one hand, the 1,6-pyrene isomer did not undergo encapsulation despite several attempts to encapsulate **46a** in a prism by changing the solvent and the temperature of the reaction (See Table 4.1). On the other hand, **46b** was successfully

encapsulated into the prism. Moreover, compounds **48** and **52** were used as potential guests and successful encapsulation into the prism was observed in both cases (Scheme 4.5).



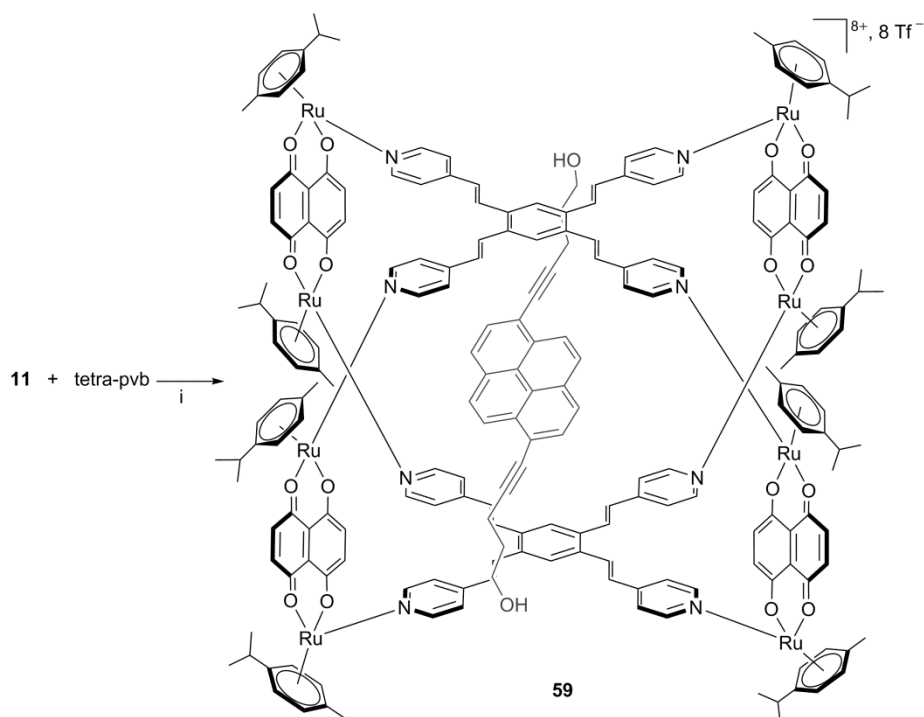
Scheme 4.5 Encapsulation of guest molecules (**46b**, **48** and **52**) into hexanuclear Ru cages. Reagents and conditions: i. MeOH, reflux, 16h, **55**: 42%, **56**: 43%, **57**: 27%, **58**: 23%

Encapsulation of the other 1,8-pyrene derivative **50** was not successful by the carceplex method. Therefore, a different route was taken to get the first generation dendrimer inside the hexanuclear metallo-prism. Compound **46b**, which was successfully encapsulated into the cage, possesses free alcohol end groups that are available for functionalisation. Hence, an esterification was attempted on the encapsulated system, aiming to attach the first generation dendron onto the pyrene moiety (Scheme 4.6). But the desired encapsulated system was not obtained. Instead, the empty cage and the free esterified compound were obtained at the end of the reaction.



Scheme 4.6 Encapsulation of guest molecule **44** into a hexanuclear Ru cage. Reagents and conditions: i. DCC, DPTS, CH_2Cl_2 , 0°C to rt, 16h.

Since the geometry of the 1,6-isomer is different from the 1,8-isomer, the encapsulation (into the Ru prism) of one and not both can be explained in terms of steric hindrance from one of the two chains in the 1,6-isomer that is too close to one of the naphthoquinone moiety, hence creating an obstruction in building the cage around the molecule. Therefore, a bigger cage was used to accommodate for the 1,6-isomer and successful encapsulation was found into a cubic arrangement with tetra-pvb spacer ligand (Scheme 4.7).



Scheme 4.7 Encapsulation of guest molecule **46a** into an octanuclear Ru cage. Reagents and conditions: i. AgCF_3SO_3 , **46a**, MeOH, reflux, 16h, 22%

Attempts to entrap the other dendrimers into the Ru cages did not result in any successful cases over a range of varying conditions: different cages (prism, rectangle and cube), different solvent systems (CH_2Cl_2 , MeOH, acetone, and mixtures of solvents), various reaction temperatures (room temperature, reflux) and different methods of encapsulation (host-guest and carceplex) (Table 4.1).

Table 4.1 Summary of different attempts made to encapsulate compounds **46-50** and **52**

| Guest | Host | Spacer ligand | Solvent of reaction | Temperature of reaction | Method | Product |
|------------|-----------|---------------------|--|-------------------------|--------------------------|-----------|
| 46a | Prism | 4-tpt | MeOH; CH ₂ Cl ₂ | rt; reflux | carceplex; host-guest | X |
| | Rectangle | dpe | MeOH; acetone; CH ₂ Cl ₂ | rt; reflux | carceplex; host-guest | X |
| | Cube | tetra-pvb | MeOH | rt; reflux | carceplex | 59 |
| | | Zn-tpp | | | carceplex; host-guest | X |
| 46b | Prism | 4-tpt | MeOH | reflux | carceplex | 55 |
| | Cube | Zn-tpp | | rt; reflux | carceplex; host-guest | X |
| 47 | Cube | tetra-pvb | MeOH; CH ₂ Cl ₂ ; THF | rt; reflux | carceplex; host-guest | X |
| | Rectangle | dpe | CH ₂ Cl ₂ | | | X |
| 48 | Prism | 4-tpt | MeOH | reflux | carceplex | 56 |
| 49 | Prism | 4-tpt; tris- pvb | MeOH; acetone; CH ₂ Cl ₂ | rt; reflux | carceplex; host-guest | X |
| | Rectangle | dpe | CH ₂ Cl ₂ | | | X |
| | Cube | tetra-pvb | CH ₂ Cl ₂ | | | X |
| 50 | Rectangle | dpe | CH ₂ Cl ₂ | rt; reflux | carceplex; host-guest | X |
| | Prism | 4-tpt | MeOH | | | X |
| | Cube | tetra-pvb | MeOH | | | X |
| 52 | Prism | 4-tpt | MeOH | reflux | carceplex | 58 |

From these attempts, no encapsulation was possible by the host-guest method. The 1,8-disubstituted pyrenes encapsulate better into these cages as compared to their 1,6- analogues. Compound **46a** was successfully encapsulated into an octanuclear cage whereas the other 1,6-derivatives bearing a dendrimer chain could not be encapsulated into these systems. For the

1,8-disubstituted molecules, encapsulation into the Ru cages was not successful for the G1 derivative. The only 1,8-disubstituted compounds that could be encapsulated into these Ru cages are **46b**, **48** and **52**. Attempts to encapsulate the G1 derivatives of both isomers into tetra-, hexa- and octanuclear Ru cages failed, which may imply that these cages are not appropriate to encapsulate these molecules.

4.4 Characterization

4.4.1 Proton NMR Spectroscopy

After attaching the dendrimers to the alcohol functional group of the pyrene molecules, **46a** and **46b**, the protons of the pyrene moiety do not undergo any chemical shifts, being far away and therefore less influenced by any changes occurring on the chains (Figure 4.1). On the other hand, shifting is observed for the protons H₁₁ and H₁₂ of the aliphatic chain, due to their closer proximity to the alcohol group. For instance, H₁₂ protons are shifted upfield by about 0.1 ppm from compound **46a** to compounds **47**, **49** and **51** and a more important upfield shift of about 0.5 ppm is observed for H₁₁ protons, as can be seen in Figure 4.1 below. Similar observations were made for the 1,8-isomer compounds (**46b**, **48**, **50**, **52**).

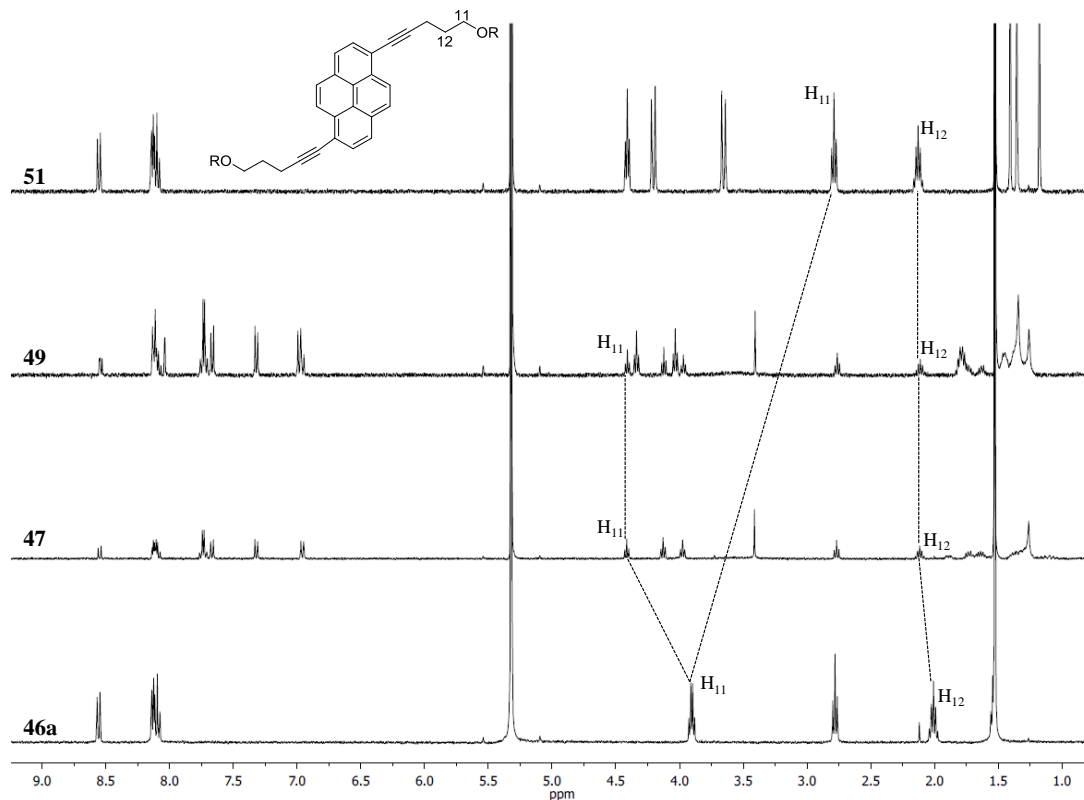


Figure 4.1 ¹H NMR spectra (400 MHz, CD₂Cl₂) of compounds **46a**, **47**, **49** and **51**

In many cases, the ^1H NMR spectra of the encapsulated systems are not well-defined, with some missing peaks. An example is the ^1H NMR spectrum of complex **58**, where the protons corresponding to the spacer ligand, 4-tpt are only barely visible as a broad peak (Figure 4.2).

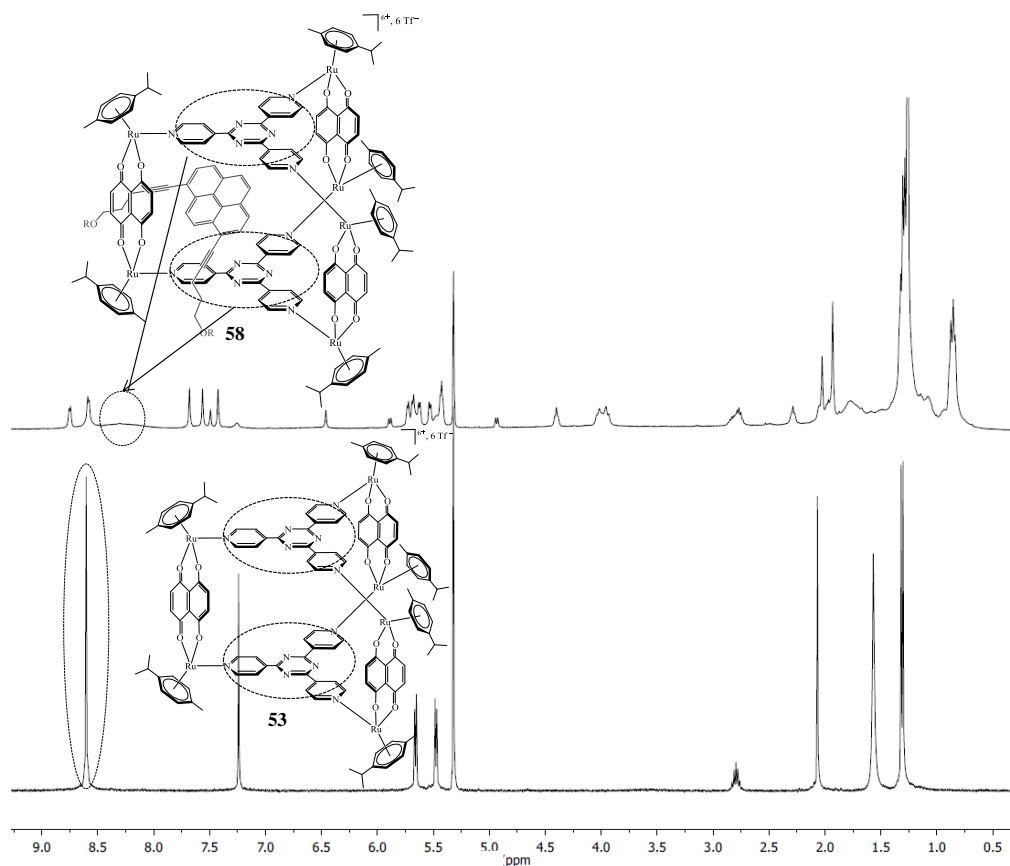


Figure 4.2 ^1H NMR spectra (400 MHz, CD_2Cl_2) of **53** and **58**

4.4.2 DOSY

Encapsulation of the pyrene compounds into the cages was followed by DOSY analysis. The displacement coefficient D , obtained as $\log D$ on the y-axis of the DOSY spectrum, allows the different components to be distinguished, provided the concentrations, the solvent and the temperature of the different measurements are the same. DOSY, known to be a good method of separating different components based on their hydrodynamic volumes, has been used to prove encapsulation of the guest molecule by the host cage.

In the case of complex **55**, which involved the entrapment of compound **46b** into prism **53**, DOSY was run on the free components (**46b** and **53**) and the encapsulated system. The stacking of the DOSY spectra in Figure 4.3 below shows the difference in the displacement of the components. Thus, **55** has a displacement value, $\log D$, of about -9.28, while the free

guest, **46b** displaces at $\log D = -8.85$. The displacement of **55** is similar to that of **53** because after encapsulation, the small guest goes inside the cavity, therefore the overall hydrodynamic volume of the encapsulated system does not differ a lot from that of the empty cage **53**.

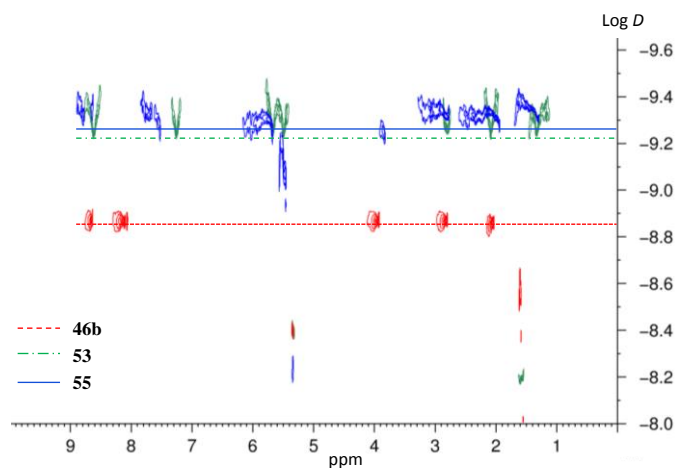


Figure 4.3 DOSY NMR spectrum (400 MHz, CD_2Cl_2) spectra of **46b**, **53** and **55**

The DOSY of complex **56** is slightly more complicated than that of **55** because the differences between the $\log D$ values are not as significant as in the previous case. The free guest, **48**, displaces at a $\log D$ value of around -9.25 while compound **56** has a $\log D = -9.30$. The empty prism **53** also displaces at a value of about -9.24, hence confirming the encapsulation of **48** into the prism (Figure 4.4).

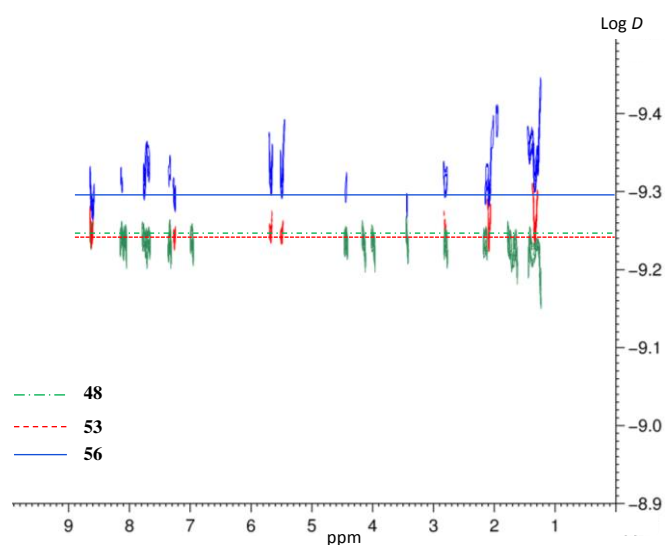


Figure 4.4 DOSY NMR spectrum (400 MHz, CD_2Cl_2) spectra of **48**, **53** and **56**

Complex **59**, which is the compound **46a** entrapped in cage **54**, has a similar DOSY spectrum as complex **55** since both involve a major change in hydrodynamic volume as a result of encapsulation. Complex **59** displaces at a log D value of about -9.33 while the free guest, **46a**, displaces at log $D = -8.90$ (Figure 4.5). The major difference in the displacement coefficient indicates that **46a** is no longer free, but instead, it displaces with the cage **54** due to the strong interaction between them.

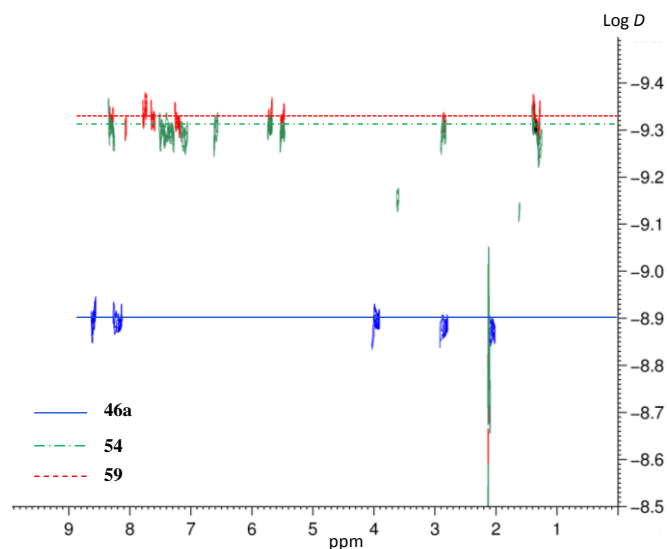


Figure 4.5 DOSY NMR spectrum (400 MHz, MeOD) spectra of **46a**, **54** and **59**

4.4.3 X-Ray Crystallography

Mono-crystals of complex **59** were obtained by slow diffusion of diethyl ether into a solution of the compound in CH_2Cl_2 . Owing to the presence of some distortion of the guest molecule, the complete X-ray structure was not obtained (Figure 4.6). DFT simulations of the encapsulated guest were used to complete the structure of **59**. The side view of the X-ray structure of **59** shows the bending of the spacer ligands into the cavity of the cage, arising from the strong π - π interactions between tetra-pvb and compound **46a**. Hence, the distances “x” and “y” have a difference of more than 1.5 Å for this system (Figure 4.6).^[115] This X-ray structure confirms that the interaction between the guest molecule and the host is not an out-of-cavity one, but an in-cavity interaction.

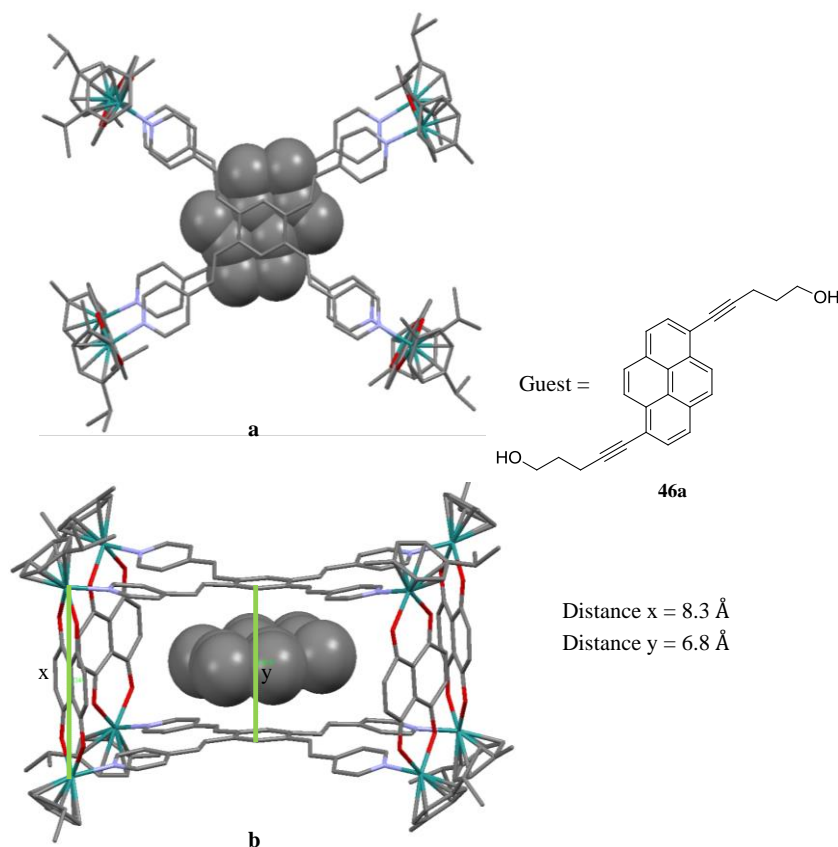


Figure 4.6 X-ray crystal structures of complex **59**: (a) top view and (b) side view

4.4.4 Mesomorphic Properties

The thermal and mesomorphic properties of compounds **47-50** were studied by differential scanning calorimetry (DSC) and polarised optical microscopy (POM). From the DSC thermogram of compound **47**, two mesophases appear to exist (Figure 4.7). The glass transition temperature (T_g) is at 26°C and two other transitions are observed at 36°C and 169°C . Preliminary analysis by POM shows a nematic phase characterised by its Schlieren texture as the only mesophase for **47** and at room temperature, compound **47** presents a nematic glass phase (Figure 4.8). Also, crystallization of **47** is observed with decreasing the temperature from T_1 to around 120°C .

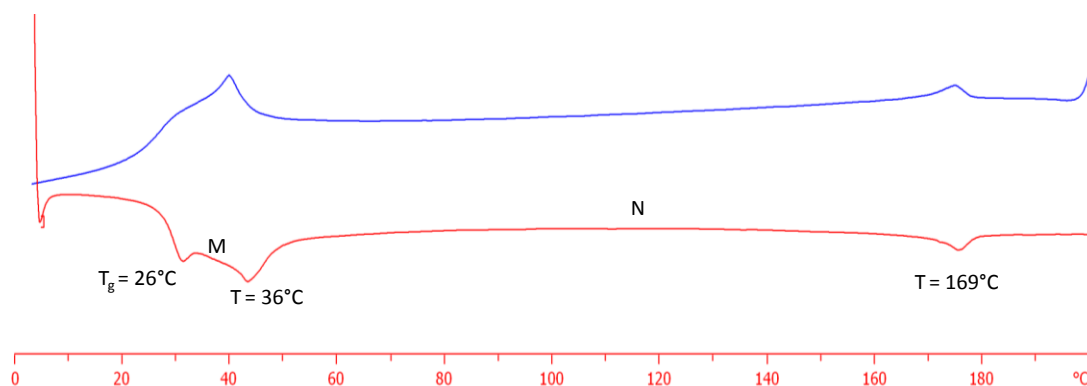


Figure 4.7 DSC thermogram of compound **47**: second heating curve (red) and second cooling curve (blue)

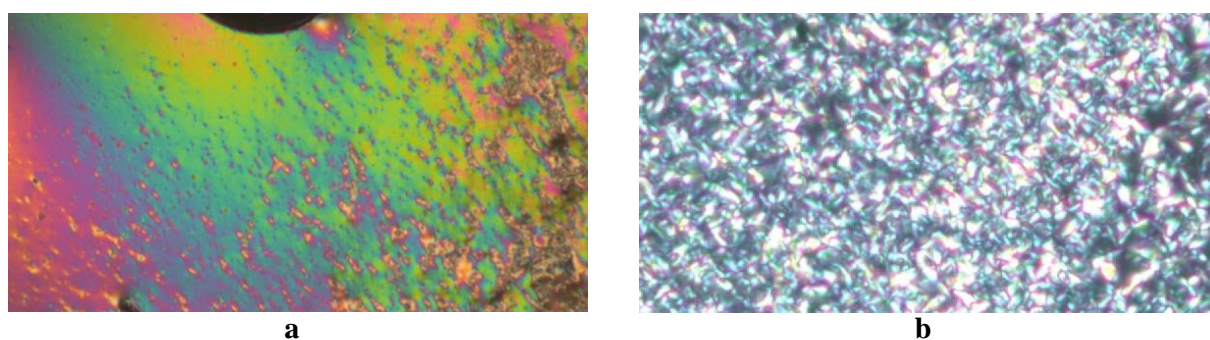


Figure 4.8 Textures of compound **47**: (a) nematic glass at 24°C and (b) nematic phase 160°C

The 1,8-isomer compound **48** was found to have more than one mesophase, from DSC analysis (Figure 4.9). The T_g was similar to compound **47** (26°C), but an overall of three mesophases was observed from the thermogram. However, from preliminary POM analysis only a Schlieren texture characteristic of a nematic phase was observed (Figure 4.10). It was also observed that the compound started to crystallise at around 124°C with lowering of the temperature from T_I .

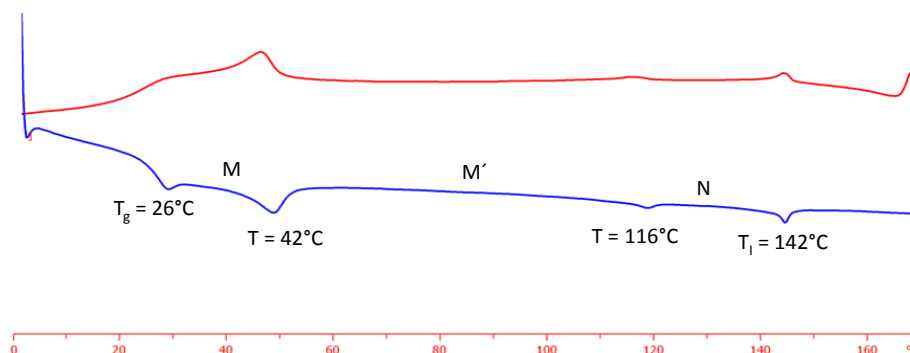


Figure 4.9 DSC thermogram of compound **48**: second heating curve (blue) and second cooling curve (red)

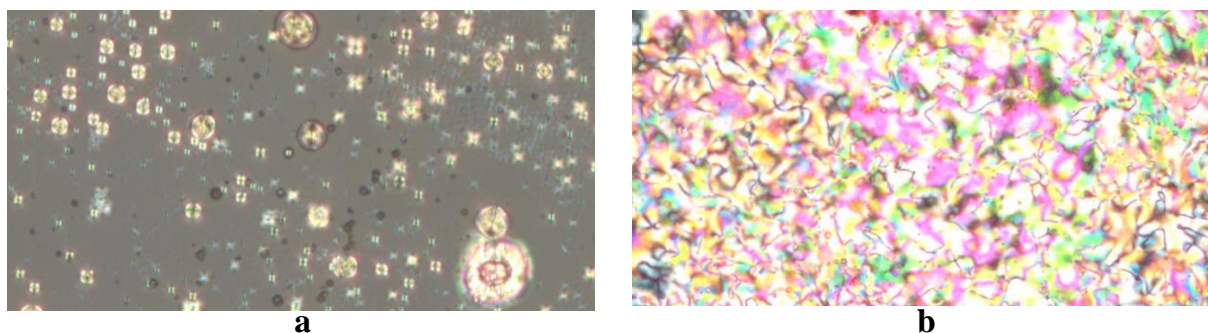


Figure 4.10 Textures of compound **48**: (a) unidentified phase at 38°C and (b) a nematic phase at 122°C

For compound **49**, the DSC thermogram is very simple, with only one mesophase before isotropy (Figure 4.11). POM images show that the only mesophase existing for this compound is the nematic phase, characterised by the Schlieren texture (Figure 4.12).

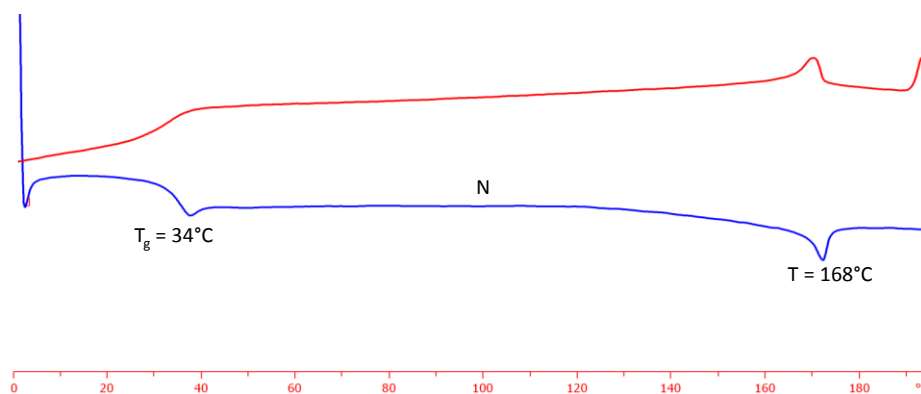


Figure 4.11 DSC thermogram of compound **49**: second heating curve (blue) and second cooling curve (red)

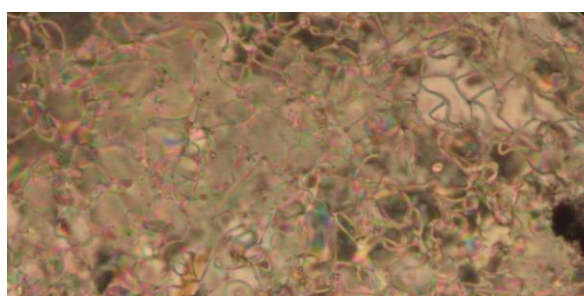


Figure 4.12 Nematic texture of compound **49** at 160°C

Compound **50**, unlike **49**, was found to have two mesophases from its DSC thermogram (Figure 4.13). From POM, the first mesophase observed with increasing temperature was a smectic A phase characterised by the conic focal and homeotropic zone. For a short span of

about 10°C a nematic phase characterised by its Schlieren texture is observed (Figure 4.14). Both compounds **49** and **50** have similar T_g of 34°C.

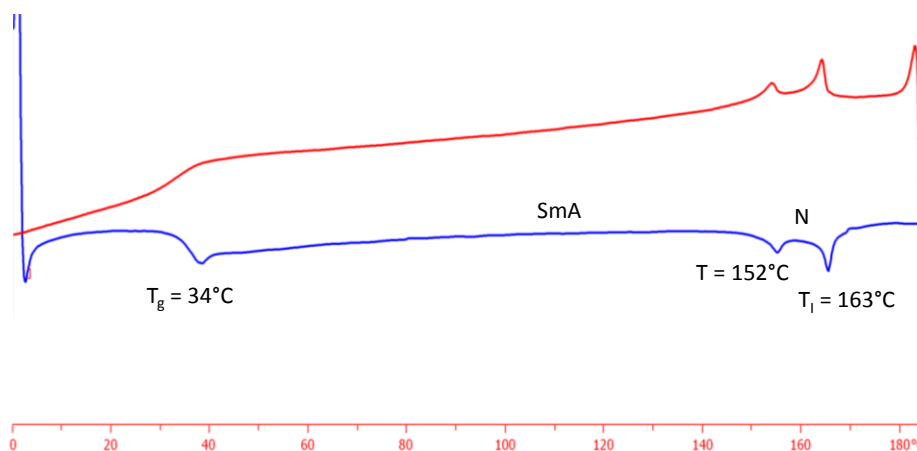


Figure 4.13 DSC thermogram of compound **50**: second heating curve (blue) and second cooling curve (red)

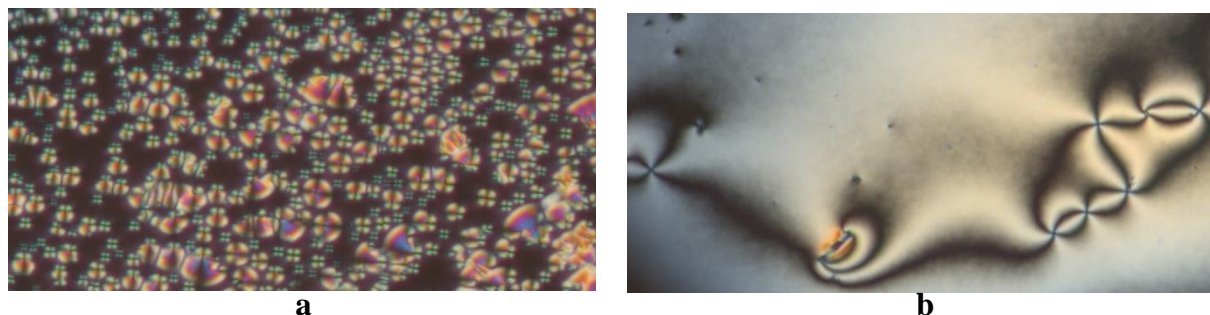


Figure 4.14 Textures of compound **50**: (a) smectic A at 135°C and (b) a nematic phase at 151°C

Compounds **47** and **48**, bearing two mesogenic cyanobiphenyl units each, were compared with the cyanobiphenyl mesogen **LV99** and a monosubstituted pyrene containing the mesogenic unit (compound **Mono-G0**, see structure in Annex 3). Similarly, for the first generation dendrons **49** and **50**, comparison was made with the corresponding G1 mesogen **LV79** and the monosubstituted pyrene containing the G1 mesogen (compound **Mono-G1**, see structure in Annex 3). The analysis for compounds **LV79**, **LV99**, **Mono-G0** and **Mono-G1** were obtained from the work done by Thi Luyen Vuong and Anaïs Pitto-Barry. The different transitions observed from DSC for these compounds are summarised in Table 4.2 with the temperatures of transition (T_g and T) and the enthalpies of transition (ΔH) for the corresponding phase transitions.

Table 4.2 Temperatures and enthalpies of transition for the mesogen bearing compounds

| Compound | T _g (°C) ^b | Transitions ^a | T (°C) ^b | ΔH (kJ·mol ⁻¹) ^b |
|----------------|----------------------------------|--------------------------|---------------------|---|
| LV99 | - | N → I | 222 | 0.7 |
| Mono-G0 | 51 | N → I | 138 | 0.7 |
| 47 | 26 | M → N | 36 | 2.3 |
| | | N → I | 169 | 1.2 |
| 48 | 26 | M → M' | 42 | 3.1 |
| | | M' → N | 116 | 0.2 |
| | | N → I | 142 | 0.5 |
| LV79 | - | N → I | 190 | 3.0 |
| Mono-G1 | 46 | N → I | 167 | 4.6 |
| 49 | 34 | N → I | 168 | 5.1 |
| 50 | 34 | SmA → N | 152 | 1.7 |
| | | N → I | 163 | 3.1 |

^a M and M': unidentified mesophases, N: nematic phase, I: isotropic phase; ^b Measurements were made at 10°C/min and all the temperatures and transition enthalpies were recorded for the second heating cycle.

Comparing two mesogens, **LV79** and **LV99**, to their mono- and disubstituted pyrenyl compounds, a decreased in T_I is observed (Table 4.2). This change may be due to an overall decrease in the strength of interactions between the molecules. In the mesogens, the alcohol end groups are stabilised by H-bonds, which get disrupted after binding to the pyrene. The pyrenyl compounds are in turn held together by π-π interactions between the pyrene units. These π-π interactions, being weaker than the H-bonds in the mesogens, result in an overall destabilization of the pyrenyl compounds with a lowering of T_I. Increasing in generation of dendrons presents an overall increase in T_I, probably resulting from increased π-π interactions arising from an increased number of aromatic units from G0 to G1.

The 1,6-isomers show higher T_I than the 1,8-isomers (Table 4.2). This can be explained in terms of the arrangement orders, the 1,6-isomers being more linear and hence stack better than the 1,8-isomer. The presence of more order in the 1,6-isomers result in higher stability and hence higher T_I than the 1,8-isomers. Moreover, from mono- to disubstitution of the pyrene compounds, an increase in T_I is observed. A possible explanation is that the

arrangements of the disubstituted compounds are more stable than the monosubstituted ones, resulting in an increase in T_I .

All the compounds present a nematic phase, with compounds **47** and **50**, the 1,8-isomers, displaying an additional unidentified phase and a smectic A phase, respectively (Table 4.2). Also, **LV99** and **LV79** do not present any T_g while the pyrene compounds all do. The disubstituted pyrenes present a lower T_g than the monosubstituted ones. The 1,6- and 1,8-isomers of a particular dendron generation present the same T_g value.

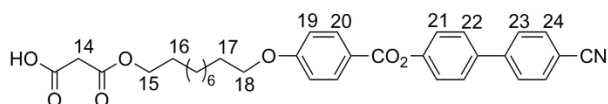
The changes in enthalpy for the compounds of same generation dendron are closely related: G0 derivatives (compounds **LV99**, **Mono-G0**, **47** and **48**) have ΔH in the range 0.5-1.2 $\text{kJ}\cdot\text{mol}^{-1}$ and the G1 derivatives (compounds **LV79**, **Mono-G1**, **49** and **50**) have ΔH between 3.0-5.1 $\text{kJ}\cdot\text{mol}^{-1}$ (Table 4.2).

The DSC and POM analyses of the encapsulated dendrimer, compound **56**, show that the latter is not liquid-crystalline. For this system, entrapment into the Ru cage results in loss of the mesomorphic property of the guest instead of transferring this property to the encapsulated system. An attempt was made by changing the counter ion, using a softer anion, dodecyl sulphate instead of triflate (compound **57**), but nevertheless, the mesomorphic properties could not be maintained.

4.5 Conclusion

A family of bifunctional, 1,6- and 1,8-pyrene-core dendrimers bearing cyanobiphenyl moieties was synthesised and all members (**47-50**) were found to be liquid-crystalline. Compounds **47-50** present a nematic phase, and compounds **48** and **50** present other phases as well, an unidentified one and a nematic phase, respectively. The temperatures and enthalpies were consistent with similar systems. The 1,8-isomer compounds, **46b** and **48**, were successfully encapsulated into Ru prism **53**, while compound **46a** was the only 1,6-isomer to be encapsulated into an octanuclear Ru system **54**; all the encapsulations were carried out by the carceplex method. A similar system bearing a different chain, polyester dendrimers, was established and in this case as well, encapsulation into the hexanuclear Ru cage was only possible for the 1,8-isomer (compound **52**). Therefore, it can be concluded that the geometry of the compounds and the length of the chains linked to the pyrene-core play a determining role in the encapsulation into the hydrophobic cavities of the cages.

4.6 Experimental Part

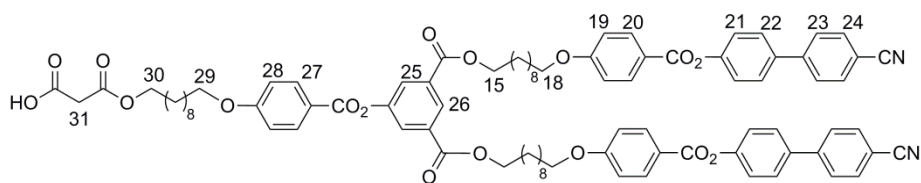
**43**

The alcohol derivative (**LV99**) (0.50 g, 1.06 mmol) and an excess of Meldrum's acid (1.52 g, 10.60 mmol) were added to dry toluene (100 mL) under argon and the mixture was stirred at 65°C. After 24h, the mixture was cooled and the solvent evaporated. The crude product was precipitated from methanol and the precipitate was run through a CC (eluent CH₂Cl₂/EtOAc 10/4). **43** was obtained as a white powder with a yield of 16% (0.14 g).

¹H NMR (400 MHz, CDCl₃, ppm): δ = 8.20 (d, ³J_{H-H} = 8.8 Hz, 8H, H₂₀, H₂₄), 7.66-7.79 (m, 6H, H₂₂, H₂₃), 7.37 (d, ³J_{H-H} = 8.6 Hz, 2H, H₂₁), 7.03 (d, ³J_{H-H} = 8.9 Hz, 2H, H₁₉), 4.24 (t, ³J_{H-H} = 6.7 Hz, 2H, H₁₈), 4.10 (t, ³J_{H-H} = 6.5 Hz, 2H, H₁₅), 3.48 (s, 2H, H₁₄), 1.87 (quint, ³J_{H-H} = 6.7 Hz, 2H, aliphatic chain), 1.71 (quint, ³J_{H-H} = 6.9 Hz, 2H, H₁₆), 1.53 (quint, ³J_{H-H} = 7.1 Hz, 2H, H₁₇), 1.35-1.43 (m, 10H, aliphatic chain).

¹³C{¹H} NMR (100 MHz, CDCl₃, ppm): δ = 168.77; 168.13; 164.90; 163.72; 151.61; 144.91; 136.75; 132.68; 132.39; 128.38; 127.73; 122.59; 121.27; 118.90; 114.40; 111.03; 68.38; 66.32; 40.00; 29.39; 22.14; 28.39; 25.98; 25.74.

MS (ESI(+)): 580.6 [M+Na]⁺

**44**

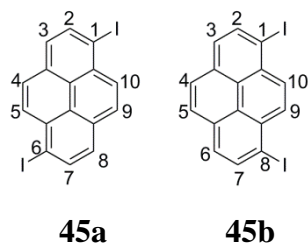
The alcohol derivative (**LV79**) (0.84 g, 0.58 mmol) and Meldrum's acid (0.80 g, 5.86 mmol) were stirred in toluene (150 mL) following the procedures as **43**. Purification was done by two CC (CH₂Cl₂/EtOAc 10/0.6 to 10/4 and CH₂Cl₂/MeOH 10/0 to 10/1). **44** was obtained in the form of a white powder with a yield of 76% (0.65 g).

¹H NMR (400 MHz, CD₂Cl₂, ppm): δ = 8.56 (t, ⁴J_{H-H} = 1.5 Hz, 1H, H₂₆), 8.14 (d, ³J_{H-H} = 8.9 Hz, 6H, H₂₀, H₂₇), 8.06 (d, ⁴J_{H-H} = 1.5 Hz, 2H, H₂₅), 7.77-7.66 (m, 8H, H₂₃, H₂₄), 7.63 (d, ³J_{H-H}

= 8.7 Hz, 4H, H₂₂), 7.33 (d, ³J_{H-H} = 8.6 Hz, 4H, H₂₁), 7.00 (d, ³J_{H-H} = 9.0 Hz, 6H, H₁₉, H₂₈), 4.35 (t, ³J_{H-H} = 6.7 Hz, 4H, H₁₅), 4.16 (t, ³J_{H-H} = 6.7 Hz, 2H, H₂₉), 4.04 (t, ³J_{H-H} = 6.0 Hz, 6H, H₁₈, H₃₀), 3.42 (s, 2H, H₃₁), 1.75-1.85 (m, 10H, aliphatic chain), 1.64-1.70 (m, 2H, aliphatic chain), 1.32-1.51 (m, 36H, aliphatic chain).

¹³C{¹H} NMR (100 MHz, CD₂Cl₂, ppm): δ = 165.12; 164.15; 152.06; 145.07; 137.07; 133.04; 132.85; 132.66; 132.56; 128.66; 128.03; 127.91; 127.49; 122.93; 121.63; 121.17; 119.18; 114.81; 114.73; 111.39; 68.83; 66.72; 66.15; 53.54; 39.89; 29.83; 29.00; 28.72; 26.34; 26.08.

MS (ESI(+)): 1473.6 [M+Na]⁺

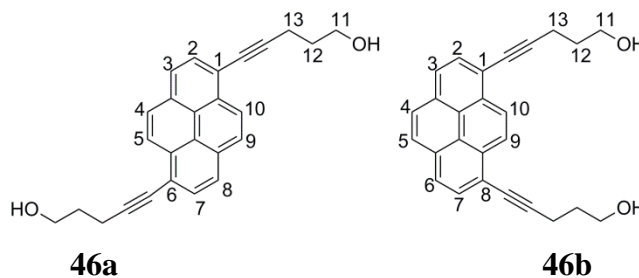


Pyrene (6.00 g, 30.00 mmol) was dissolved in acetic acid (250 mL) at 90°C. The solution was cooled to 40°C and water (20 mL), I₂ (7.15 g, 30.00 mmol), KIO₃ (2.57 g, 12.00 mmol) and concentrated H₂SO₄ (2 mL) were added. The resulting mixture was stirred at 40°C for 4h, after which it was filtered. The residue was washed with CH₂Cl₂, dried and recrystallization was done from hot toluene. **45** was obtained as a mixture of 1,6- and 1,8-isomers, **45a** and **45b** respectively, as a light brown solid with a yield of 25% (3.5 g).

¹H NMR (400 MHz, CDCl₃, ppm) for mixture **45a/45b**: δ = 8.54 (m, 2H, H₂, H₇), 8.35 (m, 2H, H₅, H₁₀), 8.08 (m, 2H, H₄, H₉), 7.90 (m, 2H, H₃, H₈).

¹³C{¹H} NMR (100 MHz, CDCl₃, ppm) for mixture **45a/45b**: δ = 97.45; 124.82; 126.71; 127.74; 129.12; 131.38; 131.72; 132.47; 133.05; 137.44.

MS (ESI(+)): 454.0 [M+H]⁺



45 (0.20 g, 0.44 mmol) was dissolved in dry and degassed CH_2Cl_2 (10 mL) under argon. CuI (0.004 g, 0.02 mmol) and degassed triethylamine (30 mL) were added to the solution and the mixture was stirred for 5 min. $\text{Pd}(\text{PPh}_3)_4$ (0.01 g, 0.01 mmol) and 4-pentyn-1-ol (0.08 mL, 0.88 mmol) were added to the mixture and stirring continued at 60°C . After overnight stirring, CH_2Cl_2 was added and extraction was done with water. The organic phase was dried over MgSO_4 and the solvent was removed. The residue was run through three CC (eluent $\text{CH}_2\text{Cl}_2/\text{MeOH}$ 10/0.4 then $\text{CH}_2\text{Cl}_2/\text{EtOAc}$ 10/4) that allowed the separation of the two isomers. Pure **46a** was obtained by recrystallization from an acetone/ CH_2Cl_2 mixture as a yellow solid with a yield of 7% (0.01 g). **46b** was purified by recrystallization from a CH_2Cl_2 /heptane mixture and was obtained as a yellow solid with a yield of 31% (0.50 g).

^1H NMR (400 MHz, CD_2Cl_2 , ppm) for **46a**: $\delta = 8.56$ (d, $^3J_{\text{H-H}} = 9.0$ Hz, 2H, H_2 , H_7), 8.08-8.14 (m, 6H, H_3 , H_4 , H_5 , H_8 , H_9 , H_{10}), 3.90 (q, $^3J_{\text{H-H}} = 5.9$ Hz, 4H, H_{11}), 2.78 (t, $^3J_{\text{H-H}} = 7.0$ Hz, 4H, H_{13}), 2.00 (quint, $^3J_{\text{H-H}} = 6.6$ Hz, 4H, H_{12}).

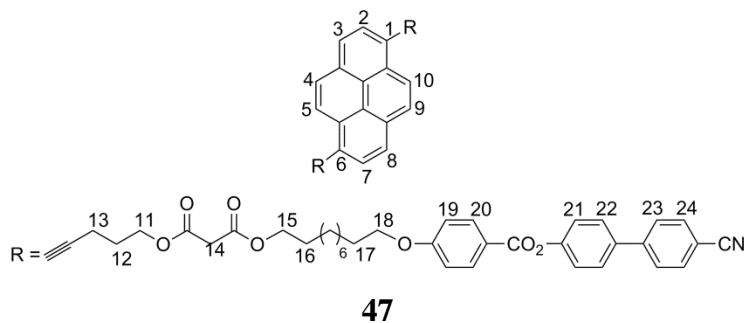
^1H NMR (400 MHz, CD_2Cl_2 , ppm) for **46b**: $\delta = 8.62$ (s, 2H, H_9 , H_{10}), 8.10 (q, $^3J_{\text{H-H}} = 7.9$ Hz, 4H, H_2 , H_3 , H_6 , H_7), 8.04 (s, 2H, H_4 , H_5), 3.91 (q, $^3J_{\text{H-H}} = 5.9$ Hz, 4H, H_{11}), 2.78 (t, $^3J_{\text{H-H}} = 7.0$ Hz, 4H, H_{13}), 2.00 (quint, $^3J_{\text{H-H}} = 6.6$ Hz, 4H, H_{12}).

$^{13}\text{C}\{^1\text{H}\}$ NMR (100 MHz, CD_2Cl_2 , ppm) for **46a**: $\delta = 130.28$; 128.28; 126.28; 125.27; 62.04; 32.16; 16.76.

$^{13}\text{C}\{^1\text{H}\}$ NMR (100 MHz, CD_2Cl_2 , ppm) for **46b**: $\delta = 132.11$; 131.27; 130.25; 127.99; 126.55; 125.30; 124.51; 79.93; 62.05; 32.16; 16.78.

MS (ESI(+)) for **46a**: 389.6 $[\text{M}+\text{Na}]^+$

MS (ESI(+)) for **46b**: 389.4 $[\text{M}+\text{Na}]^+$



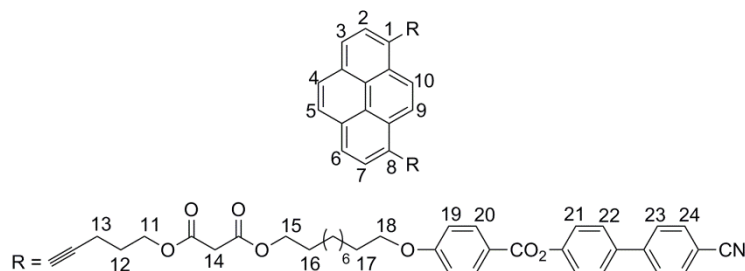
46a (0.02 g, 0.06 mmol), **51** (0.06 g, 0.13 mmol), DCC (0.07 g, 0.34 mmol) and DPTS (0.02 g, 0.06 mmol) were stirred in dry CH_2Cl_2 (50 mL) following similar procedure as **34**. The crude product was purified by two CC (eluent $\text{CH}_2\text{Cl}_2/\text{EtOAc}$ 10/0.02) followed by CC of Bio-Rad SX1 (eluent THF) and two preparative thick layer chromatographies (eluent $\text{CH}_2\text{Cl}_2/\text{EtOAc}$ 10/0.02). **47** was obtained as a pale yellow solid with a yield of 52% (0.05 g).

^1H NMR (400 MHz, CD_2Cl_2 , ppm): δ = 8.55 (d, $^3J_{\text{H-H}}$ = 9.1 Hz, 2H, H_2 , H_7), 8.07-8.14 (m, 10H, H_3 , H_4 , H_5 , H_8 , H_9 , H_{10} , H_{20}), 7.72 (q, $^3J_{\text{H-H}}$ = 6.6 Hz, 8H, H_{23} , H_{24}), 7.67 (d, $^3J_{\text{H-H}}$ = 8.6 Hz, 4H, H_{22}), 7.32 (d, $^3J_{\text{H-H}}$ = 8.6 Hz, 4H, H_{21}), 6.95 (d, $^3J_{\text{H-H}}$ = 8.7 Hz, 4H, H_{19}), 4.42 (t, $^3J_{\text{H-H}}$ = 6.3 Hz, 4H, H_{11}), 4.12 (t, $^3J_{\text{H-H}}$ = 6.7 Hz, 4H, H_{18}), 3.97 (t, $^3J_{\text{H-H}}$ = 6.6 Hz, 4H, H_{15}), 3.41 (s, 4H, H_{14}), 2.78 (t, $^3J_{\text{H-H}}$ = 7.1 Hz, 4H, H_{13}), 2.12 (q, $^3J_{\text{H-H}}$ = 6.7 Hz, 4H, H_{12}), 1.70-1.77 (m, 4H, H_{16}), 1.60-1.66 (m, 4H, H_{17}), 1.39-1.26 (m, 24H, aliphatic chain).

$^{13}\text{C}\{^1\text{H}\}$ NMR (100 MHz, CD_2Cl_2 , ppm): δ = 166.99; 166.96; 165.08; 164.12; 152.05; 145.06; 137.06; 133.03; 132.53; 131.14; 130.34; 128.65; 128.33; 128.02; 126.32; 125.31; 124.50; 122.92; 121.61; 119.33; 119.18; 114.70; 111.40; 95.41; 80.31; 68.77; 66.00; 64.53; 42.05; 29.79; 29.78; 29.64; 29.54; 29.41; 28.86; 28.35; 26.26; 26.16; 16.92.

Anal. Calcd. (found) for $\text{C}_{92}\text{H}_{88}\text{N}_2\text{O}_{14}$ (1444): C, 76.43 (76.50); H, 6.14 (6.13); N, 1.94 (1.95)%

MS (ESI(+)): 1468.6 $[\text{M}+\text{Na}]^+$

**48**

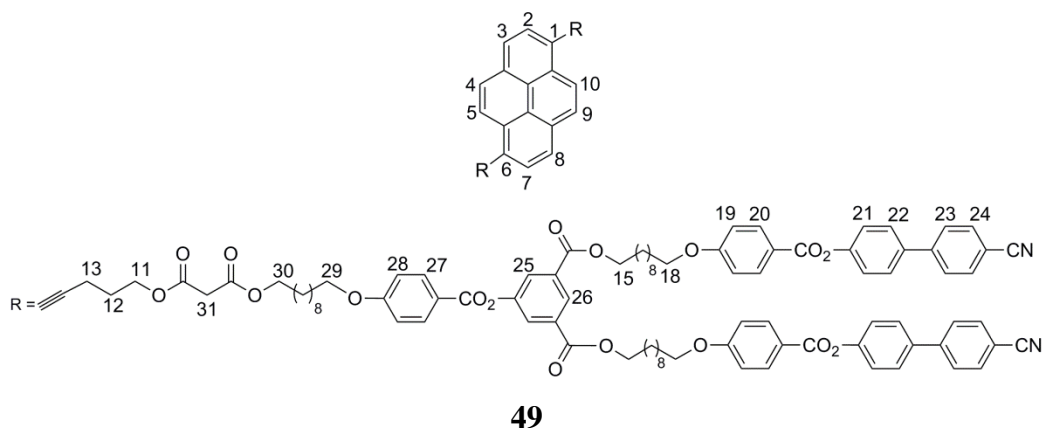
46b (0.05 g, 0.13 mmol), **51** (0.13 g, 0.27 mmol), DCC (0.15 g, 0.68 mmol) and DPTS (0.04 g, 0.13 mmol) were stirred dry CH_2Cl_2 (50 mL) following similar procedure as **34**. After overnight reaction, the solvent was removed and residue was run through CC (eluent $\text{CH}_2\text{Cl}_2/\text{EtOAc}$ 10/0.14). After two CC, the product was further purified by two preparative thick layer chromatographies (eluent $\text{CH}_2\text{Cl}_2/\text{EtOAc}$ 10/0.14). **48** was obtained as a yellow solid with a yield of 25% (0.05 g).

^1H NMR (400 MHz, CD_2Cl_2 , ppm): δ = 8.61 (s, 2H, H₉, H₁₀), 8.09-8.12 (m, 8H, H₂, H₃, H₆, H₇, H₂₀), 8.04 (s, 2H, H₄, H₅), 7.72 (q, $^3J_{\text{H-H}}$ = 8.3 Hz, 8H, H₂₃, H₂₄), 7.67 (d, $^3J_{\text{H-H}}$ = 8.7 Hz, 4H, H₂₂), 7.32 (d, $^3J_{\text{H-H}}$ = 8.6 Hz, 4H, H₂₁), 6.95 (d, $^3J_{\text{H-H}}$ = 8.9 Hz, 4H, H₁₉), 4.42 (t, $^3J_{\text{H-H}}$ = 6.2 Hz, 4H, H₁₁), 4.12 (t, $^3J_{\text{H-H}}$ = 6.7 Hz, 4H, H₁₈), 3.97 (t, $^3J_{\text{H-H}}$ = 6.5 Hz, 4H, H₁₅), 3.41 (s, 4H, H₁₄), 2.78 (t, $^3J_{\text{H-H}}$ = 7.1 Hz, 4H, H₁₃), 2.12 (quint, $^3J_{\text{H-H}}$ = 6.6 Hz, 4H, H₁₂), 1.73 (quint, $^3J_{\text{H-H}}$ = 6.7 Hz, 4H, H₁₆), 1.63 (quint, $^3J_{\text{H-H}}$ = 6.4 Hz, 4H, H₁₇), 1.39-1.25 (m, 24H, aliphatic chain).

$^{13}\text{C}\{^1\text{H}\}$ NMR (100 MHz, CD_2Cl_2 , ppm): δ = 167.00; 133.03; 132.53; 130.35; 128.65; 128.02; 125.33; 122.92; 114.68; 68.76; 66.00; 64.54; 42.04; 29.79; 29.77; 28.85; 28.38; 26.25; 26.15; 16.94.

Anal. Calcd. (found) for $\text{C}_{92}\text{H}_{88}\text{N}_2\text{O}_{14}$ (1444): C, 76.43 (76.33); H, 6.14 (6.19); N, 1.94 (1.95)%

MS (ESI(+)): 1468.6 $[\text{M}+\text{Na}]^+$



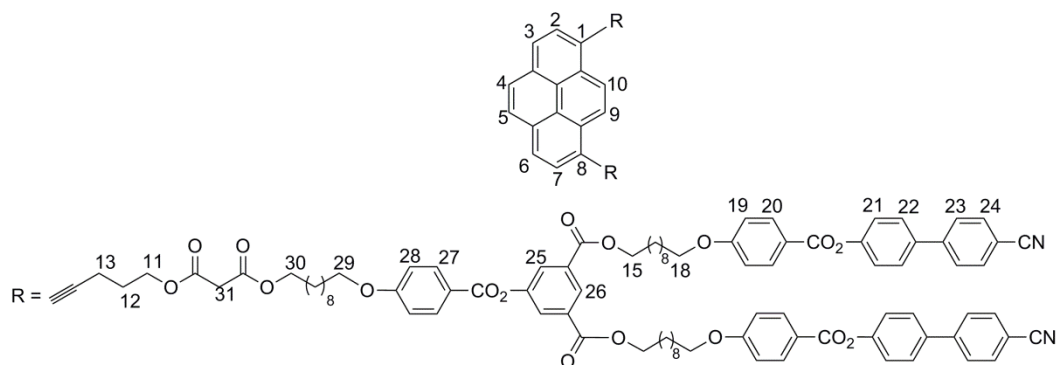
46a (0.02 g, 0.06 mmol), **52** (0.21 g, 0.15 mmol), DCC (0.07 g, 0.34 mmol) and DPTS (0.02 g, 0.06 mmol) were stirred in dry CH_2Cl_2 (50 mL) following similar procedure as **34**. The crude product was purified by two CC (eluent $\text{CH}_2\text{Cl}_2/\text{EtOAc}$ 10/0.02) followed by two preparative thick layer chromatographies (eluent $\text{CH}_2\text{Cl}_2/\text{EtOAc}$ 10/0.02). **49** was obtained as a pale yellow solid with a yield of 63% (0.14 g).

^1H NMR (400 MHz, CD_2Cl_2 , ppm): δ = 8.55-8.58 (m, 3H, H_2 , H_7 , H_{26}), 8.53 (s, 1H, H_{26}), 8.09-8.17 (m, 18H, H_3 , H_4 , H_5 , H_8 , H_9 , H_{10} , H_{20} , H_{27}), 8.04 (d, $^4J_{\text{H-H}} = 1.6$ Hz, 4H, H_{25}), 7.72 (d, $^3J_{\text{H-H}} = 8.7$ Hz, 16H, H_{23} , H_{24}), 7.66 (d, $^3J_{\text{H-H}} = 8.7$ Hz, 8H, H_{22}), 7.32 (d, $^3J_{\text{H-H}} = 8.6$ Hz, 8H, H_{21}), 6.97 (d, $^3J_{\text{H-H}} = 9.1$ Hz, 12H, H_{19} , H_{28}), 4.41 (t, $^3J_{\text{H-H}} = 6.3$ Hz, 4H, H_{11}), 4.33 (t, $^3J_{\text{H-H}} = 6.7$ Hz, 8H, H_{15}), 4.12 (t, $^3J_{\text{H-H}} = 6.7$ Hz, 4H, H_{29}), 4.03 (t, $^3J_{\text{H-H}} = 6.6$ Hz, 8H, H_{18}), 3.97 (t, $^3J_{\text{H-H}} = 6.6$ Hz, 4H, H_{30}), 3.40 (s, 4H, H_{31}), 2.76 (t, $^3J_{\text{H-H}} = 7.0$ Hz, 4H, H_{13}), 2.11 (q, $^3J_{\text{H-H}} = 8.0$ Hz, 4H, H_{12}), 1.82-1.70 (m, 20H, aliphatic chain), 1.64 (q, $^3J_{\text{H-H}} = 6.8$ Hz, 4H, aliphatic chain), 1.45-1.25 (m, 48H, aliphatic chain).

$^{13}\text{C}\{^1\text{H}\}$ NMR (100 MHz, CD_2Cl_2 , ppm): δ = 167.00; 166.97; 165.31; 165.07; 164.84; 164.30; 164.14; 152.07; 151.60; 145.03; 137.04; 133.03; 132.85; 132.65; 132.56; 130.35; 128.65; 128.34; 128.01; 127.49; 125.32; 122.93; 121.64; 114.78; 114.73; 111.40; 95.43; 80.35; 68.82; 66.14; 66.01; 64.54; 42.04; 29.85; 29.81; 29.70; 29.67; 29.62; 29.56; 29.47; 29.02; 28.88; 26.36; 26.31; 16.93.

Anal. Calcd. (found) for $\text{C}_{202}\text{H}_{206}\text{N}_4\text{O}_{34}$ (3231): C, 75.03 (74.93); H, 6.42 (6.44); N, 1.73 (1.72)%

MS (ESI(+)): 3256.3 $[\text{M}+\text{Na}]^+$

**50**

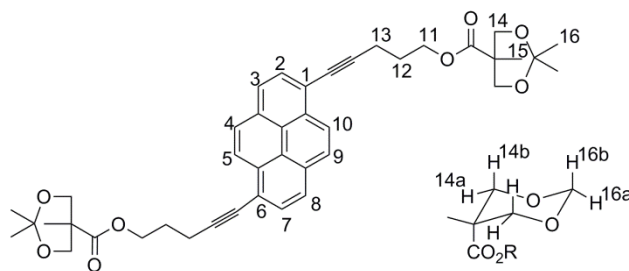
46b (0.02 g, 0.06 mmol), **44** (0.21 g, 0.15 mmol), DCC (0.07 g, 0.34 mmol) and DPTS (0.02 g, 0.06 mmol) were stirred in dry CH_2Cl_2 (50 mL) following similar procedure as **34**. The crude product was purified by three CC (thin SiO_2 , eluent $\text{CH}_2\text{Cl}_2/\text{EtOAc}$ 10/0.1) followed by two preparative thick layer chromatographies (eluent $\text{CH}_2\text{Cl}_2/\text{EtOAc}$ 10/0.1). **50** was obtained as a pale yellow solid with a yield of 55% (0.12 g).

^1H NMR (400 MHz, CD_2Cl_2 , ppm): δ = 8.61 (s, 2H, H_9 , H_{10}), 8.54 (t, $^3J_{\text{H-H}} = 1.5$ Hz, 2H, H_{26}), 8.10-8.13 (m, 18H, H_2 - H_7 , H_{20} , H_{27}), 8.03 (d, $^4J_{\text{H-H}} = 1.5$ Hz, 4H, H_{25}), 7.72 (d, $^3J_{\text{H-H}} = 8.6$ Hz, 16H, H_{23} , H_{24}), 7.66 (d, $^3J_{\text{H-H}} = 8.7$ Hz, 8H, H_{22}), 7.32 (d, $^3J_{\text{H-H}} = 8.7$ Hz, 8H, H_{21}), 6.97 (d, $^3J_{\text{H-H}} = 9.0$ Hz, 12H, H_{19} , H_{28}), 4.41 (t, $^3J_{\text{H-H}} = 6.3$ Hz, 4H, H_{11}), 4.33 (t, $^3J_{\text{H-H}} = 6.7$ Hz, 8H, H_{18}), 4.12 (t, $^3J_{\text{H-H}} = 6.8$ Hz, 4H, H_{29}), 4.03 (t, $^3J_{\text{H-H}} = 6.5$ Hz, 8H, H_{15}), 3.97 (t, $^3J_{\text{H-H}} = 6.6$ Hz, 4H, H_{30}), 3.41 (s, 4H, H_{31}), 2.77 (t, $^3J_{\text{H-H}} = 7.1$ Hz, H_{13}), 2.12 (q, $^3J_{\text{H-H}} = 6.6$ Hz, H_{12}), 1.82-1.70 (m, 20H, aliphatic chain), 1.64 (q, $^3J_{\text{H-H}} = 6.9$ Hz, 4H, aliphatic chain), 1.45-1.25 (m, 48H, aliphatic chain)

$^{13}\text{C}\{^1\text{H}\}$ NMR (100 MHz, CD_2Cl_2 , ppm): δ = 164.64; 164.40; 163.84; 163.69; 151.60; 151.13; 144.59; 136.60; 132.59; 132.39; 132.19; 132.12; 131.66; 130.88; 129.91; 128.22; 127.58; 127.46; 127.05; 126.14; 124.90; 124.04; 122.50; 121.17; 120.67; 118.88; 118.75; 114.31; 114.27; 110.94; 95.06; 79.86; 68.37; 65.69; 65.56; 64.11; 41.61; 29.41; 29.38; 29.26; 29.18; 29.12; 29.02; 28.98; 25.56; 28.42; 27.94; 25.91; 25.87; 25.83.

Anal. Calcd. (found) for $\text{C}_{202}\text{H}_{206}\text{N}_4\text{O}_{34}$ (3231): C, 75.03 (74.79); H, 6.42 (6.35); N, 1.73 (1.75)%

MS (ESI(+)): 3256.3 $[\text{M}+\text{Na}]^+$

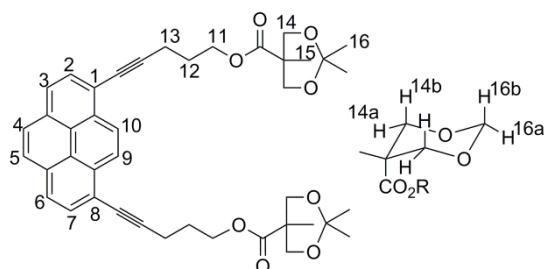
**51**

46a (0.05 g, 0.13 mmol), **zba01** (0.05 g, 0.30 mmol), DCC (0.14 g, 0.68 mmol) and DPTS (0.05 g, 0.13 mmol) and a catalytic amount of 4-ppy were stirred in dry CH_2Cl_2 (50 mL) following similar procedure as **34**. The crude product was purified by two CC (eluent CH_2Cl_2) followed by two preparative thick layer chromatographies (eluent CH_2Cl_2). **51** was obtained as a pale yellow solid with a yield of 51% (0.04 g).

^1H NMR (400 MHz, CDCl_3 , ppm): δ = 8.52 (d, $^3J_{\text{H-H}} = 9.0$ Hz, 2H, H₂, H₇), 8.08-8.11 (m, 6H, H₃-H₅, H₇-H₁₀), 4.45 (t, $^3J_{\text{H-H}} = 6.2$ Hz, 4H, H₁₃), 4.24 (d, $^3J_{\text{H-H}} = 11.6$ Hz, 4H, H_{14a}), 3.67 (d, $^3J_{\text{H-H}} = 11.6$ Hz, 4H, H_{14b}), 2.78 (t, $^3J_{\text{H-H}} = 7.1$ Hz, 4H, H₁₁), 2.14 (quint, $^3J_{\text{H-H}} = 6.7$ Hz, 4H, H₁₂), 1.44 (s, 6H, H_{16a}), 1.40 (s, 6H, H_{16b}), 1.23 (s, 6H, H₁₅).

$^{13}\text{C}\{^1\text{H}\}$ NMR (100 MHz, CDCl_3 , ppm): δ = 174.27; 131.99; 130.74; 129.94; 127.94; 125.99; 124.87; 124.18; 118.80; 98.09; 94.62; 80.28; 66.11; 63.65; 41.97; 28.04; 24.88; 22.47; 18.67; 16.63.

MS (ESI(+)): 701.4 $[\text{M}+\text{Na}]^+$

**52**

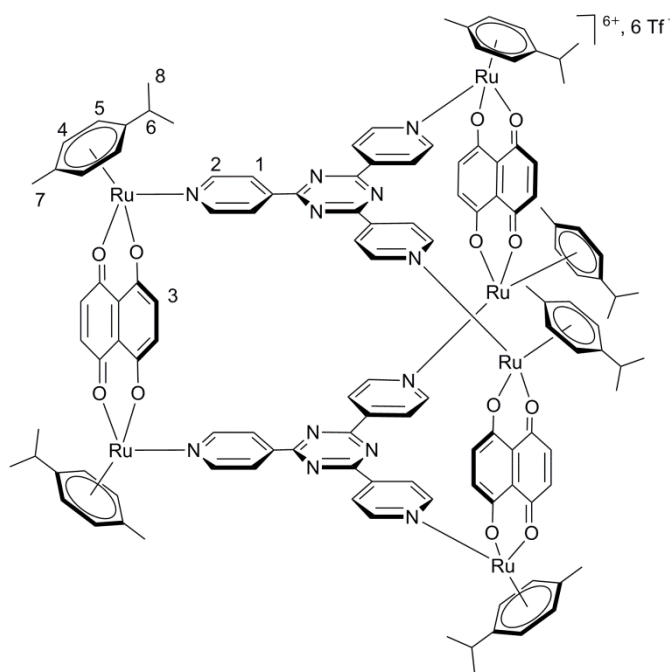
46b (0.05 g, 0.13 mmol), **zba01** (0.05 g, 0.30 mmol), DCC (0.14 g, 0.68 mmol) and DPTS (0.05 g, 0.13 mmol) and a catalytic amount of 4-ppy were stirred in dry CH_2Cl_2 (50 mL) following similar procedure as **34**. The crude product was purified by two CC (eluent CH_2Cl_2)

followed by two preparative thick layer chromatographies (eluent CH_2Cl_2). **52** was obtained as a pale yellow solid with a yield of 80% (0.07 g).

^1H NMR (400 MHz, CDCl_3 , ppm): $\delta = 8.60$ (s, 2H, H_2 , H_7), 8.08 (s, 4H, H_4 , H_5 , H_9 , H_{10}), 8.02 (s, 2H, H_3 , H_6), 4.45 (t, $^3J_{\text{H-H}} = 6.2$ Hz, 4H, H_{13}), 4.24 (d, $^3J_{\text{H-H}} = 11.6$ Hz, 4H, H_{14a}), 3.67 (d, $^3J_{\text{H-H}} = 11.6$ Hz, 4H, H_{14b}), 2.79 (t, $^3J_{\text{H-H}} = 7.1$ Hz, 4H, H_{11}), 2.15 (quint, $^3J_{\text{H-H}} = 6.6$ Hz, 4H, H_{12}), 1.44 (s, 6H, H_{16a}), 1.41 (s, 6H, H_{16b}), 1.23 (s, 6H, H_{15}).

$^{13}\text{C}\{^1\text{H}\}$ NMR (100 MHz, CDCl_3 , ppm): $\delta = 174.27$; 131.80; 130.92; 129.93; 127.66; 126.25; 124.85; 124.17; 118.83; 98.09; 94.72; 80.23; 66.10; 63.69; 49.16; 41.96; 33.95; 28.09; 25.60; 24.94; 24.83; 22.53; 18.68; 16.67.

MS (ESI(+)): 701.3 $[\text{M}+\text{Na}]^+$



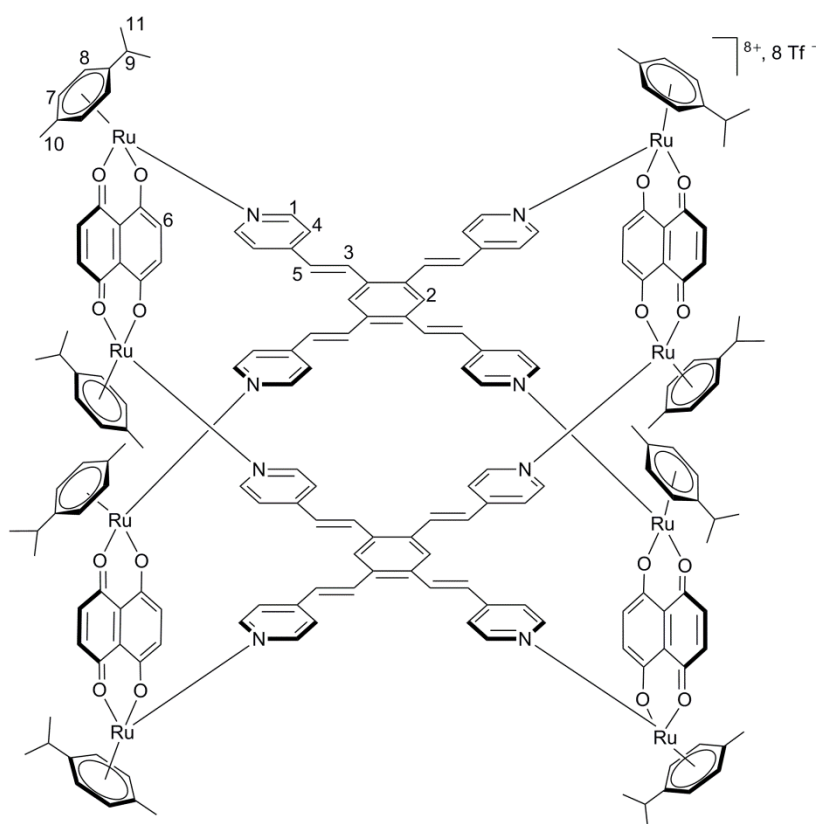
53

11 (0.04 g, 0.06 mmol) and AgCF_3SO_3 (0.03 g, 0.12 mmol) were stirred in methanol (20 mL) under reflux for 2h, after which the mixture was filtered. 4-Tpt (0.01 g, 0.04 mmol), synthesised following a literature procedure,^[116] was added to the filtrate and the mixture was stirred under reflux. After overnight reaction, the solvent was removed and the residue was dissolved in CH_2Cl_2 (3 mL) and was filtered. Diethyl ether was added to the filtrate, resulting

in the precipitation of a dark green solid, which was isolated by filtration. **53** was dried under vacuum and the yield obtained was 70% (0.04 g).

^1H NMR (400 MHz, CD_3CN , ppm): δ = 8.58 (s, 24H, H_1 , H_2), 7.24 (s, 12H, H_3), 5.73 (d, $^3J_{\text{H-H}}$ = 6.1 Hz, 12H, H_4), 5.51 (d, $^3J_{\text{H-H}}$ = 6.1 Hz, 12H, H_4), 2.84 (sept, $^3J_{\text{H-H}}$ = 7.1 Hz, 6H, H_5), 2.10 (s, 18H, H_6), 1.34 (d, $^3J_{\text{H-H}}$ = 6.9 Hz, 36H, H_7)

$^{13}\text{C}\{^1\text{H}\}$ NMR (100 MHz, CD_3CN , ppm): δ = 171.83; 170.72; 154.29; 145.25; 138.40; 125.06; 112.51; 104.93; 100.52; 85.22; 84.24; 31.57; 22.46; 17.32.

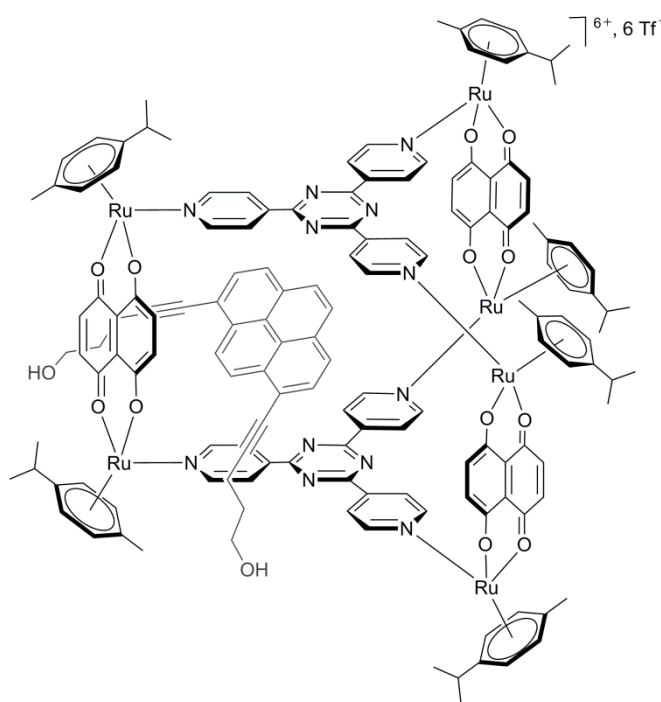


54

11 (0.06 g, 0.08 mmol) and AgCF_3SO_3 (0.04 g, 0.16 mmol) were stirred in methanol (20 mL) under reflux for 2h, after which the mixture was filtered. Tetra-pvb (0.02 g, 0.04 mmol), synthesised following to literature procedures,^[117] was added to the filtrate and the mixture was stirred under reflux. After overnight reaction, the solvent was removed and the residue was dissolved in CH_2Cl_2 (3 mL) and was filtered. Diethyl ether was added to the filtrate, resulting in the precipitation of a dark green solid, which was isolated by filtration. **54** was dried under vacuum and the yield obtained was 64% (0.06 g).

^1H NMR (400 MHz, CD_3CN , ppm): $\delta = 8.31$ (d, $^3J_{\text{H-H}} = 5.8$ Hz, 16H, H_1), 8.04 (s, 4H, H_2), 7.75 (d, $^3J_{\text{H-H}} = 16.1$ Hz, 8H, H_3), 7.65 (d, $^3J_{\text{H-H}} = 5.8$ Hz, 16H, H_4), 7.25 (s, 8H, H_5), 7.24 (d, $^3J_{\text{H-H}} = 16.1$ Hz, 8H, H_6), 7.23 (s, 8H, H_5), 5.73 (d, $^3J_{\text{H-H}} = 5.7$ Hz, 16H, H_7), 5.51 (d, $^3J_{\text{H-H}} = 5.7$ Hz, 16H, H_8), 2.85 (sept, $^3J_{\text{H-H}} = 7.0$ Hz, 8H, H_9), 2.11 (s, 24H, H_{10}), 1.33 (d, $^3J_{\text{H-H}} = 7.0$ Hz, 48H, H_{11})

$^{13}\text{C}\{^1\text{H}\}$ NMR (100 MHz, CD_3CN , ppm): $\delta = 172.01$; 171.74; 152.90; 148.32; 138.41; 135.85; 131.33; 128.56; 125.20; 124.25; 112.48; 104.59; 100.09; 85.17; 85.06; 84.18; 31.44; 22.46; 22.30; 17.32.



55

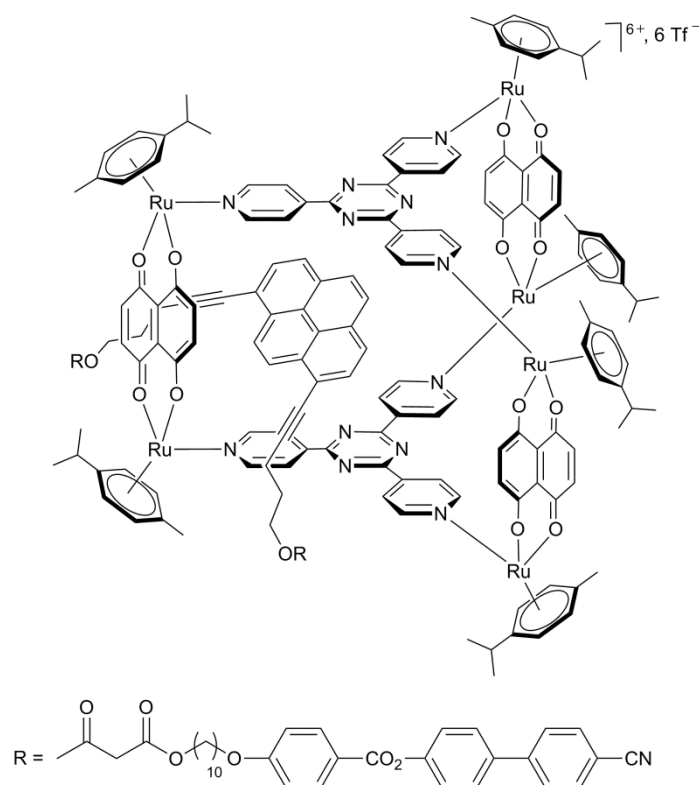
11 (0.04 g, 0.06 mmol) and AgCF_3SO_3 (0.03 g, 0.12 mmol) were stirred in methanol (20 mL) under reflux for 2h, after which the mixture was filtered. 4-Tpt (0.01 g, 0.04 mmol) and **46b** (0.008 g, 0.02 mmol) were added to the filtrate and the mixture was stirred under reflux. After overnight reaction, the solvent was removed and the residue was dissolved in CH_2Cl_2 (3 mL) and was filtered. Diethyl ether was added to the filtrate, resulting in the precipitation of a dark green solid, which was isolated by filtration. **55** was dried under vacuum and the yield obtained was 42% (0.03 g).

^1H NMR (400 MHz, CD_3CN , ppm): $\delta = 8.67$ (s, 4H, H_{pyrene}), 8.26-8.40 (m, 24H, $\text{H}_{4\text{-tpt}}$), 7.37-7.62 (m, 14H, H_{pyrene} , H_{dhnq}), 5.69 (s, 12H, $\text{H}_{p\text{-cym}}$), 5.46 (s, 12H, $\text{H}_{p\text{-cym}}$), 3.74 (s, 4H, H_{pyrene}),

2.78-2.88 (m, 6H, $H_{p\text{-cym}}$), 2.26-2.32 (m, 4H, H_{pyrene}), 2.10-2.11 (m, 4H, H_{pyrene}), 2.02 (s, 18H, $H_{p\text{-cym}}$), 1.29-1.32 (m, 36H, $H_{p\text{-cym}}$).

$^{13}\text{C}\{^1\text{H}\}$ NMR (100 MHz, CD_3OD , ppm): $\delta = 170.85$; 151.93; 137.69; 125.24; 124.16; 123.52; 122.07; 118.90; 115.73; 111.28; 103.75; 100.07; 84.70 ; 82.63; 30.53; 21.07; 15.84.

MS (ESI(+)): 1139.1 $[\text{M}-3\text{Tf}]^{3+}$



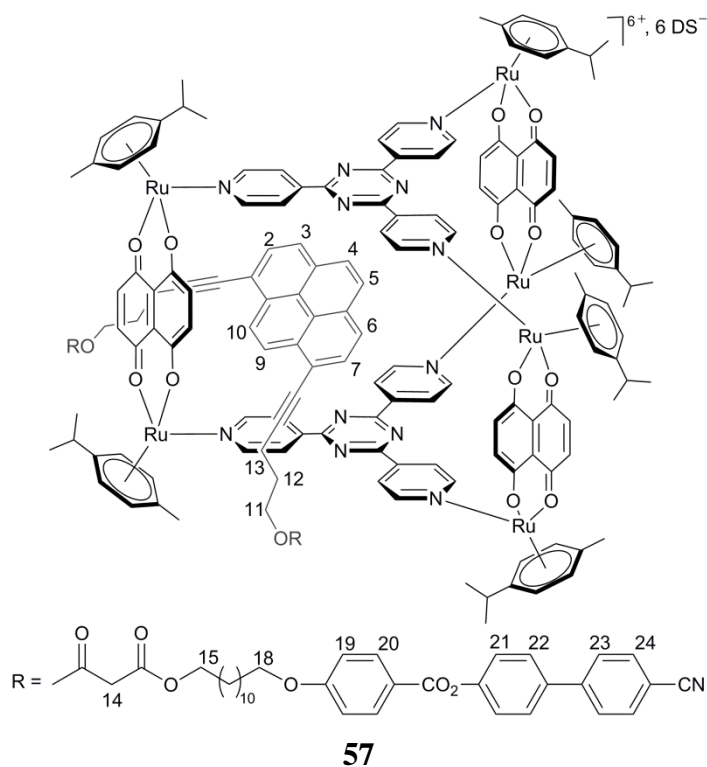
11 (0.02 g, 0.03 mmol), AgCF_3SO_3 (0.01 g, 0.06 mmol), 4-tpt (0.007 g, 0.02 mmol) and **48** (0.01 g, 0.01 mmol) were stirred in methanol (10 mL) under reflux overnight, following the same procedure as **55**. After precipitation from diethyl ether, **56** was obtained as a dark green solid with a yield of 43% (0.02 g).

^1H NMR (400 MHz, CD_2Cl_2 , ppm): $\delta = 8.60$ (s, 24H, $H_{4\text{-tpt}}$), 8.10 (d, $^3J_{\text{H-H}} = 8.7$ Hz, 8H, H_{dendron}), 7.66-7.74 (m, 16H, H_{dendron} , H_{pyrene}), 7.33 (d, $^3J_{\text{H-H}} = 8.3$ Hz, 4H, H_{dendron}), 7.24 (s, 6H, H_{dhnq}), 6.95 (d, $^3J_{\text{H-H}} = 8.5$ Hz, 4H, H_{dendron}), 5.65 (d, $^3J_{\text{H-H}} = 6.1$ Hz, 12H, $H_{p\text{-cym}}$), 5.47 (d, $^3J_{\text{H-H}} = 6.0$ Hz, 12H, $H_{p\text{-cym}}$), 4.42 (t, $^3J_{\text{H-H}} = 6.2$ Hz, 4H, H_{dendron}), 4.13 (t, $^3J_{\text{H-H}} = 6.8$ Hz, 4H, H_{dendron}), 3.98 (t, $^3J_{\text{H-H}} = 6.6$ Hz, 4H, H_{dendron}), 3.42 (s, 4H, H_{dendron}), 2.76-2.81 (m, 10H, $H_{p\text{-cym}}$,

H_{dendron}), 2.07 (s, 18H, $H_{p\text{-cym}}$), 1.90-1.96 (m, 4H, H_{dendron}), 1.34-1.38 (m, 12H, H_{dendron}), 1.30 (d, $^3J_{\text{H-H}} = 6.9$ Hz, 36H, $H_{p\text{-cym}}$).

$^{13}\text{C}\{^1\text{H}\}$ NMR (100 MHz, CD_3OD , ppm): $\delta = 170.81$; 169.51; 152.78; 144.60; 137.82; 137.23; 131.92; 125.71; 124.11; 122.27; 111.02; 103.74; 99.86; 84.57; 82.68; 71.40; 41.11; 46.90; 30.55; 23.06; 21.03; 15.88.

MS (ESI(+)): 1498.6 $[\text{M}-3\text{Tf}]^{3+}$

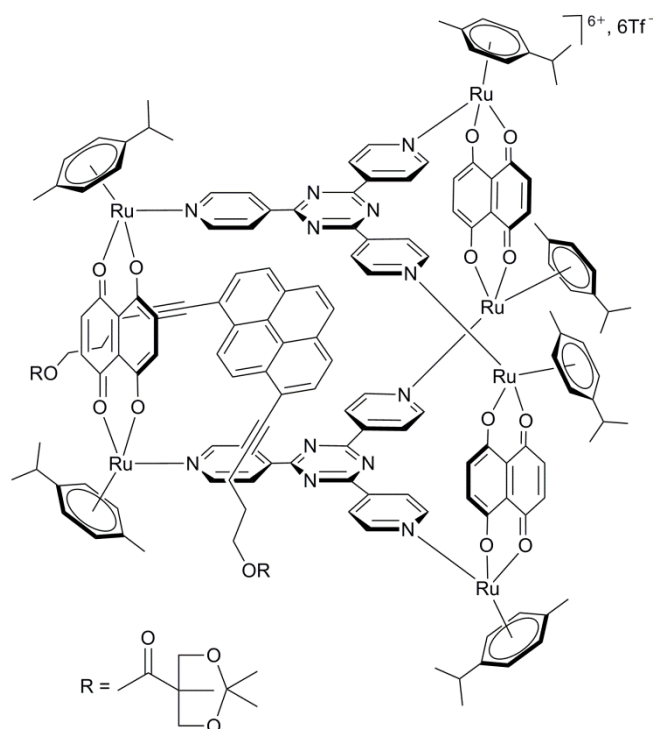


Silver nitrate (2.00 g, 11.70 mmol) was dissolved in H_2O in the dark and mixed with a solution of sodium dodecyl sulfate (0.27 g, 0.90 mmol) in H_2O at 70°C . The mixture was stirred for 3 min at 50°C in the dark, during which a white precipitate was formed. Mixture was filtered and washed abundantly with water. Silver dodecyl sulfate (AgDS) was obtained as a white solid with a yield of 30% (0.10 g). AgDS (0.01 g, 0.06 mmol), **11** (0.02 g, 0.03 mmol), 4-tpt (0.007 g, 0.02 mmol) and **48** (0.01 g, 0.01 mmol) were stirred under reflux in methanol (10 mL) overnight, following the same procedures as **55**. After precipitation from diethyl ether, **57** was obtained as a dark green solid with a yield of 27% (0.01 g).

^1H NMR (400 MHz, CD_2Cl_2 , ppm): $\delta = 8.62$ -8.68 (m, 26H, H_2 , H_7 , H_{tpt}), 8.10 (d, $^3J_{\text{H-H}} = 9.0$ Hz, 4H, H_{20}), 7.95-8.06 (m, 6H, H_3 - H_6 , H_9 , H_{10}), 7.73 (d, $^3J_{\text{H-H}} = 3.5$ Hz, 8H, H_{23} , H_{24}), 7.66

(d, $^3J_{\text{H-H}} = 8.6$ Hz, 4H, H₂₂), 7.31 (d, $^3J_{\text{H-H}} = 8.5$ Hz, 4H, H₂₁), 7.25 (s, 12H, H_{dhmq}), 6.97 (d, $^3J_{\text{H-H}} = 8.7$ Hz, 4H, H₁₉), 5.67-5.82 (m, 12H, H_{p-cym}), 5.50-5.62 (m, 12H, H_{p-cym}), 4.41-4.44 (m, 4H, H₁₁), 4.13 (t, $^3J_{\text{H-H}} = 6.5$ Hz, 4H, H₁₈), 3.90-3.97 (m, 4H, H₁₅), 3.54-3.60 (m, 12H, H_{DS}), 3.42 (s, 4H, H₁₄), 2.74-2.82 (m, 10H, H_{p-cym}, H₃), 2.11-2.15 (m, 4H, H₁₂), 2.05 (s, 18H, H_{p-cym}), 1.47-1.66 (m, 132 H, H_{DS}), 1.26-1.33 (m, 94H, H_{p-cym}, H_{DS}, H_{pyrene})

$^{13}\text{C}\{^1\text{H}\}$ NMR (100 MHz, CD₂Cl₂, ppm): $\delta = 132.61$; 132.12; 128.24; 127.60; 122.50; 114.28; 30.68; 29.60; 29.36; 29.01; 25.86; 21.99; 17.06.

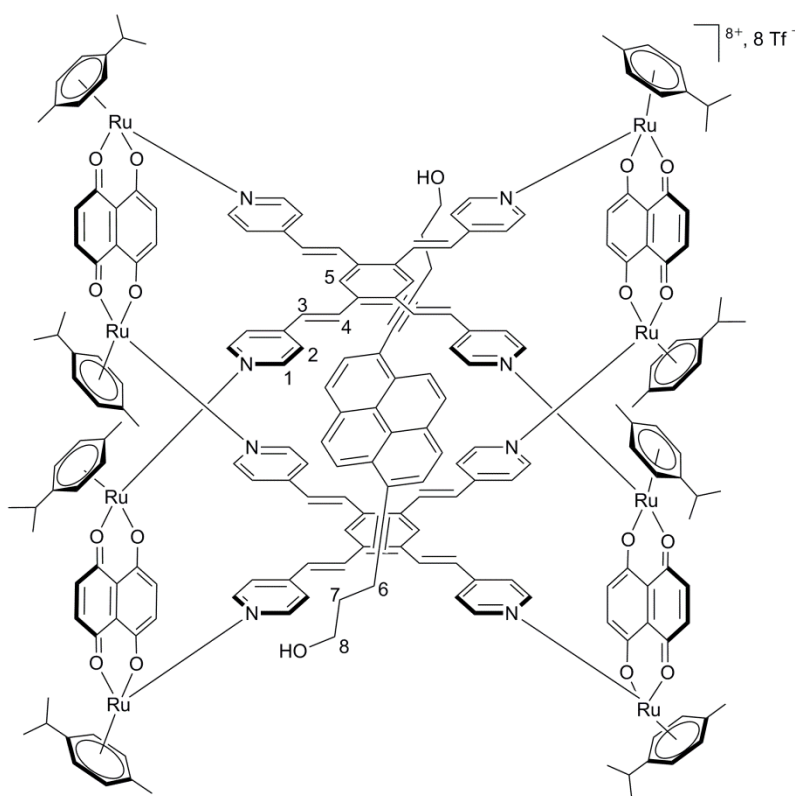


11 (0.008 g, 0.01 mmol), AgCF₃SO₃ (0.008g, 0.03 mmol), 4-tpt (0.003 g, 0.01 mmol) and **52** (0.003 g, 0.005 mmol) were stirred under reflux in methanol (10 mL) overnight, following the same procedures as **55**. After precipitation from diethyl ether, **58** was obtained as a green solid in a yield of 23% (0.01 g).

^1H NMR (400 MHz, CDCl₃, ppm): $\delta = 8.74$ (d, $^3J_{\text{H-H}} = 5.6$ Hz, 2H, H_{pyrene}), 8.57 (d, $^3J_{\text{H-H}} = 5.8$ Hz, 6H, H_{pyrene}), 7.66-7.70 (m, 2H, H_{dhmq}), 7.54-7.58 (m, 2H, H_{dhmq}), 7.48-7.52 (m, 1H, H_{dhmq}), 7.42 (s, 2H, H_{dhmq}), 7.22-7.29 (m, 3H, H_{dhmq}), 5.62-5.74 (m, 12H, H_{p-cym}), 5.43-5.54 (m, 12H, H_{p-cym}), 3.93-4.04 (m, 8H, H_{pyrene}), 2.73-2.85 (m, 6H, H_{p-cym}), 2.27-2.30 (m, 4H, H_{pyrene}),

2.02 (s, 18H, $H_{p\text{-cym}}$), 1.64-1.85 (m, 4H, H_{pyrene}), 1.25-1.32 (m, 48H, $H_{p\text{-cym}}$, H_{pyrene}), 0.85 (s, 6H, H_{pyrene}).

$^{13}\text{C}\{^1\text{H}\}$ NMR (100 MHz, CD_2Cl_2 , ppm): δ = 171.26; 170.74; 170.66; 168.05; 153.17; 142.30; 137.88; 137.53; 124.84; 124.34; 122.50; 111.61; 103.98; 100.24; 84.76; 84.67; 84.61; 82.67; 66.00; 50.02; 39.29; 37.32; 36.99; 32.67; 31.87; 30.65; 29.95; 29.62; 29.30; 27.87; 24.36; 22.63; 21.92; 19.45; 17.50; 17.01; 16.96; 13.82.



59

11 (0.06 g, 0.08 mmol) and AgCF_3SO_3 (0.04 g, 0.16 mmol) were stirred in methanol (20 mL) under reflux for 2h, after which the mixture was filtered. Tetra-pvb (0.02 g, 0.04 mmol) and **46a** (0.008 g, 0.02 mmol) were added to the filtrate and the mixture was stirred under reflux. After overnight reaction, the solvent was removed and the residue was dissolved in CH_2Cl_2 (3 mL) and was filtered. Diethyl ether was added to the filtrate, resulting in the precipitation of a dark green solid, which was isolated by filtration. **59** was dried under vacuum and the yield obtained was 22% (0.02 g).

^1H NMR (400 MHz, CD_3CN , ppm): δ = 8.30 (d, $^3J_{\text{H-H}} = 5.8$ Hz, 16H, H_1), 7.47 (d, $^3J_{\text{H-H}} = 5.8$ Hz, 16H, H_2), 7.36 (s, 8H, H_{dhnq}), 7.31 (s, 8H, H_{dhnq}), 7.11-7.15 (m, 12H, H_4 , H_5), 6.54-6.66

(m, 8H, H₃), 5.72 (d, ³J_{H-H} = 5.9 Hz, 16H, H_{p-cym}), 5.47-5.54 (m, 16H, H_{p-cym}), 3.57-3.64 (m, 4H, H₈), 2.87 (quint, ³J_{H-H} = 6.9 Hz, 8H, H_{p-cym}), 2.13 (s, 18H, H_{p-cym}), 1.75-1.81 (m, 4H, H₇), 1.56-1.66 (m, 4H, H₆), 1.32 (d, ³J_{H-H} = 7.0 Hz, 52 H, H_{p-cym}).

¹³C{¹H} NMR (100 MHz, CD₃CN, ppm): δ = 151.88; 137.36; 123.10; 103.47; 84.00; 83.10; 30.41; 21.33; 21.30; 16.28.

Chapter 5: [60]Fullerene-Ruthenium Complexes

5.1 The [60]Fullerene

After the discovery of the most stable and abundant member of the fullerenes family by Nobel Prize winners Harold W. Kroto, Robert F. Curl and Richard E. Smalley, the icosahedron molecule, [60]fullerene (C_{60}) has been subject to many studies.^[118] Consisting of 12 pentagons and 20 hexagons, the 60 sp^2 hybridised carbon atoms are linked by two types of bonds: double bonds [6,6] between two 6-membered rings of length 1.355 Å and single bonds [5,6] between a 5-membered ring and a 6-membered ring, 1.467 Å long (Figure 5.1). Hence, the 6-membered rings adopt a cyclohexatriene and not a benzene structure as the bond lengths are not all equivalent and the double bonds standing out at each carbon of the 5-membered rings give it the shape of a [5]radialene. The pyramidalised carbon atoms take up the shape of a hollow football with an inner diameter of about 1 nm (Figure 5.1).^[119] From its molecular orbital diagram, C_{60} has three degenerate low lying LUMO and is able to accept reversibly up to six electrons.^[120] Moreover, its high degree of symmetry and its molecular orbital arrangement give C_{60} interesting chemical and physical properties such as electronegativity, photophysical properties, conductivity and its redox potentials.^[121]

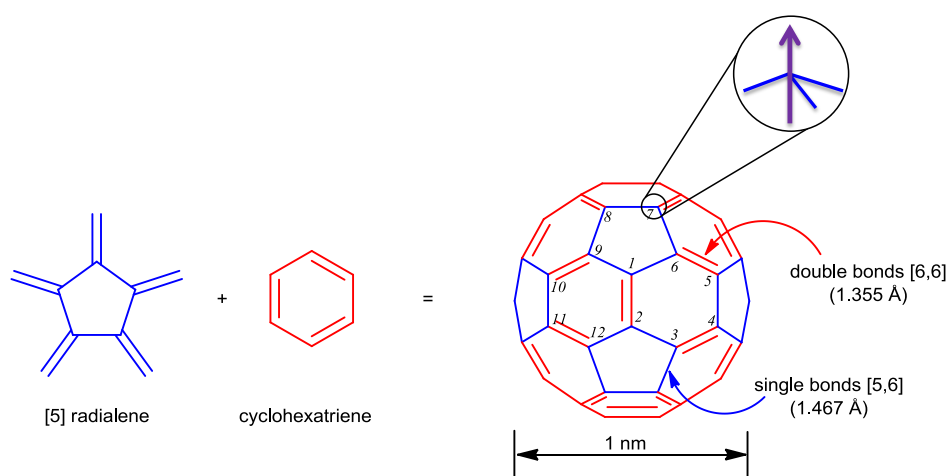


Figure 5.1 Structure of C_{60} molecule

The discovery of a cost-effective production method for fullerenes in 1990 by Krätschmer and Huffman marked the beginning of widespread research in C_{60} chemistry.^[122] But due to its high tendency of forming aggregates and its poor solubility, C_{60} needs to be functionalised to enhance its processability.^[123] The C_{60} molecule has 30 [6,6] double bonds that are all equivalent and have similar reactivity to the double bonds of electron-deficient alkenes.^[121a] Its electrophilic properties and low redox potentials make C_{60} prone to addition and redox reactions across the [6,6] double bonds. Despite the availability of several positions for

addition of addends to the C_{60} , 1,2 addition is the preferred mode as it gives the thermodynamically most stable structure. In the case of sterically demanding addends, 1,4 and 1,6 adducts are obtained rather than 1,2 adduct, as seen in Figure 5.2 below.^[124]

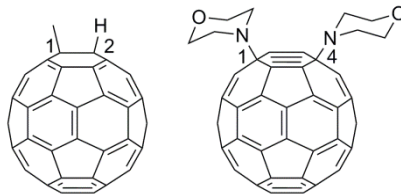
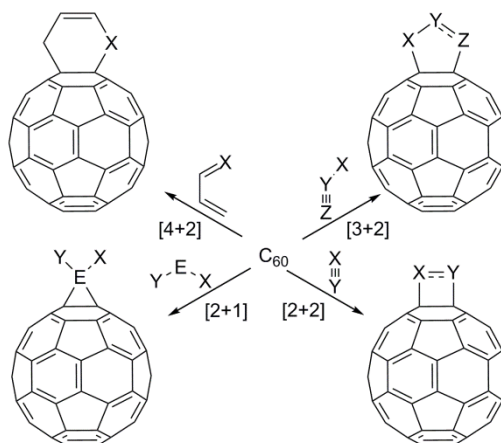


Figure 5.2 Examples of 1,2- and 1,4-adducts of C_{60}

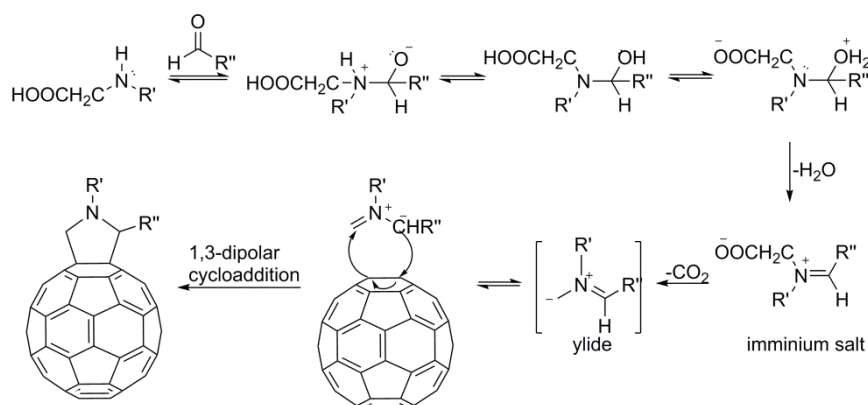
One important aspect of functionalisation of C_{60} is the number of adducts that can be obtained. The mono-functionalisation of C_{60} has been reported to be straightforward, forming one single product due to its icosahedral symmetry. Multi-functionalisation of C_{60} is also possible, even though it is more complicated than the mono-adduct formation because of the numerous isomers resulting from the process. Multi-functionalisation can occur either by stepwise multiple addition to the C_{60} molecule, which involves tedious separation of isomers and hence poor yield and selectivity for the respective isomers, or by tether-directed multiple functionalisation, allowing the formation of controlled multiple adducts of C_{60} .^[125]

C_{60} can undergo several types of reactions, for example nucleophilic and radical additions, cycloadditions, hydrogenations, complexations with transition metals and reactions with electrophiles.^[124] Among these reactions, cycloadditions are very popular to form both mono- and multi-adducts, with the possibility of attaching almost any functional group to the C_{60} molecule. During cycloaddition reactions, the [6,6] double bonds act as dienes or dienophiles. Mostly, the cycloadducts formed are stable, making them appropriate intermediates for further side chain chemistry. Different types of cycloaddition reactions are possible, such as [4+2], [3+2], [2+2] and [2+1], giving different cycloadducts (Scheme 5.1).^[124] Among these reactions, two common examples are

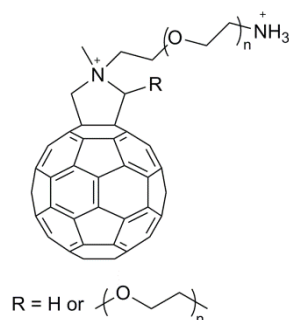
- Diels-Alder and hetero-Diels-Alder [4+2] reactions between a conjugated diene and the C_{60} acting as dienophile.
- Bingel [2+1] cyclopropanation reaction between an acidic malonate and electron-deficient [6,6] double bond of C_{60} .

Scheme 5.1 Examples of cycloaddition reactions on C_{60}

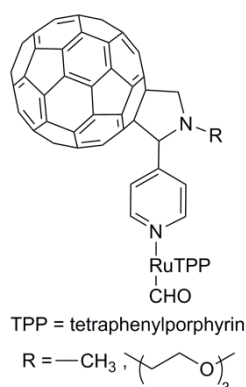
Another widely used cycloaddition reaction of C_{60} is Prato's reaction that involves a 1,3-dipolar cycloaddition of a ylide to a double bond of the C_{60} to form a fulleropyrrolidine. The ylide is formed by the decarboxylation of an iminium salt that is in turn formed by the condensation of an aldehyde with an α -amino acid (Scheme 5.2).^[126]

Scheme 5.2 Mechanism of Prato reaction^[126a]

Depending on the application of the C_{60} derivatives, R' and R'' can be carefully chosen to get the appropriate solubility and properties. For instance, Prato added PEG (polyethylene glycol) chains and made ammonium salt derivatives in order to make C_{60} derivatives hydrophilic enough for biological testing (Figure 5.3).^[126d]

Figure 5.3 Derivatives of C_{60} used for biological testing

Compared to cycloaddition reactions of C_{60} , fewer examples exist in literature for the complexation of this molecule with transition metals. The reported studies of such complexes are mainly directed towards the photophysical and electrochemical properties because of the observed intermolecular electron transfer between the metal donor and the C_{60} acceptor.^[121a, 127] In most of these cases, complexation takes place on the exterior framework of the fullerene, with the electron-rich transition metal coordinating to the electron-deficient C_{60} . Among the few examples of complexes whereby the metal centre and the C_{60} are linked *via* an intermediate moiety is the one reported by Prato; amphiphilic C_{60} -Ru-porphyrin complexes were synthesised for Langmuir-Blodgett film deposit (Figure 5.4).^[128] Likewise C_{60} and its derivatives have found a wide range of applications such as ballistic missile shield, photovoltaic cells, polymer additives, superconductors and surface coatings. Apart from these applications, C_{60} is also viewed as a potential candidate in medicinal chemistry because of its unique photo-, electrochemical and physical properties, its relative inertness under mild conditions and its negligible toxicity.^[121b]

Figure 5.4 C_{60} -porphyrin Ru complexes

Following the footsteps of Prato, many water-soluble fulleropyrrolidines have been synthesised bearing polar groups that enable them to cross cell membranes. Hence, fulleropyrrolidines found medical applications as listed below.^[121b, 129]

- Antiviral: some C₆₀ derivatives, like amino acid ones are active against the human immunodeficiency virus, a HIV. They are able to inhibit and make complexes with HIV protease by fitting inside the hydrophobic cavity hence preventing the access of substrates to the catalytic site of enzyme.^[130]
- Antioxidant: the ability of C₆₀ to take up electrons and to penetrate cell membranes has given C₆₀ the role of a radical scavenger, protecting cell growth from various toxins that can induce apoptotic injuries.
- Drug-delivery: C₆₀ functionalised with hydrophilic groups, which can be in the form of drugs and genes, allows these derivatives to cross cell membrane and bind to mitochondria. In doing so, C₆₀ is able to carry drugs and deliver them to cells.
- Anticancer: C₆₀ bearing functional groups that have biological affinity for nucleic acid/proteins and other C₆₀ derivatives upon UV exposure, show increased cytotoxicity.

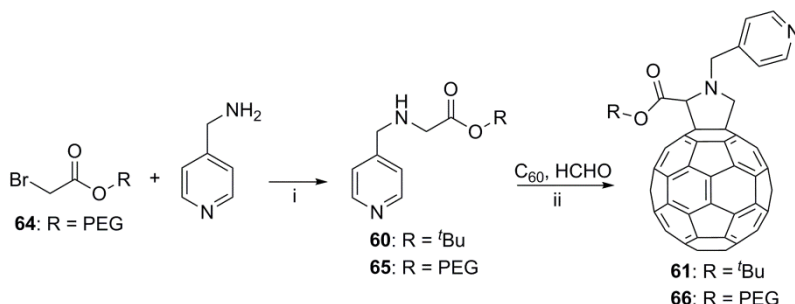
5.2 Aim

The objective of this work is to synthesise half-sandwich arene-Ru complexes with a C₆₀-based ligand for potential biological activities. The combination of these two different areas of research, the chemistry of C₆₀ and arene-Ru, is quite new and has not been well-explored so far.^[131] Hence, the aim is to study the type of interaction existing between the C₆₀ containing ligand and the Ru centre and the properties of the formed products.

5.3 Synthesis

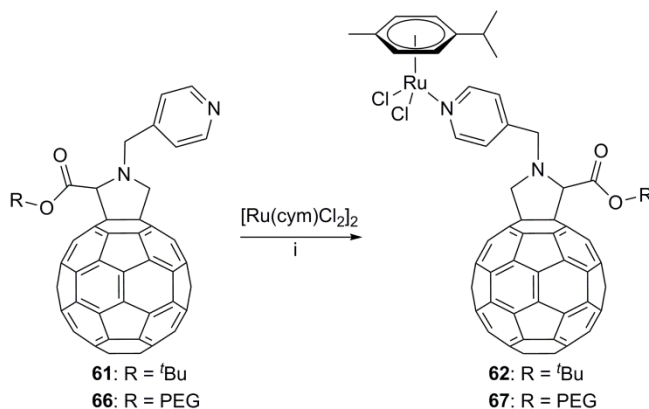
The first step of the ligand synthesis involves a nucleophilic aliphatic substitution reaction between an alkyl bromide and a primary amine, giving a higher substituted amine with the loss of HBr (Scheme 5.3).^[132] The secondary amine formed undergoes a 1,3-dipolar cycloaddition reaction with C₆₀ in the presence of *para*-formaldehyde.^[126b] As described in Scheme 5.2, such a reaction is commonly known as Prato's reaction and it involves two steps: the first one is the formation of a ylide by the decarboxylation of the iminium salt and the second step is the 1,3-dipolar cycloaddition reaction of the ylide onto a [6,6] double bond of

the C₆₀. After purification, the fulleropyrrolidines are obtained as shiny black solids that have good solubility in organic solvents (Scheme 5.3).



Scheme 5.3 Synthesis of compounds **61** and **66**. Reagents and conditions: i. NEt₃, THF, 0°C to rt, 16h, **60**: 60%, **65**: 32%, ii. toluene, 110°C, 16h, **61**: 51%, **66**: 24%

The next step is the complexation with ruthenium *para*-cymene dichloride dimer, [(η⁶-*p*-cym)Ru(μ₂-Cl)Cl]₂ whereby the labile chloride ligand is readily replaced by the nitrogen atom of the pyridyl group (Scheme 5.4).^[133] A neutral half-sandwich C₆₀-Ru-arene dichloride is formed that shows high solubility in organic solvents but is insoluble in aqueous medium when R is a tertiarybutyl group. Since water solubility is crucial for biological testing, compound **62** could not be tested straightaway.



Scheme 5.4 Synthesis of compounds **62** and **67**. Reagents and conditions: i. CH₂Cl₂, reflux, 24h, in dark, **62**: 98%, **67**: 92%

In order to make the complex more water soluble, a solubilizing group was added to the complex. The hydrophilic compound 1,3,5-triaza-7-phosphaadamantane (pta), which has been used by Dyson in making RAPTA-C, was used as ligand to improve the solubility of compound **62**. The reaction involved the abstraction of a labile chloride ligand from the Ru

complex by a Ag^+ ion from silver triflate, forming AgCl precipitate (Figure 5.5).^[134] Unexpectedly, the complex formed not only had poor water solubility, but it had lost its solubility in common organic solvents, making its characterization and purification very difficult. The mass spectrum of the compound showed the peak corresponding to the mass of the expected product, but its insolubility in water made it unsuitable for biological tests.

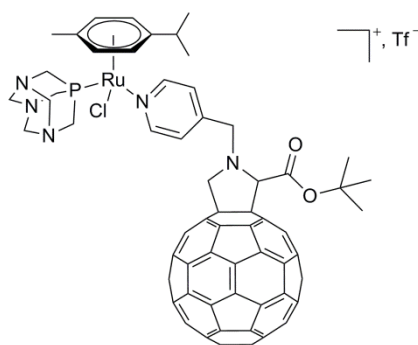
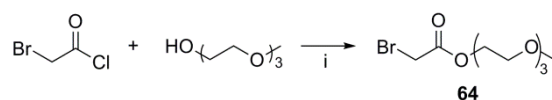


Figure 5.5 Structure of compound **63**

Another attempt was made to increase the hydrophilicity of the C_{60} -Ru complex by replacing the ester group with a PEG chain. Compound **64** was first synthesised by a reaction between bromoacetyl chloride and tri(ethylene)glycol monoethyl ether in dry CH_2Cl_2 (Scheme 5.5).^[135] The reaction was done in the presence of 4-(dimethylamino)pyridine (DMAP), which is an effective esterification catalyst that allows the reaction to occur at low temperatures, hence avoiding degradations. The nucleophilic addition of the alcohol group onto the carbonyl group of the acid chloride, followed by the elimination of HCl results in compound **64** (Scheme 5.5).



Scheme 5.5 Synthesis of compound **64**. Reagents and conditions: i. NEt_3 , DMAP, CH_2Cl_2 , 0°C to rt, 20h, quantitative yield

Compound **64** was then reacted with 4-(aminomethyl)pyridine to form **65** in the same manner as **60** and after subsequent reactions, product **67** was formed (Scheme 5.4). It was found that compound **67** showed similar solubility as compound **62**, meaning that the PEG chain was not efficient in making the complex hydrophilic. A possible explanation for the solubility problem of these two compounds might lie in the hydrophobic nature of the C_{60} moiety. The hydrophilicity of the ruthenium dichloride or the Ru-pta moieties are not able to balance the

hydrophobicity of the C₆₀. Hence, the biological activities of these complexes could not be evaluated due to their insolubility in aqueous medium.

5.4 Characterization

5.4.1 Proton NMR Spectroscopy

The ¹H NMR spectra of the C₆₀ derivatives **61** and **66** are the typically observed spectra for this family of fulleropyrrolidines. One characteristic feature of this family of compounds is that the protons closest to the C₆₀ moiety are not equivalent. This loss of equivalence and hence of conformation is due to the chiral centre on the pyrrolidine. For instance, H₃ protons, which appear as a doublet in compound **60** at 3.30 ppm, can be seen as two doublets at 4.93 and 4.30 ppm in product **61**. Similarly, H₄ protons are observed as two doublets at 4.69 and 4.14 ppm in compound **61**.

Moreover, complexation with Ru results in a major shift in the proton peaks of compound **62** compared to compound **61** (Figure 5.6). This chemical shift corresponds to H₁ protons of the pyridyl group. Complexation with Ru metal causes a downfield shift of these protons from 8.68 to 9.06 ppm. The other protons of the ligand do not undergo any major shifting as a result of complexation.

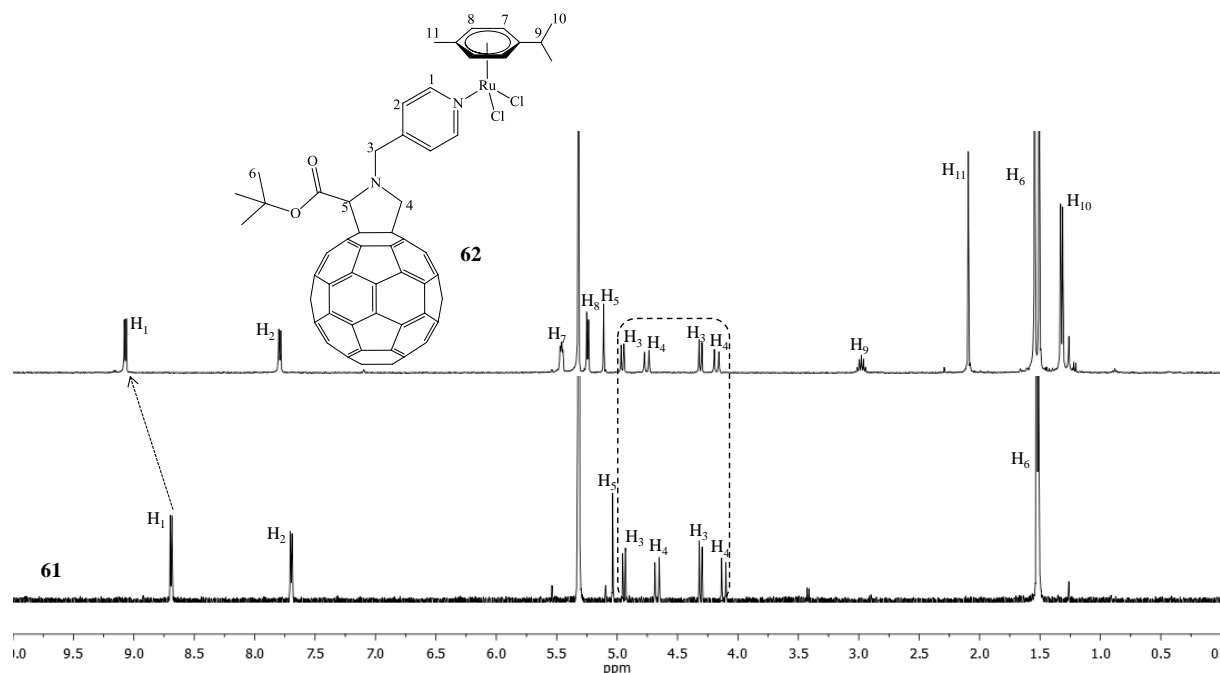


Figure 5.6 ¹H NMR (400 Hz, CD₂Cl₂) spectra of **61** and **62**

5.4.2 UV-Visible Spectroscopy

The UV-Vis spectra of compounds **61** and **62** display two bands around 308 and 429 nm. The intense, high in energy band centred at 308 nm is observed in both compounds **61** and **62**. This band is similar to the one observed at 331 nm in ruthenium *para*-cymene dichloride dimer and it is assigned to the ligand-centred $\pi \rightarrow \pi^*$ electronic transitions.^[136] The narrow band at 429 nm is considered as the fingerprint for fulleropyrrolidines, hence confirming the presence of pyrrolidine on C₆₀ for compounds **61** and **62**. Another characteristic band of these C₆₀ mono-adducts usually appear around 700 nm. But in the case of compounds **61** and **62**, this band is not visible because of its broadness and low intensity.^[126c] The maximum wavelength (λ_{\max}) and molar absorptivity (ϵ) values are listed in Table 5.1, where ϵ was determined using the Beer-Lambert law:

$$\epsilon = \frac{A}{lc} \quad \text{Equation 1}$$

where, A = absorption,

l = length of cuvette, cm

c = concentration of sample, mol·L⁻¹

Table 5.1 UV-Vis measurements of $[(\eta^6\text{-}p\text{-cym})\text{Ru}(\mu_2\text{-Cl})\text{Cl}]_2$, **61** and **62** in CH₂Cl₂

| Compound | λ_{\max} (nm) | ϵ (L·mol ⁻¹ ·cm ⁻¹) |
|---|-----------------------|---|
| $[(\eta^6\text{-}p\text{-cym})\text{Ru}(\mu_2\text{-Cl})\text{Cl}]_2$ | 331 | 1500 |
| 61 | 429 | 2400 |
| | 308 | 19300 |
| 62 | 429 | 1400 |
| | 308 | 10400 |

From the UV-Vis spectra, it can be observed that there is no electron/energy transfer between the ruthenium and C₆₀ at ground state (Figure 5.7).

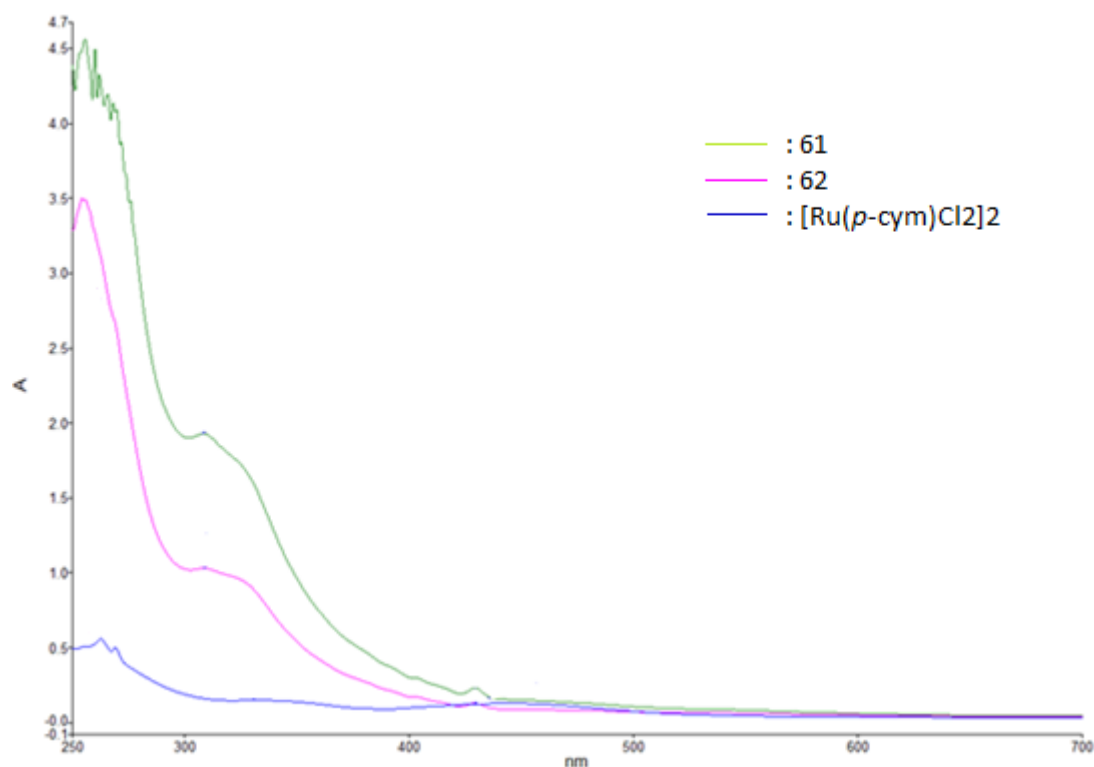
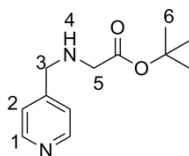


Figure 5.7 UV-Vis spectra of $[(\eta^6\text{-}p\text{-cym})\text{Ru}(\mu_2\text{-Cl})\text{Cl}]_2$, **61** and **62** in CH_2Cl_2

5.5 Conclusion

Two new fulleropyrrolidines and their corresponding arene-Ru complexes were successfully synthesised and characterised. The two half-sandwich complexes showed poor solubility in aqueous medium. Attempts to find the right equilibrium between the hydrophilicity and hydrophobicity of the complexes did not result in the desired solubility. Hence, despite the progress made in the synthetic part, the biological evaluation of C_{60} -Ru complexes could not be carried out and therefore remains to be solved.

5.6 Experimental Part



60

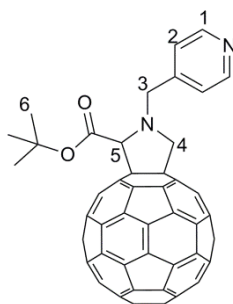
4-(Aminomethyl)pyridine (0.76 mL, 7.50 mmol) and triethylamine (2.09 mL, 15.00 mmol) were dissolved in dry THF (40 mL) at 0°C under argon. To this mixture, a THF solution (25 mL) of 2-bromoethyl propionate (0.74 mL, 5.00 mmol) was added dropwise over 2h with stirring. After 16h of reaction at rt, water (50 mL) was added to the reaction mixture and

extraction was done with CH_2Cl_2 . The combined organic phase was dried over anhydrous MgSO_4 and evaporation of the solvent gave a dark brown liquid. The crude product was purified by CC (eluent $\text{CH}_2\text{Cl}_2/\text{MeOH}$ 10/0.75). Product **60** was obtained as an orange/red liquid with a yield of 60% (0.66 g).

^1H NMR (400 MHz, CDCl_3 , ppm): $\delta = 8.54$ (d, $^3J_{\text{H-H}} = 6.0$ Hz, 2H, H_1), 7.27 (d, $^3J_{\text{H-H}} = 5.6$ Hz, 2H, H_2), 3.81 (s, 2H, H_5), 3.30 (s, 2H, H_3), 2.09 (s, 1H, H_4), 1.46 (s, 9H, H_6).

$^{13}\text{C}\{^1\text{H}\}$ NMR (100 MHz, CDCl_3 , ppm): $\delta = 171.25$; 149.54; 148.92; 123.18; 81.63; 51.89; 50.79; 28.12.

MS (ESI(+)) = 223.3 $[\text{M}+\text{H}]^+$



61

After completely dissolving C_{60} (0.36 g, 0.50 mmol) in dry toluene (300 mL) under argon and in the dark, a suspension of **60** (0.11 g, 0.50 mmol) and *para*formaldehyde (0.07 g, 2.50 mmol) in toluene (10 mL) was added to the C_{60} solution and the mixture was heated under reflux for 16h in the dark. The mixture was then cooled and the solvent was evaporated, giving a black solid. Purification of the crude product was done by two CC (eluent toluene then toluene/MeOH 10/0.5). Product **61** was obtained as shiny black solid with a yield of 51% (0.24 g).

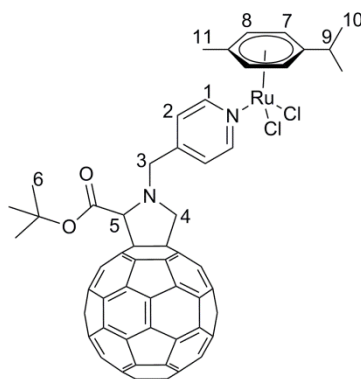
^1H NMR (400 MHz, CD_2Cl_2 , ppm): $\delta = 8.69$ (d, $^3J_{\text{H-H}} = 5.2$ Hz, 2H, H_1), 7.70 (d, $^3J_{\text{H-H}} = 5.3$ Hz, 2H, H_2), 5.04 (s, 1H, H_5), 4.96 (d, $^3J_{\text{H-H}} = 9.3$ Hz, 1H, H_3), 4.69 (d, $^3J_{\text{H-H}} = 14.0$ Hz, 1H, H_4), 4.32 (d, $^3J_{\text{H-H}} = 9.3$ Hz, 1H, H_3), 4.14 (d, $^3J_{\text{H-H}} = 14.0$ Hz, 1H, H_4), 1.53 (s, 9H, H_6).

$^{13}\text{C}\{^1\text{H}\}$ NMR (100 MHz, CD_2Cl_2 , ppm): $\delta = 168.58$; 154.49; 153.76; 152.44; 151.22; 150.14; 147.34; 146.95; 146.23; 146.01; 145.33; 145.21; 144.58; 144.44; 143.02; 142.56;

142.17; 142.11; 142.05; 142.04; 141.74; 140.18; 140.13; 138.69; 139.28; 136.33; 135.99; 132.27; 123.61; 83.16; 76.79; 72.76; 69.49; 67.73; 64.85; 54.73; 27.98.

MS (ESI(+)) = 956.1 [M+H]⁺

IR (KBr): 3434 (w, CH_{arom}); 2972 (s, CH₂); 1713 (s, C=O); 1600 (s, C=C); 1150 (s, CO_{ester}).



62

Ruthenium *para*-cymene dichloride dimer (0.05 g, 0.10 mmol) and **61** (0.19 g, 0.20 mmol) were stirred under reflux in dry CH₂Cl₂ (50 mL) under argon for 24h, and then the solvent removed. The residue obtained was dried under vacuum. Product **62** was obtained as a brown solid with a yield of 98% (0.24 g).

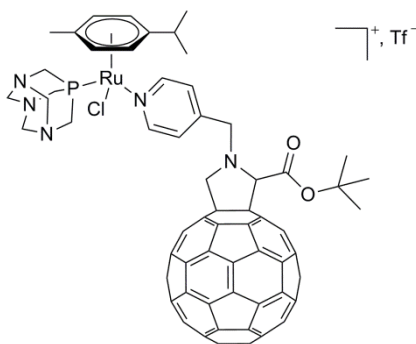
¹H NMR (400 MHz, CD₂Cl₂, ppm): δ = 9.08 (d, ³J_{H-H} = 6.6 Hz, 2H, H₁), 7.79 (d, ³J_{H-H} = 6.1 Hz, 2H, H₂), 5.45-5.47 (m, 2H, H₇), 5.25 (d, ³J_{H-H} = 6.0 Hz, 2H, H₈), 5.11 (s, 1H, H₅), 4.97 (d, ³J_{H-H} = 9.4 Hz, 1H, H₃), 4.77 (d, ³J_{H-H} = 15.1 Hz, 1H, H₄), 4.32 (d, ³J_{H-H} = 9.4 Hz, 1H, H₃), 4.20 (d, ³J_{H-H} = 15.1 Hz, 1H, H₄), 2.98 (sept, ³J_{H-H} = 6.9 Hz, 1H, H₉), 2.09 (s, 3H, H₁₁), 1.53 (s, 9H, H₆), 1.33 (d, ³J_{H-H} = 7.0 Hz, 6H, H₁₀).

¹³C{¹H} NMR (100 MHz, CD₂Cl₂, ppm): δ = 169.09; 155.45; 150.82; 147.06; 146.86; 146.63; 146.38; 146.26; 146.19; 145.98; 145.83; 145.22; 145.02; 143.60; 143.23; 142.77; 142.66; 142.37; 140.78; 136.89; 136.64; 124.62; 103.86; 97.57; 84.01; 83.50; 83.38; 82.75; 82.72; 77.42; 73.28; 70.11; 65.44; 54.67; 53.46; 31.23; 30.24; 28.61; 22.57; 22.55; 18.53.

MS (ESI(+)) = 1225.12 [M-Cl]⁺

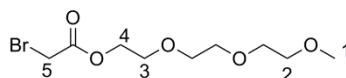
IR (KBr) = 3435 (w, CH_{arom}); 2961 (s, CH₂); 1725 (s, C=O); 1613 (s, C=C); 1150 (s, CO_{ester}).

Anal. Calcd. (found) for $C_{83}H_{32}N_2O_2Cl_2Ru$ (1261.15): C, 78.87 (79.05); H, 2.80 (2.56); N, 2.20 (2.22)%

**63**

62 (0.06 g, 0.05 mmol) and an excess of $AgCF_3SO_3$ (0.08 g, 0.32 mmol) were dissolved in CH_2Cl_2 (25 mL) and stirred at rt. After overnight stirring, the mixture was filtered and the solvent was evaporated. Methanol (20 mL) was added to dissolve the residue and pta (0.01 g, 0.10 mmol) was added. Mixture was stirred at rt for 4h. The solvent was evaporated, leaving **63** as a brown solid in a crude yield of 97% (0.06 g).

MS (ESI(+)) = 1382.5 $[M-Tf]^+$

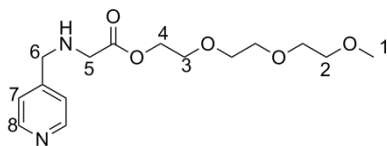
**64**

A solution of bromoacetyl chloride (0.15 g, 1.00 mmol) in dry CH_2Cl_2 (2 mL) was added dropwise to a mixture of tri(ethylene)glycol monoethyl ether (0.16 mL, 1.00 mmol), triethylamine (0.14 mL, 1.00 mmol), DMAP (0.006 g, 0.05 mmol) and CH_2Cl_2 (6 mL) under stirring at $0^\circ C$. The reaction mixture was stirred for 2h at $0^\circ C$ and for 16h at rt. The mixture was then filtered and the filtrate washed two times with HCl (1N), saturated $NaHCO_3$ and brine solution. The organic phase was dried over anhydrous $MgSO_4$ and the solvent was evaporated. Product **64** was obtained as a pale yellow liquid with a quantitative yield (0.39 g).

1H NMR (400 MHz, $CDCl_3$, ppm): δ = 4.32-4.36 (m, 2H, H_4), 4.10 (s, 1H, H_5), 3.87 (s, 1H, H_5), 3.72-3.75 (m, 2H, H_2), 3.64-3.67 (m, 6H, chain), 3.54-3.57 (m, 2H, H_3), 3.38 (s, 3H, H_1).

^{13}C NMR (100 MHz, $CDCl_3$, ppm): δ = 166.35; 75.78; 70.92; 69.65; 69.58; 67.75; 64.30; 58.02; 39.85; 24.82.

MS (ESI(+)) = 309.3 [M+Na]⁺



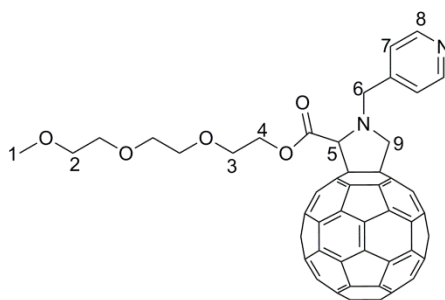
65

4-(Aminomethyl)pyridine (0.15 mL, 1.50 mmol), triethylamine (0.42 mL, 3.00 mmol) and **64** (0.28 g, 1.00 mmol) in dry THF (60+20 mL) reacted and the product was purified following same procedure as for compound **60**. Product **65** was isolated as a pale yellow liquid with a yield of 32% (0.10 g).

¹H NMR (400 MHz, CDCl₃, ppm): δ = 8.56 (d, ³J_{H-H} = 6.1 Hz, 2H, H₈), 7.28 (d, ³J_{H-H} = 6.1 Hz, 2H, H₇), 4.30 (t, ³J_{H-H} = 4.7 Hz, 2H, H₄), 3.87 (s, 2H, H₆), 3.68-3.71 (m, 2H, H₂), 3.63-3.66 (m, 6H, chain), 3.53-3.55 (m, 2H, H₃), 3.45 (s, 2H, H₅), 3.37 (s, 3H, H₁).

¹³C{¹H} NMR (100 MHz, CDCl₃, ppm): δ = 171.86; 149.27; 123.31; 71.90; 70.58; 68.96; 64.04; 61.64; 59.00; 51.72; 49.82.

MS (ESI(+)) = 313.3 [M+H]⁺



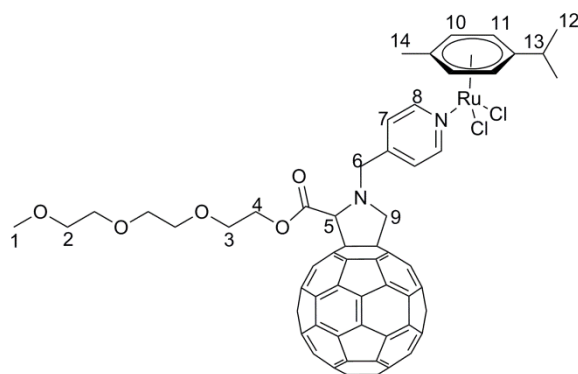
66

C₆₀ (0.13 g, 0.16 mmol), *para*-formaldehyde (0.02 g, 0.70 mmol) and **65** (0.04 g, 0.14 mmol) in dry toluene (250 mL) reacted following same procedures as compound **61**. The crude product obtained after the evaporation of the reaction solvent was purified by two CC (eluent toluene then CH₂Cl₂/MeOH 10/0.5) and a CC of Bio-Rad SX1 (eluent toluene). Product **66** was obtained as a brown solid with a yield of 24% (0.07 g).

^1H NMR (400 MHz, CD_2Cl_2 , ppm): $\delta = 8.69$ (d, $^3J_{\text{H-H}} = 4.9$ Hz, 2H, H_8), 7.70 (d, $^3J_{\text{H-H}} = 5.6$ Hz, 2H, H_7), 5.23 (s, 1H, H_5), 4.97 (d, $^3J_{\text{H-H}} = 9.4$ Hz, 1H, H_9), 4.68 (d, $^3J_{\text{H-H}} = 14.1$ Hz, 1H, H_9), 4.44-4.48 (m, 2H, H_4), 4.35 (d, $^3J_{\text{H-H}} = 9.5$ Hz, 1H, H_6), 4.14 (d, $^3J_{\text{H-H}} = 14.1$ Hz, 1H, H_6), 3.62-3.73 (m, 2H, H_3), 3.54-3.45 (m, 8H, H_2), 3.30 (s, 3H, H_1).

$^{13}\text{C}\{^1\text{H}\}$ NMR (100 MHz, CD_2Cl_2 , ppm): $\delta = 170.12$; 155.00; 150.79; 147.31; 146.87; 146.69; 145.65; 146.63; 146.37; 146.24; 146.21; 145.85; 145.83; 143.25; 143.22; 143.19; 142.83; 142.81; 142.67; 142.54; 142.39; 142.37; 142.36; 124.30; 77.12; 73.32; 72.45; 71.09; 70.99; 70.06; 69.44; 65.45; 65.19; 59.20; 55.40; 30.26.

MS (ESI(+)) = 1045.4 $[\text{M}+\text{H}]^+$



67

Ruthenium *para*-cymene dichloride dimer (0.01 g, 0.02 mmol) and **66** (0.05 g, 0.04 mmol) in dry CH_2Cl_2 (5 mL) reacted and the product was purified following same procedure as compound **62**. Product **67** was obtained as a black solid with a yield of 92% (0.05 g).

^1H NMR (400 MHz, CD_2Cl_2 , ppm): $\delta = 9.08$ (d, $^3J_{\text{H-H}} = 6.7$ Hz, 2H, H_8), 7.80 (d, $^3J_{\text{H-H}} = 6.4$ Hz, 2H, H_7), 5.44-5.47 (m, 2H, H_{11}), 5.31 (s, 1H, H_5), 5.25 (d, $^3J_{\text{H-H}} = 5.9$ Hz, 2H, H_{10}), 4.98 (d, $^3J_{\text{H-H}} = 9.5$ Hz, 1H, H_9), 4.77 (d, $^3J_{\text{H-H}} = 15.1$ Hz, 1H, H_9), 4.44-4.47 (m, 2H, H_4), 4.35 (d, $^3J_{\text{H-H}} = 9.4$ Hz, 1H, H_6), 4.20 (d, $^3J_{\text{H-H}} = 15.1$ Hz, 1H, H_6), 3.71-3.60 (m, 2H, H_3), 3.45-3.55 (m, 8H, H_2), 3.31 (s, 3H, H_1), 2.95-3.02 (m, 1H, H_{13}), 2.09 (s, 3H, H_{14}), 1.33 (d, $^3J_{\text{H-H}} = 6.9$ Hz, 6H, H_{12}).

$^{13}\text{C}\{^1\text{H}\}$ NMR (100 MHz, CD_2Cl_2 , ppm): $\delta = 170.04$; 155.47; 154.99; 154.74; 153.71; 151.40; 150.60; 148.00; 149.86; 147.05-145.85; 145.23; 145.11; 144.96; 143.63; 143.21; 142.81; 142.68-142.44; 142.38; 140.88; 140.81; 140.29; 140.15; 138.25; 136.93; 136.82; 136.10;

124.66; 103.90; 97.55; 83.45; 83.36; 82.76; 77.09; 73.20; 72.43; 71.05; 70.97; 70.95; 70.05;
69.36; 65.42; 65.28; 59.20; 31.24; 22.56; 18.54.

MS (ESI(+)) = 1363.2 [M+Na]⁺

Chapter 6: Conclusion & Perspectives

6.1 Conclusion

The first part involved the possibility of designing a new series of supramolecular assemblies comprising of H-bond held dimers and Ru clips of various lengths. Bi- and tetranuclear complexes were formed and NMR studies and DFT calculations were run in order to better understand the organization in these systems. The head-to-tail arrangement of the dimers as well as the rectangular assembly of the tetranuclear Ru compounds was hence confirmed. The general synthesis for the compounds was straight forward, and the purifications were simple.

In the second part, several problems were faced, like the poor stability of the anthracene derivatives. Along the synthetic route, the isolation of pure compounds became increasingly challenging. The final product underwent degradation during the purification step, making it very difficult to be obtained pure under the conditions used, and hence could not be used for further reactions.

Another section of the second part involves the pyrene derivatives. Better stability of these compounds enabled more advanced study of the systems. Hence, their liquid-crystalline properties were observed and their encapsulation in Ru cages was studied. Compound **54** was the successful encapsulated product of **48** into a hexanuclear Ru prism by carceplex method. However, **54** did not show any liquid-crystalline properties, even with a softer counter anion in compound **55**.

In the last part, the synthesis of arene-ruthenium compounds containing [60]fullerene was described. But, their poor water solubility did not allow their biological properties to be evaluated.

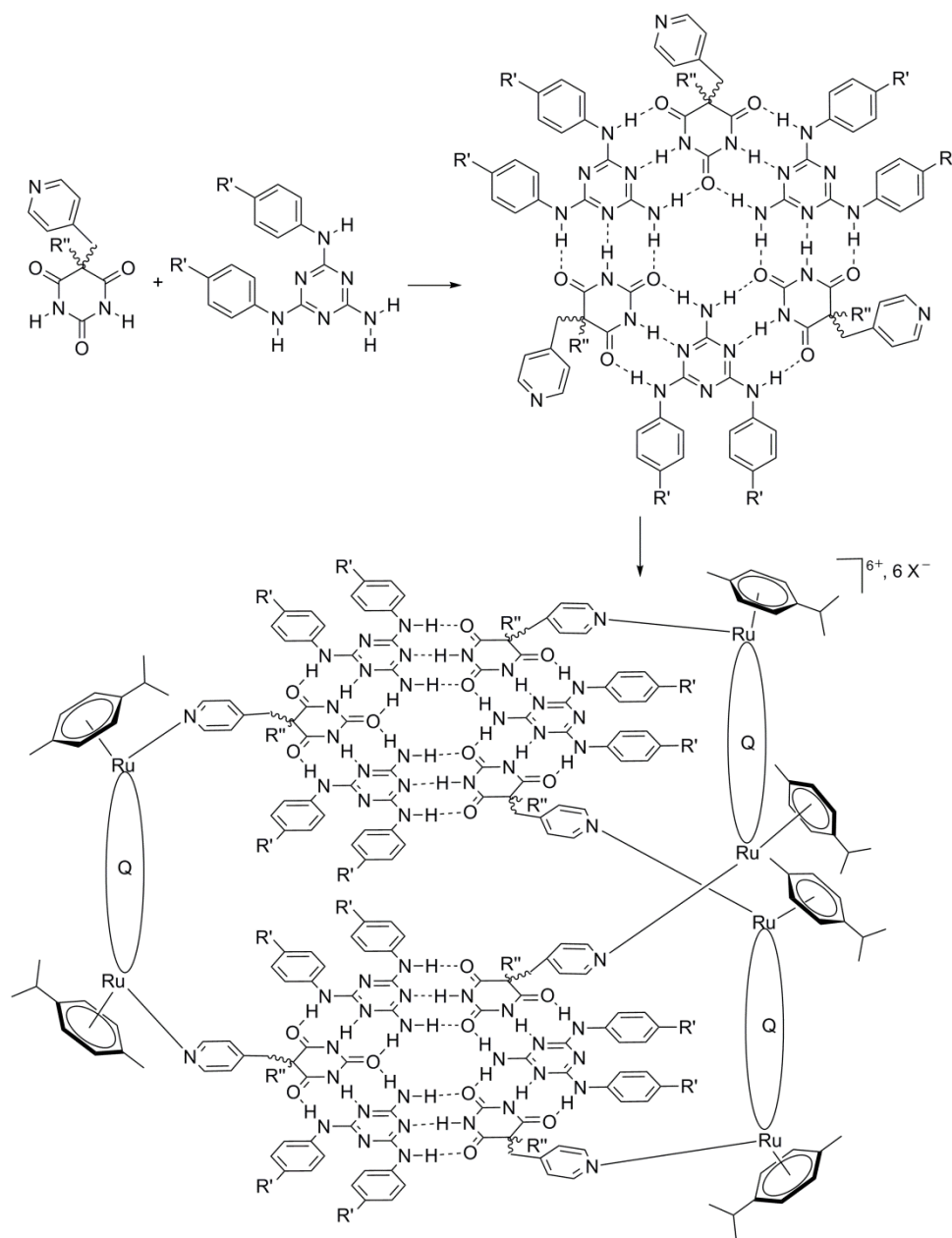
6.2 Perspectives

The work carried out in Chapter 2 can be considered as the foundation upon which a new area of research in the chemistry of supramolecules and arene-ruthenium metallo-assemblies can be built. The development of a new series of tetranuclear metallo-cages bearing a cavity has provided a new route towards host-guest chemistry.

Although this work focused on the construction of only rectangular arrangements, there exists the possibility of building prismatic and cubic systems by following similar pathways. For instance, one potential spacer ligand, held together by H-bonding, to generate hexanuclear arrangement may be the rosette-type structure shown in Scheme 6.1. This molecule is a tridentate ligand composed of two different units arranged in alternating order, with six H-bonds around each unit. Hence, 18 H-bonds exist per spacer ligand, with three coordinating sites available to link to the ruthenium centres.^[57] The possibilities of altering R' and R'' groups allows for a wide spectrum of arrangements that can be used to tune the solubility and/or the affinity of the assembly for particular systems.

After obtaining the ruthenium cages, their potential to host different guests may be studied. The larger sizes of the cavity of the different arrangements compared to the typical tpt, bpe and porphyrin-based spacer ligands, may allow a wider range of molecules to be encapsulated into these ruthenium cages.

From Chapter 4, it was observed that the encapsulation of pyrene-core dendrimers was quite challenging in the typical hexanuclear and octanuclear ruthenium cages with 4-tpt and tetrapvb spacer ligands. Therefore, another perspective might be the possibility of encapsulating these pyrene dendrimers into the above mentioned supramolecular assemblies. The larger cavity of these potential hosts might allow the pyrene dendrimers to be trapped more easily.



Scheme 6.1 Self-assembly of rosette molecules

Chapter 7: References

- [1] N. N. Greenwood, A. Earnshaw, 'Chemistry of the elements', Second ed., Elsevier, Oxford, **1997**.
- [2] S. Nishimura, H. Yoshino, *B. Chem. Soc. Jpn.* **1969**, *42*, 499-501.
- [3] T. Naota, H. Takaya, S. I. Murahashi, *Chem. Rev.* **1998**, *98*, 2599-2660.
- [4] a) R. H. Grubbs, S. Chang, *Tetrahedron* **1998**, *54*, 4413-4450; b) R. H. Grubbs, *Tetrahedron* **2004**, *60*, 7117-7140; c) S. B. Garber, J. S. Kingsbury, B. L. Gray, A. H. Hoveyda, *J. Am. Chem. Soc.* **2000**, *122*, 8168-8179.
- [5] B. Therrien, *CrystEngComm.* **2015**, *17*, 484-491.
- [6] a) M. J. Hannon, *Pure Appl. Chem.* **2007**, *79*, 2243-2261; b) J. Reedijk, *Chem. Commun. (Cambridge)* **1996**, 801-806; c) G. Süß-Fink, *Dalton Trans.* **2010**, *39*, 1673-1688.
- [7] A. Vessieres, S. Top, W. Beck, E. Hillard, G. Jaouen, *Dalton Trans.* **2006**, 529-541.
- [8] O. R. Allen, L. Croll, A. L. Gott, R. J. Knox, P. C. McGowan, *Organometallics* **2004**, *23*, 288-292.
- [9] A. V. Rudnev, L. S. Foteeva, C. Kowol, R. Berger, M. A. Jakupec, V. B. Arion, A. R. Timerbaev, B. K. Keppler, *J. Inorg. Biochem.* **2006**, *100*, 1819-1826.
- [10] a) A. Bergamo, C. Gaiddon, J. H. M. Schellens, J. H. Beijnen, G. Sava, *J. Inorg. Biochem.* **2012**, *106*, 90-99; b) A. Levina, A. Mitra, P. A. Lay, *Metallomics* **2009**, *1*, 458-470.
- [11] a) T. G. Ioannis Bratsos, Enzo Alessio, Christian G. Hartinger, Michael A. Jakupec, B. K. Keppler, *Bioinorganic Medicinal Chemistry* **2011**, 151-174; b) C. S. Allardyce, P. J. Dyson, *Platinum Met. Rev.* **2001**, *45*, 62-69.
- [12] M. Melchart, J. P. Sadler, *Bioorganometallics* **2006**, 39-64.
- [13] J. R. Durig, J. Danneman, W. D. Behnke, E. E. Mercer, *Chem. Biol. Interact.* **1976**, *13*, 287-294.
- [14] M. J. Clarke, F. C. Zhu, D. R. Frasca, *Chem. Rev.* **1999**, *99*, 2511-2533.
- [15] F. Bottomley, *Can. J. Chem.* **1977**, *55*, 2788-2791.
- [16] D. R. Frasca, J. Ciampa, J. Emerson, R. S. Umans, M. J. Clarke, *M. Based Drugs* **1996**, *3*, 197-209.
- [17] R. A. Vilaplana, F. Gonzalezvilchez, E. Gutierrezpuebla, C. Ruizvalero, *Inorg. Chim. Acta* **1994**, *224*, 15-18.
- [18] F. G. Vilchez, R. Vilaplana, G. Blasco, L. Messori, *J. Inorg. Biochem.* **1998**, *71*, 45-51.

- [19] G. Sava, S. Zorzet, T. Giraldi, G. Mestroni, G. Zassinovich, *Eur. J. Cancer Clin. On.* **1984**, *20*, 841-847.
- [20] R. E. Morris, R. E. Aird, P. D. Murdoch, H. M. Chen, J. Cummings, N. D. Hughes, S. Parsons, A. Parkin, G. Boyd, D. I. Jodrell, P. J. Sadler, *J. Med. Chem.* **2001**, *44*, 3616-3621.
- [21] a) A. Bergamo, G. Sava, *Dalton Trans.* **2007**, 1267-1272; b) C. G. Hartinger, M. A. Jakupec, S. Zorbas-Seifried, M. Groessler, A. Egger, W. Berger, H. Zorbas, P. J. Dyson, B. K. Keppler, *Chem. Biodivers.* **2008**, *5*, 2140-2155; c) G. Sava, S. Pacor, A. Bergamo, M. Cocchietto, G. Mestroni, E. Alessio, *Chem. Biol. Interact.* **1995**, *95*, 109-126; d) E. Reisner, V. B. Arion, B. K. Keppler, A. J. L. Pombeiro, *Inorg. Chim. Acta* **2008**, *361*, 1569-1583; e) M. Groessler, E. Reisner, C. G. Hartinger, R. Eichinger, O. Semenova, A. R. Timerbaev, M. A. Jakupec, V. B. Arion, B. K. Keppler, *J. Med. Chem.* **2007**, *50*, 2185-2193.
- [22] M. J. Clarke, *Coordin. Chem. Rev.* **2002**, *232*, 69-93.
- [23] a) G. S. Smith, B. Therrien, *Dalton Trans.* **2011**, *40*, 10793-10800; b) B. Therrien, *Eur. J. Inorg. Chem.* **2009**, 2445-2453; c) B. Therrien, *Coordin. Chem. Rev.* **2009**, *253*, 493-519; d) G. Süß-Fink, *J. Organomet. Chem.* **2014**, *751*, 2-19.
- [24] a) P. Crochet, V. Cadierno, *Dalton Trans.* **2014**, *43*, 12447-12462; b) P. Kumar, R. K. Gupta, D. S. Pandey, *Chem. Soc. Rev.* **2014**, *43*, 707-733; c) A. A. Nazarov, C. G. Hartinger, P. J. Dyson, *J. Organomet. Chem.* **2014**, *751*, 251-260; d) A. K. Singh, D. S. Pandey, Q. Xu, P. Braunstein, *Coordin. Chem. Rev.* **2014**, *270*, 31-56; e) A. Mishra, S. C. Kang, K. W. Chi, *Eur. J. Inorg. Chem.* **2013**, *2013*, 5222-5232; f) S. K. Singh, D. S. Pandey, *Rsc Adv.* **2014**, *4*, 1819-1840; g) A. F. A. Peacock, P. J. Sadler, *Chem. Asian J.* **2008**, *3*, 1890-1899.
- [25] W. H. Ang, A. Casini, G. Sava, P. J. Dyson, *J. Organomet. Chem.* **2011**, *696*, 989-998.
- [26] W. H. Ang, P. J. Dyson, *Eur. J. Inorg. Chem.* **2006**, 4003-4018.
- [27] C. Manzotti, G. Pratesi, E. Menta, R. Di Domenico, E. Cavalletti, H. H. Fiebig, L. R. Kelland, N. Farrell, D. Polizzi, R. Supino, G. Pezzoni, F. Zunino, *Clin. Cancer Res.* **2000**, *6*, 2626-2634.
- [28] A. Valente, M. Garcia, *Inorganics* **2014**, *2*, 96-114.
- [29] M. G. Mendoza-Ferri, C. G. Hartinger, M. A. Mendoza, M. Groessler, A. E. Egger, R. E. Eichinger, J. B. Mangrum, N. P. Farrell, M. Maruszak, P. J. Bednarski, F. Klein, M.

- A. Jakupec, A. A. Nazarov, K. Severin, B. K. Keppler, *J. Med. Chem.* **2009**, *52*, 916-925.
- [30] A. K. Gorle, A. J. Ammit, L. Wallace, F. R. Keene, J. G. Collins, *New J. Chem.* **2014**, *38*, 4049-4059.
- [31] R. Chakrabarty, P. S. Mukherjee, P. J. Stang, *Chem. Rev.* **2011**, *111*, 6810-6918.
- [32] a) M. Yoshizawa, M. Nagao, K. Kumazawa, M. Fujita, *J. Organomet. Chem.* **2005**, *690*, 5383-5388; b) W. Y. Sun, M. Yoshizawa, T. Kusakawa, M. Fujita, *Curr. Opin. Chem. Biol.* **2002**, *6*, 757-764; c) J. K. Klosterman, Y. Yamauchi, M. Fujita, *Chem. Soc. Rev.* **2009**, *38*, 1714-1725; d) Y. Inokuma, M. Kawano, M. Fujita, *Nat. Chem.* **2011**, *3*, 349-358.
- [33] T. R. Cook, V. Vajpayee, M. H. Lee, P. J. Stang, K. W. Chi, *Acc. Chem. Res.* **2013**, *46*, 2464-2474.
- [34] S. Bivaud, S. Goeb, V. Croué, P. I. Dron, M. Allain, M. Sallé, *J. Am. Chem. Soc.* **2013**, *135*, 10018-10021.
- [35] a) D. J. Cram, J. M. Cram, *Science* **1974**, *183*, 803-809; b) E. P. Kyba, R. C. Helgeson, K. Madan, G. W. Gokel, T. L. Tarnowski, S. S. Moore, D. J. Cram, *J. Am. Chem. Soc.* **1977**, *99*, 2564-2571.
- [36] a) C. J. Pedersen, *J. Am. Chem. Soc.* **1967**, *89*, 2495-2496; b) C. J. Pedersen, *J. Am. Chem. Soc.* **1967**, *89*, 7017-7036.
- [37] a) B. Dietrich, J. M. Lehn, J. P. Sauvage, *Tetrahedron Lett.* **1969**, 2885-2888; b) B. Dietrich, J. M. Lehn, J. P. Sauvage, *Tetrahedron Lett.* **1969**, 2889-2892.
- [38] B. Gomez, V. Francisco, F. Fernandez-Nieto, L. Garcia-Rio, M. Martin-Pastor, M. R. Paleo, F. J. Sardina, *Chem. Eur. J.* **2014**, *20*, 12123-12132.
- [39] C. Sanchez-Cano, M. J. Hannon, *Dalton Trans.* **2009**, 10702-10711.
- [40] J. W. Yi, N. P. E. Barry, M. A. Furrer, O. Zava, P. J. Dyson, B. Therrien, B. H. Kim, *Bioconjugate Chem.* **2012**, *23*, 461-471.
- [41] J. Freudenreich, N. P. E. Barry, G. Süß-Fink, B. Therrien, *Eur. J. Inorg. Chem.* **2010**, 2400-2405.
- [42] R. G. Chapman, N. Chopra, E. D. Cochien, J. C. Sherman, *J. Am. Chem. Soc.* **1994**, *116*, 369-370.
- [43] a) J. Mattsson, P. Govindaswamy, J. Furrer, Y. Sei, K. Yamaguchi, G. Süß-Fink, B. Therrien, *Organometallics* **2008**, *27*, 4346-4356; b) X. P. Zhou, J. Liu, S. Z. Zhan, J. R. Yang, D. Li, K. M. Ng, R. W. Y. Sun, C. M. Che, *J. Am. Chem. Soc.* **2012**, *134*, 8042-8045; c) J. Mattsson, O. Zava, A. K. Renfrew, Y. Sei, K. Yamaguchi, P. J.

- Dyson, B. Therrien, *Dalton Trans.* **2010**, 39, 8248-8255; d) N. P. E. Barry, B. Therrien, *Eur. J. Inorg. Chem.* **2009**, 4695-4700; e) P. Govindaswamy, J. Furrer, G. Süss-Fink, B. Therrien, *Z. Anorg. Allg. Chem.* **2008**, 634, 1349-1352; f) J. C. Sherman, C. B. Knobler, D. J. Cram, *J. Am. Chem. Soc.* **1991**, 113, 2194-2204.
- [44] H. Peng, C. Wang, X. Xu, C. Yu, Q. Wang, *Nanoscale* **2015**.
- [45] G. Collet, C. Grillon, M. Nadim, C. Kieda, *Gene* **2013**, 525, 208-216.
- [46] C. H. Wu, C. Cao, J. H. Kim, C. H. Hsu, H. J. Wanebo, W. D. Bowen, J. Xu, J. Marshall, *Nano Lett.* **2012**, 12, 5475-5480.
- [47] a) B. Therrien, G. Süss-Fink, P. Govindaswamy, A. K. Renfrew, P. J. Dyson, *Angew. Chem. Int. Ed.* **2008**, 47, 3773-3776; b) O. Zava, J. Mattsson, B. Therrien, P. J. Dyson, *Chem. Eur. J.* **2010**, 16, 1428-1431.
- [48] a) A. Pitto-Barry, N. P. E. Barry, O. Zava, R. Deschenaux, P. J. Dyson, B. Therrien, *Chem. Eur. J.* **2011**; b) A. Pitto-Barry, N. P. E. Barry, O. Zava, R. Deschenaux, B. Therrien, *Chem. Asian J.* **2011**, 6, 1595-1603; c) A. Pitto-Barry, O. Zava, P. J. Dyson, R. Deschenaux, B. Therrien, *Inorg. Chem.* **2012**, 51, 7119-7124.
- [49] H. Hirao, X. Wang, 'The Chemical Bond: Chemical Bonding Across the Periodic Table', First ed., Wiley-VCH, Weinheim **2014**, pp. 501-521.
- [50] a) C. G. Cannon, *Spectrochim. Acta* **1958**, 10, 341-368; b) J. Emsley, *Chem. Soc. Rev.* **1980**, 9, 91-124; c) B. Kojic-Prodic, K. Molcanov, *Acta. Chim. Slov.* **2008**, 55, 692-708.
- [51] T. L. Brown, J. H. E. LeMay, B. E. Bursten, C. J. Murphy, P. M. Woodward, 'Chemistry: The Central Science', 12 ed., Pearson Prentice Hall, Boston, **2012**, pp. 431-434.
- [52] a) P. S. Corbin, L. J. Lawless, Z. T. Li, Y. G. Ma, M. J. Witmer, S. C. Zimmerman, *Proc. Natl. Acad. Sci. U.S.A* **2002**, 99, 5099-5104; b) Y. Hisamatsu, N. Shirai, S. Ikeda, K. Odashima, *Org. Lett.* **2009**, 11, 4342-4345; c) F. H. Beijer, H. Kooijman, A. L. Spek, R. P. Sijbesma, E. W. Meijer, *Angew. Chem. Int. Ed.* **1998**, 37, 75-78; d) Y. Yang, M. Xue, L. J. Marshall, J. de Mendoza, *Org. Lett.* **2011**, 13, 3186-3189.
- [53] a) X. -Q. Li, D. -J. Feng, X. -K. Jiang, Z. -T. Li, *Tetrahedron* **2004**, 60, 8275-8284; b) J. P. Mathias, E. E. Simanek, J. A. Zerkowski, C. T. Seto, G. M. Whitesides, *J. Am. Chem. Soc.* **1994**, 116, 4316-4325; c) P. S. Corbin, S. C. Zimmerman, *J. Am. Chem. Soc.* **1998**, 120, 9710-9711; d) S. W. Kuo, *Polym. Int.* **2009**, 58, 455-464.

- [54] a) T. J. Murray, S. C. Zimmerman, *J. Am. Chem. Soc.* **1992**, *114*, 4010-4011; b) E. E. Fenlon, T. J. Murray, M. H. Baloga, S. C. Zimmerman, *J. Org. Chem.* **1993**, *58*, 6625-6628; c) S. C. Zimmerman, T. J. Murray, *Tetrahedron Lett.* **1994**, *35*, 4077-4080.
- [55] a) J. Pranata, S. G. Wierschke, W. L. Jorgensen, *J. Am. Chem. Soc.* **1991**, *113*, 2810-2819; b) W. L. Jorgensen, J. Pranata, *J. Am. Chem. Soc.* **1990**, *112*, 2008-2010.
- [56] G. M. Whitesides, E. E. Simanek, J. P. Mathias, C. T. Seto, D. N. Chin, M. Mammen, D. M. Gordon, *Acc. Chem. Res.* **1995**, *28*, 37-44.
- [57] X. B. Shao, X. K. Jiang, S. Z. Zhu, Z. T. Li, *Tetrahedron* **2004**, *60*, 9155-9162.
- [58] a) R. P. Sijbesma, F. H. Beijer, L. Brunsveld, B. J. B. Folmer, J. H. K. K. Hirschberg, R. F. M. Lange, J. K. L. Lowe, E. W. Meijer, *Science* **1997**, *278*, 1601-1604; b) T. Park, S. C. Zimmerman, S. Nakashima, *J. Am. Chem. Soc.* **2005**, *127*, 6520-6521; c) B. A. Blight, C. A. Hunter, D. A. Leigh, H. McNab, P. I. T. Thomson, *Nat. Chem.* **2011**, *3*, 244-248.
- [59] W. P. J. Appel, M. M. L. Nieuwenhuizen, M. Lutz, B. F. M. de Waal, A. R. A. Palmans, E. W. Meijer, *Chem. Sci.* **2014**, *5*, 3735-3745.
- [60] L. Brunsveld, B. J. B. Folmer, E. W. Meijer, R. P. Sijbesma, *Chem. Rev.* **2001**, *101*, 4071-4097.
- [61] a) H. M. Keizer, J. J. Gonzalez, M. Segura, P. Prados, R. P. Sijbesma, E. W. Meijer, J. de Mendoza, *Chem. Eur. J.* **2005**, *11*, 4602-4608; b) J. J. Gonzalez, P. Prados, J. de Mendoza, *Angew. Chem. Int. Ed.* **1999**, *38*, 525-528; c) U. Hahn, J. J. Gonzalez, E. Huerta, M. Segura, J. F. Eckert, F. Cardinali, J. de Mendoza, J. F. Nierengarten, *Chem. Eur. J.* **2005**, *11*, 6666-6672; d) E. Huerta, E. Cequier, J. de Mendoza, *Chem. Commun.* **2007**, 5016-5018; e) S. H. M. Sontjens, R. P. Sijbesma, M. H. P. van Genderen, E. W. Meijer, *J. Am. Chem. Soc.* **2000**, *122*, 7487-7493; f) L. J. Marshall, J. de Mendoza, *Org. Lett.* **2013**, *15*, 1548-1551.
- [62] P. S. Corbin, S. C. Zimmerman, P. A. Thiessen, N. A. Hawryluk, T. J. Murray, *J. Am. Chem. Soc.* **2001**, *123*, 10475-10488.
- [63] V. G. H. Lafitte, A. E. Aliev, P. N. Horton, M. B. Hursthouse, K. Bala, P. Golding, H. C. Hailes, *J. Am. Chem. Soc.* **2006**, *128*, 6544-6545.
- [64] T. R. Cook, Y. R. Zheng, P. J. Stang, *Chem. Rev.* **2013**, *113*, 734-777.
- [65] K. F. Morris, C. S. Johnson, *J. Am. Chem. Soc.* **1992**, *114*, 3139-3141.
- [66] D. Y. Li, G. Kagan, R. Hopson, P. G. Williard, *J. Am. Chem. Soc.* **2009**, *131*, 5627-5634.

- [67] a) C. S. Johnson, *Prog. Nucl. Mag. Res. Sp.* **1999**, *34*, 203-256; b) X. Z. Yan, S. J. Li, J. B. Pollock, T. R. Cook, J. Z. Chen, Y. Y. Zhang, X. F. Ji, Y. H. Yu, F. H. Huang, P. J. Stang, *Proc. Natl. Acad. Sci. U.S.A* **2013**, *110*, 15585-15590.
- [68] G. Ciancaleoni, C. Zuccaccia, D. Zuccaccia, A. Macchioni, *Magn. Reson. Chem.* **2008**, *46*, S72-S79.
- [69] T. D. W. Claridge, in 'High-resolution NMR Techniques in Organic Chemistry' Vol. 27, Second ed., Elsevier, Hungary, **2009**, pp. 247-302.
- [70] D. Feller, E. R. Davidson, 'Reviews in Computational Chemistry', Vol. 1, Wiley-VCH, New York, **1990**.
- [71] D. C. Young, 'Computational Chemistry: A Practical Guide for Applying Techniques to Real-World Problems', John Wiley & Sons, Inc., New York, **2004**.
- [72] a) W. F. Sun, H. J. Zhu, P. M. Barron, *Chem. Mater.* **2006**, *18*, 2602-2610; b) N. P. E. Barry, F. Edeife, B. Therrien, *Dalton Trans.* **2011**, *40*, 7172-7180.
- [73] a) I. Mathew, Y. J. Li, Z. J. Li, W. F. Sun, *Dalton Trans.* **2010**, *39*, 11201-11209; b) N. P. E. Barry, O. Zava, P. J. Dyson, B. Therrien, *Chem. Eur. J.* **2011**, *17*, 9669-9677; c) A. Vogler, H. Kunkely, *Coordin. Chem. Rev.* **2007**, *251*, 577-583.
- [74] N. P. E. Barry, O. Zava, P. J. Dyson, B. Therrien, *J. Organomet. Chem.* **2012**, *705*, 1-6.
- [75] a) M. Pope, P. Magnante, H. P. Kallmann, *J. Chem. Phys.* **1963**, *38*, 2042-2043; b) J. Sun, H. L. Zhong, E. J. Xu, D. L. Zeng, J. H. Zhang, H. G. Xu, W. Q. Zhu, Q. Fang, *Org. Electron* **2010**, *11*, 74-80.
- [76] a) N. S. Baek, Y. H. Kim, S. G. Roh, B. K. Kwak, H. K. Kim, *Adv. Funct. Mater.* **2006**, *16*, 1873-1882; b) Y. H. Kim, H. C. Jeong, S. H. Kim, K. Y. Yang, S. K. Kwon, *Adv. Funct. Mater.* **2005**, *15*, 1799-1805; c) Y. H. Kim, D. C. Shin, S. H. Kim, C. H. Ko, H. S. Yu, Y. S. Chae, S. K. Kwon, *Adv. Mater.* **2001**, *13*, 1690-1693; d) M. Zelzer, S. Kappaun, E. Zojer, C. Slugovc, *Monatsh. Chem.* **2007**, *138*, 453-464; e) I. Yamaguchi, K. Seo, Y. Kawashima, *Tetrahedron* **2010**, *66*, 6725-6732.
- [77] a) S. S. Pujari, S. A. Ingale, F. Seela, *Bioconjugate Chem.* **2014**, *25*, 1855-1870; b) Q. Y. Cao, Z. C. Wang, M. Li, J. H. Liu, *Tetrahedron Lett.* **2013**, *54*, 3933-3936; c) C. F. Ke, R. A. Smaldone, T. Kikuchi, H. Li, A. P. Davis, J. F. Stoddart, *Angew. Chem. Int. Ed.* **2013**, *52*, 381-387; d) I. Mallard, D. Landy, N. Bouchemal, S. Fourmentin, *Carbohydr. Res.* **2011**, *346*, 35-42.
- [78] a) R. Y. Tan, Z. B. Wang, Y. Li, D. J. Kozera, Z. H. Lu, D. T. Song, *Inorg. Chem.* **2012**, *51*, 7039-7049; b) Y. P. Ou, C. Y. Jiang, D. Wu, J. L. Xia, J. Yin, S. Jin, G. A.

- Yu, S. H. Liu, *Organometallics* **2011**, *30*, 5763-5770; c) M. Inouye, T. Konishi, K. Isagawa, *J. Am. Chem. Soc.* **1993**, *115*, 8091-8095; d) H. Dang, M. Levitus, M. A. Garcia-Garibay, *J. Am. Chem. Soc.* **2002**, *124*, 136-143.
- [79] a) N. Miyaura, K. Yamada, A. Suzuki, *Tetrahedron Lett.* **1979**, *20*, 3437-3440; b) N. Miyaura, A. Suzuki, *J. Chem. Soc. Chem. Commun.* **1979**, 866-867.
- [80] a) N. Miyaura, A. Suzuki, *Chem. Rev.* **1995**, *95*, 2457-2483; b) A. Suzuki, *Pure Appl. Chem.* **1991**, *63*, 419-422.
- [81] A. Suzuki, *J. Organomet. Chem.* **1999**, *576*, 147-168.
- [82] N. Miyaura, K. Yamada, H. Suginome, A. Suzuki, *J. Am. Chem. Soc.* **1985**, *107*, 972-980.
- [83] H. C. Kolb, M. G. Finn, K. B. Sharpless, *Angew. Chem. Int. Ed.* **2001**, *40*, 2004-2021.
- [84] a) B. Schulze, U. S. Schubert, *Chem. Soc. Rev.* **2014**, *43*, 2522-2571; b) J. Iehl, R. P. de Freitas, J. F. Nierengarten, *Tetrahedron Lett.* **2008**, *49*, 4063-4066; c) V. V. Rostovtsev, L. G. Green, V. V. Fokin, K. B. Sharpless, *Angew. Chem. Int. Ed.* **2002**, *41*, 2596-2599; d) Z. X. Wang, H. L. Qin, *Chem. Commun.* **2003**, 2450-2451; e) Q. H. Zhang, T. Piacham, M. Drew, M. Patek, K. Mosbach, L. Ye, *J. Am. Chem. Soc.* **2006**, *128*, 4178-4179.
- [85] K. Sivakumar, F. Xie, B. M. Cash, S. Long, H. N. Barnhill, Q. Wang, *Org. Lett.* **2004**, *6*, 4603-4606.
- [86] L. K. Rasmussen, B. C. Boren, V. V. Fokin, *Org. Lett.* **2007**, *9*, 5337-5339.
- [87] M. Meldal, C. W. Tornøe, *Chem. Rev.* **2008**, *108*, 2952-3015.
- [88] F. Himoto, T. Lovell, R. Hilgraf, V. V. Rostovtsev, L. Noodleman, K. B. Sharpless, V. V. Fokin, *J. Am. Chem. Soc.* **2005**, *127*, 210-216.
- [89] a) L. Xu, Y. J. Li, Y. L. Li, *Asian J. Org. Chem.* **2014**, *3*, 582-602; b) P. Espeel, F. E. Du Prez, *Macromolecules* **2015**, *48*, 2-14.
- [90] K. Sonogashira, Y. Tohda, N. Hagihara, *Tetrahedron Lett.* **1975**, 4467-4470.
- [91] a) G. Evano, N. Blanchard, M. Toumi, *Chem. Rev.* **2008**, *108*, 3054-3131; b) R. Chinchilla, C. Najera, *Chem. Soc. Rev.* **2011**, *40*, 5084-5121; c) R. Chinchilla, C. Najera, *Chem. Rev.* **2007**, *107*, 874-922.
- [92] J. Gil-Moltó, C. Nájera, *Eur. J. Org. Chem.* **2005**, 4073-4081.
- [93] S. Durgadas, V. K. Chatare, K. Mukkanti, S. Pal, *Appl. Organomet. Chem.* **2010**, *24*, 680-684.
- [94] H. Plenio, *Angew. Chem. Int. Ed.* **2008**, *47*, 6954-6956.
- [95] Y. Yamamoto, *Chem. Rev.* **2008**, *108*, 3199-3222.

- [96] G. P. McGlacken, I. J. S. Fairlamb, *Eur. J. Org. Chem.* **2009**, 4011-4029.
- [97] H. B. Li, G. A. Grasa, T. J. Colacot, *Org. Lett.* **2010**, *12*, 3332-3335.
- [98] S. H. Jang, H. Kim, M. J. Hwang, E. B. Jeong, H. J. Yun, D. H. Lee, Y. H. Kim, C. E. Park, Y. J. Yoon, S. K. Kwon, S. G. Lee, *B. Korean. Chem. Soc.* **2012**, *33*, 541-548.
- [99] a) J. S. Moore, S. I. Stupp, *Macromolecules* **1990**, *23*, 65-70; b) B. Dardel, R. Deschenaux, M. Even, E. Serrano, *Macromolecules* **1999**, *32*, 5193-5198; c) B. Dardel, D. Guillon, B. Heinrich, R. Deschenaux, *J. Mater. Chem.* **2001**, *11*, 2814-2831; d) A. Pitto-Barry, N. P. E. Barry, V. Russo, B. Heinrich, B. Donnio, B. Therrien, R. Deschenaux, *J. Am. Chem. Soc.* **2014**, *136*, 17616-17625.
- [100] E. J. Corey, Venkates.A, *J. Am. Chem. Soc.* **1972**, *94*, 6190-6191.
- [101] W. B. Cui, X. J. Zhang, X. X. Jiang, H. K. Tian, D. H. Yan, Y. H. Geng, X. B. Jing, F. S. Wang, *Org. Lett.* **2006**, *8*, 785-788.
- [102] P. G. M. Wuts, T. W. Greene, 'Greene's protective groups in organic synthesis', fourth ed., John Wiley & Sons, Inc, New Jersey, **2007**.
- [103] a) J. M. Aubry, C. Pierlot, J. Rigaudy, R. Schmidt, *Acc. Chem. Res.* **2003**, *36*, 668-675; b) W. Fudickar, T. Linker, *Chem. Eur. J.* **2011**, *17*, 13661-13664; c) G. R. Martinez, F. Garcia, L. H. Catalani, J. Cadet, M. C. B. Oliveira, G. E. Ronsein, S. Miyamoto, M. H. G. Medeiros, P. Di Mascio, *Tetrahedron* **2006**, *62*, 10762-10770; d) R. Schmidt, K. Schaffner, W. Trost, H. D. Brauer, *J. Phys. Chem.* **1984**, *88*, 956-958.
- [104] Y. Takaguchi, T. Tajima, Y. Yanagimoto, S. Tsuboi, K. Ohta, J. Motoyoshiya, H. Aoyama, *Org. Lett.* **2003**, *5*, 1677-1679.
- [105] W. Fudickar, T. Linker, *J. Am. Chem. Soc.* **2012**, *134*, 15071-15082.
- [106] S. K. Lee, W. J. Yang, J. J. Choi, C. H. Kim, S. J. Jeon, B. R. Cho, *Org. Lett.* **2005**, *7*, 323-326.
- [107] H. Staudinger, *Nobel Lecture* **1953**, 397-419.
- [108] a) V. Percec, M. Peterca, Y. Tsuda, B. M. Rosen, S. Uchida, M. R. Imam, G. Ungar, P. A. Heiney, *Chem. Eur. J.* **2009**, *15*, 8994-9004; b) B. Donnio, S. Buathong, I. Bury, D. Guillon, *Chem. Soc. Rev.* **2007**, *36*, 1495-1513; c) I. M. Saez, J. W. Goodby, *J. Mater. Chem.* **2005**, *15*, 26-40.
- [109] a) M. A. Mintzer, M. W. Grinstaff, *Chem. Soc. Rev.* **2011**, *40*, 173-190; b) S. H. Medina, M. E. H. El-Sayed, *Chem. Rev.* **2009**, *109*, 3141-3157.
- [110] D. A. Tomalia, *Prog. Polym. Sci.* **2005**, *30*, 294-324.
- [111] H. Ihre, A. Hult, E. Soderlind, *J. Am. Chem. Soc.* **1996**, *118*, 6388-6395.

- [112] a) V. V. Lipson, N. Y. Gorobets, *Mol. Divers.* **2009**, *13*, 399-419; b) Y. Morita, R. Kamakura, M. Takeda, Y. Yamamoto, *Chem. Commun.* **1997**, 359-360.
- [113] S. Leroy-Lhez, F. Fages, *Eur. J. Org. Chem.* **2005**, 2684-2688.
- [114] H. Bittermann, D. Siegemund, V. L. Malinovskii, R. Haner, *J. Am. Chem. Soc.* **2008**, *130*, 15285-15287.
- [115] a) N. P. E. Barry, M. Austeri, J. Lacour, B. Therrien, *Organometallics* **2009**, *28*, 4894-4897; b) Y. F. Han, Y. J. Lin, L. H. Weng, H. Berke, G. X. Jin, *Chem. Commun.* **2008**, 350-352.
- [116] H. L. Anderson, S. Anderson, J. K. M. Sanders, *J. Chem. Soc. Perkin Trans. 1* **1995**, 2231-2245.
- [117] A. J. Amoroso, A. M. W. C. Thompson, J. P. Maher, J. A. McCleverty, M. D. Ward, *Inorg. Chem.* **1995**, *34*, 4828-4835.
- [118] H. W. Kroto, J. R. Heath, S. C. O'Brien, R. F. Curl, R. E. Smalley, *Nature* **1985**, *318*, 162-163.
- [119] a) R. C. Haddon, *J. Am. Chem. Soc.* **1997**, *119*, 1797-1798; b) S. Z. Liu, Y. J. Lu, M. M. Kappes, J. A. Ibers, *Science* **1991**, *254*, 408-410.
- [120] R. C. Haddon, L. E. Brus, K. Raghavachari, *Chem. Phys. Lett.* **1986**, *125*, 459-464.
- [121] a) A. Hirsch, M. Brettreich, 'Fullerenes: Chemistry and Reactions', Wiley-VCH, Weinheim, **2004**; b) A. W. Jensen, S. R. Wilson, D. I. Schuster, *Bioorgan. Med. Chem.* **1996**, *4*, 767-779.
- [122] W. Kratschmer, L. D. Lamb, K. Fostiropoulos, D. R. Huffman, *Nature* **1990**, *347*, 354-358.
- [123] G. Brusatin, R. Signorini, *J. Mater. Chem.* **2002**, *12*, 1964-1977.
- [124] A. Hirsch, 'Principles of Fullerene Reactivity', Vol. 199, Springer, Berlin, **1999**.
- [125] Z. G. Zhou, S. R. Wilson, *Curr. Org. Chem.* **2005**, *9*, 789-811.
- [126] a) P. Piotrowski, J. Pawlowska, J. Pawlowski, A. Wieckowska, R. Bilewicz, A. Kaim, *J. Mater. Chem. A* **2014**, *2*, 2353-2362; b) M. Maggini, G. Scorrano, M. Prato, *J. Am. Chem. Soc.* **1993**, *115*, 9798-9799; c) M. Prato, M. Maggini, *Acc. Chem. Res.* **1998**, *31*, 519-526; d) A. Bagno, S. Claeson, M. Maggini, M. L. Martini, M. Prato, G. Scorrano, *Chem. Eur. J.* **2002**, *8*, 1015-1023.
- [127] a) T. Fujita, Y. Matsuo, E. Nakamura, *Chem. Mater.* **2012**, *24*, 3972-3980; b) Y. Matsuo, E. Nakamura, *Organometallics* **2003**, *22*, 2554-2563.
- [128] T. Da Ros, M. Prato, M. Carano, P. Ceroni, F. Paolucci, S. Roffia, L. Valli, D. M. Guldi, *J. Organomet. Chem.* **2000**, *599*, 62-68.

- [129] R. Bakry, R. M. Vallant, M. Najam-Ul-Haq, M. Rainer, Z. Szabo, C. W. Huck, G. K. Bonn, *Int. J. Nanomed.* **2007**, *2*, 639-649.
- [130] a) S. H. Friedman, D. L. Decamp, R. P. Sijbesma, G. Srdanov, F. Wudl, G. L. Kenyon, *J. Am. Chem. Soc.* **1993**, *115*, 6506-6509; b) R. A. Kotelnikova, G. N. Bogdanov, E. C. Frog, A. I. Kotelnikov, V. N. Shtolko, V. S. Romanova, S. M. Andreev, A. A. Kushch, N. E. Fedorova, A. A. Medzhidova, G. G. Miller, *J. Nanopart. Res.* **2003**, *5*, 561-566.
- [131] C. S. Chen, Y. F. Lin, W. Y. Yeh, *Chem. Eur. J.* **2014**, *20*, 936-940.
- [132] G. Porzi, S. Sandri, *Tetrahedron:Asymmetry* **1996**, *7*, 189-196.
- [133] C. S. Allardyce, P. J. Dyson, D. J. Ellis, S. L. Heath, *Chem. Commun.* **2001**, 1396-1397.
- [134] B. Therrien, T. R. Ward, *Angew. Chem. Int. Ed.* **1999**, *38*, 405-408.
- [135] X. H. Fu, Y. Shen, W. X. Fu, Z. B. Li, *Macromolecules* **2013**, *46*, 3753-3760.
- [136] C. S. Araujo, M. G. B. Drew, V. Felix, L. Jack, J. Madureira, M. Newell, S. Roche, T. M. Santos, J. A. Thomas, L. Yellowlees, *Inorg. Chem.* **2002**, *41*, 2250-2259.

List of Abbreviations

| | |
|----------------------|---|
| 4-ppy | 4-Pyrrolidinopyridine |
| Acac | Acetylacetonato |
| Anal. | Elemental Analysis |
| dpe | 1,2-Di(4-pyridyl)ethylene |
| Calc. | Calculated |
| CC | Column chromatography |
| Cisplatin | <i>Cis</i> -diamminedichloroplatinum(II) |
| CDI | 1,1'-Carbonyldiimidazole |
| DCC | <i>N,N'</i> -Dicyclohexylcarbodiimide |
| dClbq-H ₂ | 2,5-Dichlorido-1,4-benzoquinone |
| ΔH | Enthalpy gradient |
| DFT | Density Functional Theory |
| DMAP | 4-Dimethylaminopyridine |
| DMF | <i>N,N</i> -Dimethylformamide |
| DNA | Deoxyribonucleic acid |
| DPTS | 4-(Dimethylamino)pyridium <i>para</i> -toluenesulfonate |
| dhnq-H ₂ | 5,8-Dihydroxy-1,4-naphthoquinone |
| dhbq-H ₂ | 2,5-Dihydroxy-1,4-benzoquinone |
| DOSY | Diffusion Ordered Spectroscopy |
| DS ⁻ | Dodecylsulfate ion |
| DSC | Differential scanning calorimetry |
| EDC | <i>N</i> -(3-Dimethylaminopropyl)- <i>N'</i> -ethylcarbodiimide |
| en | Ethane-1,2-diamine |
| ESI-MS | Electrospray mass spectrometry |
| EtOH | Ethanol |
| EtOAc | Ethyl acetate |

| | |
|------------------|---|
| FDA | Food and Drug Administration |
| GIAO | Gauge-independent atomic orbitals |
| IC ₅₀ | Drug concentration necessary for 50% inhibition of cell viability |
| IR | Infrared |
| KP1019 | Imidazolium- <i>trans</i> -bis(1H-indazole)-tetraruthenate |
| LANL2DZ | Los Alamos national laboratory 2-double-z |
| M | Non-identified mesophase |
| MeOH | Methanol |
| MOPAC | Molecular orbital package |
| N | Nematic phase |
| NaAsc | Sodium ascorbate |
| NAMI-A | Imidazolium- <i>trans</i> -dimethylsulfoxide-imidazole-tetrachlororuthenate |
| NEt ₃ | Triethylamine |
| ox | Oxalato |
| pta | 1,3,5-Triaza-7-phosphaadamantane |
| <i>p</i> -Cym | <i>Para</i> -cymene |
| PEG | Polyethylene glycol |
| PAMAM | Poly(amido amine) |
| PPh ₃ | Triphenylphosphine |
| POM | Polarised optical microscopy |
| NOE | Nuclear Overhauser Effect |
| NMR | Nuclear magnetic resonance |
| ROE | Rotating-frame Overhauser Enhancement |
| rt | Room temperature |
| Sm | Smectic phase |
| ^t Bu | Tertiarybutyl |
| Tetra-pvb | 1,2,4,5-Tetrakis(2-(pyridine-4-yl)vinyl)benzene |

| | |
|----------------|--|
| T _g | Glass transition temperature |
| T _I | Isotropic temperature |
| TBAF | Tetrabutylammonium fluoride |
| TBDMSCl | Tertiarybutyldimethylchlorosilane |
| Tf | Triflate ion |
| THF | Tetrahydrofuran |
| tpp | 5,10,15-Tris(4-pyridyl)-20-phenylporphyrin |
| tpt | 2,6-Tri(pyridine-4-yl)-1,3,5-triazine |
| UPy | 2-Ureido-4-pyrimidinone |
| UV-Vis | Ultraviolet-visible |

Annex 1

Experimental Techniques

- **Thin layer chromatography**

Thin layer chromatographies (TLC) were done on aluminium sheets covered with a thin layer of silica gel 60F₂₅₄ of 0.2 mm with a fluorescent detector

- **Column chromatographies**

Column chromatographies (CC) were carried out using silica gel Brunschwig 0.063-0.2 mm or 0.040-0.063 mm and a UV detector K-2000 Knauer. For products that were not UV active, a chemical stain (KMnO₄, Na₂CO₃ and water) was used to visualise the spots.

- **Size exclusion chromatography**

Size exclusion chromatographies (SEC) were performed using size exclusion gel Bio-Rad SX1 with the range of mass operation between 600 and 14000 Da. The grains of Bio-Rad SX1 were impregnated with THF for 24h at room temperature, under argon before usage. The eluents used were THF and toluene.

- **Nuclear magnetic resonance**

NMR measurements were recorded on a Brüker AMX-400 (400 and 100 MHz) or a Brüker Advance-400. The internal standard corresponds to the residual non-deuterated solvents: CDCl₃ (δ = 7.26 ppm); CD₂Cl₂ (δ = 5.32 ppm); CD₃CN (δ = 1.94 ppm); DMSO-*d*₆ (δ = 2.50 ppm); MeOD (δ = 3.31 ppm). The multiplicities of the signals were expressed in the following abbreviations: s (singlet), d (doublet), t (triplet), q (quadruplet), quint (quintuplet), sext (sextuplet), sept (septuplet), m (multiplet), dd (doublet of doublets) ddd (doublet of doublet of doublets) and dt (doublet of triplets). The chemical shifts (δ) were expressed in ppm and the coupling constants (J) in Hz. The data were processed using MestRec and MestReNova.

- **Infrared spectroscopy**

IR measurements were carried out using KBr pellets and were analysed by PerkinElmer Spectrum One FT-IR spectroscopy. The spectra were recorded and processed on Spectrum.

- **Mass spectrometry**

The MS measurements were carried out in two departments: Service Analytique Facultaire (SAF) at the University of Neuchâtel on a LCQ-IT Finnigan for electrospray ionization [ESI (+/-)] and at the University of Fribourg on a Bruker FTMS 4.7T BioAPEX II for ESI.

- **Elemental analysis**

The elemental analyses were performed by the Mikroelementar-analytisches Laboratorium laboratory of Eidgenössische Technische Hochschule (ETH) Zürich

- **Polarised optical microscopy**

The observations made on the microscope Axioscope Zeiss equipped with a Linkam THMS 600 heating plate directed by Linkam 93. The photographs were taken with a camera AxioCam MRc (Zeiss) and registered on AxioVision Rel. 4.8.

- **Differential scanning calorimetry**

DSC measurements were performed in a measurement cell Mettler Toledo DSC1 Star^e system. The samples were analysed in aluminium crucibles of 40 μ L under an argon flow. The heating and cooling were carried out at 10°C/min. Each measurement consisted of three heating and cooling cycles. The data was processed using STARE. The temperatures of transitions were determined by the method of tangent (onset) and the enthalpies of transition were obtained from the integration of the peaks.

- **UV-Visible spectroscopy**

The UV-Vis spectra were recorded using a PerkinElmer Lambda 25 UV-Vis spectrometry in quartz cuvettes of 1 cm wide and data was processed using PerkinElmer UV WinLab.

- **X-ray structure analysis**

The crystal was mounted on a Stoe Image Plate Diffraction system equipped with a ϕ circle goniometry, using Mo K α graphite-monochromated radiation ($\lambda = 0.71073 \text{ \AA}$) with ϕ range 0–200°, increment of 1.2° and 1.0°, respectively, 2θ range from 4.0° to 52°, $D_{\text{max}}-D_{\text{min}} = 12.45-0.81 \text{ \AA}$. The structure was solved by direct methods using the program SHELXS-97. Refinement and all further calculations were carried out using SHELXL-97. In the compound, H atoms were included in calculated positions and treated as riding atoms using the SHELXL default parameters. All non H atoms were refined anisotropically, using weighed fullmatrix least-squares on F^2 .

- **Density functional theory**

Optimization was performed using a semiempirical method PM7 as implemented in MOPAC2012 and further optimization was performed with DFT methods utilizing the B3LYP hybrid functional and 6-311++G(2d,p) basis set as implemented in Gaussian09. The LANL2DZ pseudopotentials were used on the Ru centres to obtain the structures. The

magnetic shielding tensors of both ^1H and ^{13}C nuclei were calculated with the GIAO method at the same level of theory of the DFT optimizations.

Reagents

| Reactants | Quality | Supplier |
|---|-----------------|-----------------|
| Glacial acetic acid | 99.9% | Carlo Erba |
| Hydrochloric acid | 32% | Reactolab |
| Meldrum's acid | 98% | Aldrich |
| 4-Pentyn-1-ol | 97% | Aldrich |
| Bromoacetyl chloride | $\geq 95\%$ | Aldrich |
| 4-Hydroxyboronic acid | 97% | Aldrich |
| Bromine | Reagent grade | Aldrich |
| Iodine | 99.8% | Fluka |
| Sodium chloride | Technical grade | Fluka |
| <i>tert</i> -Butyldimethylsilyl chloride (TBDMSCl) | 97% | Aldrich |
| Tetrabutylammonium fluoride (TBAF) | 98% | Aldrich |
| Fullerene | $\geq 99.9\%$ | MER Corp |
| Sodium hydroxide | $> 97\%$ | Carlo Erba |
| <i>N,N'</i> -Dicyclohexylcarbodiimide (DCC) | $\geq 99\%$ | |
| 4-(Dimethylamino)pyridine (DMAP) | 99% | Acros |
| 4-Pyrrolidinopyridine | $\geq 98\%$ | Fluka |
| <i>N</i> -(3-Dimethylaminopropyl)- <i>N'</i> -ethylcarbodiimide (EDC) | $\geq 97\%$ | Fluka |
| Copper bromide | Technical grade | Acros |
| <i>tert</i> -butyl nitrite | 90% | Aldrich |
| Tetrakis(triphenylphosphine)palladium(0) | 99% | Aldrich |
| Silver trifluoromethanesulfonate | $\geq 99\%$ | Aldrich |
| Copper iodide | | Riedel |
| Sulphuric acid | 96% | Reactolab |
| <i>p</i> -Toluene sulfonic acid | 98.5% | Aldrich |
| 1,2-Bis(4-pyridyl)ethylene | 97% | Aldrich |
| 5,8-Dihydroxy-1,4-naphthoquinone | Technical grade | Aldrich |
| Ruthenium trichloride hydrate | - | Johnson Matthey |

| | | |
|--|------------------------|---------|
| Triethylamine | ≥99% | Aldrich |
| 1,3,5-Triaza-7-phosphaadamantane (pta) | 97% | Aldrich |
| <i>Para</i> formaldehyde | Reagent grade | Aldrich |
| 4-(Aminomethyl)pyridine | 98% | Aldrich |
| 4-(2-Aminoethyl)pyridine | 96% | Aldrich |
| 4-(1-Aminoethyl)pyridine | 95% | Aldrich |
| Diethyl carbonate | >98% | TCI |
| Tin(II) chloride dihydrate | ≥98% | Aldrich |
| Sodium dodecyl sulfate | ≥98.5% | Aldrich |
| Silver nitrate | ≥99% | Aldrich |
| Pyrene | ≥99% | Aldrich |
| 9,10-Dibromoanthracene | 98% | Aldrich |
| Anthraquinone | 97% | Aldrich |
| 2,6-Diaminoanthraquinone | 97% | Aldrich |
| α-Phellandrene | Technical grade | Fluka |
| Hexamethylbenzene | 99% | Aldrich |
| Guanidine carbonate | 98% | TCI |
| 1,1'-Carbonyldiimidazole (CDI) | >95% | TCI |
| 2-Tridecanone | ≥96% | Aldrich |
| Sodium hydride | 60% in paraffin liquid | TCI |
| 2,5-Dihydroxy-1,4-benzoquinone | 98% | Aldrich |
| Chloranilic acid | - | Aldrich |
| 2-Hexanone | 98% | Aldrich |
| Sodium acetate | - | Aldrich |
| <i>n</i> -Butyllithium | 2.5 M in hexanes | Aldrich |
| 4-Pentynoic acid | 95% | Aldrich |
| Magnesium Sulfate | Technical grade | Fluka |
| Tri(ethylene)glycol monoethyl ether | Technical grade | Aldrich |
| 4-Pyridinecarbonitrile | 98% | Aldrich |

Solvents

The solvents used for the reactions, extractions and chromatographies were of technical grade and distilled by rotary evaporator before use.

- **Distilled solvents**

| Solvent | Supplier |
|-------------------|-------------------|
| Ethyl acetate | Reactolab |
| Acetone | Reactolab, puriss |
| Acetonitrile | Acros |
| Dichloromethane | Reactolab |
| Ethanol | Reactolab |
| Diethyl ether | Reactolab |
| Heptane | Reactolab |
| Isopropanol | Reactolab |
| Methanol | Reactolab, puriss |
| Dimethylsulfoxide | Reactolab |
| Dimethylformamide | Aldrich |
| Tetrahydrofuran | Reactolab |
| Toluene | Reactolab |

- **Dried solvents**

| Solvent | Drying agent |
|-------------------|-------------------------------|
| Dichloromethane | P ₂ O ₅ |
| Tetrahydrofuran | KOH, then K/Na/benzophenone |
| Toluene | NaH |
| Dimethylformamide | CaH ₂ |

- **Deuterated solvents**

| Solvent | Supplier | Quality |
|-------------------|-----------------------------------|----------------|
| Chloroform | Cambridge Isotope Laboratories, D | 99.8% |
| Dichloromethane | Cambridge Isotope Laboratories, D | 99.8% |
| Dimethylsulfoxide | Cambridge Isotope Laboratories, D | 99.9% |
| Methanol | Cambridge Isotope Laboratories, D | 99.8% |
| Acetonitrile | Cambridge Isotope Laboratories, D | 99.8% |

Annex 2

In the NOE, when the population difference across the Zeeman eigenstates of a nuclear spin is driven away from its equilibrium state, either by saturation or inversion, a change in signal intensity may be observed for resonances associated with spins that are dipolar coupled to the irradiated one. In other words, if a nuclear spin is in spatial proximity with another one, with the latter being perturbed by an *rf*-pulse, the former will show a variation of signal intensity when compared to a spectrum where no spin was irradiated. A requirement for this phenomenon to take place is a dipolar coupling between the above-mentioned nuclear spins. This interaction is proportional to r^{-6} , where r is the distance between the spin pairs. It may be shown that, under conditions of linear growth of the NOE enhancements, if one perturbs the equilibrium-population difference of spin A and observes NOEs on spins B and X , the following relationship applies:

$$r_{AB} = r_{AX} \left(I_X / I_B \right)^{1/6} \quad \text{Equation 2}$$

where I_i = intensity of the i^{th} signal,

r_{Ai} = internuclear distance between the irradiated spin A and the i^{th} spin for which an NOE is observed.

In other words, if the internuclear distance r_{AX} is known, then one can readily determine the unknown distance r_{AB} .

The structures of **4** in both its monomeric and dimeric forms were preliminarily optimised with the semiempirical method PM7 as implemented in MOPAC2012. A further optimization was performed with DFT methods utilizing the B3LYP hybrid functional and 6-311++G(2d,p) basis set as implemented in Gaussian09. The LANL2DZ pseudopotentials were used on the Ru centres. The structures thus obtained were used to calculate the magnetic shielding tensors of both ^1H and ^{13}C nuclei with the GIAO method at the same level of theory of the DFT optimizations.

When analysing NOE enhancements in such dimeric structures one has to consider both intra- and intermolecular dipolar couplings, which may both supply pathways for polarization transfer. If one considers two spins A and X belonging to one molecule and their chemically-

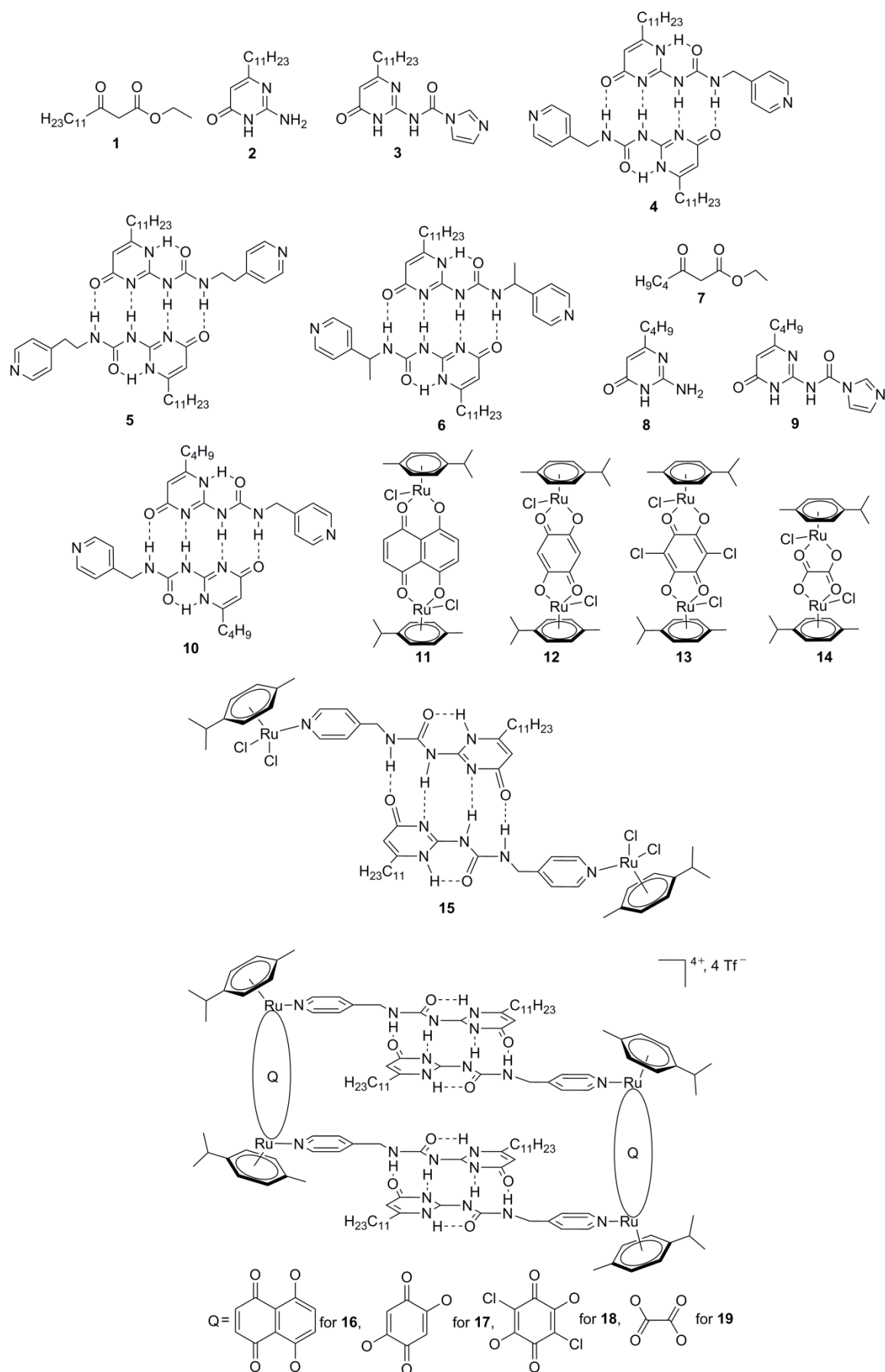
equivalent counterparts A' and X' belonging to the other molecule of the dimer, it may happen, as in our case, that $r_{AX} > r_{AX'}$. In other words, the NOE enhancement observed for, say, the spin A (and A') when perturbing the spin X (and X') may be related to both intra- and intermolecular dipolar couplings. In order to take into account these effects, Equation 2 needs to be modified by considering an effective distance $r_i^{(eff)}$ that may be related to the intensity of the enhancement I_i of the i^{th} spin that is experiencing n different polarization-transfer pathways:

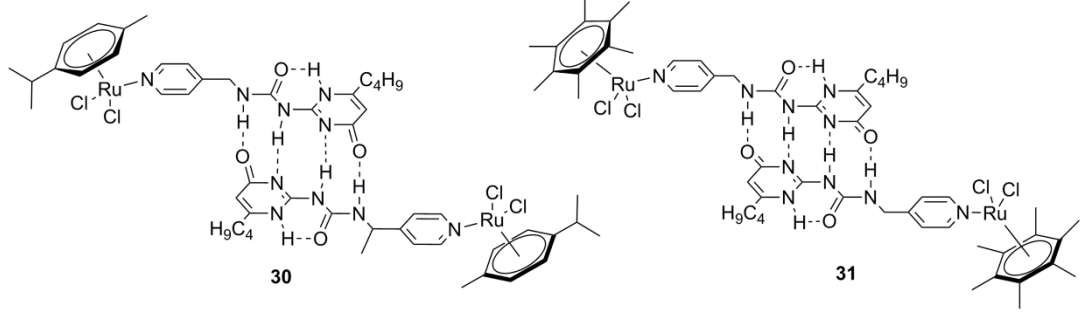
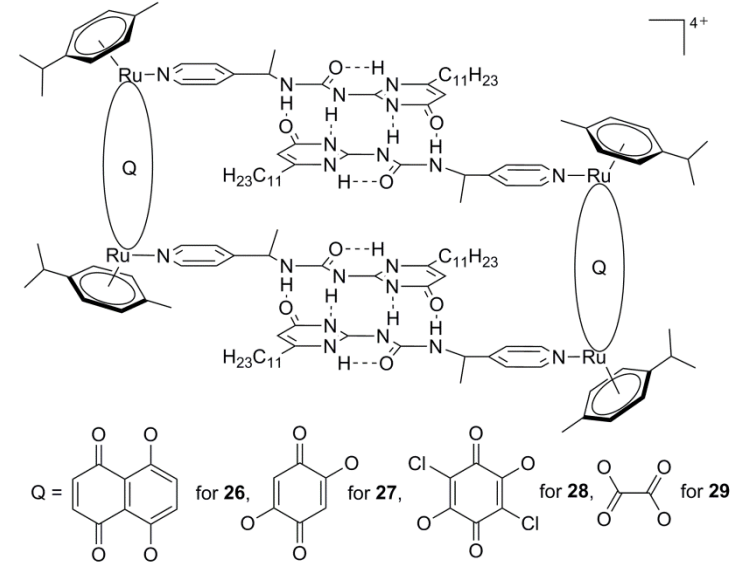
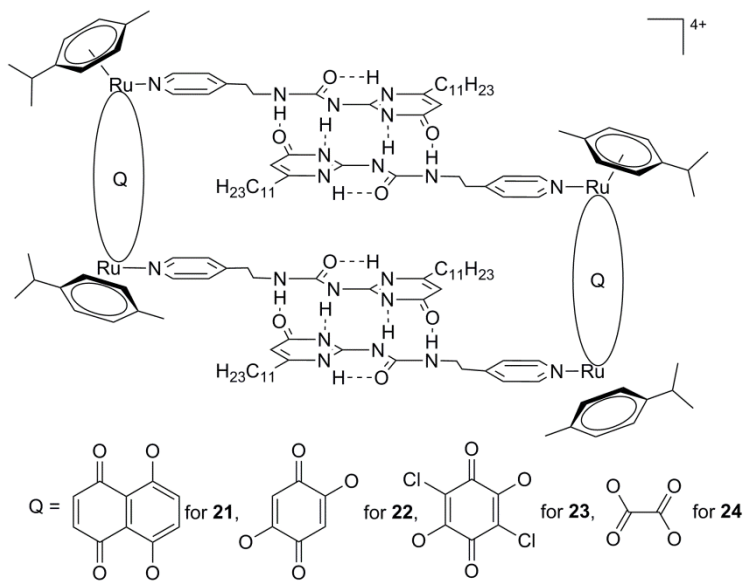
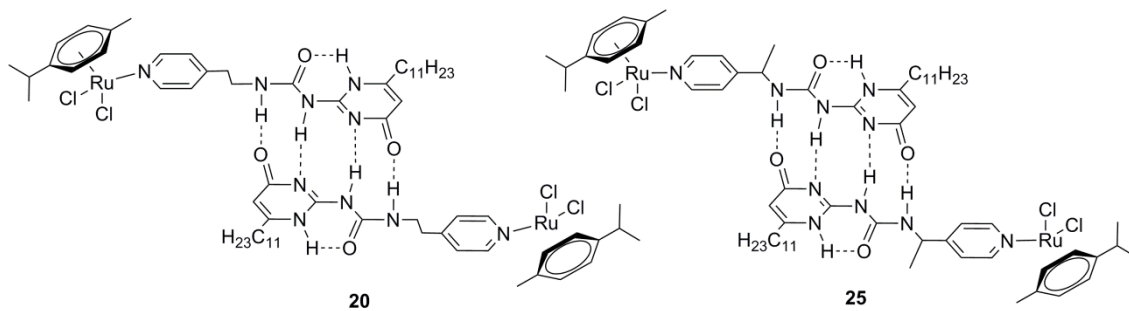
$$r_i^{(eff)} = \left[\left(\frac{1}{r_{i,1}^6} + \frac{1}{r_{i,2}^6} + \dots + \frac{1}{r_{i,n}^6} \right)^{-1} \right]^{1/6} = \left(\frac{\prod_j^n r_{i,j}^6}{\sum_j^n r_{i,j}^6} \right)^{1/6} \quad \text{Equation 3}$$

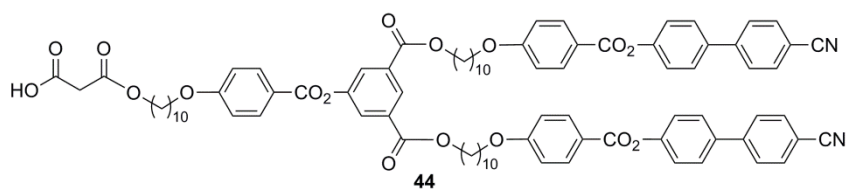
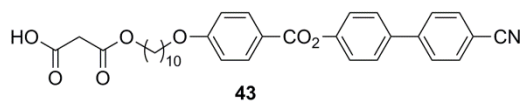
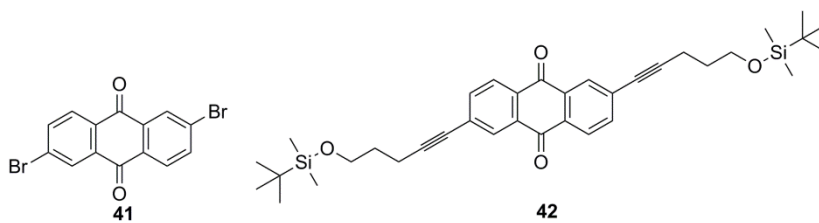
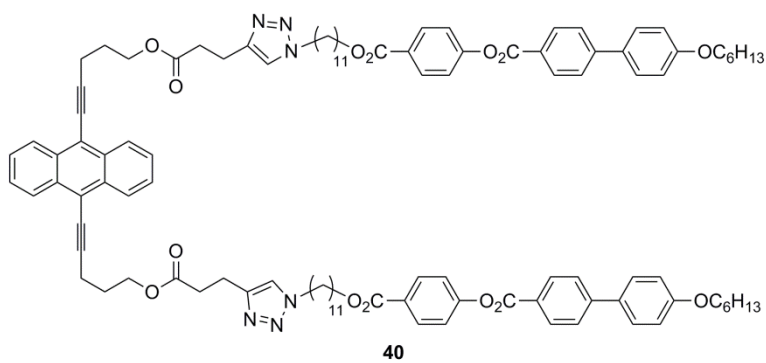
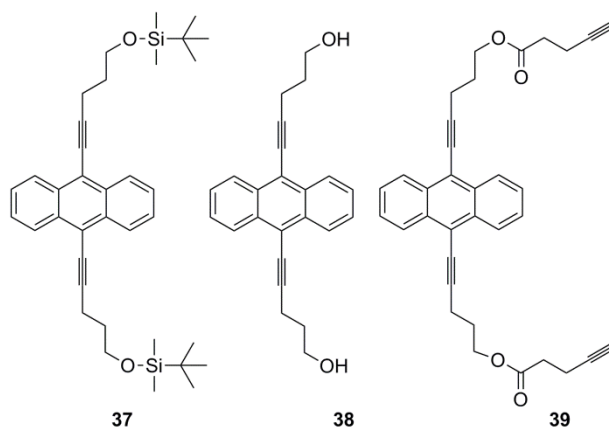
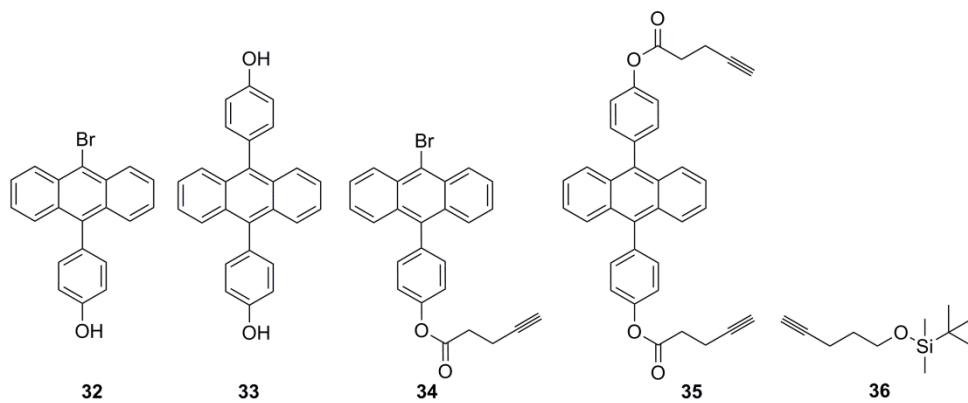
Equation 2 takes into account only intramolecular dipolar couplings whereas the effective distances of Equation 3 considers both intra- and intermolecular pathways of polarization transfer.

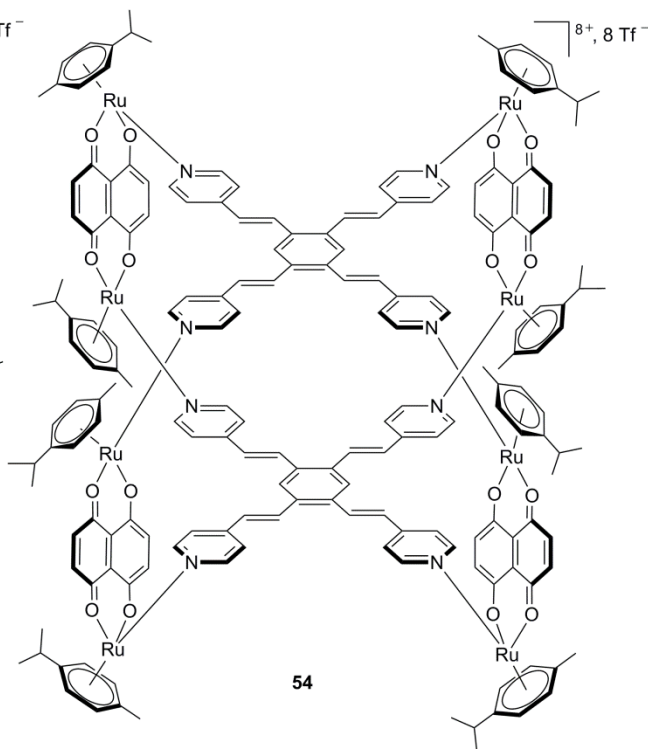
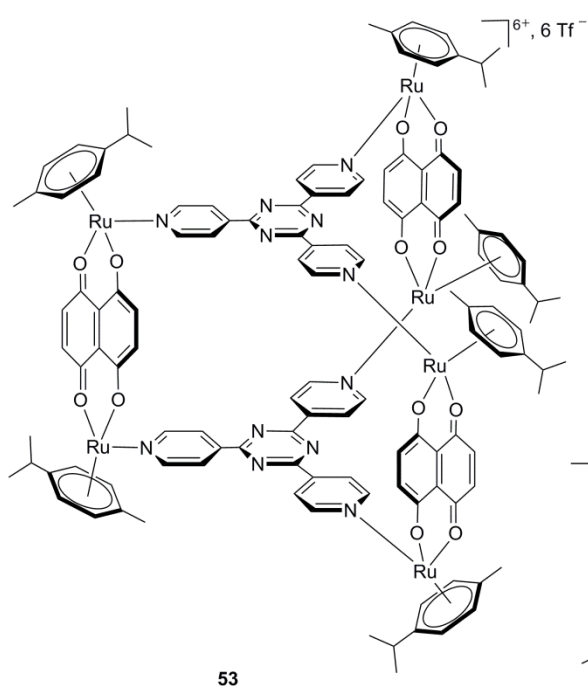
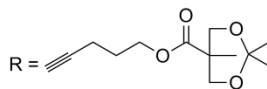
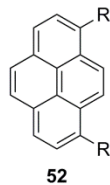
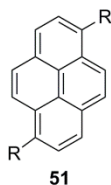
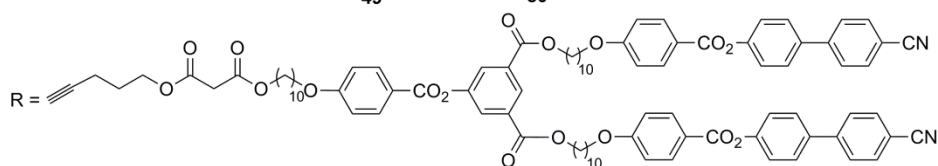
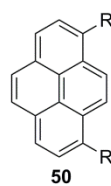
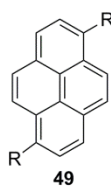
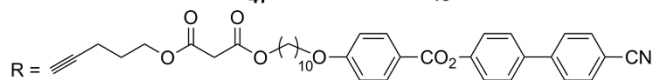
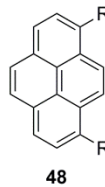
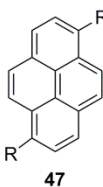
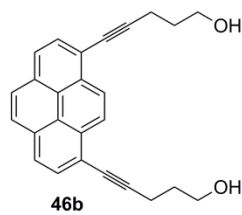
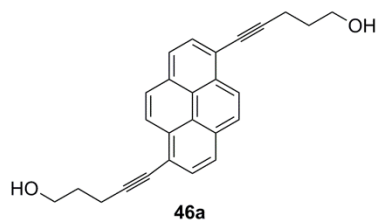
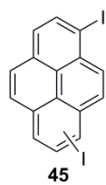
For the tetranuclear arrangement of compound **17**, the contribution of the different resonances to the peak pattern experiencing in NOE transfer in Figure 2.20 has been measured by numerical fit, assuming three Lorentzian lineshapes and performed over the space spanned by the isotropic shift, signal intensity and line broadening.

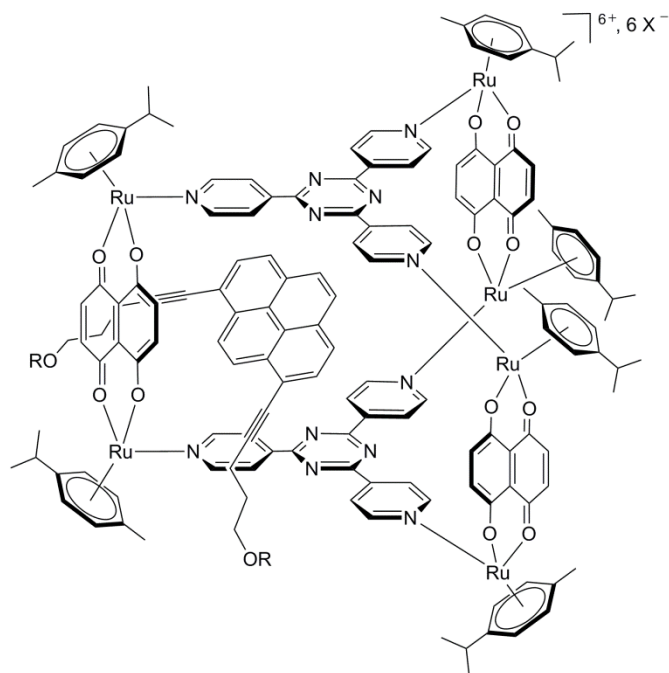
Annex 3



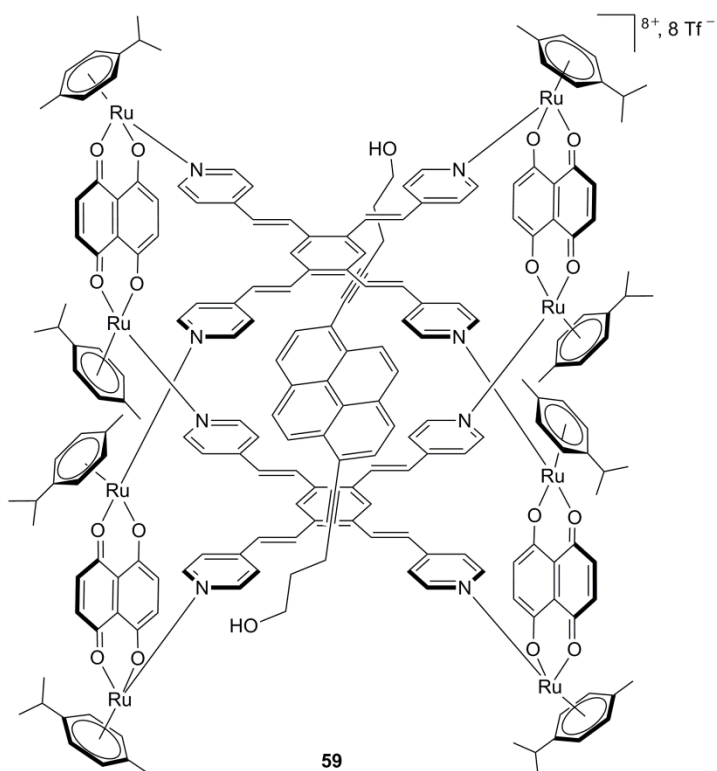
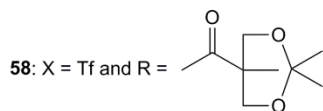
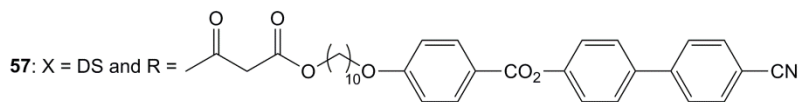
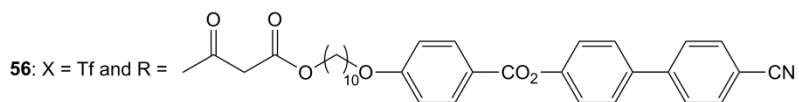








55: X = Tf and R = H



59

